



Synthesis of Crosslinked Block Copolymer Microparticles in Supercritical CO₂

Kartini Alias

Thesis submitted to the University of Nottingham

for the degree of Doctor of Philosophy

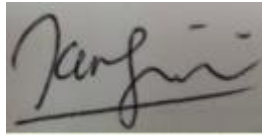
2022

Disclaimer

All work presented in this Thesis is the original work of the author, with the exception of results referenced to other sources. It has not been submitted as part of any other degree or professional qualification.

Signed

:

A rectangular box containing a handwritten signature in black ink. The signature is cursive and appears to read 'Kangni'.

Date : 31st March 2022

Acknowledgement

It was a great pleasure and a wonderful PhD journey throughout my studies at the University of Nottingham. Thank you for the opportunity given by the Al-Mighty. Many amazing people were directly or indirectly involved in enriching my knowledge of polymer synthesis and building expertise in the areas of high-pressure systems and supercritical carbon dioxide. It was almost impossible for me to produce a few important findings and achieve all the listed objectives for this study without the support of these important people. Here is a small compliment to all those people.

First and foremost, I would like to take this opportunity to thank my brilliant and wonderful supervisor, Professor Steve Howdle, for the great opportunity and trust given to shoulder an exciting and valuable research task and for his continuous guidance and support throughout my study. I am also pleased to have a passionate Post-Docs and former Post-Docs, Dr. Vincenzo Taresco, Dr. Thomas Bennett, and Dr. Olivia Monaghan, who have never had a shortage of ideas in guiding me through my day-to-day experimental work and sharing tips and tricks in handling the high-pressure autoclave. It's really beneficial!

A special thanks also goes to Dr. Alice Haddleton for being a great proof-reader and her ever-ready kind help throughout my study and thesis writing. Many thanks also go to our visiting Associate Prof. Fabricio Machado for his knowledge sharing and being a good commentor for my thesis. Further thanks goes to: Dr. Elizabeth Steer for SEM focal point reference, Ms. Nicola Weston and Ms. Denise Mclean for microtome and TEM one-on-one valuable guidance. Mr. Richard Wilson, Mr Mark Gyler and the workshop team for their technical and trouble-shooting assistance, particularly on high-pressure related things. I'd also like to thank Malaysian

Rubber Board for their sponsorship of my studies at Nottingham University in the United Kingdom.

Many thanks to each of my B10 lab mates for their knowledge sharing and their great friendship, which made my lab day more cheerful. Last but not least, a special dedication to my beloved family members, especially my husband, Mohd Azrul Md Said, and my kids, Aqilah Huda and Arif Harraz, who have sacrificed so much by all means and for their never-ending motivation and love throughout my PhD journey in this wonderful Queen's land. To my lovely parents, Umi Kalsom Salleh and Alias Samat, thank you so much for all the prayers and blessings given to me until I have finally completed my task given in order to become a better person who will come back and serve the nation (if God wills).

Being away and apart from family, friendship is the most valuable relationship that I cherish and contributed a lot to my student life in Nottingham. Thus, a special note to all my beloved friends in Nottingham and Malaysia, especially Afnan (a wonderful lady), Tini Rahim, Mek Wanie, Dazy, Yus, Shark, Zurina, Karmila, Kak Fifie, Kak Mimi, Azie, and the rest of them for your wonderful friendship. Without all your support and prayers, it is almost impossible to complete this journey. May God bless you all.

Abstract

To this end, this work aims to develop a synthesis route to structured cross-linked BCP microparticles, with different size and morphology, by RAFT-dispersion polymerisation in $scCO_2$. It is also essential that the developed method can preserve the microparticulate and internal nanostructure integrity, particularly in solvated environment. This study, which focuses on poly(methyl methacrylate)-*block*-poly(4-vinyl pyridine) (PMMA-*b*-P4VP) BCP with spherical (SPH) and lamellar (LAM) morphology, has been successful in crosslinking the BCP with divinyl benzene (DVB), ranging from 0 to 16 wt.%. The microparticle structure and the internal morphology is maintained by delaying the addition of the crosslinker and a portion of the second monomer. As a result polymerisation induced microphase separation within the microparticles is well maintained while the growing chains of the precursor PMMA-*b*-P4VP microparticles are crosslinked. The internal structures formed in the synthesised products were fully characterised by multiple instrumental techniques and promising results were revealed.

The swelling and solubility behaviour of the crosslinked microparticles exhibiting either SPH or LAM internal morphology was investigated via microscopy techniques including Tilt-TEM tomography and nitrogen adsorption isotherm. The maximum resistance point to swelling for both the SPH and LAM BCP microparticles were determined. The SPH microparticles incorporating different levels of crosslinking were found to have control over the porosity formation when swollen in ethanol. Macropores greater than 100 nm, mesopores 20 nm, sub-10 nm pores, and finally non-porous structures were all obtained by increasing the DVB concentration from 0 to 0.5, 1, and 4 wt.%, respectively.

It was demonstrated that the size and porosity of the microparticle BCP can be controlled through *in-situ* crosslinking copolymerisation by RAFT-dispersion in scCO₂. This control allows for tuning of the materials for different applications. Both the non-porous SPH (synthesised using 2.5 wt.% PDMS-MA) and the LAM particles demonstrated good potential as an enzyme support, by recording an immobilisation yield of more than 50 % during lipase immobilisation. Amongst the tested samples, the porous particles synthesised with 5 wt.% PDMS-MA and 1 wt.% crosslinker recorded the highest adsorption yield of usnic acid (79%). The extraction capacity of the majority of the microparticles synthesis using 2.5 wt.% PDMS-MA and DVB concentration ranging from 0-4 wt.% was found satisfactory for polymer stationary phase application, with the percentage of recovery meeting the estimated specification (35 to 75 %).

List of Abbreviations and Symbols

ACN	Acetonitrile
AIBN	2,2'-azobis(isobutyronitrile)
ALAM	Allyl acrylamide
ATRP	Atom-Transfer Radical Polymerisation
BCP	Block Copolymer
CHCl ₃	Chloroform
CLRP	Controlled/Living Radical Polymerisation
CPDT	2-Cyano-2-propyl dodecyl-trithiocarbonate
CRP	Controlled Radical Polymerisation
CTA	Chain Transfer Agent
CYL	Cylindrical
DDMAT	2-(Dodecylthiocarbonothioylthio)-2-methylpropionic acid
DOT	disorder-to-order transition
DRI	Differential Refractometer
DSC	Differential Scanning Calorimetry
EGDMA	Ethylene Glycol Dimethacrylate
FRP	Free Radical Polymerisation
GPC	Gel Permeation Chromatography
GYR	Gyroidal
HPLC	High Pressure Liquid Chromatography
<i>I_{block}</i>	Peak intensity (NMR)

J_{crit}	Critical Molecular Weight
LAM	Lamellar
LAMs	Less Active Monomers
MALS	Multi Angle Light Scattering
MAMs	More Active Monomers
MeOH	Methanol
MMA	Methyl Methacrylate
M_n	Number Average Molecular Weight
M_w	Weight Average Molecular Weight
$M_{n\text{Target}}$	Number Average Molecular Weight Target
NMP	Nitroxide Mediated Polymerisation
NMR	Nuclear Magnetic Resonance
nH_{block}	Number of protons
ODT	Order-to-disorder transition
PBzMA	Poly(benzyl methacrylate)
PDMS	Poly(dimethylsiloxane)
PDMS-MA	Methacrylate terminated polydimethylsiloxane
P4VP	Poly(4-vinyl pyridine)
PISA	Polymerisation Induced Self-Assembly
PMMA	Poly(methyl methacrylate)
PGA	Poly(glycerol adipate)
PVC	Poly(vinyl chloride)
PS	Polystyrene

RDRP	Reversible Deactivation Radical Polymerisation
RAFT	Reversible Addition-Fragmentation Chain-Transfer
rpm	Revolutions per minute
scCO ₂	Supercritical Carbon Dioxide
SEM	Scanning Electron Microscopy
SPH	Spherical
TEA	Triethylamine
TEM	Transmission Electron Microscopy
THF	Tetrahydrofuran
T_g	Glass Transition Temperature
Vac	Vinyl acetate
VPI	Vinyl pivalate
ρ_c	Critical Pressure
k_d	Rate of Decomposition
k_i	Rate of Initiation
k_p	Rate of Propagation
k_{tc}	Rate of Termination by Combination
k_{td}	Rate of Termination by Disproportionation
χ	Flory-Huggins Interaction Parameter

Acknowledgement	iii
Abstract.....	v
List of Abbreviations and Symbols.....	vii
Chapter 1.....	1
Introduction	1
1.1 Overview.....	2
1.2 Polymer Chemistry	3
1.2.1 Polymer Synthesis.....	3
1.2.2 Polymer Structure	5
1.3 Polymerisation Techniques.....	6
1.3.1 Free Radical Polymerisation	6
1.3.2 Reversible Deactivation Radical Polymerisation (RDRP)	9
1.3.2.1 Reversible Addition Fragmentation Chain Transfer (RAFT).....	10
1.4 Polymerisation Processes.....	14
1.4.1 Homogeneous polymerisation	14
1.4.2 Heterogeneous polymerisation	15
1.5 Block Copolymers: Definition, Synthesis, Phase Separation and Application.....	20
1.5.1 Synthesis of Block Copolymers.....	21
1.5.2 Phase Separation Behaviour	22
1.6 Supercritical Carbon Dioxide	28
1.6.1 Polymerisation in scCO ₂	30
1.7 Cross-linked polymers and their applications.....	35
1.8 Summary and Research Objective	45
1.9 References	47
Chapter 2.....	55
Experimental Technique	55
2.1 High-Pressure Equipment (HIP).....	56
2.1.1 General Set-Up	56
2.1.2 High-Pressure Autoclave	57
2.1.2.1 Standard Operating Procedure.....	58
2.1.3. <i>In-situ</i> monomer and cross-linker addition via HPLC Pump ...	62

2.1.4.	Sampling under pressure	65
2.2	Analytical Techniques.....	67
2.2.1	Nuclear Magnetic Resonance Spectroscopy (NMR)	67
2.2.2	Differential Scanning Calorimetry (DSC).....	68
2.2.3	Gel Permeation Chromatography (GPC).....	69
2.2.4	Scanning Electron Microscopy (SEM).....	70
2.3.5	Transmission Electron Microscopy (TEM)	70
2.3.5.1	Tilt TEM Tomography.....	71
2.3.6	Dynamic Light Scattering (DLS)	72
2.3.7	Porosimeter by Tri-star Machine	72
2.4	References	73
Chapter 3	74
Synthesis of Homopolymer, PMMA and Block Copolymer, PMMA-<i>b</i>-P4VP by Dispersion Polymerisation in Supercritical Carbon Dioxide.....	74
3.1	Introduction.....	75
3.2	Materials	77
3.3	Methods	78
3.3.1	Synthesis of PMMA by Free Radical Polymerisation (FRP).....	78
3.3.2	Synthesis of PMMA by RAFT Polymerisation	79
3.3.3	Synthesis of BCP PMMA- <i>b</i> -P4VP via two consecutive RAFT polymerisation	79
3.3.4	Synthesis of BCP PMMA- <i>b</i> -P4VP via RAFT in a series of shorter independent steps	82
3.4	Results and Discussion	85
3.4.1	Synthesis of PMMA by Free Radical Polymerisation (FRP).....	85
3.4.2	Synthesis of PMMA by RAFT Polymerisation	89
3.4.3	Synthesis of PMMA- <i>b</i> -P4VP via RAFT with different size and nanostructure of microparticles	92
3.4.3.1	BCP PMMA ₅₀ - <i>b</i> -P4VP ₃₃ with Spherical (SPH) nanostructure.....	92
3.4.3.2	Synthesis of PMMA ₂₀₀ - <i>b</i> -P4VP ₁₃₃ block copolymer at different block sizes with the same nanostructure, spherical (SPH).....	105

3.4.3.2	Synthesis of PMMA- <i>b</i> -P4VP block copolymer at different block size with lamellar (LAM) nanostructure.....	107
3.5	Conclusions	122
3.6	References	126
Chapter 4		129
<i>In situ</i> crosslinking of nanostructured block copolymer microparticles in super critical carbon dioxide		129
4.1	Introduction.....	130
4.2	Materials	135
4.3	Methods	136
4.3.1	<i>In situ</i> crosslinking of PMMA homopolymer	136
4.3.2	<i>In situ</i> crosslinking copolymerisation of PMMA- <i>b</i> -P4VP via RAFT.....	138
4.3.2.1	One-step addition - SPH morphology.....	138
4.3.2.2	Two-step addition - SPH morphology.....	141
4.3.2.3	Two-step addition - LAM morphology.....	143
4.3.3	Determination of crosslinking formation	145
4.3.4	Determination of Insoluble Fraction (Gel Content)	145
4.3.5	Porosity Control by Degree of Crosslinking	146
4.4	Results and Discussion	147
4.4.1	<i>In situ</i> crosslinking of PMMA homopolymer	147
4.4.2	<i>In situ</i> crosslinking copolymerisation of PMMA- <i>b</i> -P4VP via RAFT dispersion.....	154
4.4.2.1	One-step addition -SPH morphology	158
4.4.2.2	Two-step addition -SPH morphology.....	158
4.4.2.3	Physical Properties-SPH morphology.....	165
4.4.2.3.1	Dissolution Test.....	165
4.4.2.4	Porosity control by a degree of crosslinking -SPH morphology.....	175
4.4.2.5	Thermal Analysis- SPH morphology.....	185
4.4.2.6	Two-step addition -LAM morphology.....	189
4.4.2.6.1	Porosity control by a degree of crosslinking.....	194
4.4.2.6.2	Dissolution Test.....	204

4.5	Conclusion.....	208
4.6	References	210
Chapter 5.....	213	
Testing for Potential Applications.....	213	
5.1	Introduction.....	214
5.2	Experimental	220
5.2.1	Synthesis of bigger crosslinked block copolymer PMMA ₅₀₀ - <i>b</i> -P4VP ₃₃₀ particles.....	220
5.2.2	Porosity Control by Degree of Crosslinking	220
5.2.3	Lipase Immobilisation	220
5.2.3.1	Materials, Chemicals and Enzyme Preparation.....	220
5.2.3.2	Determination of Enzyme Activity.....	221
5.2.3.3	Enzyme Stability Study.....	222
5.2.3.4	Sample Miscibility Study.....	222
5.2.3.5	Immobilisation of enzyme.....	223
5.2.4	Usnic Acid adsorption	224
5.2.5	Polymer Stationary Phase for Sample Preparation	225
5.2.5.1	Chemicals and Reagents.....	225
5.2.5.2	Instrumentation.....	225
5.2.5.3	Dispersive solid-phase extraction procedure.....	227
5.3	Results & Discussion	229
5.3.1	Synthesis of bigger PMMA- <i>b</i> -P4VP particles by two-step addition method – SPH.....	229
5.3.1.1	Solubility Test.....	235
5.3.1.2	Porosity Control by Crosslinking.....	239
5.3.1.2.1	Tilt-TEM Tomography.....	241
5.3.1.2.2	Nitrogen Adsorption Isotherms.....	246
5.3.2	Enzyme Immobilisation	252
5.3.2.1	Enzyme Stability Study.....	252
5.3.2.2	Sample Miscibility.....	253
5.3.2.3	Immobilisation of Enzyme.....	254
5.3.3	Usnic Acid Adsorption Test	257

5.3.4 Polymer Stationary phase for sample preparation.....	261
5.5 Conclusion.....	266
5.6 References	267
Chapter 6.....	269
Conclusions and Future Work	269
6.1 Conclusions	270
6.2 Future Work	274
6.3 References	276

Chapter 1

Introduction

This chapter addresses the background of this study and its context. It provides a brief introduction to polymer chemistry, focusing on heterogeneous synthesis and controlled polymerisation techniques, in particular Reversible Addition Fragmentation Chain Transfer (RAFT). Subsequently, the use of $scCO_2$ as a green solvent for polymer synthesis is introduced and an overview of the unique behaviour of block copolymers in $scCO_2$, highlighting the novel technique developed to cross-link the internal domain of block copolymer, without sacrificing the particle microstructure as well as the morphology of microphase separation. The uses of these crosslinked microparticles is also investigated.

1.1 Overview

Polymers are necessity materials in almost every aspect of contemporary life. They have been used widely in making everything from simple chocolate packaging,¹ to electronic gadgets² and high-end nanomaterials devices.³⁻⁵ In modern day life we are surrounded by polymers that exist naturally for example protein and carbohydrate sources which have become a major contribution for the development of synthetic polymers that are man-made, that can serve our daily life needs. For decades, there have been a variety of traditional methods for synthesising polymers, which are widely employed in the industrial and manufacturing sectors. However, the majority of them use a lot of organic solvent and water, which contributes to high energy consumption and wastewater contamination, resulting in expensive costs. More recently, the utilisation of $scCO_2$ in polymer synthesis has been intensively researched due to the fact that it ensures greener and cleaner processing pathways.

A polymer, also known as a macromolecule, is a big molecule with a high relative molecular mass composed of long repeating monomer units with a low molecular mass that are chemically bonded together.⁶ Oligomers are polymers with a shorter chain length and a medium relative molecular mass. Polymerisation is the process by which monomers are converted into polymer chains. Each polymer has unique qualities that are determined by the type of monomer units bound together and how they are attached. Polymers that are solid and robust, such as polycarbonate and polyurethane, exist alongside polymers that are bendy and elastic, such as polyester and polyisoprene. They all have a respected application based on their behaviour and distinctive qualities to satisfy the needs of the application.

Advances in polymer chemistry are incredible. Researchers keep exploring and improving the properties of existing polymer materials to exploit niche markets or add value to existing products. Homopolymer, copolymer and now block copolymer materials have attracted considerable attention for multi-component biomaterials,⁷ biomedical sensors,⁸ tissue adhesives⁹ and semiconductor applications.^{10, 11} The interesting and unique properties of block copolymers, which are able to self-assemble into distinct, nano-sized internal morphologies such as spheres, cylinders, lamellae and the bicontinuous gyroid, have made them particularly attractive in recent years for innovation and advanced materials applications such as transdermal drug delivery, membranes and as templates to direct the structure formation of other materials.^{12 3,7}

1.2 Polymer Chemistry

1.2.1 Polymer Synthesis

The chemistry of polymer formation can be clearly defined in the case of synthetic polymers. There are two mechanisms for polymer synthesis- step growth and chain growth.

Step growth, that is also known as condensation, is a reaction in which two molecules link together giving rise to a larger molecule and eliminate a small molecule, often water. At the beginning of the reaction, this reaction mechanism produces low molecular weight oligomeric products that subsequently join together to form high molecular weight polymer. This route proceeds in a relatively slow increase in the molecular

weight of the polymer (Figure 1.1).¹³ The widely used polymers namely nylon and polyester are synthesised by this technique.¹⁴

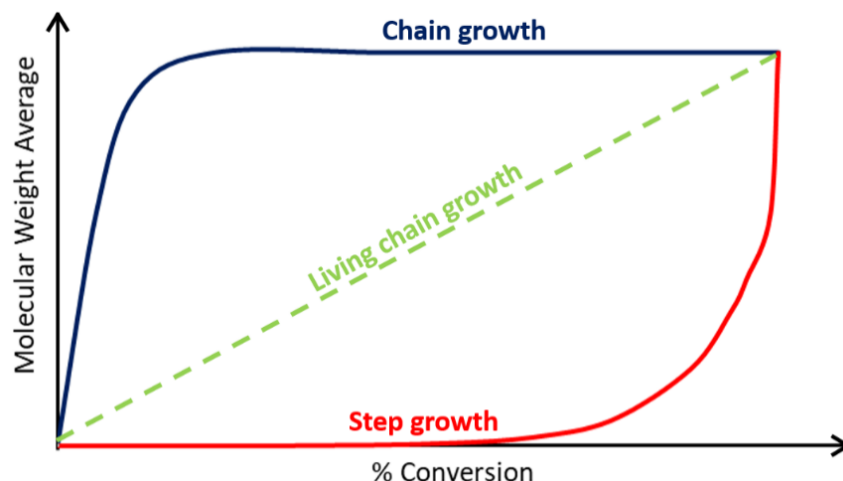


Figure 1.1. A comparison of polymerisation mechanism between Step Growth and Chain Growth.¹³

In the case of chain growth, molecules grow by the consecutive addition of monomer units to the active ends of the growing chains. This involves an active centre. In this mechanism there is no elimination of any by-product, thus it is also called an addition polymerisation. The active centre is terminated at the end of the reaction to prevent further growth, but this can be avoided through living polymerisation techniques which allow for further chain growth when feeding more monomer. This technique can easily produce a high molecular weight polymer compared to step-growth, even at low conversion (Figure 1.1).¹³ A number of polymers are synthesised by this technique such as polyvinylchloride and polyethene.¹⁴

1.2.2 Polymer Structure

Synthetic polymers can be grouped depending on their structure and shape, which is related to how the monomers are arranged and linked together. There are three fundamental polymer structures: a simple linear chain; branched, being composed of a main chain with one or more substituent side chains; and cross-linked, in which a main chain is attached to each other forming a dimensional network (Figure 1.2). Different polymer structures have different polymer properties, for example, linear polymers are usually more glassy and denser than analogous branched polymers of similar molecular weight, resulting in different glass transition temperature (T_g).

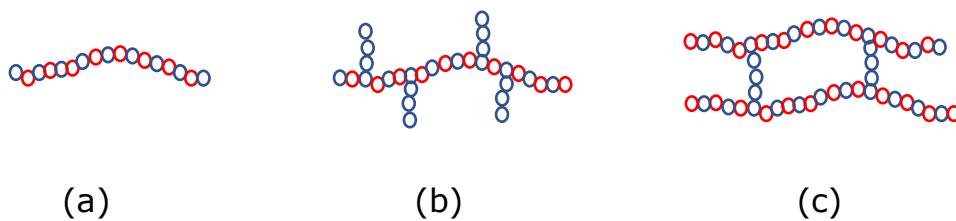


Figure 1.2. Schematic drawing representing the different polymer structures;- Linear (a), Branched (b) and Cross-linked (c)

A polymer assembled from only one type of monomer is known as homopolymer. In comparison, using two (or more) monomer species can result in the formation of block copolymers, statistical copolymers, alternating copolymers, gradient copolymers or graft polymers (Figure 1.3), depending on the synthesis route used. A block copolymer is formed of two or more segments of differing monomer groups. Alternating copolymers consist of two monomer species in alternating order whereas, statistical polymer assembles monomer units to form a specific pattern of polymer chain. Grafted polymers contain two or more polymer types where one type makes up the main chain and other segment attaches to this main chain. In contrast to block copolymers, which have an abrupt shift in

composition, and random copolymers, which have no continuous change in composition, gradient copolymers have a progressive change in monomer composition from primarily one species to mostly the other.¹⁵

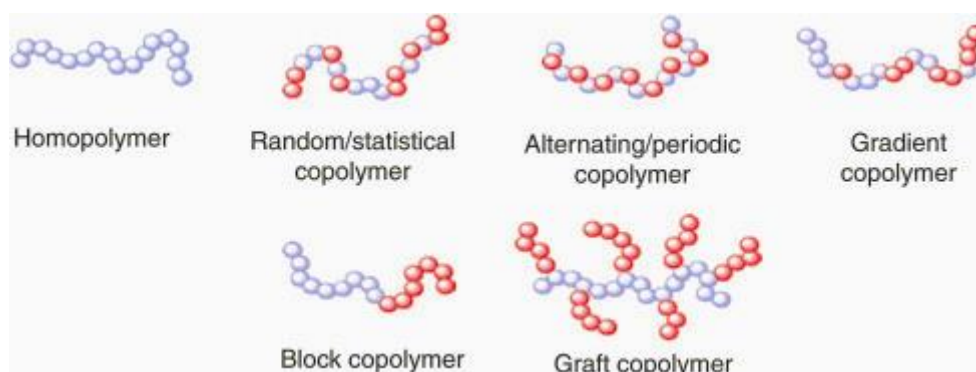


Figure 1.3. Schematic representation of homopolymer and various copolymers block -Random/statistical, alternating/ periodic , gradient, block copolymer and grafted from literature.¹⁶

1.3 Polymerisation Techniques

There are numbers of methods to synthesise polymers, and they are characterised by the polymer synthesis mechanism; step or chain growth. The chain growth mechanism involves an addition of vinyl monomers sequentially through the activating of the double bond by means of ions, radicals or coordination with a metal complex.¹³ Only radical polymerisation will be discussed further in this thesis as it was used throughout this research study.

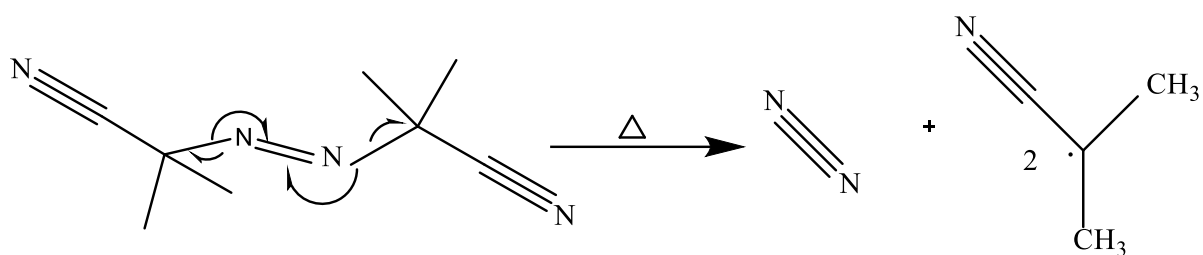
1.3.1 Free Radical Polymerisation

Free Radical Polymerisation (FRP) is classified as a chain growth polymerisation mechanism. It involves four progression phases:

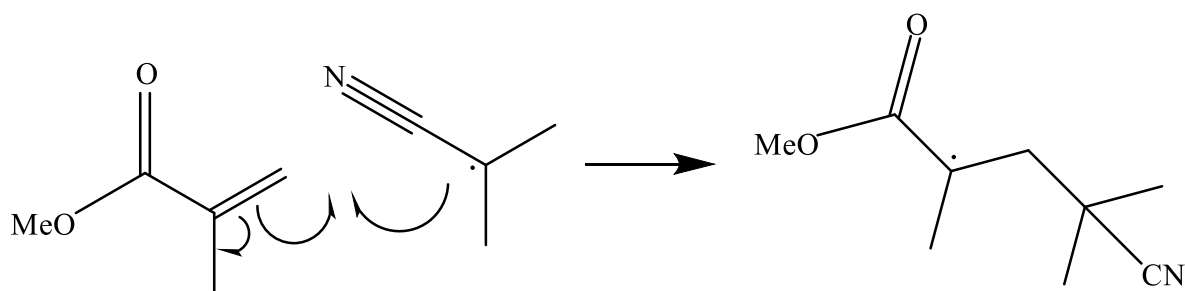
decomposition, initiation, propagation and termination by either combination or disproportionation. The process begins with decomposition of the initiator molecule to form a reactive free radical by either thermal, photochemical or electrochemical routes.¹⁷ The free radical then reacts with a monomer to initiate the formation of polymer chain by producing the active propagating species. At this point the chain length starts to grow successively by the addition of monomers to this species until all monomers available are depleted. After this, the polymer enters the last phase, namely termination, which happens by one of either two possible mechanisms, combination or disproportionation. Combination occurs when two polymer radicals combine and produces a polymer with a total chain length of the two individual chains. In contrast, disproportionation is the abstraction of a hydrogen from a second radical of polymer chain to terminated the reaction.¹³ There is also the possibility of side reaction occurring during the polymerisation that could initiate a new polymer chain prior to the termination reaction, which results in a higher molecular weight dispersity (\bar{D}) of the polymer. A solution to this is the use of Controlled Radical Polymerisation (CRP). This offers a method for producing polymer that are well controlled with low dispersity which are particularly usefully for advanced application. Furthermore, CRP processes allow the end-groups of polymer chains to be further reacted when exposed to additional initiator and monomer species resulting in the ability to synthesise block copolymers.

In this study, the polymerisation of MMA was initiated using an azo compound, namely 2,2'-azobis(isobutyronitrile) (AIBN). The phases of the MMA polymerisation is illustrated in Figure 1.4(a)-Figure 1.4(e).

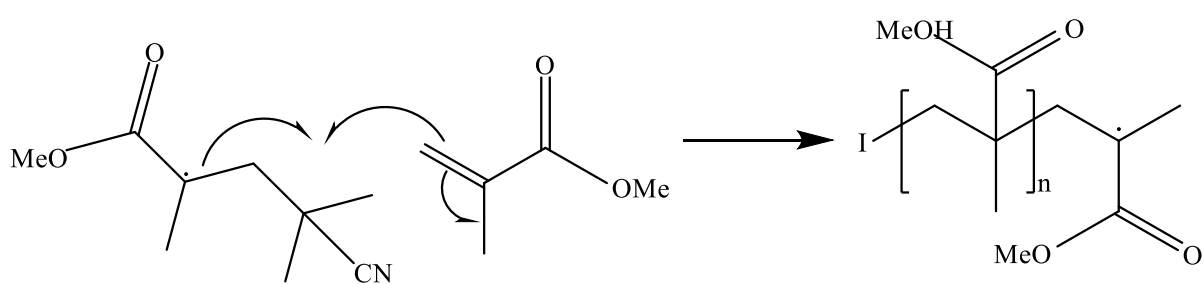
(a)



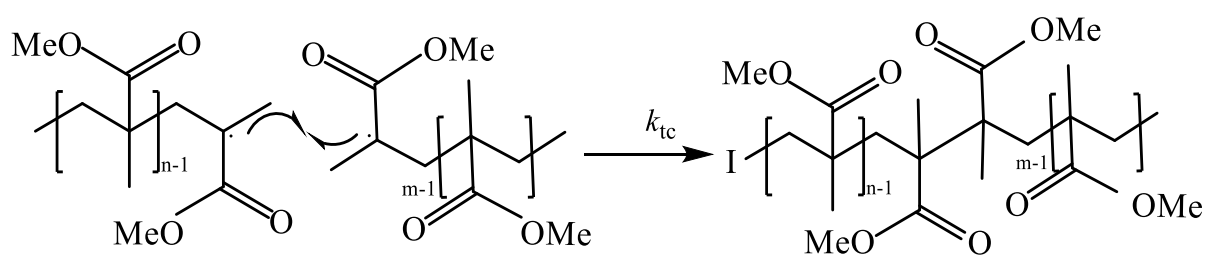
(b)



(c)



(d)



(e)

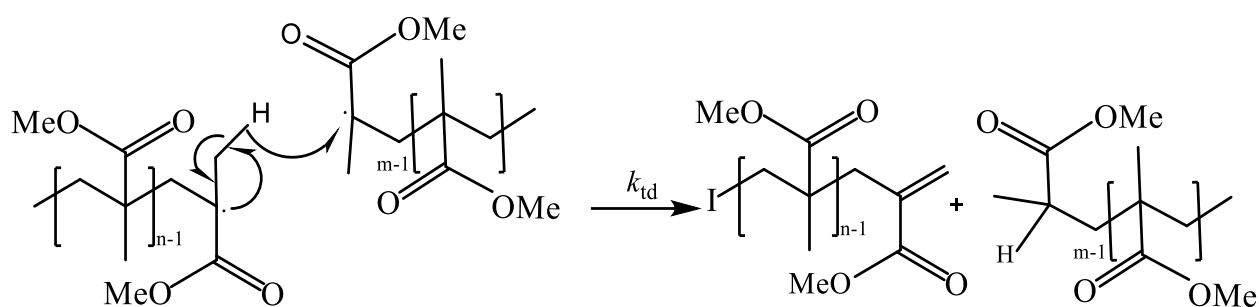


Figure 1.4. Schematic of the thermal decomposition of AIBN (a), the initiation of a MMA monomer unit by an AIBN radical (b), propagation of a growing MMA polymer chain (c) and termination reactions by combination (d) and disproportionation (e) (I: abbreviation for initiating molecule and n : the degree of polymerisation.)

1.3.2 Reversible Deactivation Radical Polymerisation (RDRP)

Reversible Deactivation Radical Polymerisation (RDRP), formerly known as Controlled/Living Radical Polymerisation (CLRP), methods have been developed to more precisely control the polymerisation process, leading to low molecular weight dispersity (\mathcal{D}) and the ability to target specific polymer molecular weight values. These approaches can overcome the drawbacks of FRP by reducing the polymeric radical concentration (termination step is suppressed) to attain further 'living' behaviour. This results in the favouring of propagation over termination, which allows higher control over the polymerisation. Furthermore, the concentration of propagating chain ends is constant which cause all the chains grow at almost the same rate and molecular weight increases linearly with conversion as well as low dispersity close to 1.¹⁸

There are now three well-known methods of RDRP, namely Atom Transfer Radical Polymerisation (ATRP), Nitroxide Mediated Polymerisation (NMP) and Reversible-Addition Fragmentation Chain-Transfer (RAFT). According to literature, both ATRP and NMP polymerisation are controlled by the persistent radical effect.¹⁹ Whilst RAFT involves a degenerative chain transfer mechanism. In all cases, the direction of the equilibrium favours the dormant species over the polymeric radical species. Hence, the concentration of polymer radicals is minimised and the termination is suppressed relative to the propagation step. This study makes use of RAFT polymerisation specifically, so it will be discussed further in the next section.

1.3.2.1 Reversible Addition Fragmentation Chain Transfer (RAFT)

RAFT is the most versatile RDRP technique due to its tolerance to most functional groups.²⁰ It enables a precisely targeted molecular weight, a narrow molecular weight distribution (\mathcal{D}) and the ability to change the polymer architecture, such as to produce a block copolymers, etc.²¹ In comparison to FRP it requires one more additional reagent, the RAFT agent, that is responsible for controlling the polymerisation process by the formation of a reversible-deactivation radical.²²

RAFT agents are generally defined into classes based on their central functional atoms, typically either a dithioester, a trithiocarbonate, a dithiocarbamate or a xanthate (Figure 1.5). They are classically thiocarbonylthio based compounds (Figure 1.6). In addition to the central atoms, RAFT agents also consist of an R- and a Z-group; the R-group is the free radical leaving group which must be able to reinitiate polymerisation, whilst the Z-group controls the C=S bond reactivity and influences rate of

radical addition or fragmentation.²⁰ During selection of the RAFT agent, the C=S bond must be more reactive to radical addition than the C=C bond of the monomer in the intended reaction. This is referring to the right assortment of Z and R group (Figure 1.6) of the RAFT agent.

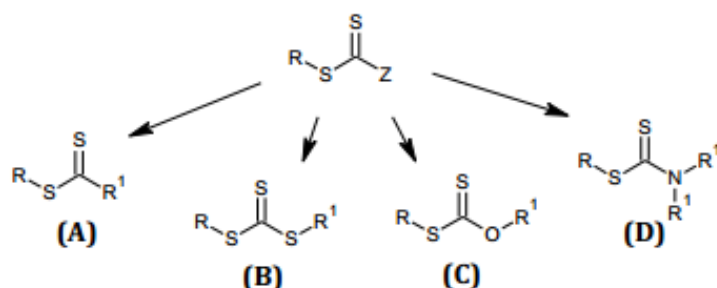


Figure 1.5. The most common RAFT agents used in polymerisation, dithioester (A), trithiocarbonate (B), xanthate (C) and dithiocarbamate (D).

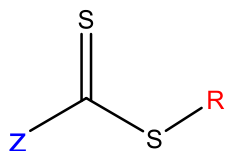


Figure 1.6. General structure of thiocarbonylthio chain transfer, the RAFT agent.

In the case of monomers, there are two classified groups namely more active monomers (MAMs) and less active monomers (LAMs) (Figure 1.7). MAMs produce relatively more stabilised radicals due to the presence of substituents and steric factor resulting in electronic stabilisation, consequently a Z-group (Figure 1.7b) is required to aid the stabilisation of the intermediate radical to favour radical addition on the C=S bond. Trithiocarbonates ($Z=S$ -alkyl) and dithioester ($Z=$ aryl) are the best candidates to control MAMs polymerisation. In contrast, LAMs have high

reactivity, making them poor homolytic groups. In order to favour fragmentation of the propagating species, the RAFT agent needs a less stable intermediate radical, such as a Xanthate (Z=O-alkyl) or a dithiocarbamate (Z=N-alkyl). More stable intermediates will perform as a radical descend and this bounds polymerisation.²³

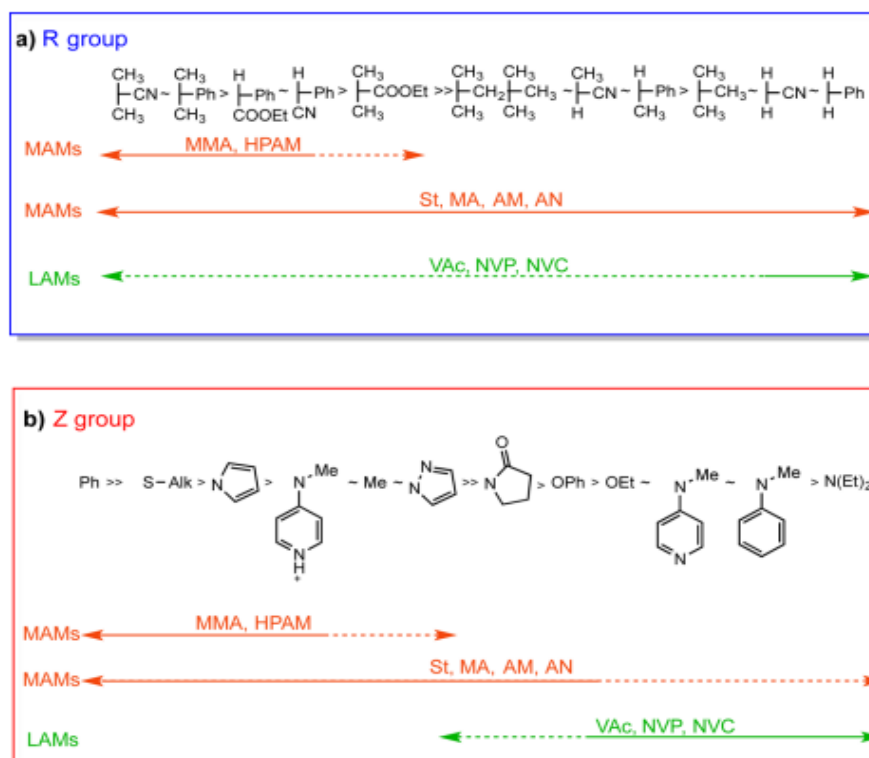


Figure 1.7. Guidance principles for selection of various RAFT agents and monomers in RAFT polymerisation a) R-Group of RAFT agents, b) Z-Group of RAFT agents²³

The RAFT process take place by the addition of monomer units into the S-R bond of the RAFT agent to produce a polymer, with the theoretical molecular weight being determined by its concentration relative to the monomer. The polymer chains can also be seen to retain RAFT end group, thus enabling them to act as so called 'macro-RAFT agents' to control the polymerisation of a second monomer unit and produce block copolymers.

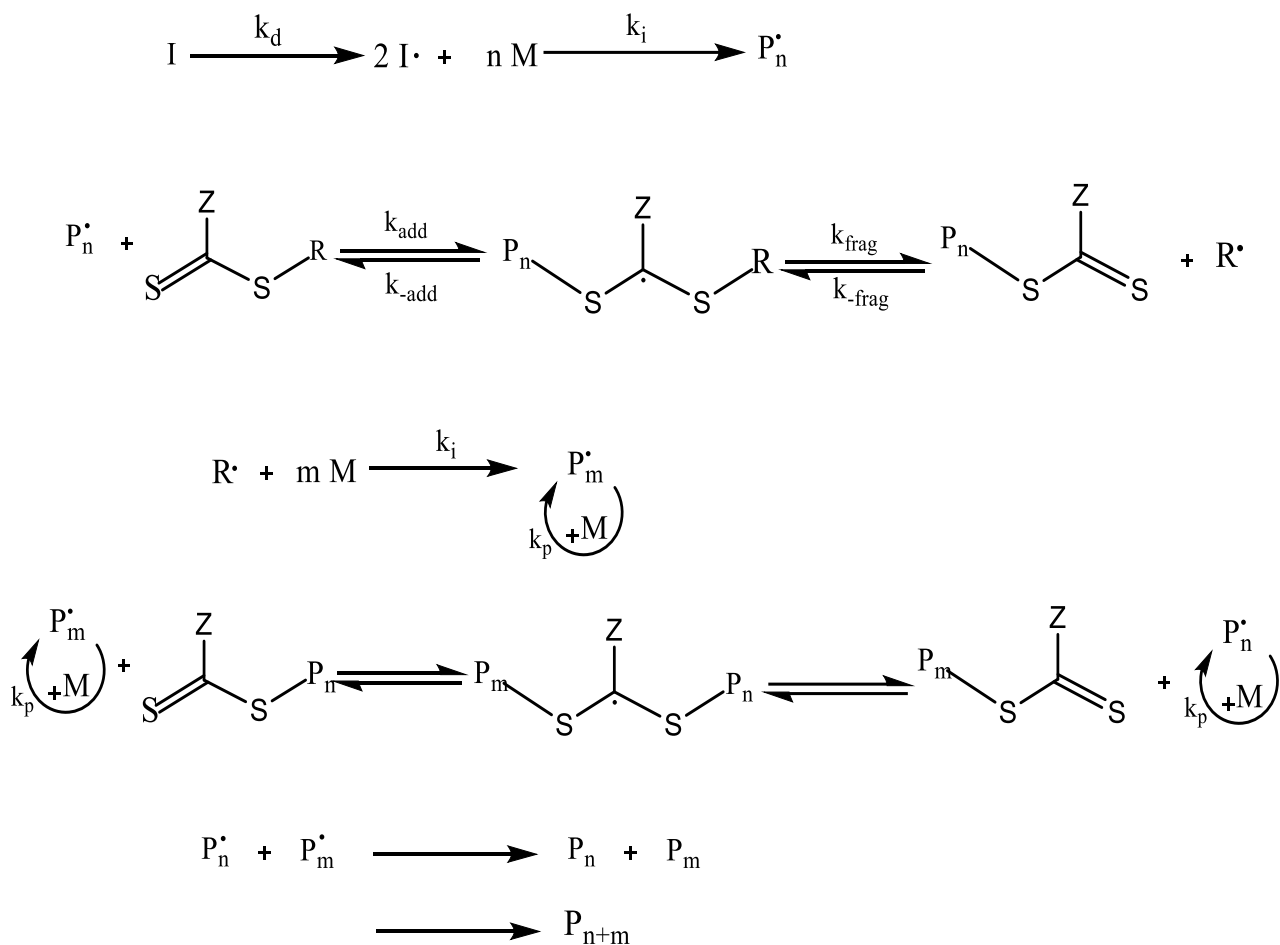


Figure 1.8. Mechanism of RAFT polymerisation as adapted from the literature.²⁴

The mechanism of RAFT polymerisation is illustrated in Figure 1.8. First, the initiator decomposes and initiates the growth of a polymer chain as in FRP. The propagating polymer then reacts with the C=S bond of the RAFT agent to form an intermediate radical, stabilised by the Z group. This radical then fragments to release the R-group, which initiates further monomer propagation reactions. An equilibrium is then rapidly established between the growing polymer chains and the intermediate radical species, which fragments to release a polymeric radical. This polymeric radical undergoes further propagation before once again reacting with the RAFT agent and releasing another polymeric radical. From this rapid activation-deactivation equilibrium, all chains are given an equal opportunity to grow

at the same rate and termination reactions are reduced resulting in low \bar{M}_n of the end polymer.²² Finally, termination occurs by combination or disproportionation, as elaborated in FRP. This method was utilised in this study as a basis to develop a synthesis route of crosslinking the PMMA-*b*-P4VP block copolymers (Figure 1.9).

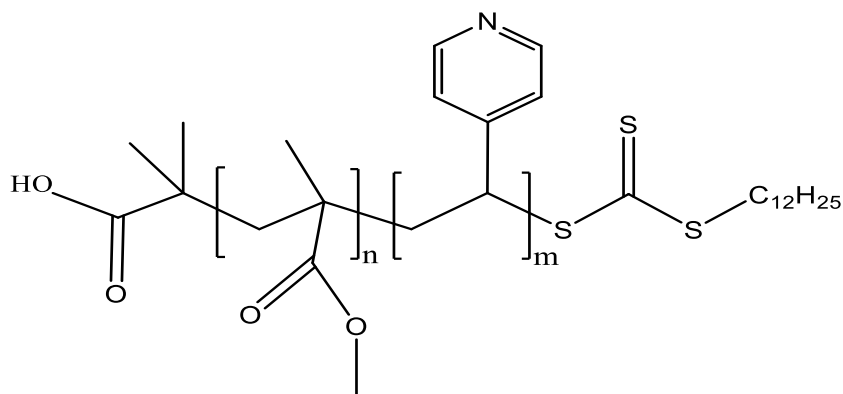


Figure 1.9. Molecular structure of block copolymer PMMA-*b*-P4VP with DDMAT as a RAFT end group.

1.4 Polymerisation Processes

Polymerisation can take place in two different ways of processing: either homogeneous or heterogeneous, depending on the phases that exist and the forms of the medium. There are specific techniques involved according to these two different processes as given in the following sections.

1.4.1 Homogeneous polymerisation

Homogeneous polymerisations occur in one phase, in which all reactants including monomers and initiators, can be homogeneously dissolved in the

same phase. This type of polymerisation can be conducted either in bulk or in solution. Bulk polymerisation proceeds only with the presence of monomers and initiators in the reaction medium in which the monomer acts as a solvent. It is generally used in the production of condensation polymers in which the process is easier in comparison to chain polymerisation of vinyl polymer. A few limitations have been discovered in its use. The viscosity of the medium increases as the reaction progresses, making stirring and heating transfer more difficult. The captured heat causes an auto-acceleration gel effect, also known as the Tromsdorff-Norris effect.²⁵

In solution polymerisation, both the monomer and the initiator are dissolved in a solvent and the reaction takes place in this solution. The presence of a solvent lowers the viscosity reducing the chance of auto-acceleration. This technique, however, needs an additional step for product recovery, which often demands the use of large volumes of solvent.²⁶ In addition, the presence of a solvent allows for chain transfer between the propagating radical and the solvent, which can be detrimental to the propagation process.

1.4.2 Heterogeneous polymerisation

Heterogeneous polymerisation occurs in two or more immiscible phases. For example, in ethylene polymerisation, the monomer is in the gas state and the formed polymer can be either liquid or solid. Another good example is precipitation polymerisation, which begins under homogeneous conditions but as the polymer forms it precipitates as it is no longer soluble in the reaction medium. The polymerisation process then continues within or on the surface of the precipitated polymer particles. Polymer particles with poor morphology are typically produced by this type of polymerisation. In addition to precipitation, there are another three categories of

heterogeneous polymerisation namely emulsion, suspension and dispersion.

Emulsion polymerisation is a system that includes water, an initiator (usually water-soluble), a water-insoluble monomer, and a colloidal stabiliser, all of which can be added or formed in situ.²⁷ During the polymerisation process, the monomer exists in surfactant-stabilised monomer droplets, which are depleted as the polymerisation proceeds. In the continuous phase, initiation occurs, leading to the formation of oligomers. When the critical degree of polymerisation (J_{crit}) is reached, the oligomers diffuse into monomer swollen micelles, where they continue to propagate until full conversion is achieved.²⁸ This mechanism generates polymer particles ranging in size from 0.05 to 1 μm depending on the components and conditions used. Particles produced using this method are widely used in paints²⁹, coatings⁹, adhesives^{30, 31} and finishes³².

Both the monomer and the initiator are insoluble in the continuous phase of suspension polymerisation. Mechanical agitation is used to mix the system and form droplets. Polymerisation then occurs within the droplets, resulting in polymer particles with diameters in the hundreds of microns. This method is widely used in the manufacture of commercial polymers such as poly(vinyl chloride) (PVC) and polystyrene.³³ Dispersion polymerisation is similar to precipitation polymerisation, in which the presence of a stabiliser prevents the precipitation of growing polymers. These sorts of polymerisation are widely utilised in industry in combination with radical polymerisation. Hence, this study has proposed to make use of this approach by combining the radical and dispersion polymerisation routes of method.³⁴

1.4.2.1 Dispersion polymerisation

The dispersion polymerisation technique is a straightforward method to make relatively large solid particles. Polymer beads with uniform sizes ranging from 0.1 to 10 μm are increasingly being employed in coatings, electronics, microelectronics, biomedical, and information technology applications.^{26, 35} The majority of these applications require good particle size control and a restricted size distribution.³⁶

Dispersion polymerisation was first created as a process that took place in a hydrocarbon environment.³⁷ However, the usefulness of this type of polymerisation was substantially enhanced when it was extended to polar solvents, such as ethanol or methanol.^{4, 38} The creation of uniform-sized particles was achieved using an atom transfer radical dispersion polymerisation of styrene in ethanol.³⁹ This was achieved by employing a 'two-stage' dual-process polymerisation approach, with the first stage including a standard free radical polymerisation and the second stage involving a reverse ATRP. To prepare particles of uniform size, the initial nucleation stage has to be accomplished in a relatively short amount of time. The large percentage of retained chain end functionality made it easy to modify the particles further.

In 2005, S. Kawaguchi and K. Ito proposed that dispersion polymerisation takes place following five stages as shown in Figure 1.10:

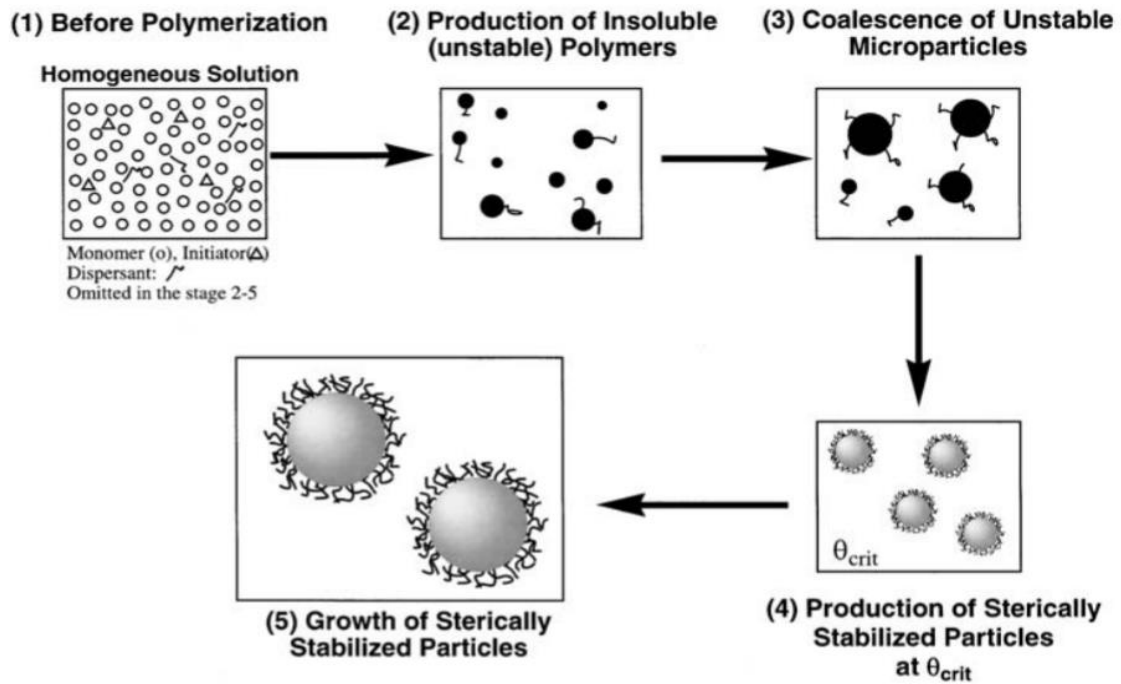


Figure 1.10. Schematic model for the particle nucleation and growth of sterically-stabilised particles in dispersion polymerisation.⁴⁰

1. The reaction mixture dissolves entirely into the continuous phase prior to polymerisation.
2. Upon heating, the initiator decomposes producing free radicals, which propagate in the continuous phase to create linear oligomers, polymers, and/or graft copolymers. The solubility of these polymers is determined by their molecular weight (MW) and graft copolymer makeup. Polymers with a molecular weight greater than a critical value precipitate and coagulate, forming unstable particles.
3. These particles coagulate when they come into contact with one another, and the coagulation continues until sterically-stabilized particles develop.
4. When all of the particles have enough stabiliser polymer chains on their surfaces to provide colloidal stability, this is referred to as the critical point.
5. After this point, no new nuclei or particles are formed, and the particles may grow by diffusive capture of oligomers and coagulation of very small

unstable particles (nuclei, precursors) produced in the continuous phase, as well as polymerisation of the monomer included within the particles, until the monomer is consumed entirely. The overall number of such sterically stabilised particles remains constant, and their size is solely determined by the amount of polymer created.

This technique produces polymer particles ranging in size from 0.1 to 10 micrometres.^{26, 41, 42} A stabiliser is a key component in dispersion polymerisation because it prevents the growing polymeric particles from coagulating once they are produced. The most frequent method of particle stabilisation is through the use of steric stabiliser, which inhibits nearby particles from interacting.^{43 40} However, due to a lack of solvents that are miscible with a monomer but immiscible with the polymer, this polymerisation is less researched than other heterogeneous polymerisations such as emulsion polymerisation. A possible continuous phase that meets this criteria is supercritical carbon dioxide (scCO₂), which is becoming one of the most often used continuous phase solvents today.⁴⁴

The surfactant that has been used for this study is poly(dimethylsiloxane) monomethacrylate (PDMS-MA) (Figure 1.11). It consists of a CO₂-philic (siloxane chain) macromonomer that prevent precipitation of particles by migrating to the surface of each particle during the reaction, as previously shown by Guan et al.⁹⁵ As a result, uniform spherical particles without agglomeration are formed, with typical size ranges from 0.1 – 10 µm.¹¹⁰

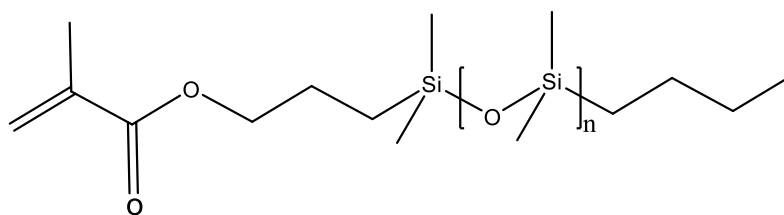


Figure 1.11. The structure of PDMS-MA that was used in this study.

1.5 Block Copolymers: Definition, Synthesis, Phase Separation and Application

Block copolymers are made up of at least two homopolymer segments that are chemically linked together by covalent bonds to form a single, linear polymer chain. Because of the introduction of innovative non-terminating 'living' polymerisation processes, polymer chains with opposing chemical compatibilities, such as amphiphilic copolymers, now include a living end group that can be reinitiated to create an extra block.⁴⁵⁻⁴⁷ These blocks may be thermodynamically incompatible due to the low entropy of mixing per unit volume and the inverse relationship between entropy and molecular weight. Block copolymers, which are formed by merely linking polymer chains, produce complex nanostructures with various morphologies in distinct molecular sizes (5–100 nm) in bulk. In addition because the polymer chain is covalently linked, macro-separation is avoided and structural organisation is at the nanoscale scale.⁴⁸ As a result of this nanostructuring, block copolymers, including synthesis methods, phase separation behaviour, properties and their potential applications have been comprehensively studied over the last 50 years.

1.5.1 Synthesis of Block Copolymers

These days, methods to prepare block copolymers have been well-established. The fabrication of block copolymers has aroused great interest due to their enchanting phase separation behaviour and diverse areas of application, covering traditional and advanced materials.

In 1956, Szwarc and co-workers discovered that a second batch of styrene monomer polymerised from the living ends of a previously prepared polymer.⁴⁵ This method of preparing living polymers by anionic polymerisation became the basis of block copolymer synthesis at the time.

As time went on, researchers found that anionic polymerisation with a carbon-centred anion was severely disrupted by trace impurities, thus requiring rigorous reagent purification beyond the level achievable in an industrial setting. Currently, for dispersion polymerisation specifically, RAFT has shown to be an effective route to well-defined block copolymer products when compared with competing CRP methods, especially when performed in $scCO_2$.⁴⁹ This technique efficiently assists polymer chemist to prepare wide range of block copolymer architectures that are useful for many applications.

Block copolymers are typically synthesised by a polymerisation process in which the polymer chains retain a living end group that can be reinitiated to grow an additional block by infusing the reaction system with fresh monomer and initiator. A diblock copolymer is made by the consecutive polymerisation of two different monomers by the RAFT reaction, as shown in Figure 1.12. A homopolymer formed from the first RAFT polymerisation acts as a macro-CTA to control the polymerisation of the second monomer. In this study, block copolymers of PMMA-*b*-P4VP were synthesised, where the MMA block was grown first and used as a macro-CTA for 4VP. This synthesis order was chosen due to the established efficacy of PMMA as the first block as reported from literature⁵⁰⁻⁵². Chapter

3 provides a more extensive overview of the RAFT dispersion polymerisation method for the production of block copolymers in this study.

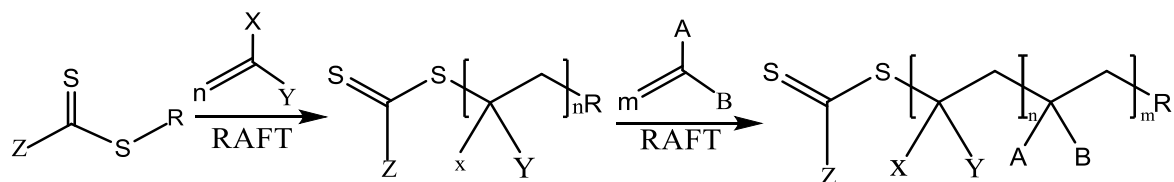


Figure 1.12. Block copolymer synthesis by RAFT polymerisation.

1.5.2 Phase Separation Behaviour

Phase separation of block copolymers occurs due to the chemical incompatibility of the two blocks and their inability to separate on the macroscale as a consequence of being covalently linked. This leads to nanoscale morphology or domains. That is, the covalent connections that hold the blocks together inhibit 'macrophase' separation but allow 'microphase' separation or self-assembly in bulk or in concentrated and dilute solutions.⁵³⁻⁵⁵ The spatial scales are determined by the lengths of the chains, whilst their morphologies are determined by their relative compositions. According to J.Jennings et al., the ordered nanoscale domains are generated in bulk block copolymers, whereas in a dilute solution of a solvent that favours one block, block copolymers display surfactant-like character and self-assemble into distinct nanoparticles, as illustrated in Figure 1.13. The phase behaviour of bulk linear diblock copolymers was found to be of the most significance in this study.⁵⁶

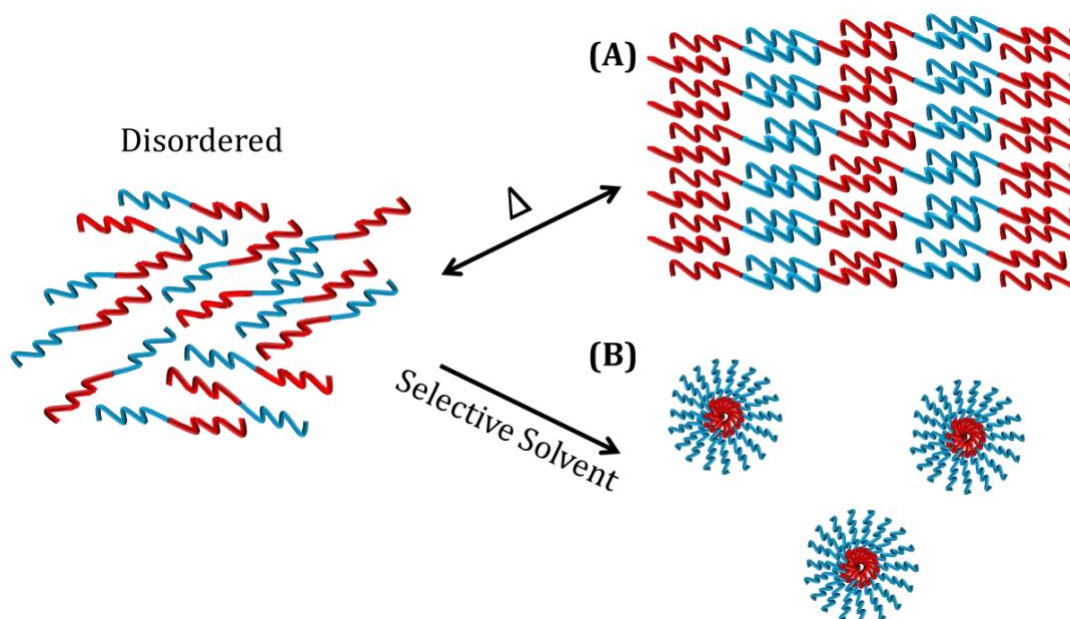


Figure 1.13. Schematic of microphase separation phenomenon of diblock copolymer in the bulk (A) or in the presence of a selective solvent (B).⁵⁶

The disorder-to-order transition (DOT) is the reversible change of state of a block copolymer from a homogeneous mixture (disordered state) to a self-assembled structure (ordered state). The order-to-disorder transition (ODT) is the reverse situation. To produce the ordered state, the block copolymer requires movement, which can be achieved by heating both blocks above their T_g s or by adding a solvent. The development of phase separation once in the movable rubbery state is a balance of enthalpy and entropy. Phase separation minimises unfavourable segment-segment interactions, lowering the enthalpy of the system, whereas chain extending reduces conformational entropy and favours the ordered state.

The Flory-Huggins interaction parameter (χ), which changes between polymer pairings, and the total degree of polymerisation of the block copolymer (N) determines the level of repulsion between the two blocks.

According to the principle, phase separation must dominate when the resultant of the interaction parameter and the degree of polymerisation is greater than 10.5 for diblock copolymers (Equation 1.1).⁵⁷

$$\chi N > 10.5 \quad \text{(Equation 1.1)}$$

The interaction parameter is related to the temperature (T) and two more parameters that rely on the structure of the block copolymer and the volume fraction (α and β) (Equation 1.2).⁵⁷ As a result, phase separation may not always occur.

$$\chi = (\alpha / T) + \beta \quad \text{(Equation 1.2)}$$

An increase in polymer-polymer interaction (χ) occurs as temperature falls, and phase separation typically happens upon cooling, a phenomenon known as the upper order-disorder transition (UODT). There are a few polymers that arrange when heated, which is known as lower disorder-order transition (LDOT) behaviour.⁵⁸ Within a certain temperature range, such block copolymers can transition from disordered -to- ordered- to-disordered.

The relative size, or volume fraction (f), of the two blocks determines the appearance of the phase separated morphology. The thermodynamically favoured (equilibrium) shape is characterised by a reduction in interfacial area and thus a decrease in enthalpic interactions. When the two blocks have identical volumes (f=0.5), the system often generates flat surfaces and lamellar morphology. As asymmetry rises, it becomes more advantageous to curve the interfaces towards the minority block, resulting in morphological change. At volume fractions greater than

0.5, the following morphologies have been seen in most systems: lamellar – gyroid/bicontinuous – cylindrical – spherical (Figure 1.14).^{59, 60}

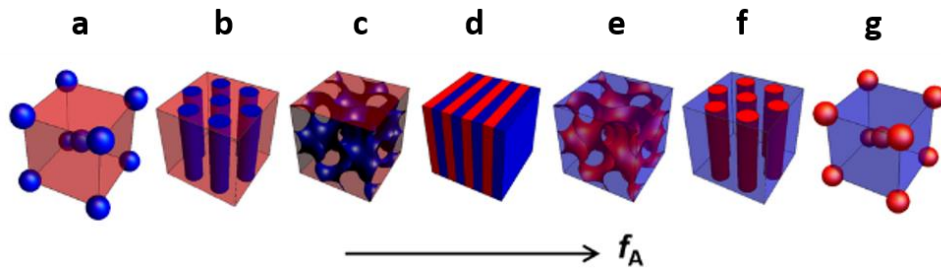


Figure 1.14. Schematic showing how the morphology of a block copolymer changes as the volume fraction of monomer A (shown in blue) increases from left to right. The following morphologies are formed; spherical (a), cylindrical (b), gyroid (c), lamellar (d), inverse gyroid (e), inverse cylindrical (f) and inverse spherical (g).⁶¹

The relationship between the three parameters and which morphology is preferred has been the subject of many scientific studies, culminating in the plotting of a theoretical phase diagram (Figure 1.15). Although all theoretical morphologies have been experimentally created, some only occur over a restricted range of parameters and, as a result, require longer annealing times to attain homogeneity than others.⁶²

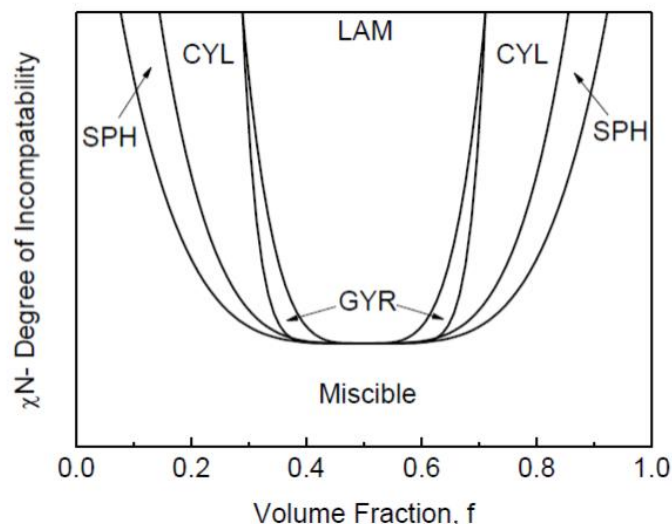


Figure 1.15. Theoretical relationship of the three parameters in constructing phase separation of linear block copolymer. (SPH) showing region of spherical, (CYL) = cylindrical, (GYR)= gyroidal and (LAM)= lamellar morphology, along with a miscible region.⁶³

Due to their supramolecular connections, adjustable size, and spontaneous production, these self-assembling structures have a wide range of applications such as in drug delivery^{5, 12, 64}, gas separation,^{65, 66} and photonics,⁶⁷ to name a few. In particular, the fabrication of hierarchically porous materials with further processing of nanostructured block copolymer particles is of interest because the block copolymer structures can be used for chromatography column materials,⁶⁸ protein sorption⁶⁹ and catalytic supports.⁷⁰ Hence, these systems will be the focus of this study.

In 2012, Howdle and co-workers demonstrated a simple and consistent route for the preparation of novel block copolymer microparticles with controlled molecular architecture and nanostructure using a one-pot scCO₂ method.⁷¹ The RAFT dispersion technique in scCO₂ displayed excellent control over a variety of different monomer types, leading to block copolymers that might be problematic or impossible to achieve in a

microparticulate form through more conservative routes. Furthermore, a wide series of nanostructured block copolymer morphologies were observed, and could be targeted by control of the mass fractions of the blocks, as well as by changing the constituent blocks, signifying an effect of CO₂ sorption on the block copolymer phase behaviour.^{54, 72} In a recent publication, a unique ABC triblock terpolymer with a complex internal nanostructure was successfully synthesised, resulting in a 'lamellar with spheres' [L+ S (II)] type morphology. It has been characterised and shown to have potential photocatalytic applications.⁷³

In this study, an early trial to synthesise a PMMA-*b*-P4VP block copolymer was given some impressive results, which have seen to reproduce almost the same behaviour of phase separation as reported previously by this group.^{56, 71} PMMA was selected as the first block because methacrylate monomers are often efficient macro-chain transfer agents (macro-CTA) and a good propagating radical which are proficiently able to initiate polymerisation of a new block.²² Furthermore, the polymerisation of this monomer in scCO₂ to produce microparticles had also already been optimised by our group, and is not a trivial undertaking. The few examples of phase separation morphology reported by the group that involved PMMA and P4VP is shown in Figure 1.16.

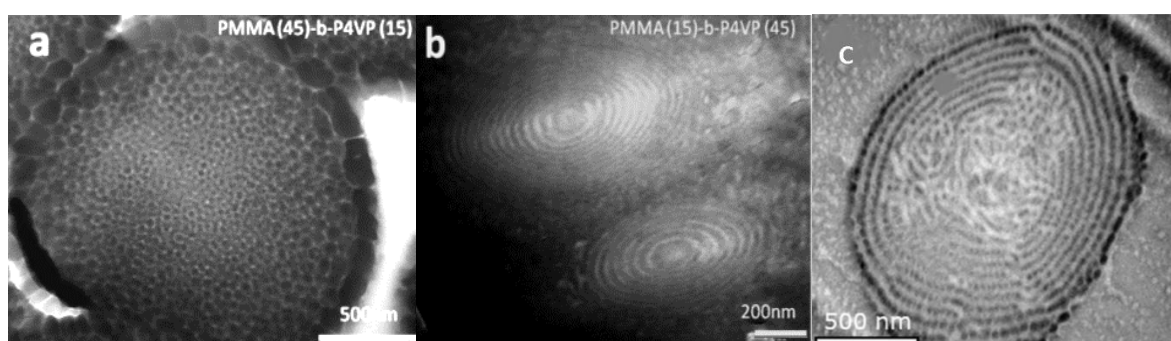


Figure 1.16. The morphology of phase separation of block copolymer by RAFT dispersion polymerisation in scCO₂ reported by the Howdle group a) SPH, b) LAM and c) [L+ S (II)]^{56, 71, 73}

1.6 Supercritical Carbon Dioxide

The extreme conditions demanded for polymer production, including high temperatures, water, and energy consumption, are exceedingly harmful to the environment and cannot be sustained. For example, conventional polymeric particle synthesis often requires solution chemistry and the use of a high concentration of organic solvents. This technology has numerous uses in a variety of significant industries, including cosmetics, electronics, food, biomedical, pharmaceuticals, and fertiliser that could raise serious air and water pollution concerns.⁷⁴⁻⁷⁷ As a result, technologies for synthesis that are both effective and environmentally friendly are of great interest. There has been a steady increase in interest in using ecologically friendly supercritical fluids in place of standard organic solvents in chemical operations. ScCO₂ appears to be a feasible choice due to its superior qualities and properties as well as sustainability.

Carbon dioxide is a well-known supercritical fluid that has been studied in recent years as a possible replacement for the aqueous and organic solvents used in polymerisation. It provides a number of advantages, including being ecologically friendly, being a tuneable solvent, resistant to chain transfer, and having a low viscosity, allowing for high initiator efficiency and fluid handling.

ScCO₂ is a liquid phase of carbon dioxide that is formed at or above its critical temperature ($T_c = 31.1\text{ }^\circ\text{C}$) and critical pressure ($p_c = 73.8\text{ }^\circ\text{C}$) (Figure 1.17). It has exclusive physical properties, demonstrating a diffusion coefficient similar to a gas whilst having liquid like densities letting for the solvation of many compounds.⁷⁸ It is readily available, nontoxic, economical, biocompatible, chemically inert and does not accumulate in the system, and hence represents an extremely promising solvent for chemical

extraction and materials processing, among other applications. This is not a new finding because there are numerous CO₂ -responsive materials, including polymers,⁷⁹ carbon nanotubes,⁸⁰ nanofibrous membranes,⁶⁵ hydrogels⁸¹ and ionic liquids,⁸² that have been established and reported since 1986.⁸³ Furthermore, scCO₂ fluids have been used widely in a large number of chemical processing due to their highly adjustable properties. Several applications were reported such as extraction of organic compounds from black liquor,⁸⁴ extraction of oil from seeds^{85, 86} and extraction of caffeine from coffee beans⁸⁷ at commercial levels. At present, scCO₂ is also being frequently used as a solvent in polymerisation process^{49, 88-91} to replace the use of organic solvents that are harmful to both human and the environment. In this study, scCO₂ will be utilised as a medium for polymer synthesis and details of these reactions will be discussed further below.

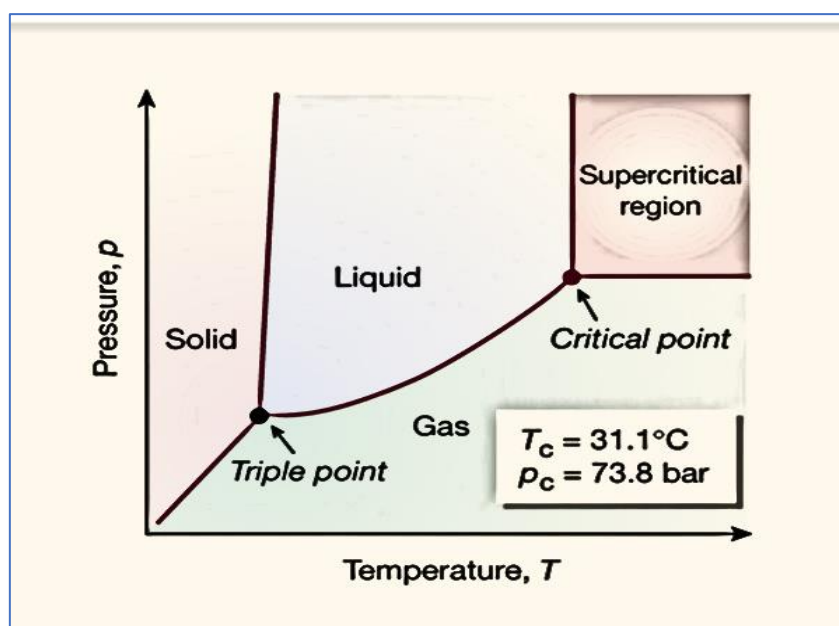


Figure 1.17. Pressure -temperature phase diagram showing the supercritical fluid region for carbon dioxide.⁹²

1.6.1 Polymerisation in scCO₂

Many distinct polymer synthesis strategies have been carried out in scCO₂, using a variety of processes, including ring opening and radical reactions.^{93, 94} ScCO₂ is ideal for radical polymerisation because it has a low reactivity towards radicals, making chain transfer to the solvent uncommon. The radical initiator decomposition kinetics and initiator efficiency have also been reported to be influenced by scCO₂.⁹⁵

The solubility of the reactants and products is the most significant element to consider while polymerising in scCO₂. The majority of polymers are not soluble in scCO₂ at low temperatures and pressures, with the exception of fluorinated and siloxane polymers. Heterogeneous radical polymerisation is the most common method used in scCO₂, making it a versatile medium for the creation of polymer particles of various sizes (Figure 1.18).⁹⁶⁻⁹⁹

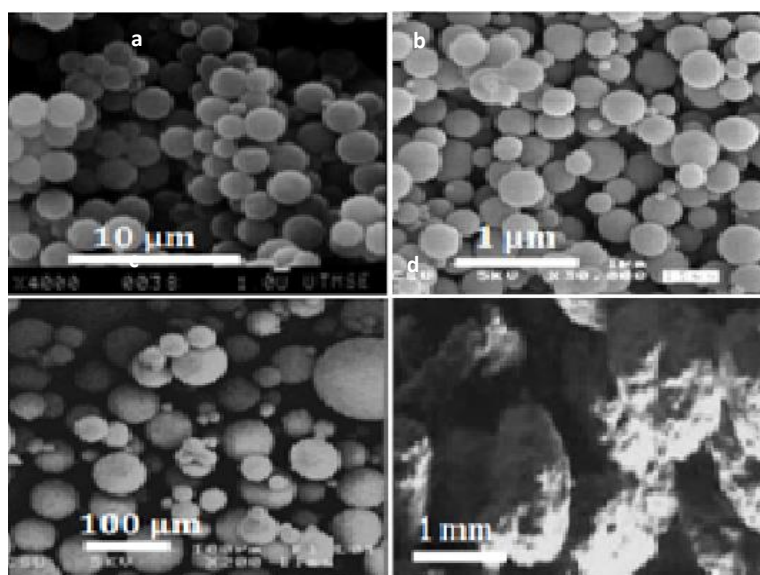


Figure 1.18. SEM images of polymer particles from four different types of heterogeneous polymerisations in scCO₂, Dispersion⁹⁹ (a), Emulsion⁹⁶ (b), Precipitation⁹⁸ (c) and Suspension⁹⁷ (d).

The solvent's environmental friendliness is one of the benefits of heterogeneous polymerisations in scCO₂ in comparison to organic solvents. Furthermore, the product can be easily separated from the continuous phase by venting the reaction vessel to atmospheric pressure. Similarly, scCO₂ is a diverse media for heterogeneous polymerisation due to the insolubility of many polymers in CO₂ and its inertness to reactivity with most chemical functions.¹⁰⁰ As noted in Section 1.5.2, the Howdle group has been actively producing polymers by exploiting the special properties of scCO₂ for nearly a decade. A synthetic route that creates nanostructured BCPs microparticle via a one-pot synthesis using RAFT dispersion polymerisation in scCO₂ (Figure 1.19) has been well established.

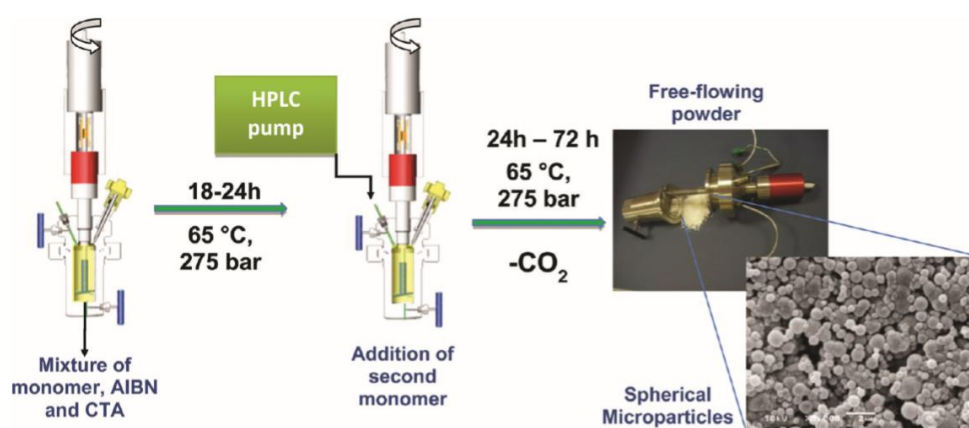


Figure 1.19. One-pot synthesis method for the clean preparation of nanostructured polymeric microparticles in scCO₂.⁷¹

Subsequently, an improvised modular and dependable on-line sampling method (Figure 1.20) was designed and proven to be effective in gathering kinetic data for a variety of polymer reactions in scCO₂.¹⁰¹

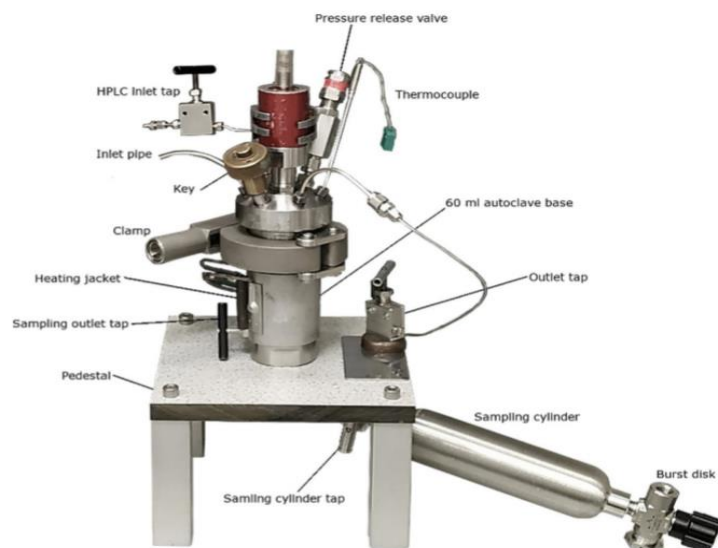
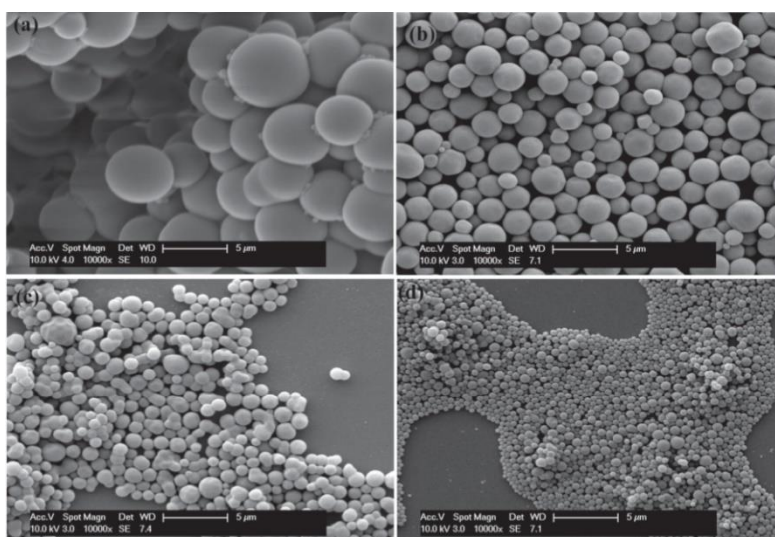


Figure 1.20. On-line sampling system for polymerisation reaction in $scCO_2$ developed by the Howdle group.¹⁰¹

Efforts continue to explore this green polymerisation route by synthesising particles that are more relevant to industry needs. Beginning with improved particle size control of the most prevalent particle in the manufacturing industry, poly(methyl methacrylate), combining control of both the initial monomer and stabiliser loadings produced particles with diameters ranging from 0.3 to 5.3 μm (Figure 1.21a).¹⁰² This method is also scale-able, with synthesis of PMMA particles on the 1 L scale also report (Figure 1.21b).¹⁰³



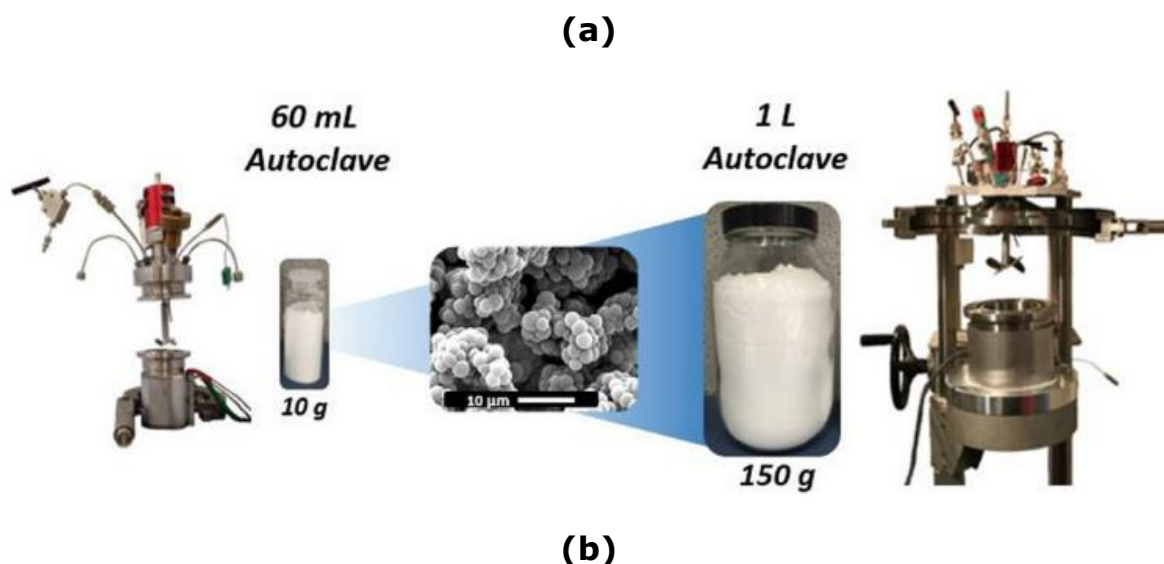


Figure 1.21. (a) SEM images of PMMA particles in different sizes obtained by varying the amount of stabilizer, PDMS-MA.¹⁰² (b) The 1L scale-up of PMMA via Free radical dispersion polymerisation in Howdle group.¹⁰³

This was expanded on with the synthesis of brightly coloured and electrophoretically active PMMA particles being reported, which are cost effective for commercialisation (Figure 1.22).¹⁰⁴

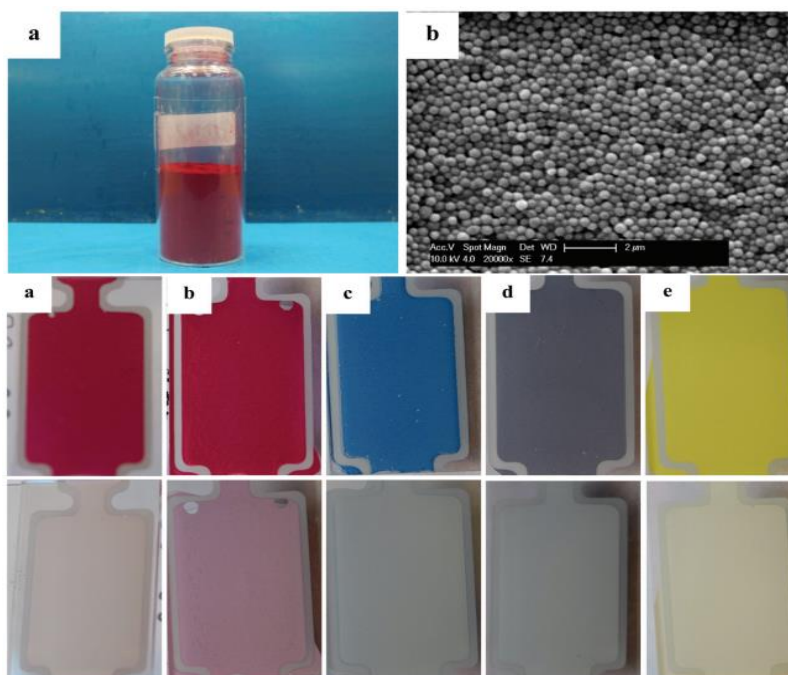


Figure 1.22. (Top: a & b) PMMA brightly coloured and electrophoretically active particles and its SEM image.¹⁰² (Bottom: a-e) Out-of-plane electrophoresis test cell images of magenta particles by Howdle group.¹⁰⁴

Moving to an alternative soft polymer component of poly(butyl acrylate (PBA), Haddleton et al. presented a simple and novel method of synthesis of phase-separated particles in scCO₂ that does not require any chemical control agents or post-polymerisation drying steps (Figure 1.23).¹⁰⁵

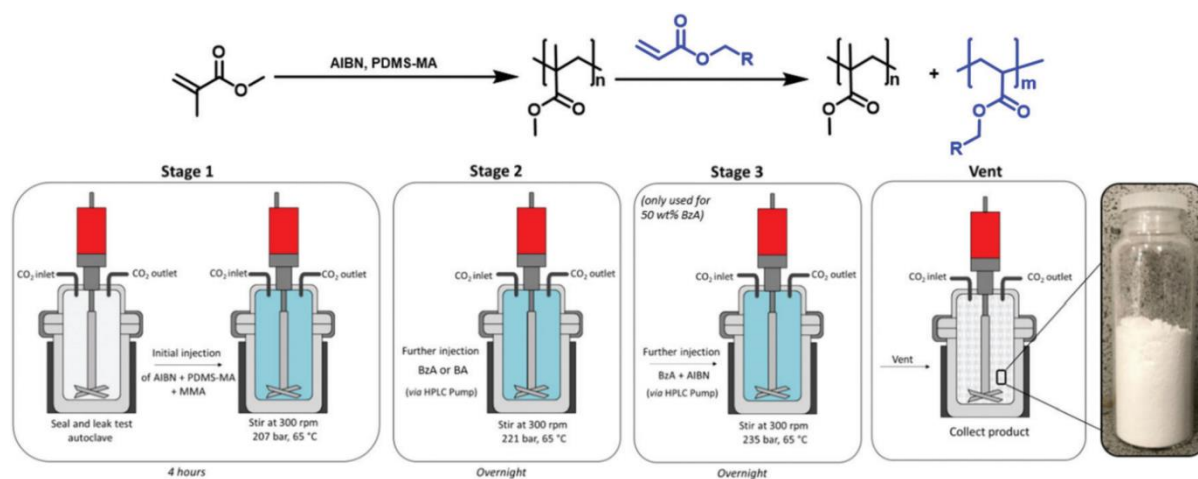


Figure 1.23. Schematic of the reaction procedure used in producing two-phase polymer particles in supercritical carbon dioxide.¹⁰⁵

In addition, a simpler and adaptable technique for the custom production of macro- and mesoporous block copolymer microparticles was reported. However, this approach takes hours, but is freely scalable for the manufacture of grams of material.⁹¹ Hence, this research continues Howdle's legacy of focusing on a dispersion polymerisation reaction that produces monodisperse polymer microparticles using scCO₂ as the continuous media (solvent). This approach has been well-established and widely used by the group, especially for high-pressure reactions involving block copolymer production.

Dispersion polymerisation is a widely used technique to synthesise monodisperse polymer microspheres in scCO₂ that can be applied to

numerous applications such as coatings, biochemical analysis, electronics and microelectronics.^{2, 9, 106, 107} Previously in 2014 Pham et al. was reported the successful polymerisation of vinyl acetate (VAc) and vinyl pivalate (VPi) by using the similar technique. Recently, Xu et al. made a series of poly(dodecafluoroheptyl methacrylate)-*b*-poly(methyl-methacrylate) (PDFMA-*b*-PMMA) diblock copolymer and Alauhdin et al. synthesised a variety of poly(methyl methacrylate)-based block copolymers, both in 2017.^{28, 108, 109}

The synthesis of block copolymers (BCP) in scCO₂ has received a lot of attention because scCO₂ is a green processing solvent that allows for the production of dry powders with micron-sized particles. Furthermore, because of their propensity to spontaneously self-assemble into interior arrays of nano-sized domains, the block copolymer microparticles generated through this procedure offer a lot of application potential. However, at higher temperatures or in the presence of solvents, such materials are still susceptible to morphological loss and degradation. To obtain the qualities needed to make them ideal for a particular use, these microparticles require additional processing or modification stages. Routes that use the crosslinking process as an alternative to these typical fabrication pathways are gaining popularity and this study has focused on them. This process will be discussed further in the following section.

1.7 Cross-linked polymers and their applications

Chemical cross-linking or physical gelation can be utilised to construct networks. Cross-links are formed by covalent chemical bonding or physical interaction. The number of cross-links has an effect on the swelling capacity (degree of swelling) of the produced networks (cross-linking density).

Reaction conditions (temperature, pressure, etc.) can also be used to alter the porosity of a network.¹¹¹

In general, cross-linked polymers have a number of interesting properties that make them appealing materials. Cross-linking can be used to stabilise the structure of a polymer solution. Depending on the environment, the resulting polymer networks (or gels) are elastic and have good mechanical properties. When polymer networks absorb water or chemical solvents, they swell. When a phase transition is generated in cross-linked responsive polymers, the properties of the macroscopic network for example elasticity and swelling behaviour change due to a change in chain configuration.⁸

Amongst all cross-linked polymer materials present in the literature, the author focused her attention only on a particular family of polymers and they will be reported and discussed throughout this report. In 2010, the synthesis of a cross-linked poly(styrene-co-butadiene) core by incorporation of a core-shell modifier was reported, which resulted in toughening polymeric materials.¹¹² In addition, Qiu et al. have demonstrated that the cross-linking of block copolymers synthesised via RAFT dispersion polymerisation gave better fluid sustainability.³⁸ Furthermore, Xu and co-workers made a temperature-responsive block copolymer (reversible shell-crosslinking micelles) that has potential as therapeutic nanocarriers in biomedicine based on pH-triggered release behaviour concept.¹¹³ More recently, there was another finding reported by Q. Qu discussing the cross-linked material resistance to fluid and its ability to preserve the internal morphology and colloidal stability upon exposure to dimethylformamide (DMF).¹¹⁴

Numerous reaction methods for cross-linking polymer particles have been established to date. There are two practical techniques that are widely used: post-polymerisation chemical reactions and *in situ* crosslinking via copolymerisation using a comonomer with two or more reactive sites. The first entails pre-synthesis of polymer particles containing reactive groups, followed by chemical reactions with a crosslinker. Xu et al. described a route to pre-polymerise tri-block copolymer-unimers, bearing amine groups that can react with a dialdehyde crosslinker and form shell-crosslinked micelles (Figure 1.24).¹¹³

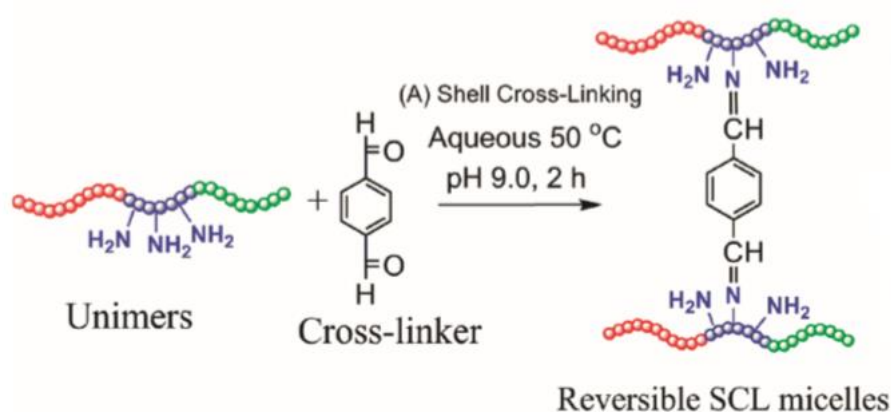


Figure 1.24. Cross-linking of a triblock copolymer micelles in aqueous solution.¹¹³

Later in 2016, Qiu and colleagues demonstrated for the first time that nanoparticles bearing aldehyde groups may be formed by PISA and crosslinked with butanediamine, resulting in core-crosslinked nanoparticles which maintained morphologies (Figure 1.25).³⁸ Literatures show that post-polymerisation crosslinking can also possibly be attained through transition metal complexation (Figure 1.26)¹¹⁵ or a sol-gel reaction (Figure 1.27).¹¹⁶

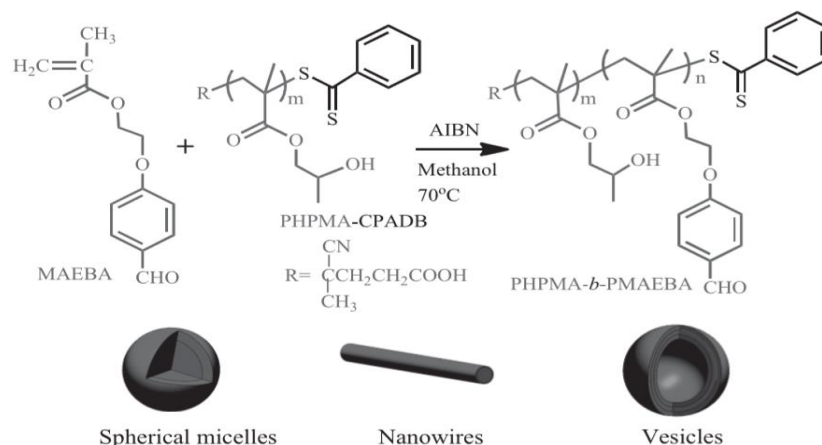


Figure 1.25. Preparation of the diblock copolymer nano-objects via RAFT dispersion polymerisation in methanol at 70 °C.³⁸

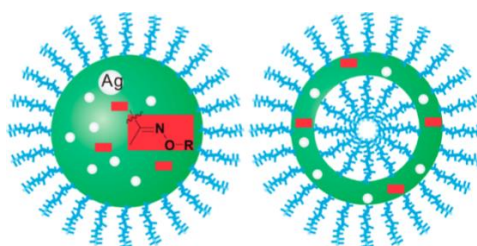


Figure 1.26. Multifunctionalisation of silver nanoparticles.¹¹⁵

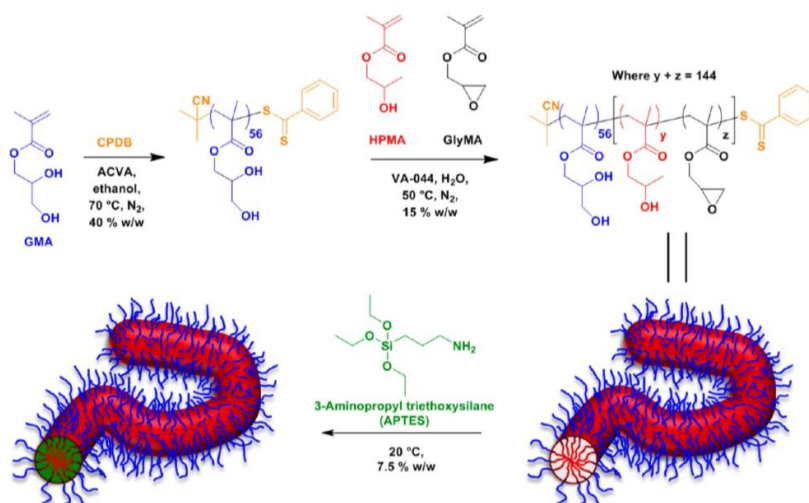


Figure 1.27. Synthesis of a macro-CTA via RAFT solution polymerisation and its subsequent chain extension via statistical copolymerisation to form diblock copolymer worms via polymerisation-induced self-assembly (PISA). Such worms are then cross-linked in a two-step post-polymerisation process.¹¹⁶

A unique feature of the post-polymerisation crosslinking technique is its potential application to a pre-established synthesis route for precursor BCP particles that have already achieved shape and/or particle size control. Additionally, it enables the pre-production and storage of polymer particles with varying characteristics for subsequent crosslinking operations.¹¹⁷ However, there are significant drawbacks because it requires many steps: precursor particle manufacturing and purification, re-dispersion or dissolution, and a second purification phase following crosslinking. As a result, it is deemed to be a time-consuming and expensive method with limited industrial viability was created.

The second approach is *in situ* crosslinking in which divinyl comonomers are used to form covalent crosslinks during the polymerisation step. Since 2011, the structural stabilisation of PISA-generated nano objects has been explored by using this technique with a divinyl comonomer. As a result, the chain movement of a growing polymer was found to reduce much upon crosslinking which usually interrupts the copolymerisation through macrogelation and/or obstructs morphology progression (Figure 1.28).¹¹¹

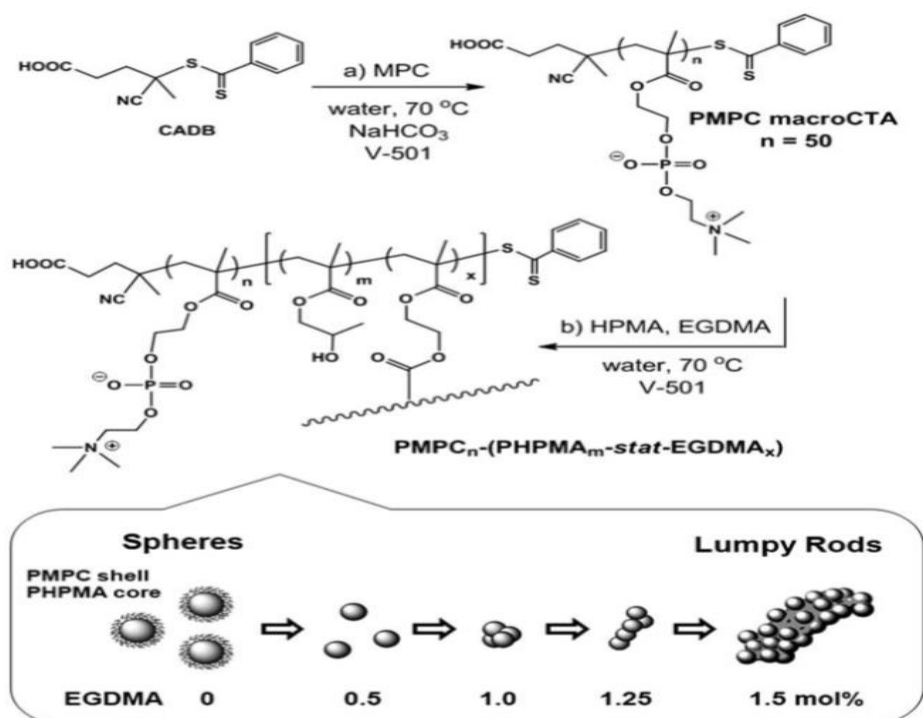


Figure 1.28. Synthesis of nanoparticles with spherical, worm-like or 'lumpy rod' morphologies by RAFT aqueous dispersion polymerisation at 70 °C. In each case the extent of cross-linking dictates the final particle morphology that is obtained.¹¹¹

An elegant solution to this drawback was reported by the Armes group where they studied a method of delaying crosslinker addition for the *in situ* crosslinking of vesicles with a symmetric divinyl comonomer (Figure 1.29 and 1.30).^{118, 119} Following the consumption of the core-forming monomer, ethylene glycol dimethyl acrylate (EGDMA) was added to generate a strongly crosslinked third block. The delayed addition of a crosslinker only accelerates crosslinking significantly towards the end of the reaction and allows for maintaining control over polymerisation and particle morphology.

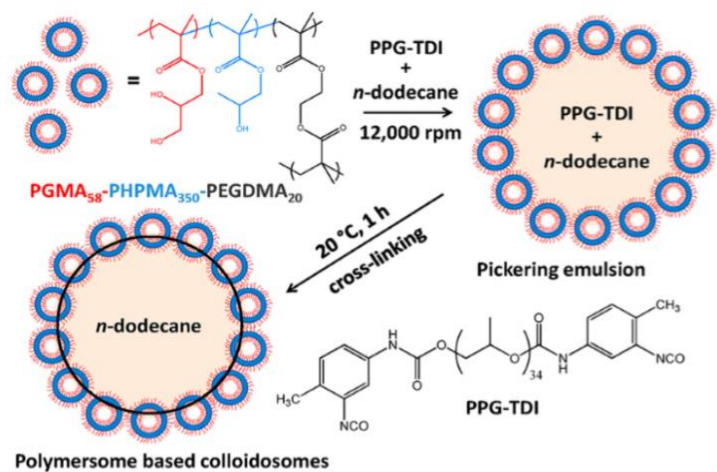


Figure 1.29. Schematic representation of the preparation of covalently cross-linked colloidosomes using cross-linked polymersomes, n-dodecane as the internal oil phase and an oil-soluble polymeric crosslinker.¹¹⁹

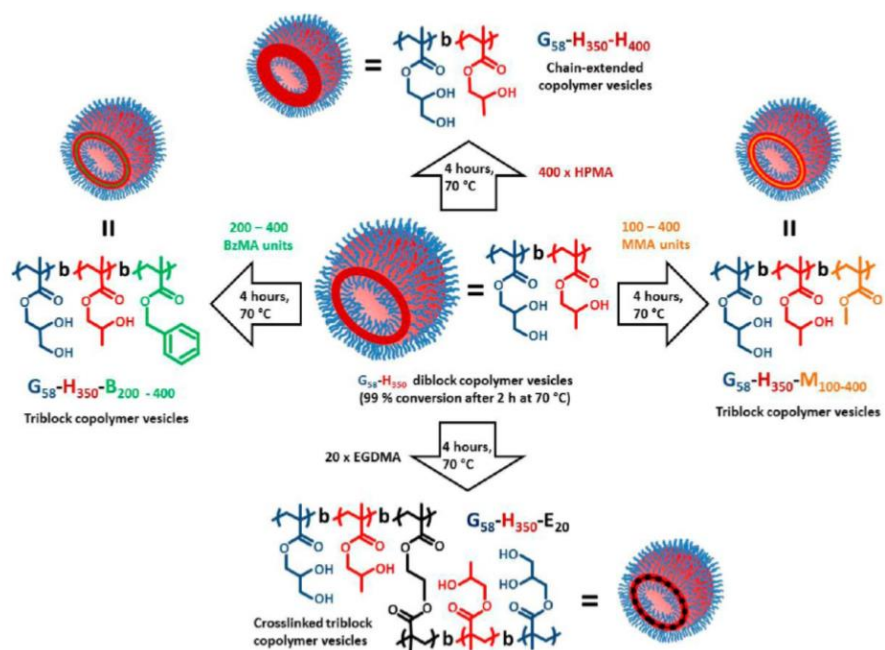


Figure 1.30. Reaction scheme for the synthesis of methacrylic triblock copolymer vesicles via RAFT polymerisation of a third comonomer from a linear diblock copolymer vesicle precursor. Such *in situ* syntheses provide a good test of the pseudoliving character that can be achieved under RAFT aqueous dispersion polymerisation conditions at 70 °C.¹¹⁸

Another possibility is to utilise an asymmetric crosslinker, which has two vinyl groups with varying reactivity and is inserted at the start of the polymerisation process.¹¹⁴ Qu et al. established that the asymmetric crosslinker allyl acrylamide (ALAM) can be used to stabilise higher order morphologies such as vesicles (Figure 1.31).¹¹⁴ This method enables the formation of vesicles with a higher degree of crosslinking (2–5 mol percent ALAM) than those formed with the symmetric crosslinker *N,N'*-methylene bisacrylamide (BIS) (1 mol%). They later demonstrated that these crosslinked vesicles maintain the RAFT end group's viability for chain extension into triblock copolymer vesicles (Figure 1.32).⁵⁵

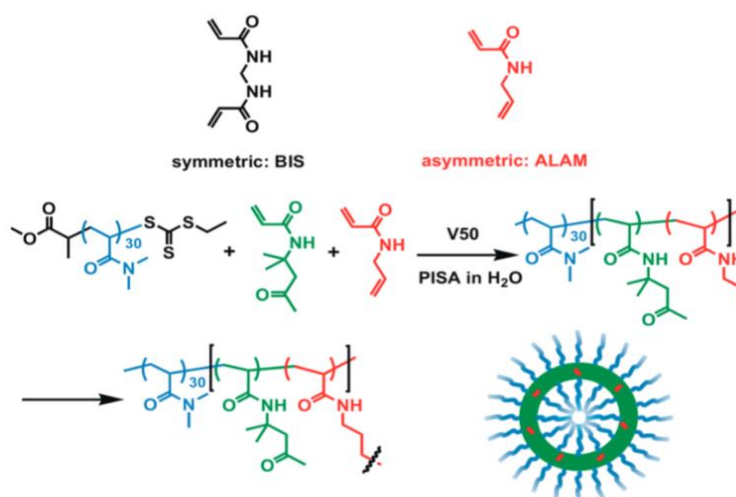


Figure 1.31. Structure of crosslinkers and synthesis of in situ cross linked vesicles.¹¹⁴

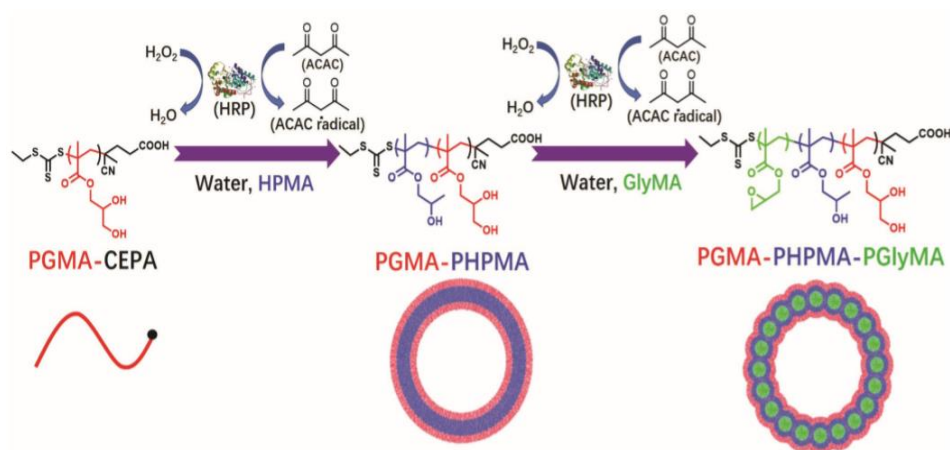


Figure 1.32. Synthesis of poly(glycerol monomethacrylate)-*b*-poly(2-hydroxypropyl methacrylate) diblock copolymer vesicles and poly(glycerol monomethacrylate)-*b*-poly(2-hydroxypropyl methacrylate)-*b*-poly(glycidyl methacrylate) triblock copolymer vesicles via enzyme-initiated RAFT polymerisation in water.⁵⁵

Recently, the Howdle group published a versatile technique to transform nanostructured microparticles, that have been synthesised by RAFT dispersion polymerisation in $scCO_2$, into porous microparticles via swelling/rapid deswelling process.⁹¹ It was verified that the porosity can be customised over a wide size range from 20 to 200 nm, and assorted morphologies from secluded spherical pores, short porous channels, to interconnected pore networks, could be achieved by varying the block ratio and block length (Figure 1.33).⁹¹

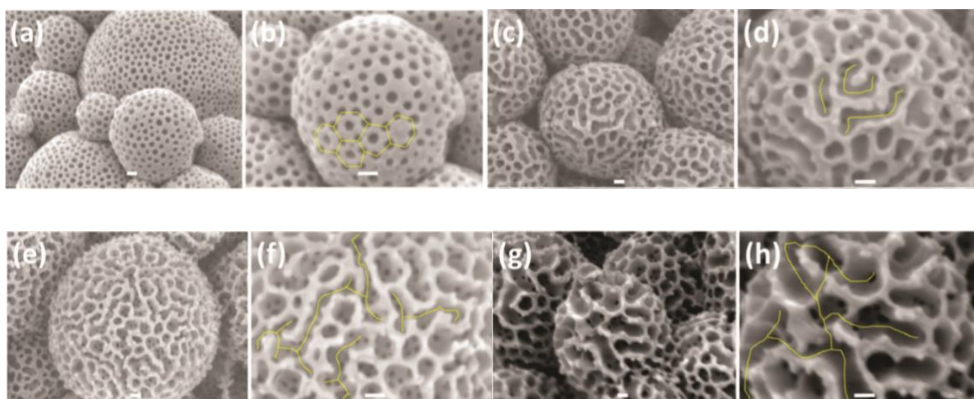


Figure 1.33. Controlled nanoporosity introduced into block copolymer microparticles by selective swelling/deswelling in ethanol with hexane at different block ratio and block length. The yellow lines in (b, d, f, h) mark the surface pore evolution from secluded spherical pores to short channels, and to interconnected channels.⁹¹

To increase the versatility of these materials for a variety of applications such as column chromatography, drug delivery, and slow release, it is critical to ensure that the particle structure and internal morphology can be sufficiently maintained when exposed to a fluid (for example, an organic solvent). To the author's knowledge, little attention has been paid to the internal crosslinking of such bigger, micron-sized particles, particularly those with hierarchical structures formed *in situ* via polymerisation-induced microphase separation.

Taking into account the published literature and the knowledge gap in this field, we concentrated on developing a method for selectively crosslinking the internal phase separated domains of BCP microparticles during their one-pot polymerisation in $scCO_2$. This should enhance their structural integrity in the presence of solvents or, indeed, any other stimuli. This technique permits *in situ* crosslinking of nanostructured BCP microparticles without impairing their polymerisation-induced phase separation morphologies. (Figure 1.34).¹²⁰ The details of results obtained from this reaction are discussed in detailed in chapter 4.

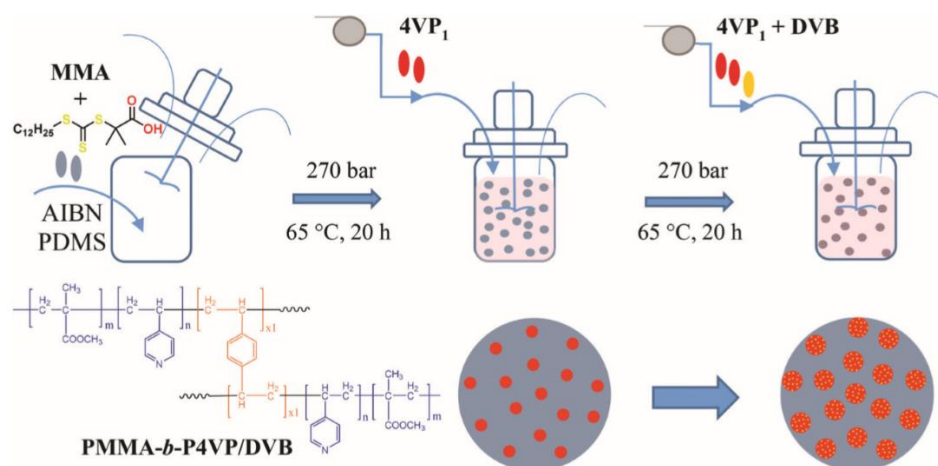


Figure 1.34 The *in situ* crosslinking of PMMA-*b*-P4VP microparticles by RAFT dispersion polymerisation in $scCO_2$ in a one-pot, two-step process.

1.8 Summary and Research Objective

This first chapter discusses, in detail, the theory and basics underlying this research project. It begins with an overview before delving into the definitions of polymer, block copolymer, polymer production methods, and applications. Later in the chapter, the key concepts used in this study are discussed, including $scCO_2$ —its characteristics and behaviour, heterogeneous polymerisation, controlled/living radical polymerisation, RAFT dispersion polymerisation, phase separation behaviour of block copolymers, and finally, crosslinking as a primary method for enhancing the morphology for targeted application. The second chapter provides details of the high-pressure system employed in this study, including the equipment configuration for the polymer reactions and the analytical techniques used for testing and characterisation of the materials, as well as product performance.

To begin with, the third chapter compiles all the efforts made during the early experimental phase aimed at synthesising homopolymer PMMA by both FRP and RAFT. In tandem with these studies, the crosslinking agent (EGDMA) was incorporated into the FRP PMMA dispersion polymerisation process by simply adding it to the reaction mixture with the other components at the beginning of the reaction. This one-pot method was used to observe the effect of crosslinking on the morphology and thermal properties of the PMMA microparticles.

The following chapter, Chapter 4, discusses the synthesis of the block copolymer, PMMA-*b*-P4VP, and reveals the correct technique, tips and tricks for incorporating the crosslinker into this block copolymer without compromising both the overall microparticle structure and the internal phase separated morphology formed. This is important and has become a prime area of interest in this study due to the application demand for technologically complex materials in various areas, such as for micron-sized carriers for therapeutics or as chemically resistant templates for other compounds.

Finally, in Chapter 5, the newly discovered crosslinking approach is used to fabricate stationary phase polymer materials for sample preparation and to test their performance in other applications, including drug adsorption/sorption and enzyme immobilisation.

1.9 References

1. L. Hartman, *Packaging Digest*, 2008, **45**, 50-56.
2. H. C. Kim, S. M. Park and W. Hinsberg, *Journal*, 2010, **110**, 146-177.
3. A. M. Wagner, D. S. Spencer and N. A. Peppas, *Journal of Applied Polymer Science*, 2018, **135**, 17.
4. F. Mastrotto, A. F. Breen, G. Sicilia, S. Murdan, A. D. Johnstone, G. E. Marsh, C. Grainger-Boulton, N. A. Russell, C. Alexander and G. Mantovani, *Polym. Chem.*, 2016, **7**, 6714-6724.
5. Z. Jiao, W. Fan, Z. Wang and X. Wang, *Journal of Drug Delivery Science and Technology*, 2018, **44**, 13-18.
6. N. Hadjichristidis, *Complex Macromolecular Architectures : Synthesis, Characterization, and Self-assembly.*, John Wiley & Sons Asia, Singapore, 2011.
7. O. J. G. M. Goor, S. I. S. Hendrikse, P. Y. W. Dankers and E. W. Meijer, *Chem. Soc. Rev.*, 2017, **46**, 6621-6637.
8. A. Kaynak and A. Zolfagharian, *Stimuli-Responsive Polymer Systems—Recent Manufacturing Techniques and Applications*, MDPI - Multidisciplinary Digital Publishing Institute, 2019.
9. M. F. Maitz, *Biosurface and Biotribology*, 2015, **1**, 161-176.
10. J. Xu, S. Wang, G.-J. N. Wang, C. Zhu, S. Luo, L. Jin, X. Gu, S. Chen, V. R. Feig, J. W. F. To, S. Rondeau-Gagné, J. Park, B. C. Schroeder, C. Lu, J. Y. Oh, Y. Wang, Y.-H. Kim, H. Yan, R. Sinclair, D. Zhou, G. Xue, B. Murmann, C. Linder, W. Cai, J. B. H. Tok, J. W. Chung and Z. Bao, *Science (New York, N.Y.)*, 2017, **355**, 59.
11. C. Janáky and K. Rajeshwar, *Progress in polymer science*, 2015, **43**, 96-135.
12. C. Pegoraro, S. Macneil and G. Battaglia, *Nanoscale*, 2012, **4**, 1881-1894.
13. G. Odian, *Principles of Polymerisation*, John Willey & Sons, Inc., 4th Edition edn., 2004.

14. J. W. Nicholson. *The Chemistry of Polymers*, Cambridge, U.K. : RSC Pub., Cambridge, U.K., 3rd ed. edn., 2006.
15. U. Beginn, *Colloid and polymer science*, 2008, **286**, 1465-1474.
16. V. Postupalenko, T. Einfalt, M. Lomora, I. A. Dinu and C. G. Palivan, *Journal*, 2016, 341-371.
17. C. E. Carraher, Jr., *Introduction to polymer chemistry*, Boca Raton ; London, 4th ed. edn., 2017.
18. R. Braslau, *Journal of the American Chemical Society*, 2003, **125**, 3399-3400.
19. H. Fischer, *Chemical reviews*, 2001, **101**, 3581-3610.
20. J. C. Foster, S. C. Radzinski and J. B. Matson, *Journal*, 2017, **55**, 2865-2876.
21. A. M. Gregory, K. J. Thurecht and S. M. Howdle, *Macromolecules*, 2008, **41**, 1215-1222.
22. D. Keddie, *Journal*, 2014, **43**, 496-505.
23. S. b. Perrier, *Macromolecules*, 2017, **50**, 7433-7447.
24. G. Moad, E. Rizzardo and S. Thang, *Journal*, 2009, **62**, 1402-1472.
25. J. M. G. Cowie, *Polymers : Chemistry and Physics of Modern Materials*, Boca Raton, 3rd ed. edn., 2008.
26. H. Warson, *Journal*, 1998, **45**, 329-330.
27. A. v. Herk and ProQuest, *Chemistry and technology of emulsion polymerisation [electronic resource] / editor, A.M. van Herk*, Chichester, West Sussex, U.K. : John Wiley & Sons Inc., Chichester, West Sussex, U.K., 2nd edn., 2013.
28. M. Alauhdin, Thesis (PhD)--University of Nottingham, 2017., 2017.
29. M. Eren and H. K. Can, *Progress in organic coatings*, 2019, **135**, 424-437.
30. L. Shaofen, *Journal*, 2017, 541-598.
31. J. Sakdapipanich, N. Thananusont, N. Pukkate and Y. Tanaka, *Journal of applied polymer science*, 2007, **103**, 2767-2767.
32. F. Naz, M. Zuber, K. Mehmood Zia, M. Salman, J. Chakraborty, I. Nath and F. Verpoort, *Carbohydrate polymers*, 2018, **200**, 54-62.

33. C. E. Carraher Jr, *Carraher's Polymer Chemistry, Ninth Edition*, Bosa Roca: CRC Press LLC, Bosa Roca, 2013.
34. J. K. Oh, *Journal of polymer science. Part A, Polymer chemistry*, 2008, **46**, 6983-7001.
35. R. Arshady, *Journal of molecular recognition*, 1996, **9**, 536-542.
36. T. Senninger, V. Darcos, K. Matyjaszewski, D. Lastecoueres, L. Sanchez and J.-B. Verlhac, *Journal*, 2002.
37. K. Matyjaszewski and J. Spanswick, *Journal*, 2012, **3**, 377-428.
38. L. Qiu, C. R. Xu, F. Zhong, C. Y. Hong and C. Y. Pan, *Macromolecular Chemistry and Physics*, 2016, **217**, 1047-1056.
39. K. Min and K. Matyjaszewski, *Macromolecules*, 2007, **40**, 7217-7222.
40. S. Kawaguchi and K. Ito, *Advances in polymer science*, 2005, **175**, 299-328.
41. *Polymer Particles*, Berlin, Heidelberg: Springer Berlin Heidelberg, Berlin, Heidelberg.
42. C. Barner-Kowollik, *Handbook of RAFT polymerization / edited by Christopher Barner-Kowollik*, Weinheim : Wiley-VCH, Weinheim, 2008.
43. A. P. Richez, H. N. Yow, S. Biggs and O. J. Cayre, 2013.
44. J. M. DeSimone, E. E. Maury, Y. Z. Menceloglu, J. B. McClain, T. J. Romack and J. R. Combes, *Science*, 1994, **265**, 356-359.
45. M. Szwarc, *Nature*, 1956, **178**, 1168-1169.
46. N. Bertrand, J. Wu, X. Y. Xu, N. Kamaly and O. C. Farokhzad, *Advanced Drug Delivery Reviews*, 2014, **66**, 2-25.
47. H. W. Melville and A. S. Dunn, *Nature (London)*, 1952, **169**, 699-700.
48. J. Rodríguez-Hernández, *Journal*, 2017, 131-161.
49. J. Jennings, G. He, S. M. Howdle and P. B. Zetterlund, *Chem. Soc. Rev.*, 2016, **45**, 5055-5084.
50. Y. D. Luo, I. C. Chou, W. Y. Chiu and C. F. Lee, *Journal of Polymer Science Part A: Polymer Chemistry*, 2009, **47**, 4435-4445.

51. C. Chang, H. Wei, D.-Q. Wu, B. Yang, N. Chen, S.-X. Cheng, X.-Z. Zhang and R.-X. Zhuo, *International journal of pharmaceuticals*, 2011, **420**, 333.
52. C. Du, X. Ma, C. J. Wu, M. Cai and L. Wu, *J. Appl. Polym. Sci.*, 2014, **131**.
53. H. A. Klok and S. Lecommandoux, *Advanced materials (Weinheim)*, 2001, **13**, 1217-1229.
54. M. Alauhdin, T. M. Bennett, G. He, S. P. Bassett, G. Portale, W. Bras, D. Hermida-Merino and S. M. Howdle, *Polym. Chem.*, 2019, **10**, 860-871.
55. Q. Xu, Y. Zhang, X. Li, J. He, J. Tan and L. Zhang, *Polym. Chem.*, 2018, **9**, 4908-4916.
56. J. Jennings, Thesis (PhD)--University of Nottingham, 2013., 2007.
57. F. S. Bates and G. H. Fredrickson, *Annual review of physical chemistry*, 1990, **41**, 525-557.
58. J. Kon Kim, U. Jeong, D. Yeol Ryu and T. P. Russell, *Nature materials*, 2002, **1**, 114-117.
59. F. S. Bates, *Science (American Association for the Advancement of Science)*, 1991, **251**, 898-905.
60. I. W. Hamley, *The physics of block copolymers / Ian W. Hamley*, Oxford : Oxford University Press, Oxford, 1998.
61. N. A. Lynd, A. J. Meuler and M. A. Hillmyer, *Progress in Polymer Science*, 2008, **33**, 875-893.
62. Y. Mai and A. Eisenberg, *Chemical Society reviews*, 2012, **41**, 5969-5985.
63. A. H. Hofman, G. Ten Brinke and K. Loos, *Polymer*, 2016, **107**, 343-356.
64. O. R. Davies, A. L. Lewis, M. J. Whitaker, H. Tai, K. M. Shakesheff and S. M. Howdle, *Advanced drug delivery reviews*, 2008, **60**, 373.
65. H. Che, M. Huo, L. Peng, T. Fang, N. Liu, L. Feng, Y. Wei and J. Yuan, *Angewandte Chemie International Edition*, 2015, **54**, 8934-8938.

66. M. G. Buonomenna, W. Yave and G. Golemme, *RSC advances*, 2012, **2**, 10745-10773.
67. A. Urbas, R. Sharp, Y. Fink, E. L. Thomas, M. Xenidou and L. J. Fetters, *Advanced materials (Weinheim)*, 2000, **12**, 812-814.
68. M. J. Benes^ˇ, D. Horák and F. Svec, *Journal of Separation Science*, 2005, **23**, 1855-1875.
69. J. Alvarez, G. Saudino, V. Musteata, P. Madhavan, A. Genovese, A. R. Behzad, R. Sougrat, C. Boi, K.-V. Peinemann and S. P. Nunes, *Scientific reports*, 2019, **9**, 13987-13910.
70. R. Say, S. Emir, B. Garipcan, S. Patir and A. Denizli, *Advances in polymer technology*, 2003, **22**, 355-364.
71. J. Jennings, M. Beija, A. P. Richez, S. D. Cooper, P. E. Mignot, K. J. Thurecht, K. S. Jack and S. M. Howdle, *Journal of the American Chemical Society*, 2012, **134**, 4772.
72. S. P. Bassett, N. A. Birkin, J. Jennings, E. Chapman, R. K. O'Reilly, S. M. Howdle and H. Willcock, *Polym. Chem.*, 2017, **8**, 4557-4564.
73. R. R. Larder, T. M. Bennett, L. S. Blankenship, J. A. Fernandes, B. K. Husband, R. L. Atkinson, M. J. Derry, D. T. W. Toolan, H. A. Centurion, P. D. Topham, R. V. Gonçalves, V. Taresco and S. M. Howdle, *Polymer chemistry*, 2021, **12**, 2904-2913.
74. J. J. Licari, *Coating materials for electronic applications : polymers, processes, reliability, testing / by James J. Licari*, Norwich, N.Y. : Noyes Publications : William Andrew Pub., Norwich, N.Y., 2003.
75. I. M. Martins, M. F. Barreiro, M. Coelho and A. E. Rodrigues, *Chemical engineering journal (Lausanne, Switzerland : 1996)*, 2014, **245**, 191-200.
76. M. Tzika, S. Alexandridou and C. Kiparissides, *Powder technology*, 2003, **132**, 16-24.
77. J. Siepmann and F. Siepmann, *International journal of pharmaceuticals*, 2013, **457**, 437-445.
78. J. Kendall, D. Canelas, J. Young and J. Desimone, *Journal*, 1999, **99**, 543-563.

79. J. Kainz, P. D. L. Werz, C. Troll and B. Rieger, *RSC Adv.*, 2015, **5**, 9556-9560.
80. Z. Guo, Y. Feng, S. He, M. Qu, H. L. Chen, H. Liu, Y. Wu and Y. Wang, *Adv. Mater.*, 2013, **25**, 584-590.
81. W. Zheng, G. Yang, N. N. Shao, L. Chen, B. Ou, S. Jiang, G. Chen and H. Yang, *J. Am. Chem. Soc.*, 2017, **139**, 13811-13820.
82. Y. Shi, D. Xiong, H. Wang, Y. Zhao and J. Wang, *Langmuir : the ACS journal of surfaces and colloids*, 2016, **32**, 6895.
83. A. Darabi, P. G. Jessop and M. F. Cunningham, *Chem. Soc. Rev.*, 2016, **45**, 4391-4436.
84. T. Fujii, Y. Matsuo and S. Kawasaki, *Ind. Eng. Chem. Res.*, 2018, **57**, 5717-5721.
85. U. Salgın, S. Salgın, D. D. Ekici and G. Uludal, *The Journal of Supercritical Fluids*, 2016, **118**, 194-202.
86. J. A. R. Uribe, J. I. N. Perez, H. C. Kaul, G. R. Rubio and C. G. Alcocer, *The Journal of Supercritical Fluids*, 2011, **56**, 174-178.
87. I. De Marco, S. Riemma and R. Iannone, *The Journal of Supercritical Fluids*, 2018, **133**, 393-400.
88. J. Pinto, D. Morselli, V. Bernardo, B. Notario, D. Fragouli, M. A. Rodriguez-Perez and A. Athanassiou, *Polymer*, 2017, **124**, 176-185.
89. S. P. Bassett, N. A. Birkin, J. Jennings, E. Champman, R. K. O'Reilly, S. M. Howdle and H. Willcock, 2017.
90. M. Benedetti, T. R. Congdon, S. P. Bassett, M. Alauhdin, S. M. Howdle, D. M. Haddleton, R. Pisano, M. Sangermano and T. L. Schiller, *Polym. Chem.*, 2017, **8**, 972-975.
91. G. He, T. M. Bennett, M. Alauhdin, M. W. Fay, X. Liu, S. T. Schwab, C.-G. Sun and S. M. Howdle, *Polym. Chem.*, 2018, **9**, 3808-3819.
92. H. Nakayama, M. Murai, M. Tono-oka, K. Masuda and K. Ishii, *Journal of Physical Chemistry A*, 2007, **111**, 1410-1418.
93. J. L. Kendall, D. A. Canelas, J. L. Young and J. M. DeSimone, *Chemical reviews*, 1999, **99**, 543-564.

94. T. Wang, Y. Liu and J. Hao, *Colloid and Polymer Science*, 2014, **292**, 2497-2508.
95. Z. Guan, J. R. Combes, Y. Z. Menciloglu and J. M. DeSimone, *Macromolecules*, 1993, **26**, 2663-2669.
96. W. Ye and J. M. DeSimone, *Macromolecules*, 2005, **38**, 2180-2190.
97. Y. A. Hussain, T. Liu and G. W. Roberts, *Industrial & engineering chemistry research*, 2012, **51**, 11401-11408.
98. T. Liu, P. Garner, J. M. DeSimone, G. W. Roberts and G. D. Bothun, *Macromolecules*, 2006, **39**, 6489-6494.
99. M. L. O'Neill, M. Z. Yates, K. P. Johnston, C. D. Smith and S. P. Wilkinson, *Macromolecules*, 1998, **31**, 2838-2847.
100. J. L. Young and J. M. DeSimone, *Macromolecules*, 2005, **38**, 4542-4544.
101. K. Kortsen, A. A. C. Pacheco, J. C. Lentz, V. Taresco and S. M. Howdle, *The Journal of supercritical fluids*, 2021, **167**.
102. T. D. McAllister, L. D. Farrand and S. M. Howdle, *Macromolecular Chemistry and Physics*, 2016, **217**, 2294-2301.
103. A. J. Haddleton, S. P. Bassett and S. M. Howdle, *The Journal of supercritical fluids*, 2020, **160**, 104785.
104. T. D. McAllister, T. M. Bennett, C. Petrillo, C. Topping, L. D. Farrand, N. Smith and S. M. Howdle, *Journal of Materials Chemistry C*, 2019, **7**, 12194-12203.
105. A. J. Haddleton, T. M. Bennett, X. Chen, R. L. Atkinson, V. Taresco and S. M. Howdle, *Polymer chemistry*, 2020, **11**, 529-539.
106. J. Jennings, M. Beija, J. T. Kennon, H. Willcock, R. K. O'Reilly, S. Rimmer and S. M. Howdle, *Macromolecules*, 2013, **46**, 6843-6851.
107. J. Sedó, J. Saiz-Poseu, F. Busqué and D. Ruiz-Molina, *Advanced materials (Deerfield Beach, Fla.)*, 2013, **25**, 653.
108. A. Xu, Q. Lu, Z. Huo, J. Ma, B. Geng, U. Azhar, L. Zhang and S. Zhang, *RSC Adv.*, 2017, **7**, 51612-51620.
109. Q. Pham, Y. Haldorai, V. Nguyen, C. Kang and J.-J. Shim, *Korean Journal of Chemical Engineering*, 2014, **31**, 2101-2107.

110. A. I. Cooper, *Journal*, 2000, **10**, 207-234.
111. S. Sugihara, S. P. Armes, A. Blanazs and A. L. Lewis, *Soft Matter*, 2011, **7**, 10787-10793.
112. M. Chen, C. Zhou, Z. Liu, C. Cao, Z. Liu, H. Yang and H. Zhang, *Polymer International*, 2010, **59**, 980-985.
113. J. D. F. Xuewei Xu, ‡ and Charles L. McCormick, *Macromolecules*, 2011, **44**, 1327-1334.
114. Q. Qu, G. Liu, X. Lv, B. Zhang and Z. An, *ACS Macro Letters*, 2016, **5**, 316-320.
115. W. Zhou, Q. Qu, W. Yu and Z. An, *ACS Macro Letters*, 2014, **3**, 1220-1224.
116. J. R. Lovett, L. P. D. Ratcliffe, N. J. Warren, S. P. Armes, M. J. Smallridge, R. B. Cracknell and B. R. Saunders, *Macromolecules*, 2016, **49**, 2928.
117. J. Qiu, B. Charleux and K. Matyjaszewski, *Progress in Polymer Science*, 2001, **26**, 2083-2134.
118. P. Chambon, A. Blanazs, G. Battaglia and S. P. Armes, *Macromolecules*, 2012, **45**, 5081-5090.
119. K. L. Thompson, P. Chambon, R. Verber and S. P. Armes, *Journal of the American Chemical Society*, 2012, **134**, 12450.
120. G. He, T. M. Bennett, K. Alias, L. Jiang, S. T. Schwab, M. Alauhdin and S. M. Howdle, *Polymer chemistry*, 2019, **10**, 3960-3972.

Chapter 2

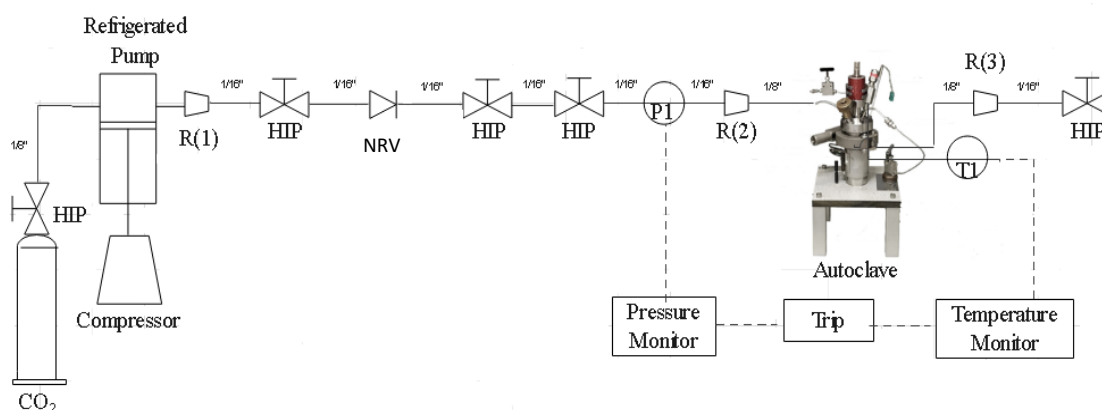
Experimental Technique

This chapter describes the apparatus of experimentation and the analytical techniques used throughout this research study. The first half of this chapter outlines the high-pressure equipment used. The general arrangement of the equipment and the reactors used for the dispersion supercritical CO₂ polymerisation (scCO₂) is detailed. The second half of this chapter discusses the analytical methods for characterising the synthesised products in this study.

2.1 High-Pressure Equipment (HIP)

2.1.1 General Set-Up

The High-Pressure Equipment (HIP) set-up in B10 laboratory, School of Chemistry, University of Nottingham, is designed in-house to meet the nature of the reaction in scCO_2 , by combining the experience of workshop employees and collaboration work with suppliers. The setup includes a compressed CO_2 cylinder as a source of CO_2 , a high-pressure pump to dispense a sufficient amount of CO_2 gas, a stainless-steel high-pressure autoclave, connected pipe work, and an electronic controller with a temperature and pressure monitor as well as a built-in trip system for safety. The schematic layout for the high-pressure equipment setup currently used in our laboratory is shown below in Figure 2.1, it shows how the CO_2 cylinder and high-pressure pump are connected to the autoclave.



Key:

- 1) HIP: High Pressure Equipment valves to control the CO_2 flow.
- 2) NRV: Non return valve to allow only single direction of the CO_2 flow into the autoclave, prevention of contamination of reagents transported from one autoclave to another through a pressure different and avoided reagents flowing back into the main line.
- 3) R(1)-R(3): Reducing union to reduce the CO_2 pressure between 2 different size of pipe line.
- 4) P(1) : Pressure transducer.
- 5) T(1) : Internal thermocouple to monitor the desired temperature.

Figure 2.1. Schematic diagram for high pressure equipment set up, including pipe diameters.¹

2.1.2 High-Pressure Autoclave

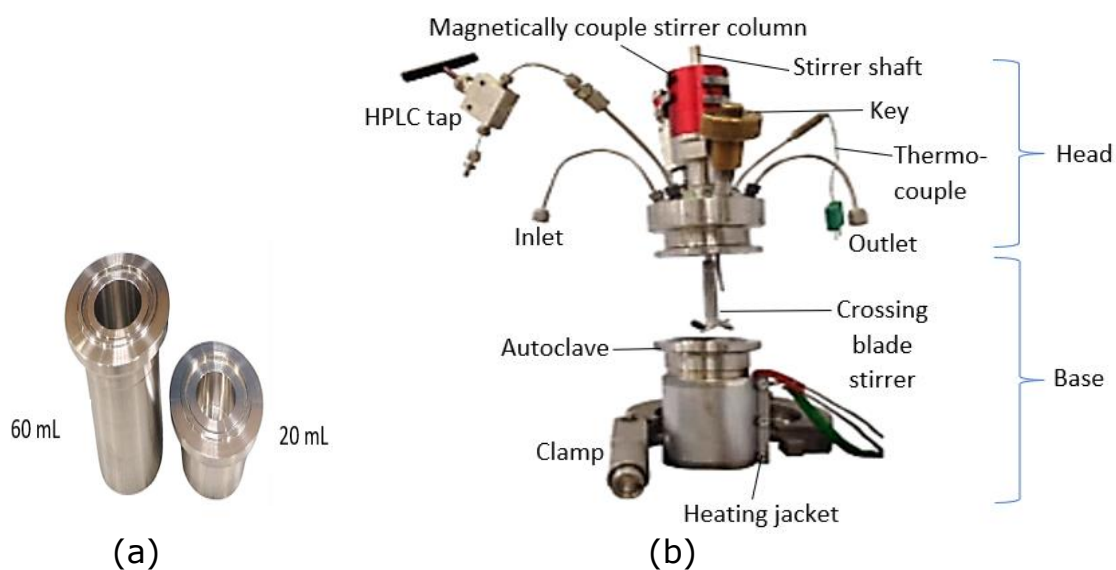


Figure 2.2. a) Two different base units, 20mL and 60mL volume capacity of autoclave's stainless-steel base for scCO₂ reaction and b) An autoclave set-up consists of 2 parts; the autoclave head and base.

A high-pressure autoclave, the reaction vessel, is made of stainless steel 316. It was created in two volume sizes: 20 mL and 60 mL (Figure 2.2a). It consists of two parts: the head and the base of the autoclave (Figure 2.2b). In the head of the autoclave there is a magnetically-coupled stirrer column. It holds the stirrer shaft which extends down into the base with crossing blade at the end for efficient mixing of the reaction content. The head also contains an inlet and outlet pipe and also a thermocouple. For the purpose of high-pressure reaction in this study, which involved polymerisation of crosslinked block copolymer, the reaction vessel, an autoclave, was equipped with a HPLC pump (Figure 2.3) for addition of the

monomer of the 2nd block and incorporation of crosslinker during synthesis. Hence, an additional inlet for the HPLC tap is built into the autoclave head. The reaction vessel is equipped with a pressure release valve as a safety feature to cause an electrical trip which disconnects power to the heating bar, reducing the temperature and subsequently the pressure. This event will take place if the reaction pressure exceeds the maximum limit, 300 bars.

The base of the autoclave is held together with the head by a clamp and sealed with an O-ring. A unique key is used to lock or unlock the clamp for the final sealing of the autoclave. The heating jacket fits around the autoclave base and is controlled throughout the reaction by Cal 3200 digital heating controller (RS, UK) (Figure 2.2b). The temperature throughout the reaction was monitored by a thermocouple (K-type). In addition, the pressure was monitored by a quartz piezoelectric transducer (345 bars, RDP Electronics) connected to a digital read out box. The stirrer was driven by a stirring motor (IKA Eurostar Digital) with stirring rates ranging between 50 rpm-2000 rpm.

2.1.2.1 Standard Operating Procedure

To maintain safety a standard operating procedure was followed for each high-pressure reaction and is detailed in this section.

- 1) The autoclave was assembled by clamping the head and base together and sandwiching an O-ring between them. The clamp was locked by fastening with the safety key, which was then secured into the autoclave's head. Subsequently, the inlet and outlet pipes were connected to the high-pressure circuit and tightened with spanners.

Do's & Don'ts/ Tips & Tricks:

- a) Do grasp both spanners with one hand while tightening the joint. This will prevent overtightening.
- b) Don't tighten too much as it can shorten the life of the internal thread.

2) A leak test was carried out by pressurising the autoclave to approximately 100 bar and with 'Snoop' all leak fittings were inspected.

Do's & Don'ts/ Tips & Tricks:

- a) Do pressurise at a pressure greater than 100 bar (for example, 140 bar) if the reaction will take more than 24 hours. This is to ensure the system is leak-free.
- b) Don't forget to connect the internal thermocouple to monitor the temperature of the system with pressure introduction.
- c) Don't spill the snoop while inspecting the fittings, as it can cause a trip if it gets onto the heating jacket. Use tissue to avoid spilling.

3) The autoclave was vented to ambient pressure through the outlet tap if leaks were spotted. The leaking fittings were then adjusted.

Do's & Don'ts/ Tips & Tricks:

- a) Use a bit of Teflon tape to seal the safety key if the leak is spotted at this part.
- b) Don't tighten fittings while the autoclave is under pressure.

4) In the case of block copolymer synthesis, the HPLC pump was connected to the autoclave set-up with the adapter nut in the autoclave's head. The pipework from the HPLC pump was also leak tested at the same condition as above.

Do's & Don'ts/ Tips & Tricks:

a) Do check the flowrate of the HPLC pump by running through acetone and closing the tap at one point to ensure it can hold the pressure.

5) Then step 2 and 3 were repeated until no leaks were detected. The autoclave was then vented to atmospheric pressure and the safety key was opened to purge the autoclave with a CO₂ flow at around 2 bar while weighing and degassing the reactants.

Do's & Don'ts/ Tips & Tricks:

a) Don't forget to close the outlet tap before purging the autoclave.

6) The reactants, including RAFT agent, initiator, surfactant, and monomer, were then added into the autoclave through the open key hole under a positive pressure of CO₂, to avoid oxygen entering the vessel.

Do's & Don'ts/ Tips & Tricks:

a) Use a syringe and long needle to add the reactant into the autoclave.

b) To grow the block copolymer, weigh the powder of the 1st block into the autoclave body.

7) The autoclave was then sealed by the safety key and pressurised to approximately 50 bar. The stirrer was turned on to stir the reactant and the required speed was set accordingly.

Do's & Don'ts/ Tips & Tricks:

a) The ideal speed to begin with is 300 rpm. A higher speed (up to 450 rpm) can give better homogenisation in stirring for the block copolymer synthesis.

b) Don't forget to connect the heating jacket to the control box and set temperature to 0 °C.

8) The autoclave was then set to the required temperature and pressure. The typical temperature and pressure for particles reactions was 65 °C and 207 bar (The safety limit of the pressure set for the system is 310 bar).

Do's & Don'ts/ Tips & Tricks:

- a) First, heat the autoclave to 55 °C and let it stabilise.
- b) Then, gradually add CO₂ to pressurise to approximately 152 bar. If the temperature drops, stop pressurisation and allow to stabilise before resuming pressurisation.
- c) Finally, increase the temperature to 65 °C and top up CO₂ to 207 bar, the final required pressure before allowing it to stabilise.

9) The reaction was left to proceed for as long as it was necessary.

Do's & Don'ts/ Tips & Tricks:

- a) Don't forget to close the inlet tap.

10) The autoclave was allowed to cool to room temperature by setting the temperature on the control box to 0 °C upon the completion of reaction time. Then the stirrer was switched off, and the autoclave was vented.

Do's & Don'ts/ Tips & Tricks:

- a) Don't depressurize the autoclave rapidly since some particles, such as PMMA, become more electrostatic and difficult to handle, particularly during the weighing process.

11) The clamp was then removed by unscrewing the safety key and the Swagelok fittings were loosened to collect the final product.

Do's & Don'ts/ Tips & Tricks:

- a) If the polymer product synthesised is a soft material with a low transition glass (T_g) temperature or low molecular weight (for example, PMMA with $M_n=15,000$ kDa), cool down the autoclave

- further to 10 °C by immersing it in an ice-bucket before slowly pressurising it. This will increase the chances of getting particles.
- b) Don't forget to remove the heating jacket before immersion into the ice-bucket.

2.1.3. *In-situ* monomer and cross-linker addition via HPLC Pump

The additional equipment namely a HPLC pump is attached to the autoclave set-up to enable the *in-situ* addition of monomer or crosslinker. In the case of block copolymer synthesis, the addition of monomer to grow the second block is done after the polymerisation of the first block. The schematic of the set-up is shown in figure 2.3.

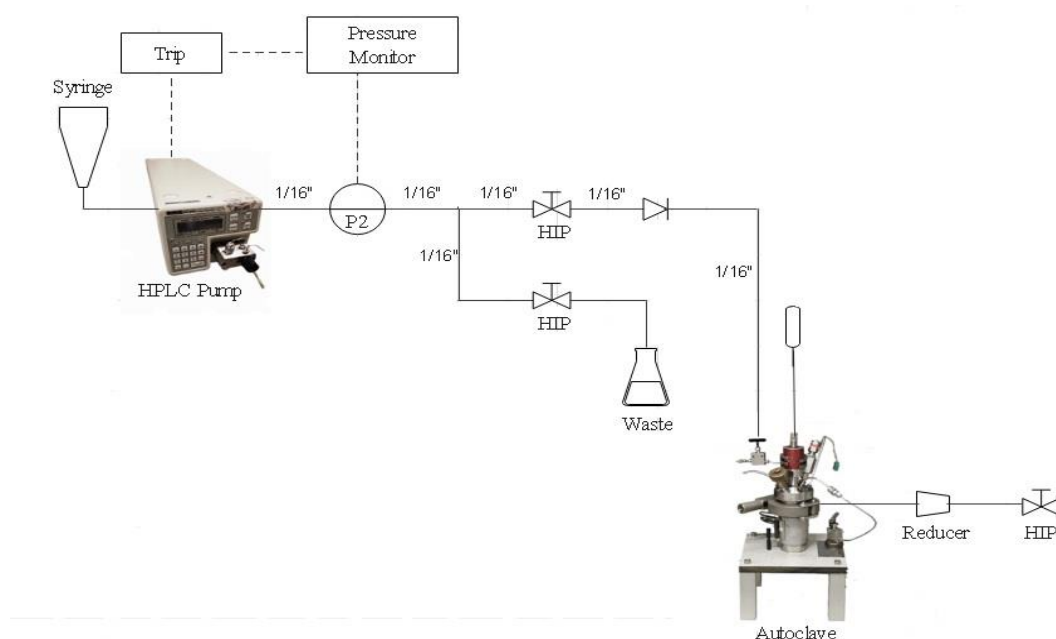


Figure 2.3. Schematic of the set-up for the HPLC pump attached to the high-pressure autoclave in $scCO_2$ reaction.

The following is the standard operating procedure for monomer addition via a HPLC pump:

- 1) The procedure continues on from the standard operating procedure as mentioned in section 2.2.2.1 no. 9.

Do's & Don'ts/ Tips & Tricks:

- a) Don't forget to disconnect the outlet piping of HPLC pump from the autoclave head after the leak test as stated above in section 2.2.2.1 no. 4.

- 2) The appropriate amount of solvent was pumped into the outlet piping through the purge setting of the HPLC pump, and the outlet tap to the purge vial was opened to allow the solvent to flow out, leaving the pipe empty to approximately 5cm from the syringe end. The syringe was later replenished with monomer or monomer-crosslinker solution as needed for the reaction. The 5cm gap between solvent and monomer solution is important to prevent them from mixing.

Do's & Don'ts/ Tips & Tricks:

- a) Use solvent that can solubilise the monomer for example acetone is suitable for methyl methacrylate.
- b) This step is a good trick to ease the addition of monomer solution via the HPLC pump.

- 3) The monomer or monomer-crosslinker solution from the syringe was next pumped into the pipework until it reached the end of the pipe before connecting it to the HPLC inlet tap on the autoclave head.

Do's & Don'ts/ Tips & Tricks:

- a) Use tissue to detect if the monomer has reached the end pipe since the acetone is quickly dried compared to the monomer solution.

4) The flow rate of addition was set on the HPLC control panel and the pipe filled with monomer was connected to the HPLC inlet tap on the autoclave head. The pumping continued to cause the pressure of the HPLC pump to increase to almost the same level as the current pressure in the autoclave.

Do's & Don'ts/ Tips & Tricks:

a) The typical flow rate used for monomer addition by HPLC pump is 1 mL/min. If the addition caused particle fusion, reduce the flow rate to less than 1 mL/min.

5) The HPLC tap was then opened, once the same pressure was reached, to allow the process of monomer addition into the autoclave. Utilize the stop watch to obtain the required volume.

Do's & Don'ts/ Tips & Tricks:

a) If the pressure in the autoclave surpassed 275 bar following the addition process, slowly vent it through the outlet tap before leaving it to polymerise.

6) When the required volume of monomer is added, the HPLC pump is turned off and the HPLC inlet tap on the autoclave head is closed. Before disconnecting the HPLC setup from the autoclave, the outlet tap on the HPLC pump was opened to relieve residual pressure.

7) The HPLC setup was then disconnected from the autoclave by loosening the fitting that connected the outlet pipe to the autoclave head's inlet HPLC tap. Use the tissue and a beaker to collect any remaining monomer solution from the pipe.

8) The HPLC pipes were then rinsed with solvent to prevent the pipework from becoming clogged with residual monomer solution. The residual monomer solution might polymerise inside the pipe over time.

2.1.4. Sampling under pressure

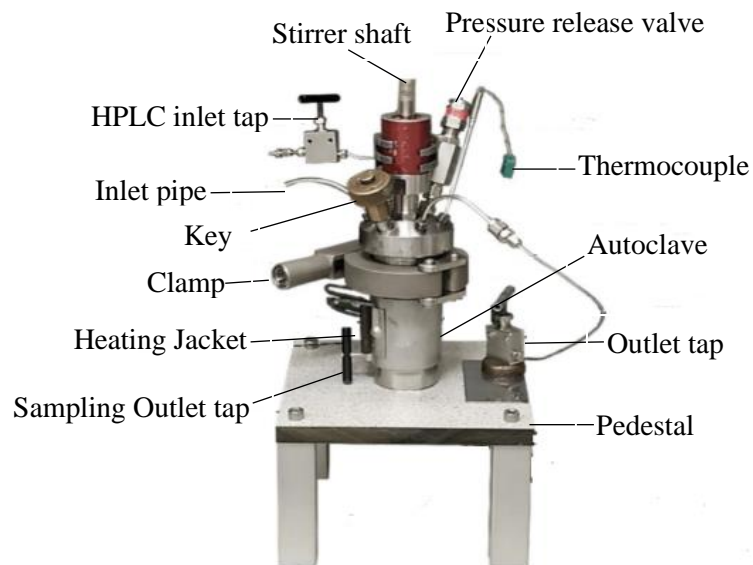


Figure 2.4. The Autoclave set-up for sampling under pressure.²

- 1) A sampling tube was put into the autoclave's bottom cavity and fastened in place with an autoclave engineer nut to facilitate sampling under pressure. The sampling outlet tap (Figure 2.4) was then opened for about 10 seconds before closing and removing the sampling tube.
- 2) Each time interval was usually divided into three to five aliquots. The first sample was discarded, and the remaining four were taken for testing.

OR

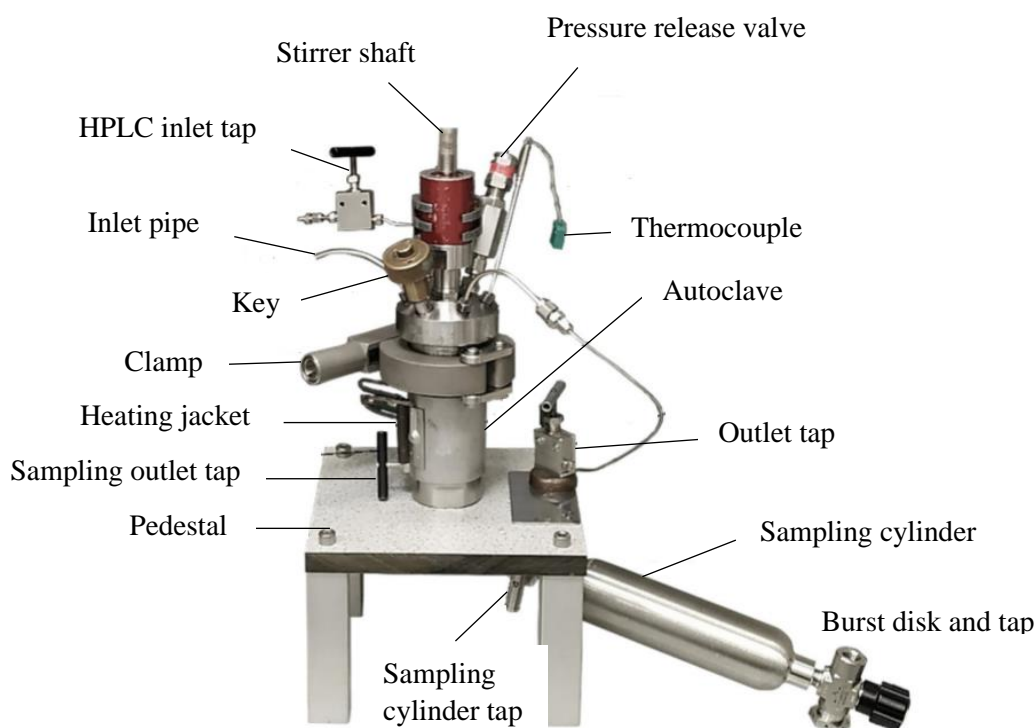


Figure 2.5. An Autoclave set-up with on-line high pressure reaction sampling unlocked with the cylinder system.²

- 1) The sample cylinder was loaded with 5 ml of a deuterated solvent prior to on-line sampling. An internal standard can be introduced to the solvent if necessary.
- 2) The resulting mixture was analysed immediately by NMR using a deuterated solvent, but basic lab solvents can also be employed. The Autoclave Engineer connection was then used to connect the cylinder system to the sample output.
- 3) CO₂ was supplied to the autoclave with all taps tightly closed to increase the internal pressure by 15 bar. The sampling outlet tap was then opened, causing the pressure to drop by 15 bar and filling the 1/8-inch tube with roughly 0.18 ml of autoclave content.

- 4) The sample cylinder tap was opened after the sampling outlet tap was closed. The contents of the high-pressure 1/8-inch tube are released directly into the cylinder chamber and collected in the deuterated solvent.
- 5) The cylinder system was then removed from the autoclave, and the sample, which had been dissolved in the selected deuterated solvent, was recovered by pouring the contents back down the 1/8-inch tube into a glass vial.

2.2 Analytical Techniques

2.2.1 Nuclear Magnetic Resonance Spectroscopy (NMR)

Determination of percentage conversion of monomer to its polymer was conducted by using proton nuclear magnetic resonance (^1H NMR). In addition, this technique was utilised in the analysis of the block copolymer to determine the weight fraction of polymer blocks. Polymers obtained were dissolved in CDCl_3 , at a concentration ranged between $0.3 - 0.5 \text{ mg mL}^{-1}$, filtered and analysed by a Bruker DPX 400 MHz spectrometer. Peaks distinctive to the polymer and the monomer (Table 2.1) were integrated for the calculation.

Table 2.1. List of ^1H NMR chemical shift regions for monomers and polymers referred in this study.

Polymer	Monomer Chemical Shift in CDCl_3 (ppm)	nH	Polymer Chemical Shift in CDCl_3 (ppm)	nH
PMMA	3.8	3	3.6	3
P4VP	5.5	4	6.1-6.8	2

By integrating the polymer peaks for each block, the weight fraction of PMMA within a block copolymer, PMMA-*b*-P4VP was calculated. The peak intensities (I_{block}) were then normalised to the number of protons (nH_{block}) to determine the degree of polymerisation fraction of PMMA (DPf_{PMMA}) (Equation 2.1).

$$DPf_{PMMA} = \frac{\frac{I_{block1}}{nH_{block1}}}{\left(\frac{I_{block1}}{nH_{block1}}\right) + (I_{block2}/nH_{block2})} \quad \text{(Equation 2.1)}$$

The DPf_{PMMA} results was then used to calculate the PMMA weight fraction by taking into account the monomer molar masses (Mr_{MMA} and Mr_{4VP}) using Equation 2.2.

$$W_{PMMA} = \frac{DPf_{PMMA} \times Mr_{MMA}}{(DPf_{PMMA} \times Mr_{MMA}) + (DPf_{P4VP} \times Mr_{4VP})} \quad \text{(Equation 2.2)}$$

2.2.2 Differential Scanning Calorimetry (DSC)

The temperature at which a polymer changes from a hard, glassy state to a soft, rubbery one is known as the glass transition temperature (T_g). It varies from polymer to polymer, hence it is useful for identifying a polymer. The T_g of polymeric materials synthesised in this study was obtained using differential scanning calorimetry (DSC). This is a technique which compares the difference between the energy input into a substance and a reference (or blank) as a function of temperature (or time), while both the reference and the sample are subjected to a controlled temperature rise.³

The sample (1-5 mg) was weighed into a T-zero sample pan (TA instruments) with a reference T-zero pan remaining empty. The pans were heated at a rate of 10 °C min⁻¹, from -80 °C to 250 °C for block copolymer, PMMA-*b*-P4VP samples. The analysis was carried out on a TA-Q2000 (TA Instruments) that was calibrated with an indium standard under nitrogen gas flow. To remove any thermal history of the individual samples, two heating cycles were recorded, with the T_g being measured from the second cycle. The data were analysed with Universal Analysis software.

2.2.3 Gel Permeation Chromatography (GPC)

Gel Permeation Chromatography (GPC) was used to analyse the molecular weight and dispersity of polymer samples in this study. In the case of PMMA, it was performed in THF as mobile phase at ambient temperature using Agilent mixed-C column in series with a flow rate of 1 ml/min. This system was equipped with both Multi Angle light scattering (MALS) detection (DAWN 8⁺) and differential refractometer (dRI). Whilst in the case of block copolymer, PMMA-*b*-P4VP mixture of chloroform/ethanol/triethylamine (90/10/0.5 by volume)⁴ was used as a mobile phase in conjunction with Agilent mixed D column (at flow rate of 0.5 mL min⁻¹ and 25°C) by another GPC unit with Wyatt module for Refractive Index (dRI) detection (Optilab rEX). Both dRI detectors were calibrated with PMMA narrow standards with molecular weight ranging from 750 to 1.8 x 10⁶ g mol⁻¹. Responses from the detector were analysed by the ASTRA 6.1 software.

Samples were dissolved in the solvent at approximately 1-5 mg mL⁻¹ and filtered prior to injection through 0.45 µm PTFE syringe filters (Agilent). A blank sample (solvent used to dissolve the GPC sample) was always analysed at the start of the sample queue as a quality control check of the GPC system.

2.2.4 Scanning Electron Microscopy (SEM)

Scanning Electron Microscopy (SEM) was utilized to characterise the overall polymer microparticle morphology. This analysis required a specific sample preparation. Some dried fine powders were mounted on aluminium SEM stubs using carbon tape. Subsequently, the stubs were coated with a platinum (Pt) layer prior to analysis (~6 – 8 nm). These coating prevent sample damage and minimise charge build up during imaging process. The stubs were then placed in a JEOL 6490LV SEM for imaging analysis at low magnification ranging from 500-10,000x. Higher magnification imaging, of the porous samples in particular, was carried out using a JEOL 7000F FEG-SEM at an accelerating voltage of 5kV.

In addition to particle morphology, the particle sizes were also calculated from the images by taking the average diameter of 100 particles using the ImageJ[®] software. The particle size distribution was evaluated from the coefficient of variance value derived from Equation 2.3.

$$Cv = \left(\frac{\sigma}{Dn} \right) \times 100 \quad (\text{Equation 2.3})$$

2.3.5 Transmission Electron Microscopy (TEM)

The internal morphology behaviour of PMMA-*b*-P4VP block copolymer particles was imaged using transmission electron microscopy (TEM). As sample preparation, microparticles of non-porous samples were embedded in epoxy resin (Agar 100) and cured at 55 °C for 48 hrs. Thin sections (~80-100 nm) of the embedded samples were microtomed using an RMC MT-X ultramicrotome with a diamond knife (Leica Diatome Ultra 45^o) at room temperature. The microtomed sections were floated on water and subsequently placed on copper TEM grids (Sigma Aldrich). The sections of the PMMA-*b*-P4VP were stained with Iodine vapour, which selectively

adsorbed to non PMMA domains, for about 2 hrs. The staining provides additional contrast in the TEM images.^{1, 5, 6}

The porous microparticle samples were mounted similarly, but were cut with a cryo-ultra-microtome. The samples were initially placed on the surface of a drop of sucrose solution (5%) on a sample stick before being frozen in liquid nitrogen. Using a glass knife, the frozen microparticles were ultra microtomed into thin pieces of 100 nm at 60 °C. These copper grid cross-sections were then photographed using a FEI Tecnai BioTwin-12 TEM at 100 kV at room temperature.

Imaging of the samples took place on a FEI Tecnai BioTwin-12 microscope in bright field mode. The accelerating voltage was 100 kV. The images were acquired using a Gatan SIS Megaview IV digital camera. The beam intensity, magnification and image focus were adjusted during imaging to obtain the best image of the analysed samples. The internal domain sizes were measured by counting over 100 domains in the TEM images using the ImageJ[®] software.

2.3.5.1 Tilt TEM Tomography

A JEOL 2100Plus equipped with a Gatan US1000 CCD camera at 200 kV was used to record images manually at 1-degree steps in a single axis tilt series, using a Gatan 916 room temperature tomography holder. Post-acquisition alignment and reconstruction was performed using the IMOD software (<http://bio3d.colorado.edu/imod/>) utilising the WBP and SIRT reconstructions. The sample was initially prepared by depositing onto a lacey carbon support TEM grid pre-prepared with 10nm gold fiducial markers to aid computer alignment. This technique was used to give a fully 3-dimensional structure projection which is not readily comprehended in a 2-dimensional conventional TEM.⁷

2.3.6 Dynamic Light Scattering (DLS)

This is a well-established technique for measuring the size and size distribution of particles in suspension. Powder samples were washed by centrifuging in dodecane 1-3 times (10 minutes, 4000 rpm), before being dried in vacuum oven. Subsequently, a 0.25 wt.% solids dispersion in dodecane was prepared with 3 wt.% Span-85 as a dispersing agent. This mixture was then homogenised using a sonicator and shaker. A minimum of 1 mL was transferred into a glass cuvette and placed into the instrument compartment for analysis. The particle size and distribution of samples were obtained by Dynamic Light Scattering (DLS) Malvern Instruments Zetasizer.

2.3.7 Porosimeter by Tri-star Machine

The porosity and surface area of the produced samples were determined using a N₂ adsorption technique at 77 K on a Micromeritics ASAP 2420 equipment. Prior to the measurements, the samples were degassed for 16 hours at 70 °C. The surface area was calculated using the Brunauer–Emmett–Teller (BET) method and N₂ adsorption isotherm data between 0.05 and 0.3 relative pressure. Using the Micromeritics programme, the density functional theory (DFT)⁸ approach was applied to extract the pore size distribution from the adsorption branch. When a material has both mesopores and macropores, it is required to evaluate the pore width distribution in terms of pore volume and surface area; mesopores add to surface area, whilst macropores greatly enhance pore volume.

2.4 References

1. M. Alauhdin, Thesis (PhD)--University of Nottingham, 2017., 2017.
2. K. Kortsen, A. A. C. Pacheco, J. C. Lentz, V. Taresco and S. M. Howdle, *The Journal of supercritical fluids*, 2021, **167**.
3. D. Walton and P. Lorimer, *Polymers.*, Oxford Science Publications, United States, 2000.
4. M. Shoji, M. Eguchi, J. M. Layman, M. P. Cashion, T. E. Long and H. Nishide, *Macromolecular chemistry and physics*, 2009, **210**, 579-584.
5. J. Jennings, Thesis (PhD)--University of Nottingham, 2013., 2007.
6. G. He, T. M. Bennett, M. Alauhdin, M. W. Fay, X. Liu, S. T. Schwab, C.-G. Sun and S. M. Howdle, *Polym. Chem.*, 2018, **9**, 3808-3819.
7. G. He, T. M. Bennett, K. Alias, L. Jiang, S. T. Schwab, M. Alauhdin and S. M. Howdle, *Polymer Chemistry*, 2019, **10**, 3960-3972.
8. Y. Ren, Z. Ma, R. E. Morris, Z. Liu, F. Jiao, S. Dai and P. G. Bruce, *Nature communications*, 2013, **4**, 2015-2015.

Chapter 3

Synthesis of Homopolymer, PMMA and Block Copolymer, PMMA-*b*-P4VP by Dispersion Polymerisation in Supercritical Carbon Dioxide

The first stage in the synthesis route of crosslinked microparticles was the formation of homopolymer, namely poly(methyl methacrylate) (PMMA) that has been utilised as a first block of the block copolymer in this study. Initially, both free radical (FRP) and controlled radical polymerisation (CLRP) techniques were utilised, with the aim of producing dry, free-flowing powders through dispersion polymerisation in scCO₂. The findings from both these techniques were compared and discussed further, by comparison of characterisation obtained from various analytical techniques. Subsequently, chain extension of these polymers was performed to achieve the nanostructured-block copolymer PMMA-*b*-P4VP microparticles, via reversible addition-fragmentation chain transfer (RAFT) dispersion polymerisation in scCO₂. Two different techniques that had been previously developed within the group and yielded the desired morphology of phase separation, namely spherical (SPH) and lamellar (LAM), were used. This study effectively created an optimal approach for producing a fine, free-flowing powder of block copolymer with an internal LAM nanostructure. This block copolymer, which was synthesised using both processes, will be examined in further detail in this chapter. It was synthesised in a variety of sizes and internal nanostructures.

3.1 Introduction

Previously in the group, block copolymerisation of various types of monomers has been carried out. A key characteristic of the monomers previously studied is their ability to dissolve in scCO₂. Hence, vinyl compounds including methyl methacrylate, vinyl pyridine, styrene and acrylamide are the most heavily reported in the literature.¹⁻¹¹ Based on these findings, this study focused on two monomers, namely methyl methacrylate (MMA) and 4-vinyl pyridine (4VP).

PMMA is a common and versatile polymer. It has been used widely in a number of applications due to its good properties and well-known performance; rigidity and dimensional stability, excellent optical properties, hardness and resistance to scratching, transparency and outstanding resistance to sun rays and weather aging.^{12, 13} It is physically a stiff, hard and colourless polymer, with a T_g range of 100 °C to 130 °C depending on its chain length and architecture.^{14, 15} It has been reported to play an effective role in providing a good propagating radical in block copolymerisation as a "living" CO₂-insoluble first block.¹⁶ In previous theses, as reported by Gregory in 2008, Jennings in 2007 and Mohammad in 2017, a variety of monomers, including *N,N*-dimethyl amino ethyl methacrylate, ethyl methacrylate, *n*-butyl methacrylate, tert-butyl methacrylate, 1H,1H,2H,2H-perfluorooctyl methacrylate, benzyl methacrylate, *N,N*-dimethyl acrylamide, styrene and 4-vinyl pyridine were chain extended from PMMA in scCO₂ to produce block copolymers with varied degrees of success.^{1, 7, 17}

Unlike PMMA, P4VP is a physically flexible polymer chain with high stability, good pH responsiveness and biocompatibility, with a very different T_g from PMMA (150 – 160 °C).¹⁸ The unique functionality of the nitrogen

within the aromatic pendants yields basicity and coordinative ability to P4VP, providing potential for chemical modification. It is also a well-known chelating agent for a wide range of inorganic species.¹⁹ This feature enables its application in electronic, optical, catalytic, and photonic materials (to name just a few).²⁰⁻²² PS-*b*-P4VP has been identified as a good block copolymer for aqueous metal reduction, due to the presence of a genuine chemical bonding site in the nitrogen-donating pyridine group. The acidic composition of the medium used penetrated the hydrophobic PS block and swelled the P4VP block, enabling metal ions to coordinate within nanodomains.²⁰ Additionally, the capability of P4VP to selectively synthesise gold nanoparticles as a result of the strong association between the P4VP block and the substrate via a multilayer of LAM parallel formed with the PS block, PMMA-*b*-P4VP, was reported.²³ M.B. Gawande et al. prepared a catalyst using a micelle solution of PS-*b*-P4VP to act as photocatalyst for water splitting.²²

Thus, the combination of these two blocks, PMMA and P4VP, is investigated further in this study in order to uncover additional properties that may be generated via dispersion polymerisation in scCO₂. The use of green synthesis routes involving supercritical carbon dioxide in the production of polymers is an area of focus in our group. Numerous attempts have been made to utilise this technology to improve and gain insight into a variety of processes, most notably the conventional processing and synthesis of polymers. A simple one-pot method for the synthesis of PMMA was developed, which resulted in a fine free-flowing powder with confirmation of discrete particles produced by microscopy analysis.²⁴ The set-up of a 1 L reactor was recently established to enable the scale-up of these reactions, with comparable results to the small scale, 60 mL standard autoclave in the group reported.²⁵ More recent progress includes the development of a more adaptable and reliable on-line sampling system for

polymerisation reactions in scCO_2 , allowing for more in-depth study of the reaction kinetics.²⁶

However, further advancement is required to improve the quality of the block copolymer particles produced using a two-stage reaction. The addition of monomer to the first block, resulting in chain extension, was carried out via HPLC pump into the high-pressure autoclave. This method allows for gradual exposure of the growing particles to newly added monomer, which if not controlled may result in particle fusion.¹ A novel and versatile method for the preparation of nanostructured block copolymer microparticles was also developed via a two-stage procedure, utilising the living nature of pre-synthesised RAFT functional polymer chains. Additionally, the PMMA was reactive/living even after months of storage. As a result, large batches of PMMA living microparticles can be produced and stored, ready for further processing on demand.⁷

3.2 Materials

Methyl methacrylate (MMA, ProSciTech, 99%) and 4-vinylpyridine (4VP, Acros, 99%) were purified by passing through a neutral alumina column and stored at $-20\text{ }^\circ\text{C}$. 2,2'-azobis(isobutyronitrile) (AIBN, Sigma Aldrich, 98%) was re-crystallized in methanol. Methacrylate-terminated polydimethylsiloxane (PDMS-MA, $M_n = 10,000\text{ g mol}^{-1}$, ABCR GmbH & Co.), 2-(dodecylthiocarbonothioylthio)-2-methylpropionic acid (DDMAT, Sigma Aldrich, 98%, HPLC Grade), 2-yno-2-propyl dodecyl-trithiocarbonate (CPDT, Sigma Aldrich, 97%, HPLC Grade), CDCl_3 (Aldrich, 99.9%), HPLC grade THF (Acros), chloroform (Aldrich, 99.9%), and iodine (Fisher) were all used as received. Agar 100 resin (Agar Scientific) was used as received, and a formulation of medium hardness was used for embedding samples.

High purity carbon dioxide (>99.99%, BOC Gases, SFC Grade) was also used as received.

3.3 Methods

3.3.1 Synthesis of PMMA by Free Radical Polymerisation (FRP)

Synthesis of PMMA by free radical polymerisation reactions were carried out in a 20 mL stainless-steel high-pressure autoclave fitted with an overhead stirrer with a suitably designed paddle blade and motorized driver controlled at 300 rpm. Before each reaction, the autoclave set-up was leak tested by pressurising to approximately 800 psi and all the joints were checked with 'snoop', a leak detecting fluid. The reactant mixture, consisting of MMA (3.33 mL), AIBN (1 wt% with respect to MMA) and PDMS-MA (5 wt% with respect to MMA), was degassed by bubbling with argon and stirring with a magnetic bar for about 30 minutes to remove the oxygen. During this period the autoclave was purged with CO₂ (~ 30 psi) and left under positive pressure by opening the keyhole.

After degassing, the reactant mixture was injected into the autoclave by using a glass syringe under a positive pressure of CO₂ (15-40 psi). The autoclave was sealed, pressurised to 650 psi, heated to 65 °C and gradually pressurised further to the reaction pressure of 3500 psi over a period of 5 mins. The reaction was left to stabilise and then stirred at 300 rpm for 4 hours. The autoclave was then allowed to cool to room temperature by setting the temperature of the control box to 0 °C and depressurised once below 30 °C prior to product collection.

3.3.2 Synthesis of PMMA by RAFT Polymerisation

The following experiments were performed in an attempt to establish good reproducibility of PMMA microparticle synthesis by RAFT dispersion polymerisation. The reaction was carried out in a 20 mL autoclave, with the same reaction condition as discussed in Section 3.3.1. The experiment was started with the leak test, followed by the degassing the reactant mixture consisting of MMA (3.33 mL, 31.26 mmol), DDMAT (21.66 mg, 0.0594 mmol), AIBN (10.28 mg, 0.0626 mmol), and PDMS-MA (157 mg, 5 wt.% with respect to MMA) for about 20-30 minutes. Subsequently, the mixture of reactants was injected into the autoclave under a positive pressure of CO₂ (15-40 psi).

The autoclave was then sealed, pressurised to 650 psi, heated to 65 °C and pressurised further to the reaction condition for about 3500 psi gradually, which took approximately 15-20 minutes, and left to stabilise under stirring at 300 rpm for 24 hours. Once the reaction was completed, the temperature was set to 0 °C and autoclave was allowed to cool to room temperature before being depressurised. The resulting products were collected and kept in a sealed glass vial for future chain extension of block copolymerisation.

3.3.3 Synthesis of BCP PMMA-*b*-P4VP via two consecutive RAFT polymerisation

Initial trials of synthesising the block copolymer of PMMA-*b*-P4VP with targeted molecular weight of 50,000 g/mol for the PMMA first block and 33,000 g/mol for the P4VP block were performed. The experiment followed the well-established high-pressure 20 mL autoclave setup as employed in

the previous experiments in Sections 3.3.1 and 3.3.2. The first block polymerisation of PMMA, conducted as described above in section 3.3.2, consumed 2.5 g MMA (24.9 mmol), 18.33 mg DDMAT (0.0503 mmol), 8.33 mg AIBN (0.0507 mmol) and 0.2083 g PDMS-MA. After a given polymerisation time of the first block, 24 hours typically, some sample was removed through the HIP outlet tap (see Figure 2.4 in Chapter 2 for a more detailed illustration) and characterized accordingly.

The second block (P4VP) was then grown from the PMMA macro-CTA microparticles by addition of the monomer into the autoclave, under pressure, using an HPLC pump. Before addition, the mixture of 4VP (1.666 g, 0.0158 mol) and some additional initiator (AIBN, 2.1 mg, 0.0128 mmol) were degassed for about 20-30 minutes. To ensure the reaction was completed in 24 hours, additional initiator was needed because the k_p value (initiator propagation rate constant) of 4VP is relatively low.²⁷ The mixture was then pumped-in through the inlet pipe dedicated for HPLC addition, on the top of the autoclave, at 0.5 mL/ min, once the pressure of the pump reached approximately the same as the autoclave pressure. The reaction was left to further polymerise for 20 hours at about 3500-4000 psi depending on where the final pressure settled down following the addition. In total the whole reaction took 3 days to complete (Figure 3.1).

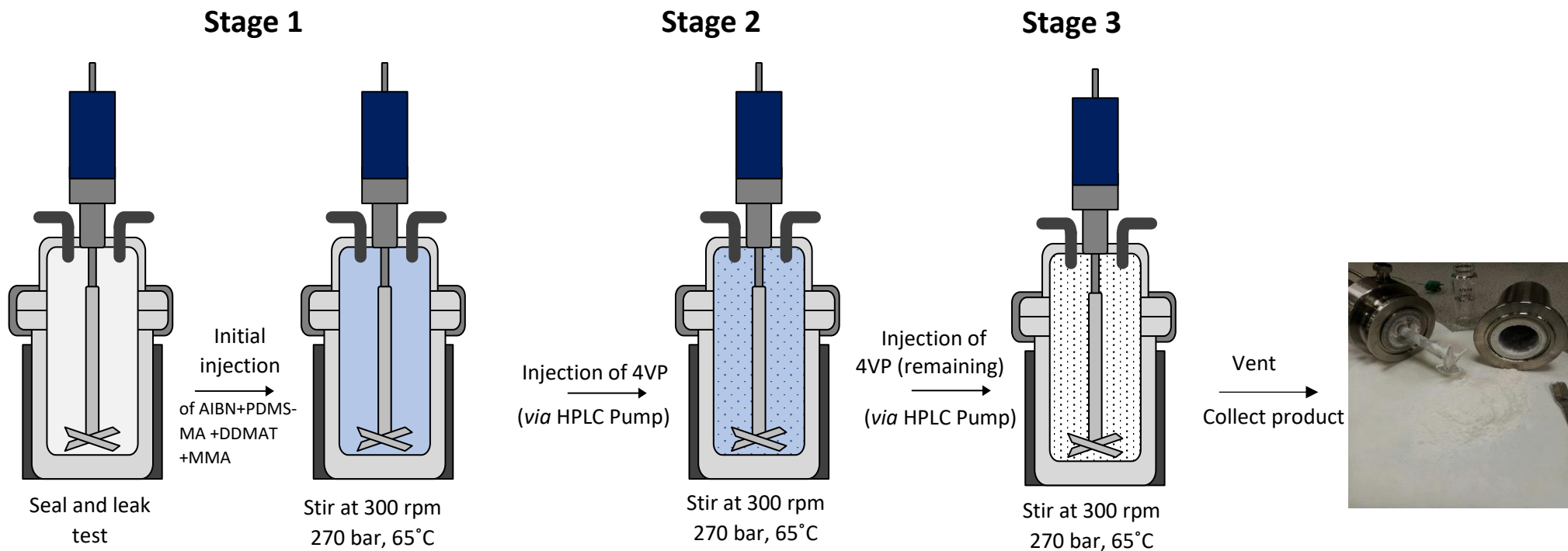


Figure 3.1. Synthesis of BCP via two consecutive RAFT polymerisation.² It involves 3 stages; the initial injection to grow the 1st block PMMA-RAFT particles (stage 1), the injection of certain portion of 4VP for chain extension and induce phase separation morphology (stage 2) and then the injection of the remaining 4VP (stage 3).

3.3.4 Synthesis of BCP PMMA-*b*-P4VP via RAFT in a series of shorter independent steps

a) The polymerisation of PMMA-chain transfer agent (PMMA-CTA) homopolymer was conducted first and this can be stored for future chain extension. The following procedure is a typical way of producing the PMMA-RAFT homopolymer, with molecular weight of 25,000 g/mol. MMA (9.4 g), DDMAT (137.1 mg), AIBN (61.7 mg) and PDMS-MA (0.47 g) were used. Upon completion of the reaction, the autoclave was first cooled to 25 °C then the heating jacket was removed, and the autoclave was further cooled to 10 °C in the ice box before being depressurised. This step is necessary when synthesising PMMA with shorter chain lengths, or low T_g as it tends to form softer product as opposed to dry powder. The product was typically collected as a solid / powder and kept dry at room temperature for further chain extension processes (Figure 3.2).

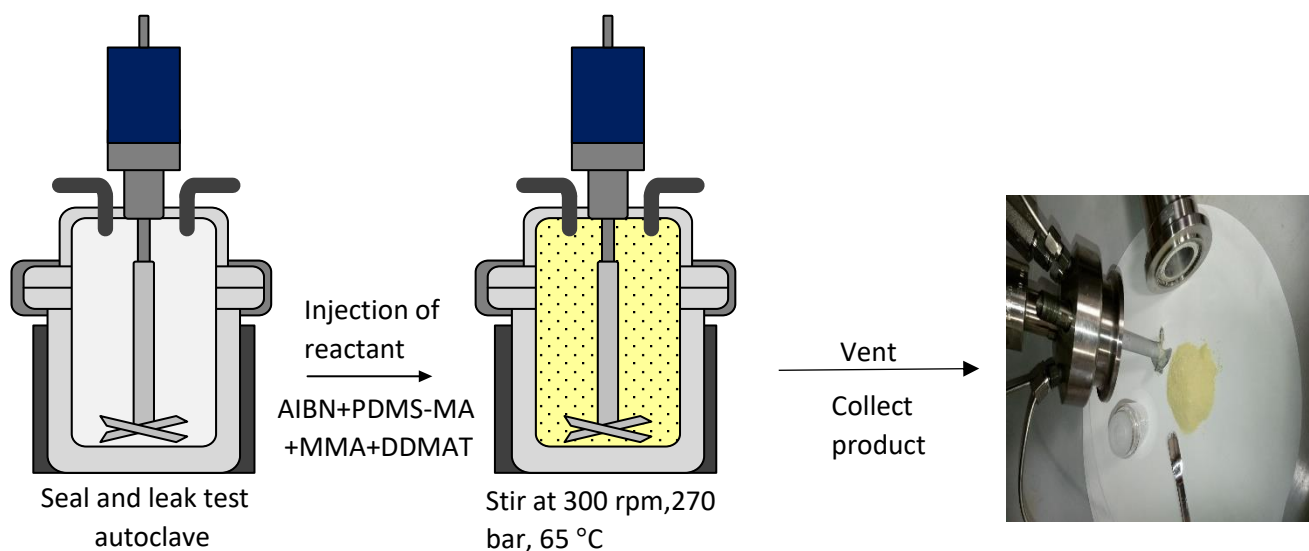


Figure 3.2. Synthesis of RAFT-terminated PMMA homopolymer (PMMA-CTA) by RAFT dispersion polymerisation in $scCO_2$ in a one-pot, batch method. All reactants needed for polymerisation was injected into the autoclave at the start of reaction. The yellow colour shows the presence of RAFT agent, DDMAT.

b) The synthesis of BCP PMMA₂₅-*b*-P4VP₇₅ (where the subscripts denote the target molecular weight values in kg/mol) with total molecular weight of 100,000 g/mol is described as follows. A 60 mL autoclave was charged with pre-synthesised PMMA-CTA (section 3.3.4a) (3.76 g, assumed M_n PMMA = 25,000 g/mol) and PDMS-MA (0.562 mg, 5wt% w.r.t. 4VP) before it was clamped shut and purged with CO₂ (50-60 psi) for 15 minutes. The autoclave was sealed and pressurised with the addition of CO₂ to 800 psi. The stirrer was turned on and adjusted to ~400 rpm. The heater was set to 65 °C and, once reached, additional CO₂ was added to reach a pressure of ~3000 psi and the system was left for ~16 hours for re-dispersion of PMMA-CTA particles. After that, degassed 4VP (11.24 g) and AIBN (24.6 mg) were added via an HPLC pump at 1 mLmin⁻¹. Additional CO₂ was then added as required to reach a final reaction pressure of 3500-4000 psi. The reaction was then left for a further 16 hours. Once the reaction was completed, the heating was removed and the autoclave was allowed to cool to room temperature. The autoclave was then further cooled to 10 °C in the ice box before being depressurised. This step is necessary when synthesising PMMA with shorter chain lengths, or low T_g as it tends to form softer product as opposed to dry powder. The resulting products were collected and kept at room temperature in a sealed vial for characterisation and future chain extension of block copolymerisation (Figure 3.3).

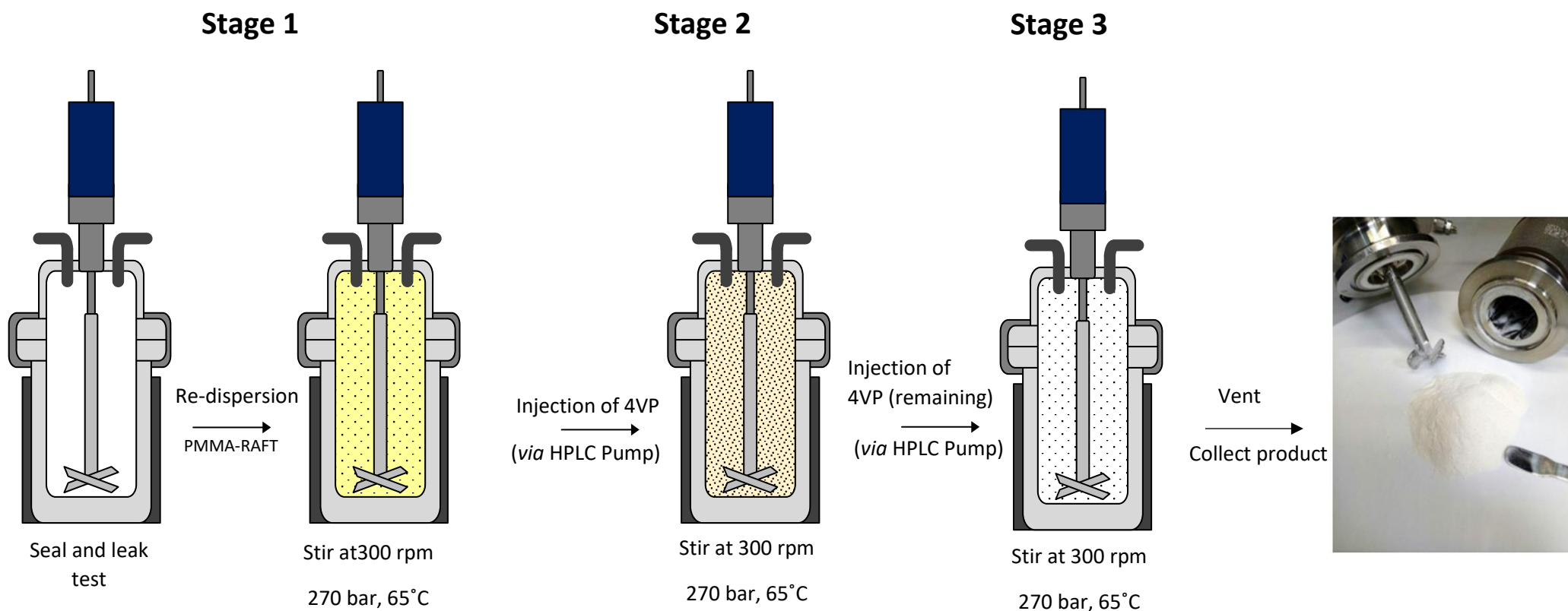


Figure 3.3. Chain extension of PMMA-CTA via high pressure addition of second monomer.⁷ It involves 3 stages; the re-dispersion of PMMA-CTA particles (stage 1), the injection of a certain portion of 4VP for chain extension (stage 2) and the injection of remaining 4VP (stage 3).

3.4 Results and Discussion

3.4.1 Synthesis of PMMA by Free Radical Polymerisation (FRP)

Preliminary reactions to synthesise the PMMA by free radical dispersion polymerisation on the 20 mL scale were designed to explore the reproducibility and repeatability of the process. After optimization good reproducibility and repeatability were obtained as can be seen in Table 3.1 (entry 1-3). The polymers obtained were characterised by GPC to determine the molecular weight, DSC to measure the T_g , NMR to quantify the conversion of the reaction and SEM to observe the morphology of the particles formed.

All reactions produced white, free-flowing powders with a yield of more than 85% (Table 3.1, entry 1-3). The reaction gave high conversion of monomer into polymer ranging from 95% – 99% (Table 3.1, entry 1-3). The conversion of monomer MMA into polymer, PMMA was identified using ^1H NMR, in which the pendant OCH_3 peak shifted from 3.8 ppm to 3.6 ppm in CDCl_3 (Figure 3.5). Similar T_g values to each other were obtained and this was reproducible in repeat reactions (Figure 3.6, Table 3.1, entry 1-3).

Table 3.1. Analysis of PMMA products from 20 mL batch reactions by FRP in scCO_2 .

Entry	Polymer	Yield (%) ^a	M_n (g/mol) ^b	\bar{D} ^a	Conversion (%) ^c	T_g (°C) ^d	Particle Size (µm) ^e
1	PMMA-FRP1	85	177,300	1.4	99	126	1.3 ±0.3
2	PMMA-FRP2	96	179,200	1.5	98	126	1.2 ±0.3
3	PMMA-FRP3	92	153,200	1.5	95	125	1.3 ±0.3

The reactions were conducted at 65°C and 270 bar, stirred at 300 rpm for 4 hrs. The reactants consist of MMA (3.33 mL), AIBN (1 wt.% with respect to MMA), and PDMS-MA (5 wt.% with respect to MMA). ^a determined by gravimetry, ^bdetermined via GPC, ^cdetermined by NMR, ^ddetermined by DSC, ^edetermined by SEM and ImageJ.

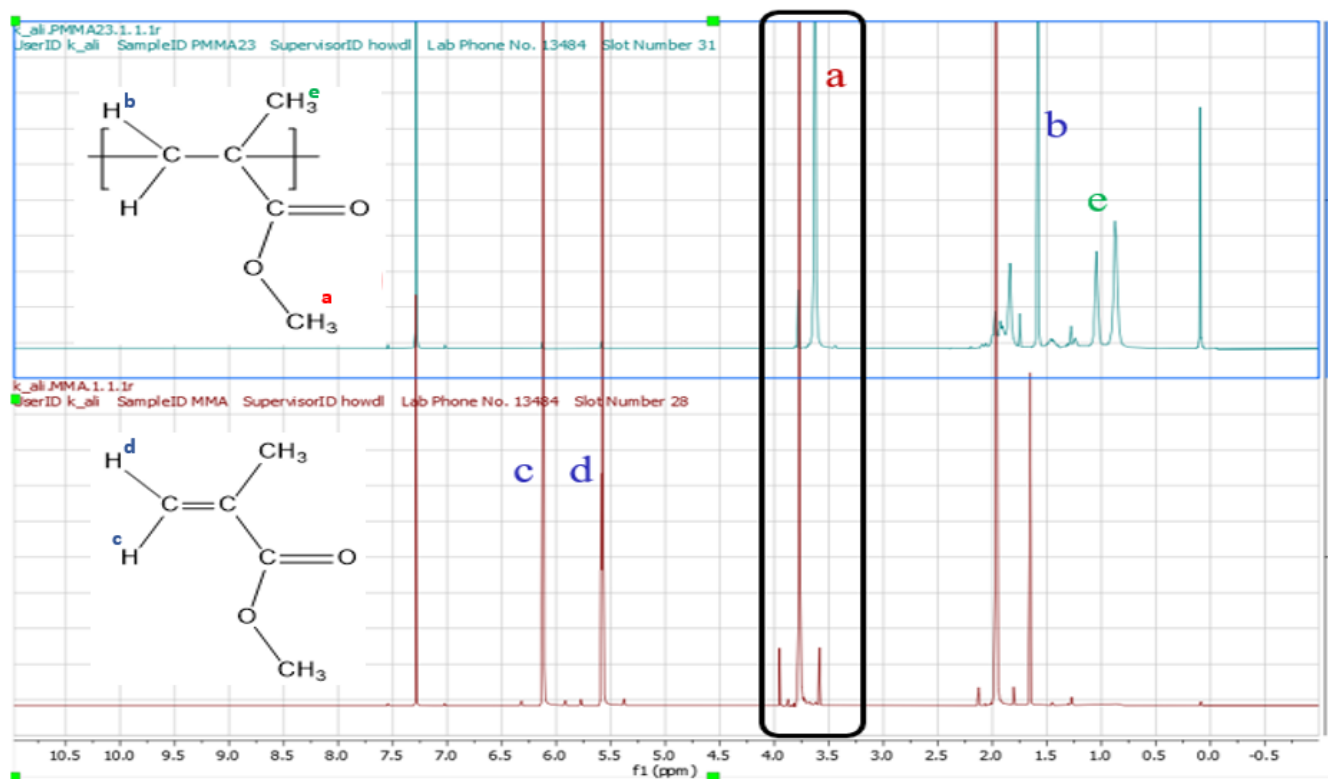


Figure 3.5. ¹H NMR value for MMA (bottom, in red) to PMMA (polymer) conversion (top, in blue). The MMA monomer was confirmed by the two peaks at 6.1 ppm and 5.6 ppm (c and d), which represents vinyl proton. Whereas polymerization of MMA into PMMA was confirmed by the methoxy protons peak shifted from 3.8 ppm to 3.6 ppm (a) and the two peaks at 1.6 ppm and 0.8 ppm (b and e) corresponds to the methylene protons of PMMA main chain in CDCl₃.

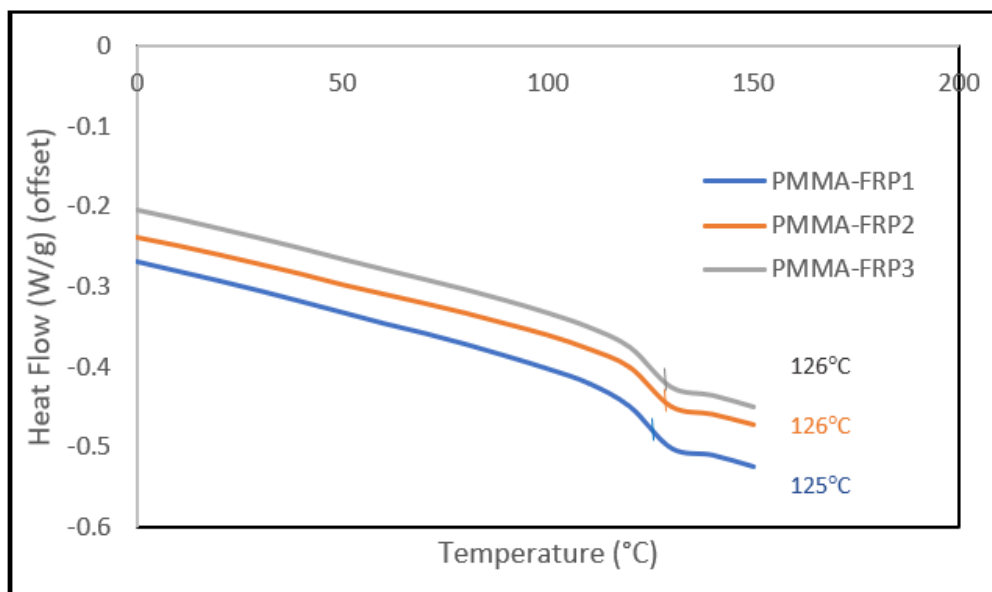


Figure 3.6. DSC of PMMA obtained from repeats of the 20 mL autoclave reaction show a good reproducibility and repeatability (Table 3.1, entry 1-3).

GPC provides the number average molecular weight (M_n) and dispersity (\mathcal{D}) values, which ranged from 153,200-179,200 g/mol and 1.4-1.5 respectively (Table 3.1, entry 1-3 and Figure 3.7). These are comparable to what is typically expected from free radical polymerisation (dispersity value, $\mathcal{D} = 1.5-2.0$) based on the previous study performed by other members in the group and as reported by G. Odian in 2004.²⁸ The dispersity obtained is lower than expected for typical a FRP, likely because the presence of $scCO_2$ increases the overall diffusivity of the system. This has the effect of considerably reducing the large viscosity increase that occurs towards the end of polymerisations in the bulk, thus improving the reaction control.³

The SEM presents clear images showing distinct spherical particles were synthesised successfully for all experiments. All reactions gave similar morphology and shape, with uniform size in the range of 1.2 -1.3 μm (Figure 3.8 and Table 3.1, entry 1-3).

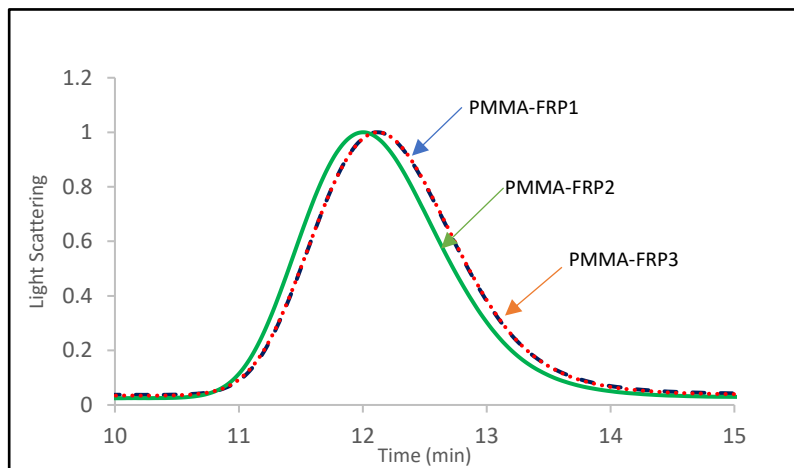


Figure 3.7. GPC traces obtained from repeats (Table 3.1, entry 1-3) of the 20 mL autoclave reaction with good reproducibility and repeatability.

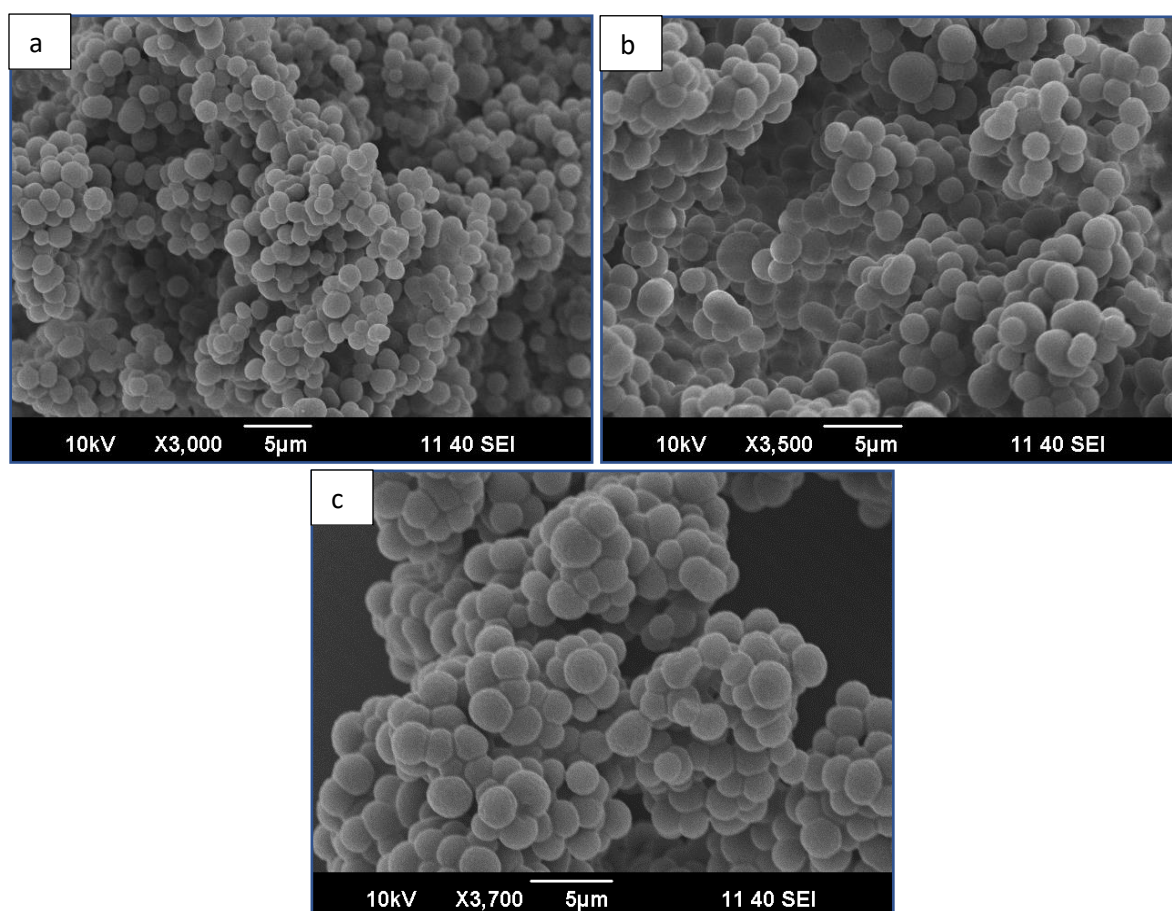


Figure 3.8. SEM images of PMMA synthesised from 20 mL autoclave reactions show a good reproducibility and repeatability of reaction. PMMA-FRP1 (a), PMMA-FRP2 (b), PMMA-FRP3 (c) (Table 3.1, entry 1-3).

3.4.2 Synthesis of PMMA by RAFT Polymerisation

Controlled / living radical polymerisations (CLRP) reactions were carried out to synthesise PMMA by RAFT dispersion polymerisation, once again with the aim of establishing good repeatability and reproducibility. These reactions were performed using two different RAFT agents, namely DDMAT and CPDT in the 20 mL base small-scale autoclave. The triplicates results are presented as shown in Table 3.2. The polymers obtained were characterised using GPC, ^1H NMR, DSC and SEM.

The number average molecular weights (M_n) of the PMMA series were close to the targeted (50,000 g/mol), ranging between 42,600 – 49,500 g/mol (Table 3.2, entry 1-3). The consistently lower molecular weight values of the products when compared with the theoretical values is attributed to the termination of the reactions before 100 % monomer conversion was achieved, as corroborated using ^1H NMR spectroscopy (Table 3.2, entry 1-3). The molecular weight dispersity of each polymer was reasonably low, with values lower than 1.4 across all of the samples (Figure 3.9, Table 3.2, entry 1-3). These values are in agreement with reports by Jennings et al. for the same polymers synthesised with analogous RAFT agents in scCO_2 , indicating that the RAFT process here was controlling the polymerisation effectively.^{1, 2}

To highlight the significant difference in M_n between DDMAT and CPDT as presented in GPC traces (Figure 3.9), the group recently demonstrated that CPDT is one of the most active CTAs and is particularly effective at controlling polymerisation of more activated monomers (MAMs) such as MMA; the cyanoalkyl-R group acts as an effective re-initiation group for MMA.²⁹ This discovery supports the explanation of the closeness of the experimental M_n to the targeted value obtained by CPDT (Table 3.2, entry 1).

The T_g values recorded were also found to be close to each other, ranging from 100 – 116 °C (Table 3.2, entry 1-3). SEM images showed particle sizes ranging from 1.2 μm - 1.4 μm (Table 3.2, entry 1-3). From a literature review, the T_g for PMMA ranges from 80°C-123°C, with the exact value depending heavily on the polymer molecular weight, but is nevertheless in agreement with our data.^{30, 31} The particle size was measured using ImageJ software, by calculation from an average of at least 100 particles. SEM images showed spherical particles in all cases (Figure 3.10), therefore demonstrating successful dispersion polymerisation in scCO_2 .¹

Table 3.2. Analysis of PMMA products from 20 mL batch reactions by Reversible Addition Fragmentation Polymerisation (RAFT) in scCO_2 .

Entry	Polymer	Yield (%)^a	M_n (g/mol)^b	\bar{D}^a	Conversion (%)^c	T_g (°C)^d	Particle size (μm)^e
1	PMMA-RAFT1 (CPDT)	90	49,510	1.3	98	114	1.2 ± 0.33
2	PMMA-RAFT2 (DDMAT)	89	45,110	1.3	99	116	1.4 ± 0.37
3	PMMA-RAFT3 (DDMAT)	95	42,550	1.4	98	100	1.3 ± 0.38

The reactions were conducted at 65 °C and 270 bar, stirred at 300 rpm for 16 hrs. The reactants consist of MMA (3.33 mL), with molar ratio of [MMA]:[RAFT]=500:1, [RAFT]:[AIBN] =1:1 and PDMS-MA (5 wt.% with respect to MMA). ^a- determined by gravimetry, ^b-determined via GPC, ^c-conversion calculated from ¹H NMR, ^d-determined by DSC, ^e- determined by SEM.

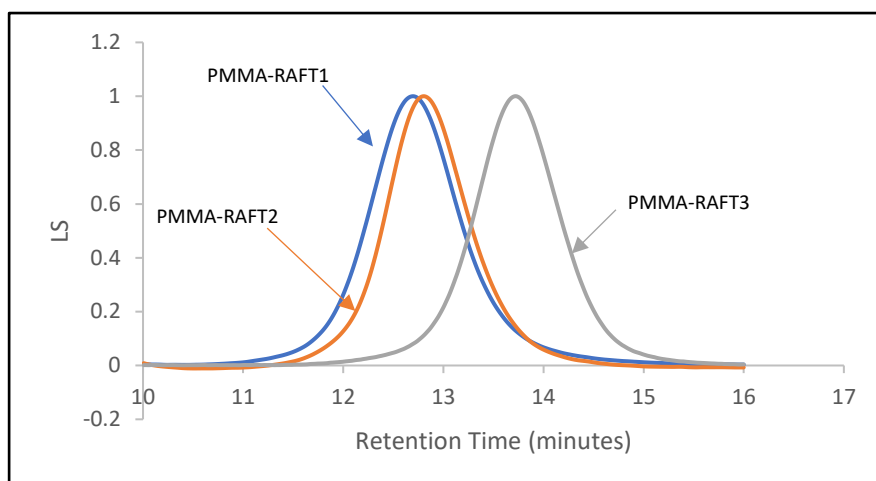


Figure 3.9. GPC traces obtained from repeats (Table 3.2, entry 1-3) of the 20 mL autoclave reactions by RAFT polymerisation in $scCO_2$.

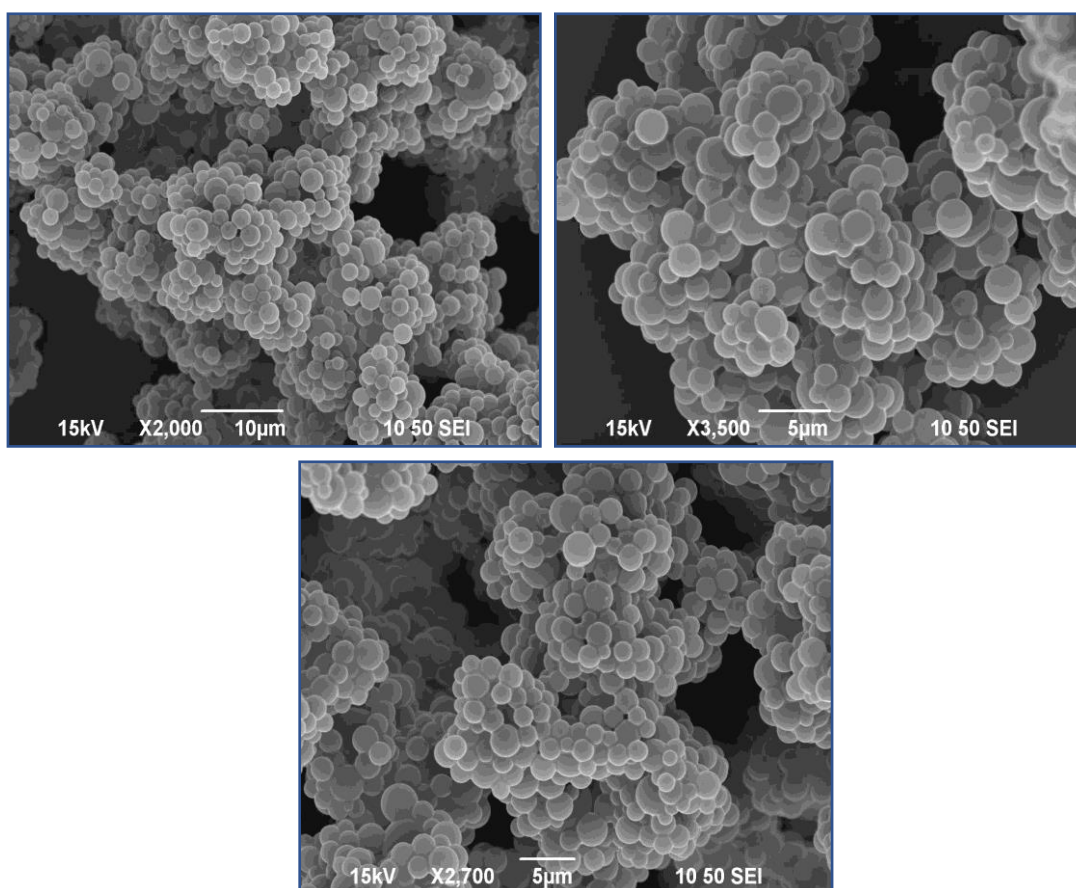


Figure 3.10. SEM images obtained from repeats of the 20 mL autoclave reaction by Reversible Addition Fragmentation (RAFT) Polymerisation in $scCO_2$, all images show discrete particles being obtained (Table 3.2, entry 1-3).

3.4.3 Synthesis of PMMA-*b*-P4VP via RAFT with different size and nanostructure of microparticles

3.4.3.1 BCP PMMA₅₀-*b*-P4VP₃₃ with Spherical (SPH) nanostructure

The objective of this section is to synthesise a medium molecular weight block copolymer, PMMA-*b*-P4VP, with a targeted molecular weight of 83,000 g/mol via one-pot dispersion polymerisation using DDMAT as the RAFT agent in scCO₂. The combination of PMMA and P4VP was chosen due to their unique properties, as described briefly in Section 3.1, and their different CO₂-philicity, where PMMA has high CO₂-philicity and absorbs CO₂ whereas P4VP is less swollen by CO₂.

The initial reaction was performed to synthesise the block copolymer PMMA₅₀-*b*-P4VP₃₃, where the subscripts denote the target molecular weight in kg mol⁻¹, by using methods reported previously.⁵ The reaction was done on the small scale in a 20 mL autoclave and the medium scale in 60 mL autoclave, to determine whether comparable polymerisation products could be obtained between the two vessels.

For each reaction, PDMS-MA was used as the stabiliser at a concentration of 5 wt. % relative to the monomer, DDMAT was chosen as the RAFT agent, and AIBN as the initiator. A [CTA]:[I] ratio of 1:1 was chosen, based on previous reports of the RAFT dispersion polymerisation of block copolymers in scCO₂.^{1,7} Synthesis of the first PMMA block was carried out for 24 hours at 65 °C and 3500 psi, with a 300 rpm stirring rate. This was followed by the addition of an appropriate amount of the second monomer, 4VP, and additional initiator required for the chain extension, using an HPLC pump. The target block ratio of PMMA/P4VP was kept at a constant molar value of 60/40. The reaction was then allowed to react for a further 24 hours to ensure close to full conversion of the second monomer

was achieved. In the case of 4VP, because the k_p of 4VP is relatively low, additional initiator is needed to ensure the efficient formation of block copolymer.²⁷

For the two reactions (Table 3.3, entry 1 and 2), the monomer conversion values for the first blocks were 93% and 98% for the 20 mL and the 60 mL autoclaves, respectively, as determined by taking ^1H NMR spectra from a small amount of the homopolymer product collected prior to the addition of the second monomer. The molecular weight of the PMMA first block sampled from the 20 mL autoclave was 32,230 g/mol considerably much lower than targeted value (50,000 g/mol) and had a high \mathcal{D} of 1.8 (Table 3.3, entry 1). In contrast, the M_n and \mathcal{D} values for the homopolymer aliquot sampled from the 60 mL autoclave were much closer to the expected values for a well-controlled RAFT polymerisation (Table 3.3, entry 2). Interestingly, at the end of reaction the M_n of the final block copolymer from the 20 mL autoclave was slightly closer to the targeted value in comparison to the block copolymer produced in the 60 mL autoclave. It seems clear that the 20 mL reaction was not fully RAFT controlled, so the higher molecular weight is probably because of a second smaller population of uncontrolled free radical chains. Both block copolymers gave acceptable dispersity values below 2.0, but the product from the 60 mL autoclave was considerably lower and more what would be expected for a block copolymerisation of these two monomers.^{5, 9} The increased \mathcal{D} value of the 20 mL PMMA₅₀-*b*-P4VP₃₃ sample suggests that there are a higher proportion of dead polymer chains present and a partial loss of polymerisation control during the reaction. This conclusion is further supported by the presence of a low molecular weight shoulder in the GPC trace of the PMMA homopolymer collected from this reaction (Figure 3.11a); it is clear that the RAFT process was not working as effectively, even towards the beginning of this reaction and that there was a higher proportion of non-RAFT initiated growing chains. Nevertheless, both of the block copolymers were powders, and the success of the block

copolymerisation was initially proven by the shift of the final product GPC peak to higher M_n values relative to the PMMA first block samples (Figure 3.11a -3.11b).

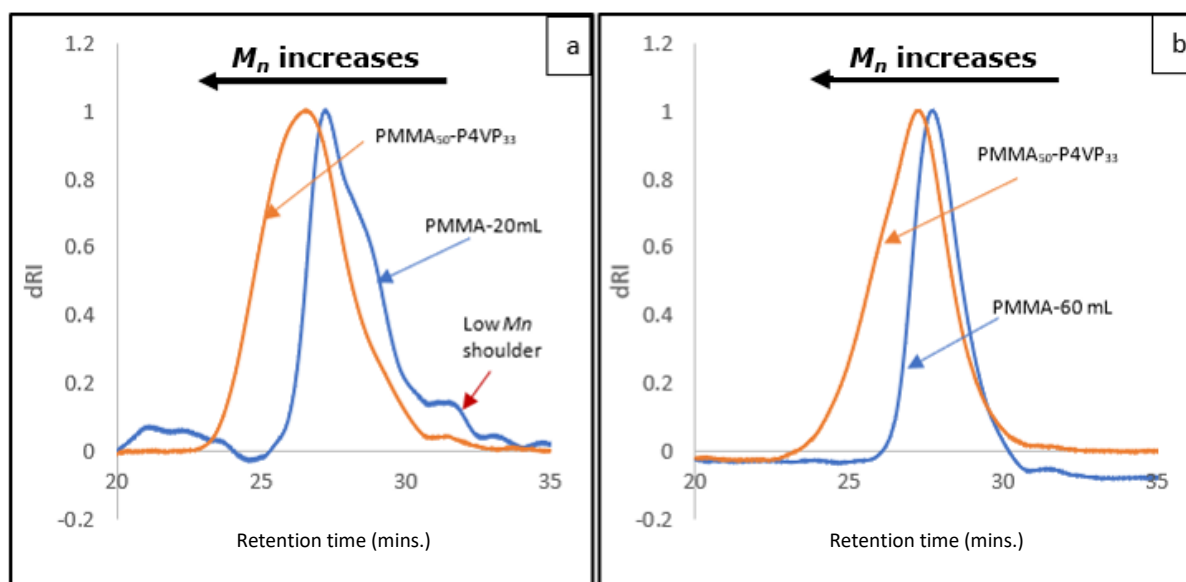


Figure 3.11. GPC traces of the first block, PMMA and final block copolymer PMMA₅₀-*b*-P4VP₃₃ in CHCl₃/EtOH/TEA (90:10:0.5) for both reaction in 20 mL (a) and 60 mL (b) autoclave (Table 3.3, entry 1 and 2). The low M_n shoulder shows the presence of a higher proportion of dead polymer chains that resulted in a partial loss of polymerisation control during the reaction in the 20 mL autoclave.

In addition, the DSC analysis (Figure 3.12) of both block copolymers also showed two separate transitions, one for PMMA ($T_g = 126^\circ\text{C}$ - 127°C) and one for P4VP ($T_g = 150^\circ\text{C}$ - 151°C) (Table 3.4). This indicates that both blocks were present and also suggests that they are in a phase separated state, as expected.

Table 3.3 Summary of comparison results of PMMA₅₀-*b*-P4VP₃₃ from 20 mL and 60 mL batch reactions by RAFT dispersion polymerisation in scCO₂.^a

Entry	Block Copolymer	f_{PMMA}^b	Morphology ^c	Conversion of PMMA ^d (%)	M_n PMMA (g/mol) ^e	M_n PMMA-P4VP (g/mol) ^e	\bar{D}^e (M/MV) ^f	Particle size ^g (M/MV) ^f (μm)
1	PMMA ₅₀ -P4VP ₃₃ (20 mL autoclave)	0.53	SPH	93	32,230	80,480	1.8/1.9	0.77 /1.7
2	PMMA ₅₀ -P4VP ₃₃ (60 mL autoclave)	0.64	SPH	98	50,290	70,840	1.2/1.6	0.80/ 1.6

^aFor the PMMA 1st block the molar ratio of CTA/AIBN=1:1 and 5 wt.% stabiliser w.r.t. monomer; for the chain extension of 4VP, macro-RAFT/AIBN=1:0.25 mol mol⁻¹; the reaction time for PMMA is 18-24 h and 16-24 h for P4VP conducted at 65 °C and 270 bar, stirring rate =300 rpm. ^b-calculated from Equation 4.1, ^c-determined via TEM, ^d-determined via NMR, ^e-determined by GPC (CHCl₃/EtOH/TEA), ^f-M, refers to first block, MV, refers to BCP, ^g-determined via SEM. (Notes: Target M_n value for PMMA= 50, 000 g/mol and target M_n value for PMMA-*b*-P4VP= 83,000 g/mol).

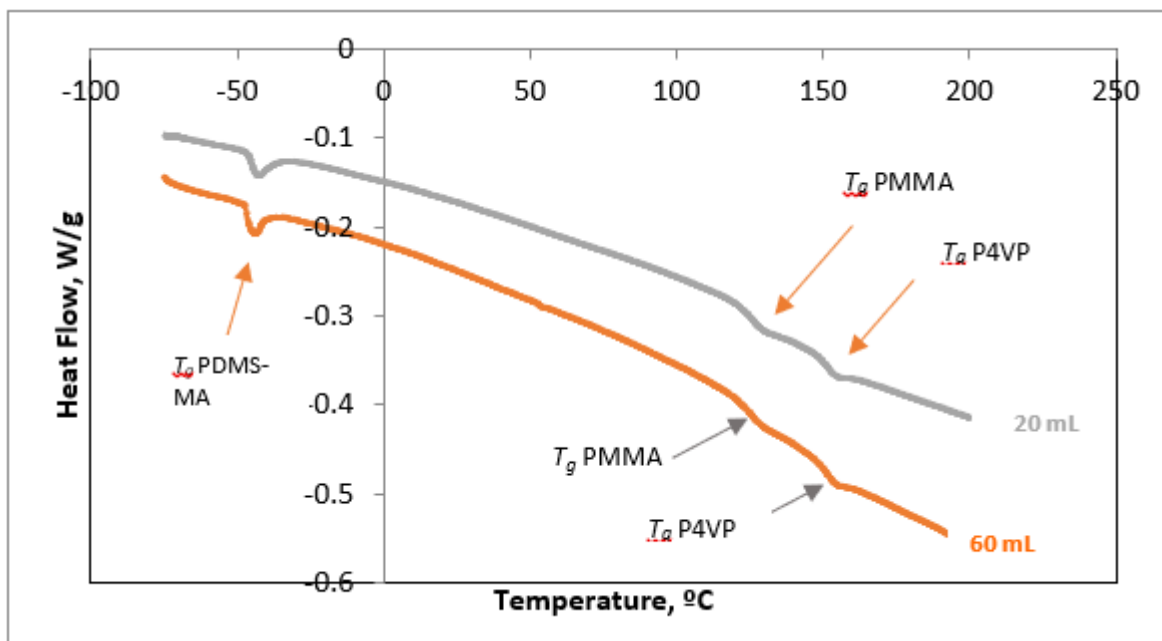


Figure 3.12. T_g s of PMMA₅₀-*b*-P4VP₃₃ block copolymer synthesised in the 20 and 60 mL autoclaves (Table 3.3, entry 1 and 2) shows two separate transitions, suggesting that they are in a phase separated state.

Table 3.4. Summary of T_g s of the first block, PMMA and block copolymer of PMMA-*b*-P4VP synthesised in both 20 and 60 mL autoclave.

	20 mL autoclave	60 mL autoclave
	T_gs (°C)	T_gs (°C)
PMMA	126	127
P4VP	150	151

SEM analysis and particle sizing were carried out to assess the particle morphology. The results indicated that the final product obtained from the 60 mL autoclave gave a superior morphology of discrete particles (Figure 3.13d and Table 3.3, entry 2). In comparison, some clumpy particles were observed for the product synthesised in the 20 mL autoclave (Figure 3.13b and Table 3.3, entry 1). The measurement of particle size was done by measuring a total of 100 distinct spherical particles using

ImageJ. This process was performed on the PMMA first block particles and the final block copolymer particles, with an increase in particle size observed, as expected, between the PMMA (around 0.77 μm) and the relative block copolymers being observed (up to 1.7 μm) (Table 3.3). Only 15% of the stabiliser is covalently bonded to the final products, the vast majority of the PDMS-MA is physisorbed but is required for stabilisation.²⁹ But this appears to also contribute to the clumping of the particles in the “dry state” and Giles et al. showed³² that the SEM images of clumpy particles were significantly improved by dispersion of the particles in hexane or dodecane prior to imaging.

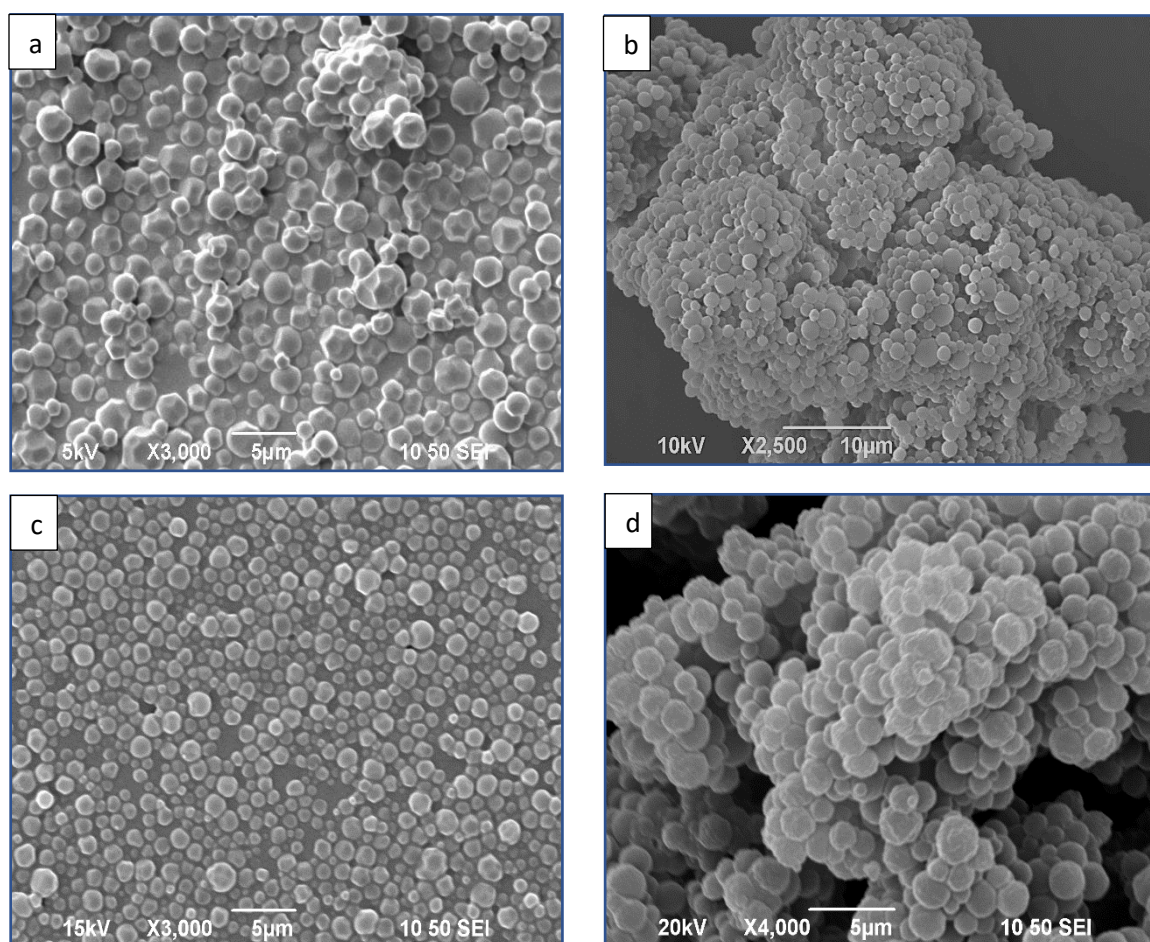


Figure 3.13. SEM images of the first block, PMMA (a and c) and final block copolymer, PMMA₅₀-*b*-P4VP₃₃ (b and d) synthesised in 20 mL autoclave (a and b) and 60 mL autoclave (c and d) (Table 3.3, entry 1 and 2). Each product shows discrete particles with some clumpy formation in the 20 mL autoclave.

The internal particle phase behaviour of these block copolymers was investigated by TEM imaging. The thin sectioning by microtome cutting allows cross-sections through micron-sized particles to be viewed using an electron beam, revealing the internal structure. BCP microparticles synthesised in scCO₂ were previously imaged to investigate their internal phase behaviour.³³ The volume fraction of the two blocks within a copolymer is a key factor determining the morphology.³⁴ Volume fraction with respect to PMMA (f_{PMMA}) was calculated from the weight fraction measured by ¹H NMR (w_{PMMA}) and the block densities (D_{PMMA} , D_{block2}), where available (Equation 3.1). Densities of PMMA (1.17 g cm⁻³) and P4VP (1.114 g cm⁻³) were taken from the literature.²⁷ In this study, volume fraction studied of PMMA is $f_{\text{PMMA}} = 0.6$.

$$f_{\text{PMMA}} = \frac{w_{\text{PMMA}} / D_{\text{PMMA}}}{w_{\text{PMMA}} / D_{\text{PMMA}} + w_{\text{block2}} / D_{\text{block2}}} \quad \text{(Equation 3.1)}$$

TEM images were taken after staining with iodine vapour for 2 hours to improve the domain contrast as reported previously.^{1, 5, 7} It was observed that a spherical (SPH) morphology was obtained for both products synthesised in 60 and 20 mL autoclave (Figure 3.14 and Table 3.3, entry 1 and 2), even though the microparticles from the 20 mL autoclave were fused in the SEM (Figure 3.13b). In 2009, Shoji et al. reported that $w_{\text{PMMA}} = 0.15$ and 0.55 , PMMA-*b*-P4VP self-assemble into disordered and lamellar (LAM) morphologies.³⁵ However, more recently both Jennings and Alauhdin reported that the presence of scCO₂ in addition to f_{PMMA} had a significant effect on the morphology of PMMA-*b*-P4VP. This was attributed to the fact that the two blocks have different CO₂-philicities, resulting in different swelling behaviour in this medium and an artificial increase in the f_{PMMA} values above what would be expected solely based on composition.^{1, 8} As a result, they discovered that when PMMA was used as the minority block,

the particles took on the morphology of a more symmetrical block copolymer, i.e., a LAM morphology.

In contrast, when the block copolymers were more symmetrical in composition, a SPH morphology was formed in which the P4VP domains were surrounded by a PMMA matrix, rather than the expected lamellar phase. This demonstrated that the scCO₂ had an effect on the system's thermodynamics.^{1, 7} Further investigation of this phenomenon revealed that when blocks shared a similar CO₂-philicity, the resulting morphology matched the expected diblock copolymer phase diagram. By contrast, a large difference in CO₂-philicity induced a morphological shift away from the expected phase diagram, resulting in unexpected morphologies. A block with a higher CO₂ -philicity will absorb more CO₂ than one with a lower CO₂ -philicity, resulting in a volume fraction that is effectively greater than expected based on the chemical composition alone. As a result, the phase diagram of the block copolymer is shifted by the effect of swelling of the PMMA block by CO₂.¹

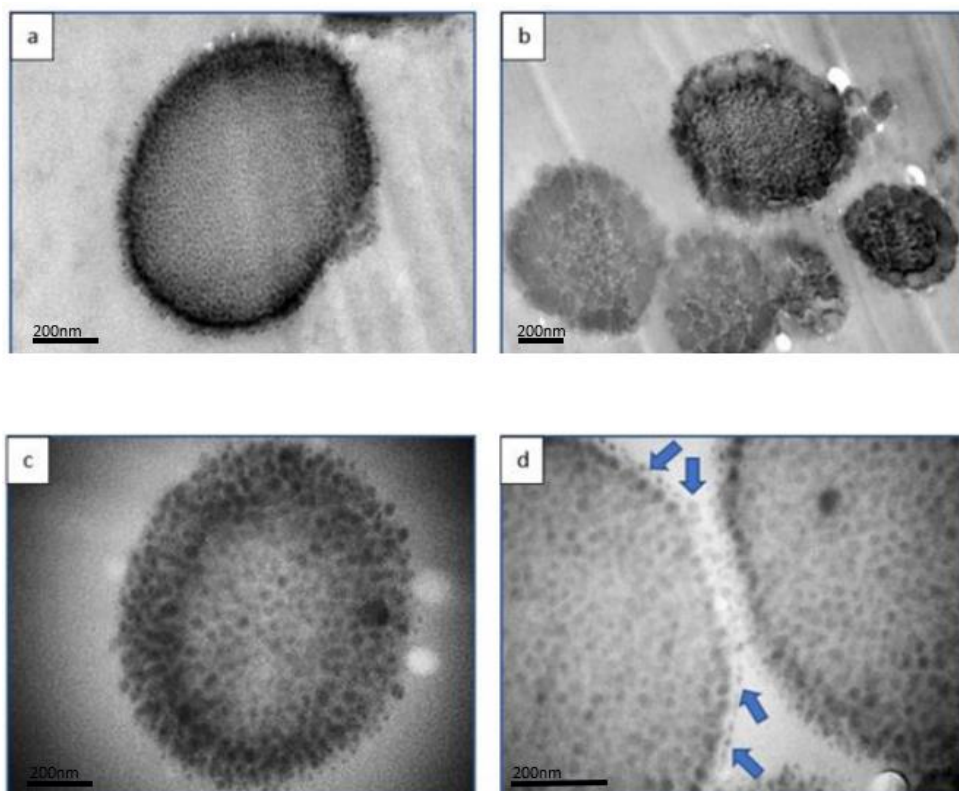


Figure 3.14. TEM images of the internal nanostructures block copolymer, PMMA₅₀-P4VP₃₃ microparticles synthesised in a 20 mL (a & b) and 60 mL (c & d) autoclave (Table 3.3, entry 1 and 2). Samples were stained with iodine vapour for 2 hours prior to imaging to enhance the contrast of the P4VP domains. The remaining PDMS-MA that acts as a stabiliser attached the methacrylate terminal group to the surface of the PMMA particle (blue arrows) (d).

A few more reactions in the 60 mL autoclave were performed to establish the repeatability and reproducibility, since subsequent reactions in this study will use this medium scale autoclave. The same procedure described in the beginning of this section (Section 3.3.3) was repeated. The triplicate results were tabulated as shown in Table 3.5 (entry 1-3). ¹H NMR spectroscopy analysis (Figure 3.15) of the BCP, PMMA₅₀-*b*-P4VP₃₃ confirmed that close targeted value of PMMA/P4VP molar block ratios of 60/40 were achieved for all reactions (Table 3.5, entry 1-3).

Table 3.5. Polymerisation of PMMA₅₀-*b*-P4VP₃₃ in 60 mL autoclave by two consecutive RAFT dispersion in scCO₂^a for repeatability and reproducibility record.

Entry	Sample	T _g ^b (°C) (M/MV)	PMMA/P4VP ^c	M _n ^d PMMA (g/mol)	Đ ^d	M _n ^d BCP (g/mol)	Đ ^d	Particle size ^e (μm)	Morphology ^f
1	PMMA ₅₀ - <i>b</i> -P4VP ₃₃ -1	127/151	64/36	50,290	1.2	70,840	1.6	1.5±0.4	SPH
2	PMMA ₅₀ - <i>b</i> -P4VP ₃₃ -2	124/151	68/32	44,210	1.3	64,400	1.7	1.6±0.4	SPH
3	PMMA ₅₀ - <i>b</i> -P4VP ₃₃ -3	126/152	61/39	59,890	1.3	83,410	1.5	1.6±0.3	SPH

^aFor the PMMA 1st block the molar ratio of CTA/AIBN=1:1 and 5 wt.% stabiliser w.r.t. monomer; for the chain extension of 4VP, macro-RAFT/AIBN=1:0.25 mol mol⁻¹; the reaction time for PMMA is 18-24 h and 16-24 h for P4VP conducted at 65 °C and 270 bar, stirring rate = 300 rpm. ^b-determined by DSC, M, refers to first block, MV, refers to BCP ^c- determined via ¹H NMR, ^d- determined via GPC, (CHCl₃/EtOH/TEA), ^e- determined by SEM and ImageJ, ^f- determined by TEM

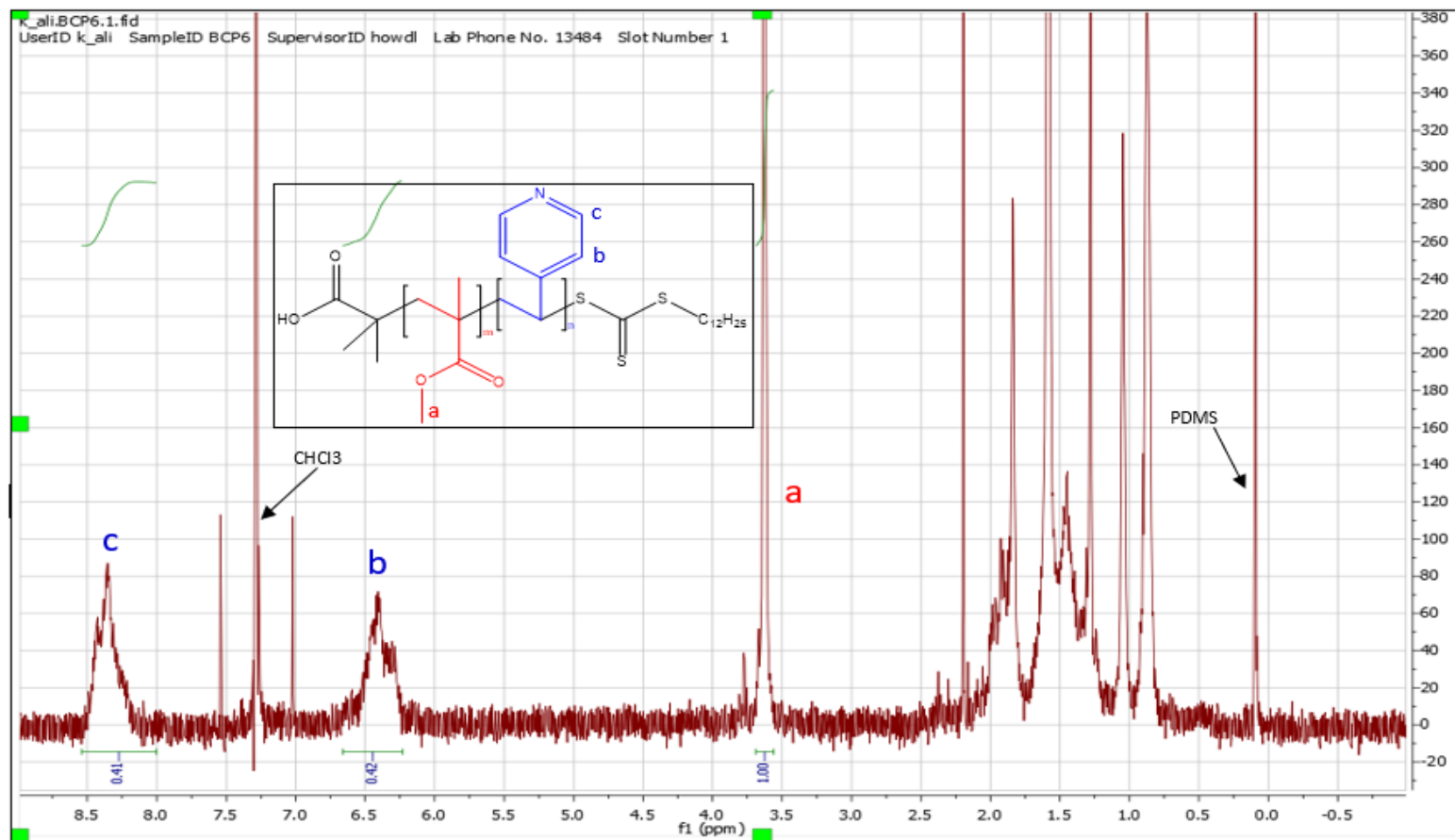


Figure 3.15. ¹H NMR spectrum of BCP, PMMA₅₀-*b*-P4VP₃₃ in CDCl₃ in 60 mL autoclave (Table 3.3, entry 2). The block copolymerisation of PMMA-*b*-P4VP was confirmed by the methoxy protons peak shifted from 3.8 ppm to 3.6 ppm (a) for PMMA and from 5.5 ppm to 6.1 -6.8 (b and c) for P4VP in CDCl₃.

The GPC analysis of the first block, PMMA and the final block copolymer PMMA-*b*-P4VP showed promising experimental M_n values and acceptable molecular weight distribution, very close to theoretical, demonstrating that the RAFT agent was efficiently controlling the polymerisation (Figure 3.16 and Table 3.5, entry 1-3).

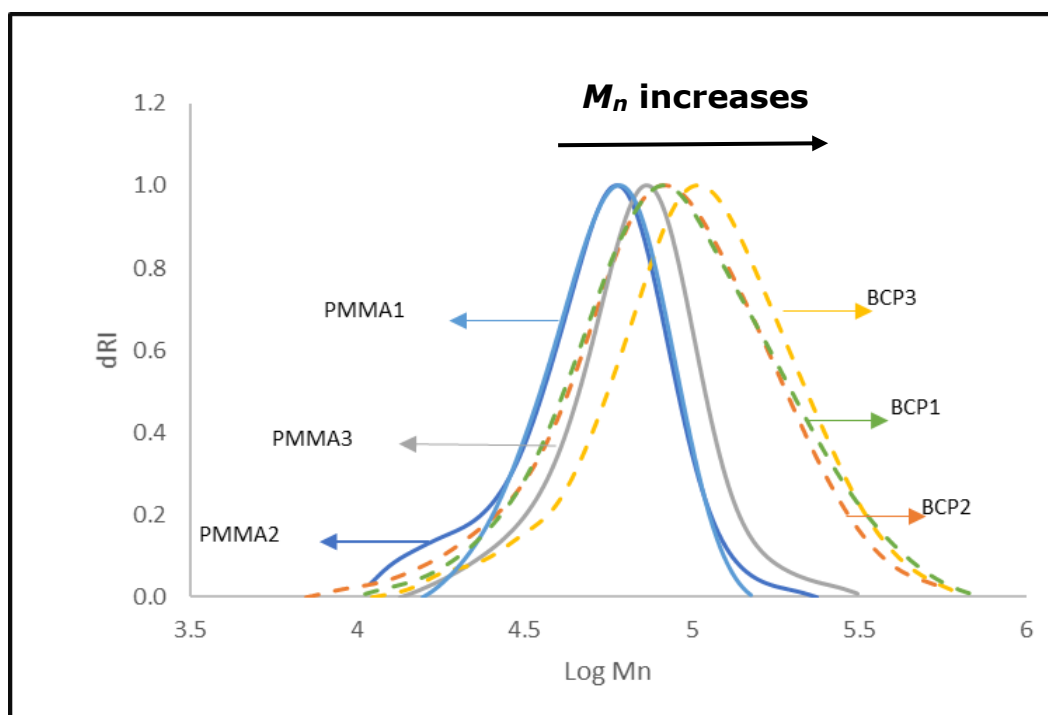


Figure 3.16. GPC traces of the first block, PMMA and final block copolymer for PMMA₅₀-*b*-P4VP₃₃ in CHCl₃/EtOH/TEA (90:10:0.5) synthesised in 60 mL autoclave showing a good repeatability of block copolymerisation reaction (Table 3.5, entry 1-3). The GPC peaks of BCP products shifted to relatively higher molecular weight than PMMA, first block.

In addition, the DSC analysis (Figure 3.17) of the block copolymers showed two separated clear transition for PMMA ($T_g = 124^\circ\text{C}$ - 127°C) and P4VP ($T_g = 151^\circ\text{C}$ - 152°C), indicating that both blocks were present. The fact that the GPC data show good chain extension is reasonable evidence that we have BCP and not homopolymer mixture.

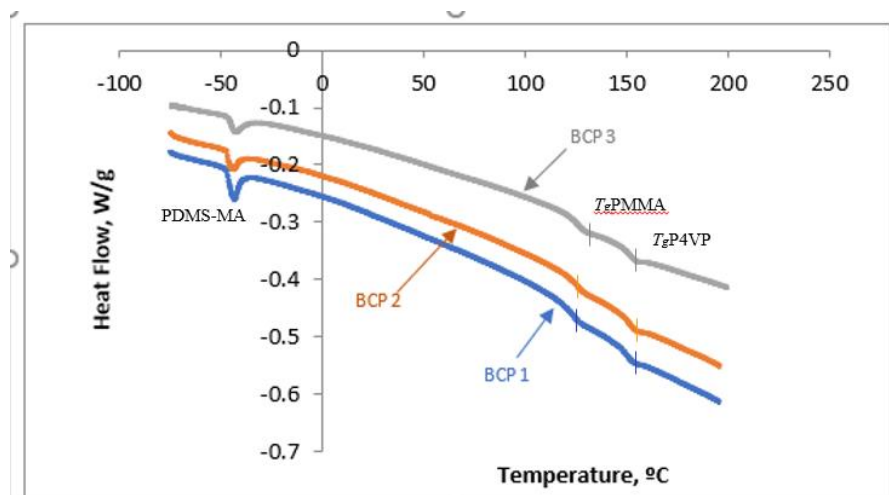


Figure 3.17. T_g s of PMMA₅₀-*b*-P4VP₃₃ block copolymers from the repeat synthesis in 60 mL autoclave (Table 3.5, entry 1-3) by DSC analysis.

SEM analysis and particle sizing were carried out to assess whether particles had been formed. The results indicated that the final product was monodisperse, well-defined, discrete particles (Figure 3.18a) with particle size the range 1.5-1.6 μm .

As before, the internal particle phase behaviour of these block copolymers was investigated by TEM imaging. It was observed that a spherical morphology was successfully obtained for all of the repeat block copolymers synthesis (Figure 3.18b).

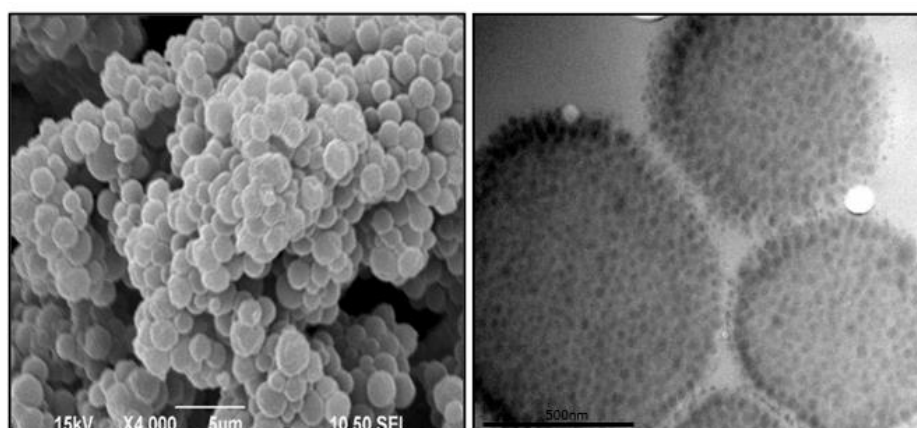


Figure 3.18 The SEM (a) and TEM (b) of PMMA₅₀-*b*-P4VP₃₃ block copolymer synthesised in 60 mL autoclave (Table 3.5) showing discrete particles and SPH morphology.

3.4.3.2 Synthesis of PMMA₂₀₀-*b*-P4VP₁₃₃ block copolymer at different block sizes with the same nanostructure, Spherical (SPH).

The following reaction was used to synthesise a block copolymer of the same composition but various sizes. The PMMA/P4VP target block ratio was kept constant at 60/40, while the degree of polymerisation of the longer chain, PMMA₂₀₀-*b*-P4VP₁₃₃, was varied ($M_{nTargeted} = 333,000$ g/mol). ¹H-NMR spectroscopy confirmed that a molar block ratio of 45/55 PMMA/P4VP was achieved, which is significantly different to the target value (Figure 3.19). In addition, GPC analysis revealed an M_n value of 194,400 g/mol ($\mathcal{D} = 1.9$), which is significantly lower than the target value, indicating that the RAFT agent was less effective at controlling polymerisation at higher molecular weights (Figure 3.20). This result is consistent with the difficulty of synthesising well-defined polymers with high molecular weights via RAFT polymerisation when monomers with low propagation rate coefficients (k_p) values are used (i.e., 4VP, styrene, etc.).^{10, 36} But, the M_n value of the first block, PMMA ($M_n = 161,600$ g/mol) was closer to targeted value ($M_{nTargetedPMMA} = 200,000$ g/mol) with higher dispersity ($\mathcal{D} = 3.6$). It might be due to the solubility issue of PMMA in the mixture of mobile phase (CHCl₃/EtOH/TEA). This result corroborated the peak with huge shoulder (Figure 3.20). Despite this, the M_n value for PMMA₂₀₀-*b*-P4VP₁₃₃ ($M_n = 194,400$ g/mol) is significantly higher than that for PMMA₅₀-P4VP₃₃ ($M_n = 83,410$ g/mol) (Table 3.5, Entry 3), and the molecular weight distribution remains unimodal despite the broad GPC traces. However, the BCP peak doesn't show an increase in M_n value compared to the first block, PMMA (Figure 3.20) indicating the failure of block copolymerisation.

The DSC analysis revealed two transitions, giving an early indication that phase separation of each block was occurring (Figure 3.21b). The SEM indicated agglomerated particles from the longer chain of products (Figure 3.21a).

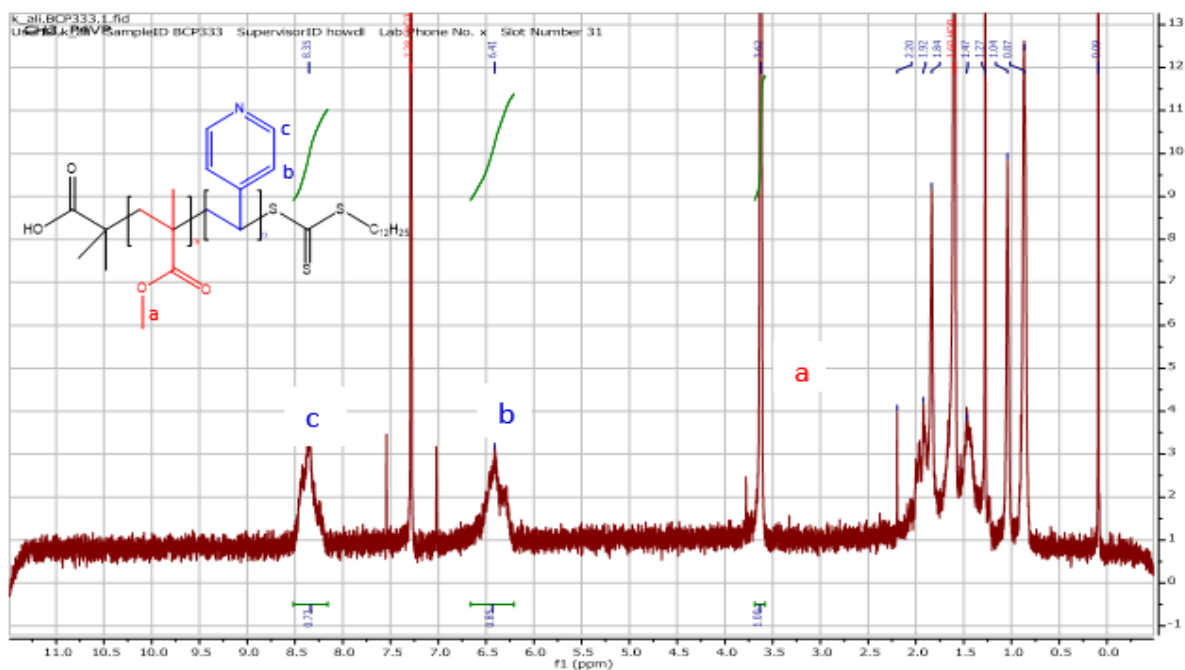


Figure 3.19. ^1H NMR spectrum of BCP, $\text{PMMA}_{200}\text{-}b\text{-P4VP}_{133}$ in CDCl_3 in 60 mL autoclave. ^1H -NMR spectroscopy confirmed that a molar block ratio of 45/55 PMMA/P4VP was achieved, which is significantly different to the targeted value, 60/40.

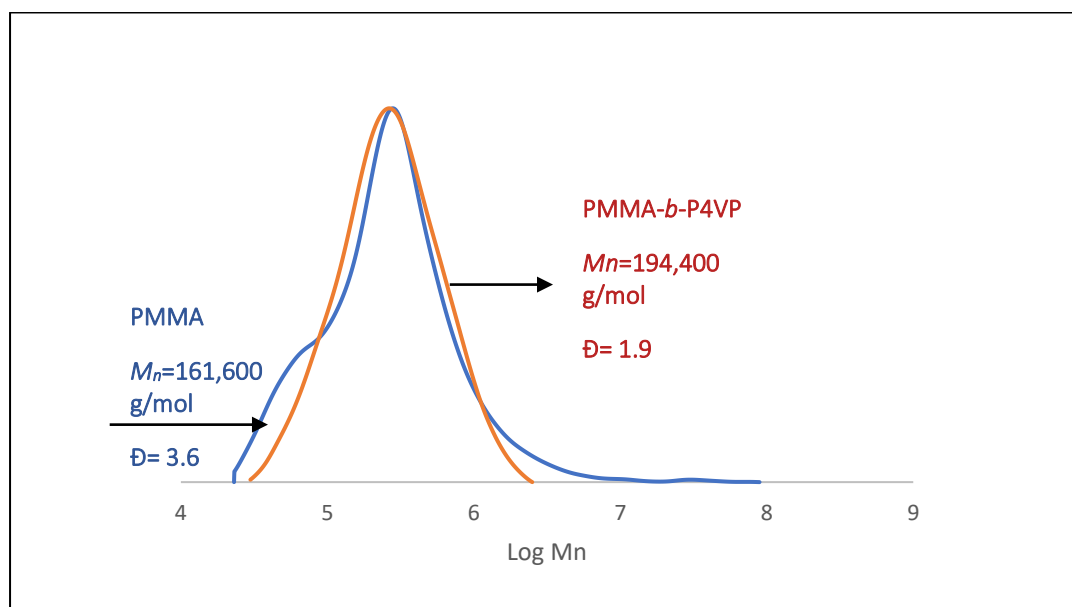


Figure 3.20. The GPC traces of longer chain BCP, $\text{PMMA}_{200}\text{-}b\text{-P4VP}_{133}$ in $\text{CHCl}_3/\text{EtOH}/\text{TEA}$ (90:10:0.5) synthesised in a 60 mL autoclave. The peak of the final product, BCP doesn't show an increase in M_n in comparison to the first block, PMMA indicating the failure of block copolymerisation.

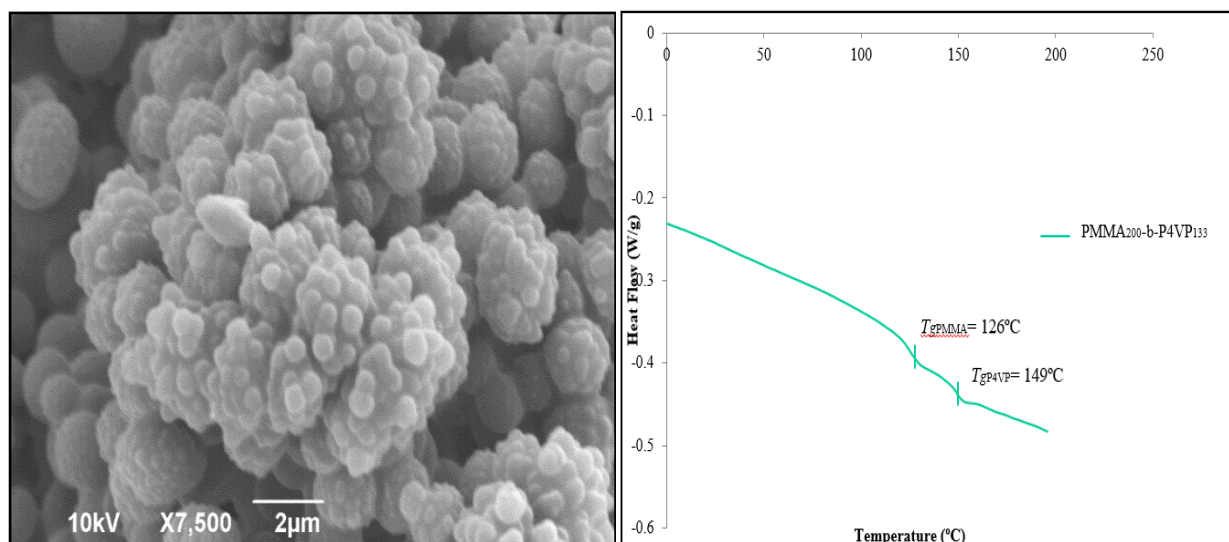


Figure 3.21. a) SEM image and b) DSC traces of longer chain BCP, PMMA₂₀₀-*b*-P4VP₁₃₃. SEM images shows fused particles, but the DSC indicate the presence of both block PMMA and P4VP in this sample.

3.4.3.3 Synthesis of PMMA-*b*-P4VP block copolymer at different block size with Lamellar (LAM) nanostructure.

The work was progressed further to target block copolymers with a different internal morphology (LAM) using the same block copolymer system PMMA-*b*-P4VP. The reaction conditions needed to yield the lamellar (LAM) morphology can be predicted theoretically by the experimental phase diagram in scCO₂.^{4, 5,37} It is predicted that a combination of a PMMA block with shorter chain lengths and a P4VP block with longer chain lengths are expected to form lamellar morphology, assuming their molecular weight values are high enough to induce microphase separation.² There are two targeted block length combinations previously established in the group; 1) 15,000 g/mol for PMMA block and 45,000 g/mol for P4VP block (PMMA₁₅-*b*-P4VP₄₅, Total M_n = 60,000 g/mol) and 2) 25,000 g/mol for PMMA block and 75,000 g/mol for P4VP block (PMMA₂₅-*b*-P4VP₇₅, Total M_n = 100,000 g/mol). The target block ratio of PMMA/P4VP was kept at a constant molar

value of 25/75. The method used to synthesise these block copolymers was via two consecutive RAFT polymerisations as described in Section 3.3.3.

In the case of the BCP with target M_n total of 60,000 g/mol (Table 3.6, entry 1), the ^1H NMR spectroscopy analysis indicated a PMMA/P4VP weight ratio value of 10/90, which is quite far off the targeted value, 25/75 (Figure 3.22). The GPC data indicated a bimodal peak for the final product of block copolymer without any peak observed for the first block, PMMA (Figure 3.23a). The bimodal peak indicates the formation of homopolymers of P4VP along with a block copolymer, whereas incomplete conversion of the low MMA volume (< 4 mL) used at the beginning of the reaction may account for the absence of the PMMA peak. One transition was then observed in the DSC analysis (Figure 3.23b), which seems to support the unsatisfactory results of weight ratio value. The SEM images showed fusing of the microparticles (Figure 3.24a). On top of that, the TEM, stained with iodine to enhance the P4VP domain, showed fully black spheres for almost all the particles imaged (Figure 3.24b). This indicated that the particles are mainly formed from P4VP. This was not unexpected as 4VP was the major monomer (12 mL) used for chain extension compared to 4 mL of PMMA to grow the first block.

Table 3.6. Synthesis of BCP, PMMA-*b*-P4VP via two consecutive RAFT dispersion polymerisations in scCO₂ as described in Section 3.3.3 (Figure 3.1) to get LAM morphology.

Entry	BCP	Morphology^a	Particle size^b (μm)	W_M/W_{MV}^c	M_n M^d (g/mol)^e	M_n M/MV (g/mol)^e	Đ^e (M/MV)^d	T_g^f (°C)
1	PMMA ₁₅ - P4VP ₄₅	-	1.5 ± 0.4	10/90	-	- (bimodal)	-	151
2	PMMA ₂₅ - P4VP ₇₅	LAM	1.6 ± 0.4	20/80	-	90,040	1.9	153

For the PMMA 1st block the molar ratio of CTA/AIBN= 1:1 and 5 wt.% stabiliser w.r.t. monomer, the reactions were conducted at 65°C and 270 bar, stirring rate ~300 rpm for ~16 h. For the chain extension of 4VP, macro-RAFT/AIBN= 1:0.25 mol mol⁻¹ was added by HPLC pump and left for another 16 h. ^a- determined via TEM, ^b- determined via SEM and ImageJ, ^c- Weight fraction determined via NMR (W_{PMMA}/ W_{P4VP}), ^d-determined by GPC (CHCl₃/EtOH/TEA), ^e - M, refers to PMMA, MV, refers to PMMA-P4VP, ^f- determined via DSC.

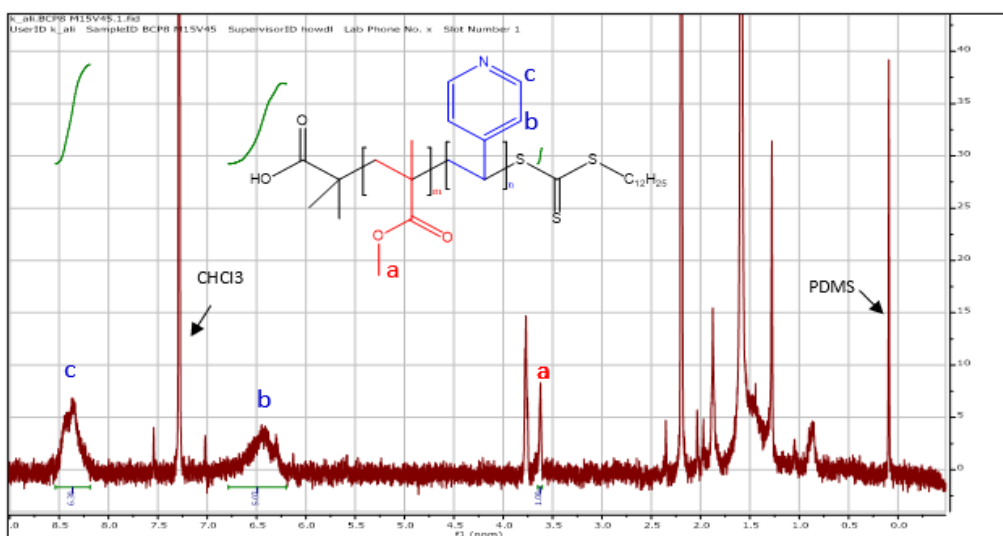


Figure 3.22. ^1H NMR spectrum of block copolymer $\text{PMMA}_{150}\text{-}b\text{-P4VP}_{450}$ ($M_{n\text{targeted}} = 60,000$ g/mol) (Table 3.6, entry 1) enabling the proportion of P4VP to be calculated. There's no conversion of MMA into PMMA obtained for this reaction (see peak (a)).

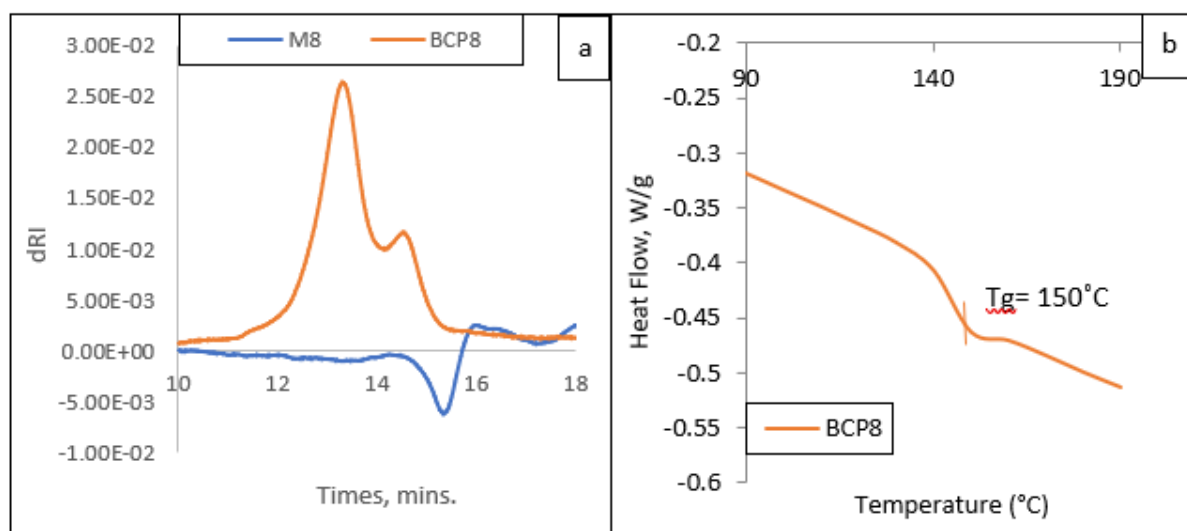


Figure 3.23 (a) GPC trace of both the first block, PMMA (M8)- no peak observed and final BCP, $\text{PMMA}_{15}\text{-}b\text{-P4VP}_{45}$ (BCP8, $M_{n\text{targeted}} = 60,000$ g/mol, (Table 3.6, entry 1) -bimodal peak obtained. (b) DSC results of BCP8, $\text{PMMA}_{15}\text{-}b\text{-P4VP}_{45}$ (Table 3.6, entry 1) – only one transition recorded.

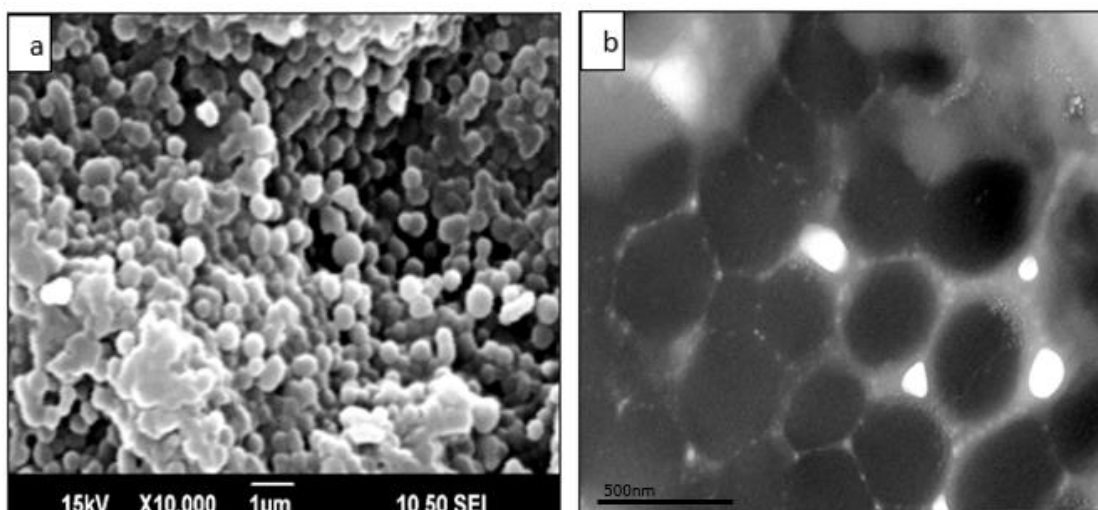


Figure 3.24. SEM (a) and TEM (b) images of BCP formed of PMMA₁₅-*b*-P4VP₄₅ ($M_{ntargeted}$ = 60,000 g/mol, Table 3.6, entry 1). The black spheres were found for almost all the particles imaged in TEM indicating that the particles are mainly formed from P4VP.

By contrast, promising results were obtained for the 100,000 g/mol BCP (Table 3.6, entry 2); the ¹H NMR spectroscopy produced a weight ratio of PMMA/P4VP of 20/80 that was close to the target value of 25/75 (Figure 3.25).

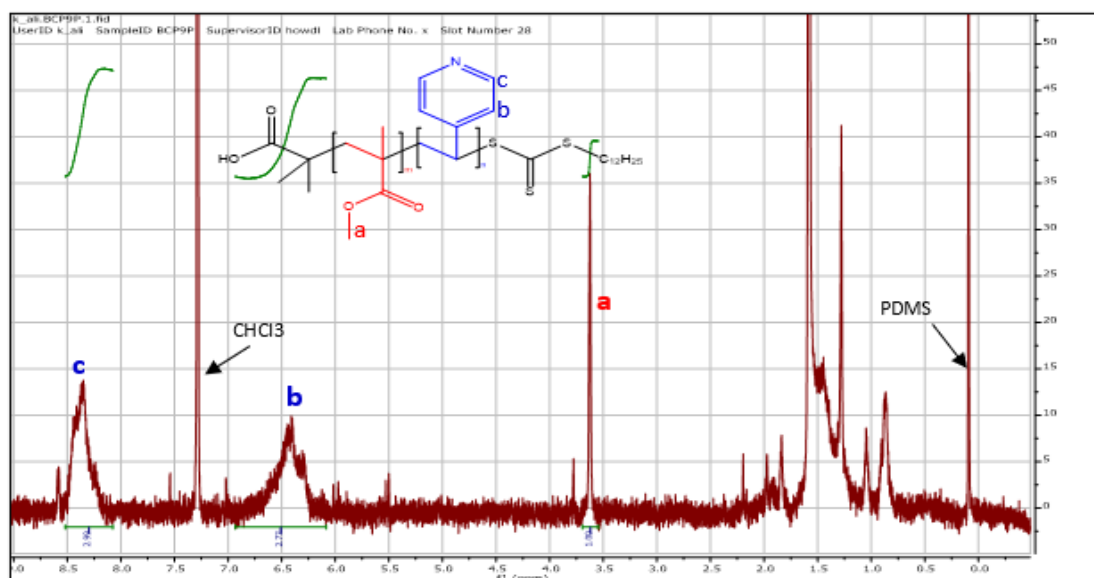


Figure 3.25. The block copolymerisation of PMMA₂₅-*b*-P4VP₇₅ ($M_{ntargeted}$ = 100,000 g/mol, Table 3.6, entry 2) was confirmed by the proton chemical shifted from 3.8 ppm to 3.6 ppm for PMMA and from 5.5 ppm to 6.1 -6.8 for P4VP in CDCl₃.

The GPC (Figure 3.26a) gave a unimodal peak, indicating a M_n value of 90,040 g/mol ($\mathcal{D} = 1.9$), showing close results to the targeted molecular weight ($M_n = 100,000$ g/mol). There was no peak obtained for the first block of PMMA as before. Our previous study reported that this small volume caused slow kinetics due to the fact that it was a highly dilute reaction solution.¹

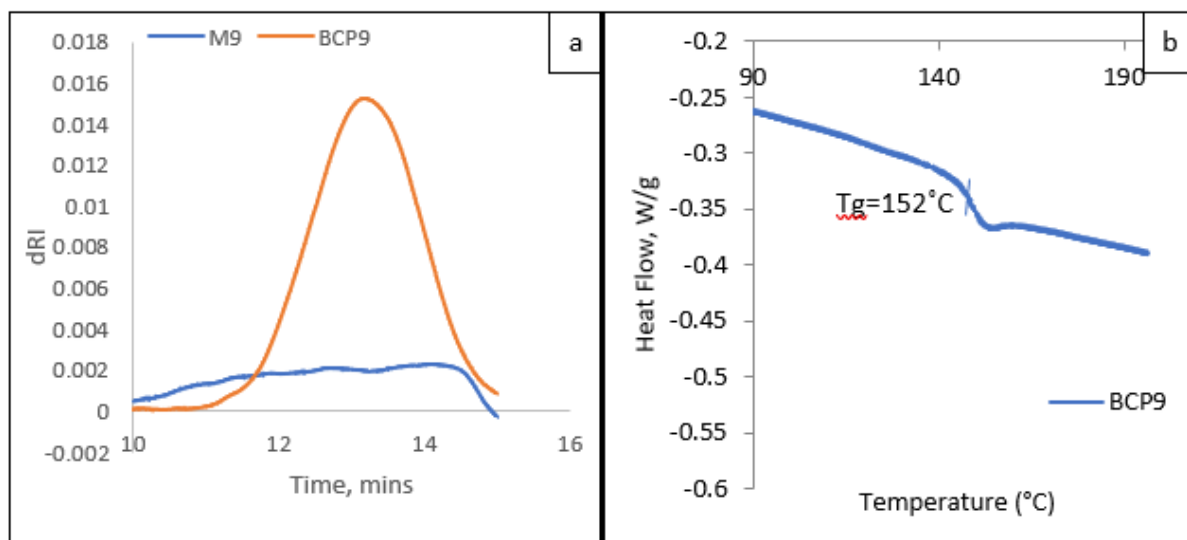


Figure 3.26. (a). GPC trace of both, the first block, PMMA (M9) - no peak observed and final BCP, PMMA₂₅-*b*-P4VP₇₅ (BCP9, $M_{n\text{targeted}} = 100,000$ g/mol, Table 3.6, entry 2) - unimodal peak. (b) DSC results of BCP9, PMMA₂₅-*b*-P4VP₇₅ (Table 3.6, entry 2) - only one transition recorded.

The SEM analysis (Figure 3.27a) showed more well-defined, discrete particles were produced in comparison to the low molecular weight BCP ($M_n = 60,000$ g/mol). Hence, TEM analysis was performed on these particles to determine the internal phase separation morphology. From the TEM images, the lamellar (LAM) morphology internal phase separation was successfully formed (Figure 3.27b).

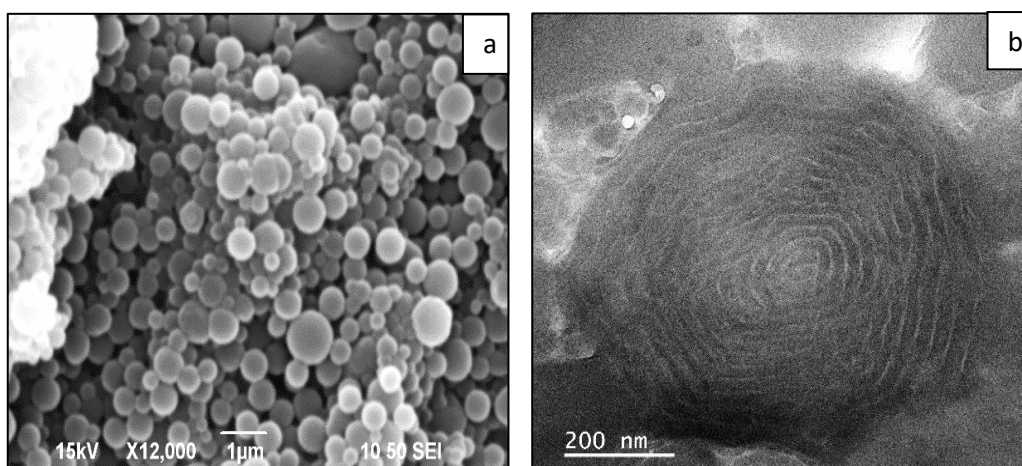


Figure 3.27. SEM (a) and TEM (b) images of BCP, PMMA₂₅-*b*-P4VP₇₅ ($M_{ntargeted}$ = 100,000 g/mol, Table 3.6, entry 2), with lamellar (LAM) morphology.

Another method devised by the group was used to validate the preceding findings. It was essentially to synthesise block copolymers in fewer independent steps (as stated in Section 3.3.4). By pre-synthesising the first block, and subsequently using the PMMA as a macro-chain transfer agent (CTA). The yellowish powdered PMMA-CTA (Figure 3.28) can be re-dispersed, with additional surfactant, for approximately 8-16 hours followed by the addition of the second monomer, 4VP, via an HPLC pump. A few reactions were carried out to improve the morphology of the LAM, while maintaining the block ratio ($w_{PMMA}:w_{P4VP} = 0.25:0.75$) and total molecular weight ($M_{ntargeted1} = 60,000$ g/mol and $M_{ntargeted2} = 100,000$ g/mol) as discussed previously.



Figure 3.28. The pre-synthesised batch of PMMA-CTA ($M_n = 15,000$ g/mol). This was added to the autoclave and redispersed before addition of 4VP.

The GPC results of both BCP systems (Figure 3.29) showed two peaks. One caused by the first block and one for the final BCP product, which is shifted to higher molecular weight relative to the peak for the first block. This indicated that the chain extension process of both block copolymers, $M_{ntargeted1} = 60,000$ g/mol (Table 3.7, entry 2) and $M_{ntargeted2} = 100,000$ g/mol (Table 3.7, entry 1) were successful. The molecular weight obtained for both was close to the target value, with good dispersity below 1.9, especially for low molecular weight block ($M_{ntargeted1} = 60,000$ g/mol, Table 3.7, entry 2). The dispersity of the PMMA-CTA is higher ($\mathcal{D} = 1.5$) than its related BCP, PMMA-*b*-P4VP ($\mathcal{D} = 1.4$). This is a result of a higher solubility of the final BCP in the mixture solvent system used for the GPC analysis namely, chloroform: ethanol: triethylamine = 90: 10: 0.5. GPC traces of higher molecular weight BCP ($M_{ntargeted2} = 100,000$ g/mol, Table 3.7, entry 1) showed high molecular weight shoulders (Figure 3.29) which, as kinetics revealed, only exhibited towards high conversion.² This indicated that side reactions such as chain transfer to polymer, which seemed to be enhanced in $scCO_2$, were most likely facilitated by the lower viscosity.⁴ The two-transitions observed in the DSC analysis (Figure 3.30), representing the T_g of PMMA and P4VP, were an early indication that phase separation had occurred.

Table 3.7. Synthesis of BCP via RAFT dispersion polymerisation in a series of shorter independent steps in scCO₂ as described in Section 3.3.4 (Figure 3.2 and 3.3) to get LAM morphology.

Block Copolymer	Entry	Morphology^a	Particle Size^b (µm)	W_{PMMA}/W_{P4VP}^c	M_n PMMA (g/mol)^d	M_n PMMA-P4VP (g/mol)^d	Đ^d (M/MV)^e	T_g^f (M/MV)^e (°C)
PMMA₂₅-P4VP₇₅	1	SPH ^g	1.8± 0.4	22/78	25, 520	107, 500	1.3 / 1.8	125 / 153
	2	LAM	1.2± 0.3	23/77	15,900	65, 400	1.5 / 1.4	122/151
PMMA₁₅-P4VP₄₅	3	LAM	0.9± 0.3	24/76	15,740	61,090	1.09/1.5	123/150
	4	LAM	1.2± 0.3	23/77	12,790	62,140	1.75/1.8	120/153

The reactions were conducted by synthesising the PMMA-CTA at 65 °C and 275 bar, stirring rate =300 rpm for ~16 hrs with molar ratio R : I = 1 : 1 and 5 wt.% stabiliser w.r.t. MMA. For the chain extension of 4VP, PMMA-CTA/AIBN= 1:0.25 mol mol⁻¹ and the 4VP was added after the redispersion of PMMA-CTA with additional 5 wt.% stabiliser w.r.t 4VP in scCO₂ for ~16 hrs, then the reaction was left for another 16 hrs. ^a- determined via TEM, ^b- determined via SEM and ImageJ, ^c- Weight fraction determined via NMR (W_{PMMA}/ W_{P4VP}), ^d-determined by GPC (CHCl₃/EtOH/TEA), ^e- M, refers to PMMA, MV, refers to PMMA-*b*-

P4VP, f^- determined via DSC, g^- BCP with high M_n ($M_{ntargeted}=100,000$ g/mol) phase separated to form SPH morphology instead of LAM, this shows that the RAFT polymerisation loss of control at high molecular weight.

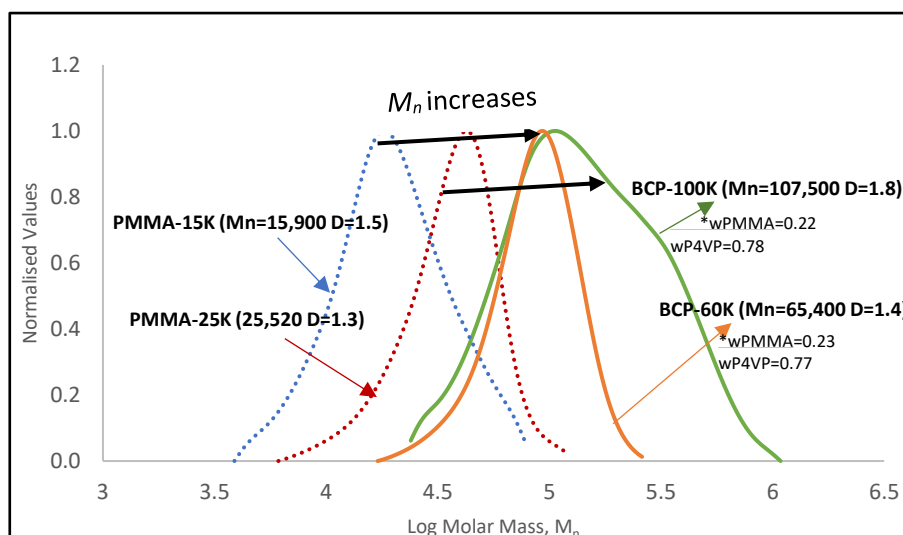


Figure 3.29. GPC traces of the 1st block-PMMA and the final product BCP, PMMA-*b*-P4VP ($M_{ntargeted1}$ = 60,000 g/mol, Table 3.7, entry 2 and $M_{ntargeted2}$ = 100,000 g/mol, Table 3.7, entry 1) from re-dispersion of PMMA-CTA. GPC traces of higher molecular weight showed high molecular weight shoulders indicated that side reactions such as chain transfer to polymer. Both products with the same target of block ratio, $w_{PMMA}:w_{P4VP} = 0.25:0.75$.

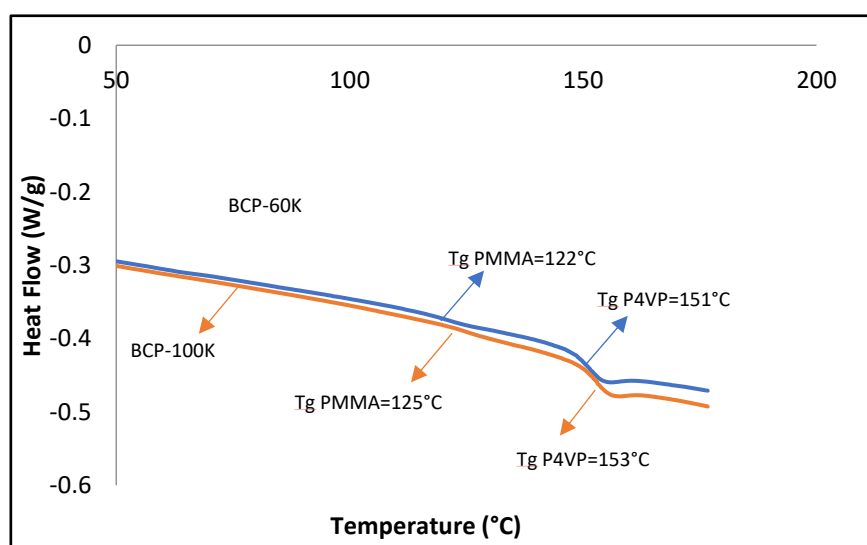


Figure 3.30 DSC traces of the BCP, PMMA-*b*-P4VP ($M_{ntargeted1}$ = 60,000 g/mol, Table 3.7, entry 2 and $M_{ntargeted2}$ = 100,000 g/mol, Table 3.7, entry 1) grown from re-dispersion of PMMA-CTA. Both BCPs recorded two T_g transition represent each block as an early indication of phase separation has occurred.

The SEM analysis showed high levels of agglomeration of the BCP (Figure 3.31b & d) particles for both molecular weights compared to the pure PMMA-CTA (Figure 3.31a & c) particles. The uneven spherical shape of particles indicates that fusing had occurred because of the swelling effect of excess 4VP added during the chain extension process.⁵ However, these particles were still able to form phase separated morphologies, as shown in the TEM analysis (Figure 3.32). Unfortunately, the higher molecular weight BCP ($M_n = 100,000$ g/mol) had formed SPH (Figure 3.32 a & b) instead of the desired LAM morphology. Only BCP at $M_n = 60,000$ g/mol formed the phase separated LAM morphology (Figure 3.32 c & d).

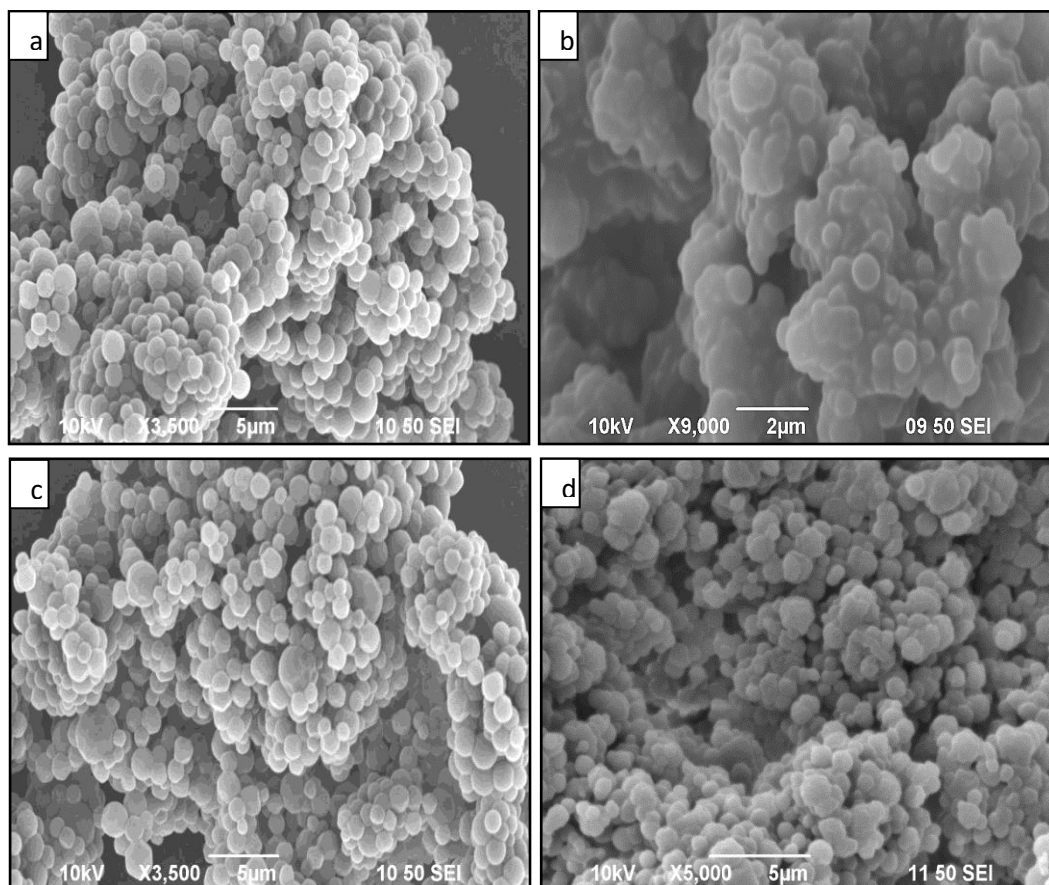


Figure 3.31. SEM images of PMMA₂₅ (a), PMMA₂₅-b-P4VP₇₅ ($M_{n\text{targeted}2} = 100,000$ g/mol, Table 3.7, entry 1) (b), PMMA₁₅ (c) and PMMA₁₅-b-P4VP₄₅ ($M_{n\text{targeted}1} = 60,000$ g/mol, Table 3.7, entry 2) (d) via re-dispersion of PMMA-CTA. All images produced discrete microparticles except for BCP with higher $M_n = 100,000$ g/mol has some particle fusion (b).

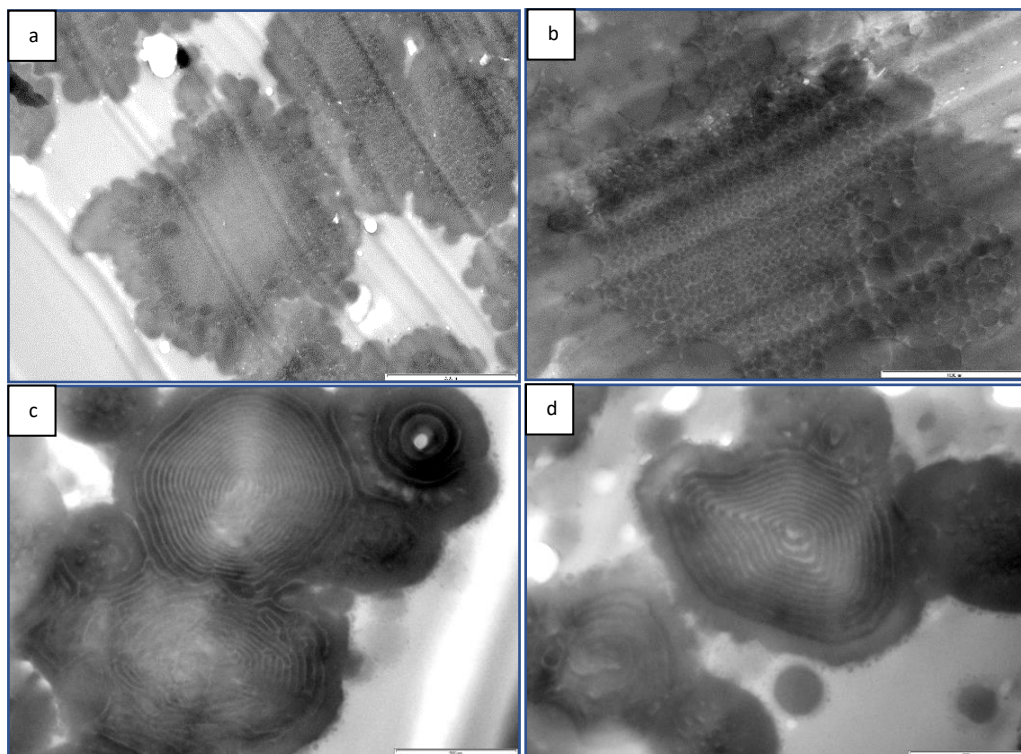


Figure 3.32. TEM images of PMMA₂₅-*b*-P4VP₇₅ ($M_{ntargeted2}$ = 100,000 g/mol, Table 3.7, entry 1) revealed the formation of SPH morphology (a-b) and PMMA₁₅-*b*-P4VP₄₅ ($M_{ntargeted1}$ = 60,000 g/mol, Table 3.7, entry 2) has successfully formed LAM morphology instead (c-d). Both BCP were synthesised by re-dispersion of PMMA-CTA.

In summary, the BCP PMMA-*b*-P4VP with LAM morphology was successfully synthesised using RAFT dispersion polymerisation in scCO₂. From this study, it was found that the PMMA₂₅-*b*-P4VP₇₅ ($M_{ntargeted2}$ = 100,000 g/mol, Table 3.6, entry 2), with a higher molecular weight, was synthesised by two consecutive polymerisation methods as described in Section 3.3.3. However, the GPC results did not show successful chain extension, as the PMMA peak did not appear to compare with the final product peak of the block copolymer. In addition, the DSC supported the GPC findings as only one transition, relating to the P4VP was observed. The SEM showed discrete particles and the TEM analysis indicated the formation of LAM morphology.

In the case of PMMA₁₅-*b*-P4VP₄₅ ($M_{n\text{targeted}1} = 60,000$ g/mol), a series of shorter independent steps was used to produce good microparticles with a targeted LAM morphology, as described in Section 3.3.4. The initial reaction (Table 3.7, Entry 2) showed good agreement with other repeat reactions (Table 3.7, Entry 3 & 4) and were close to the target value $M_{n\text{targeted}1} = 60,000$ g/mol. Replicates results (Table 3.7, Entry 3 & 4), with acceptable differences in block ratio and molecular weight, had comparable GPC traces (Figure 3.33). However, Entry 4 had a much higher dispersity than Entry 3, for both PMMA and the corresponding BCP product. These findings are corroborated by the larger particle size obtained, at 1.2 μm versus 0.9 μm . Additionally, the SEM image (Figure 3.35) clearly demonstrates that the majority of the particles in Entry 4 were agglomerated. In general, the particle sizes ranged between 0.9 and 1.2 μm , with a standard deviation of 0.3, indicate that there is no significant difference between them. The same trend was recorded by the DSC analysis, the T_g value (Figure 3.34) obtained for Entry 3 and Entry 4, were close to each other (Table 3.7). In both reactions, the TEM confirmed the formation of LAM morphology (Figure 3.36).

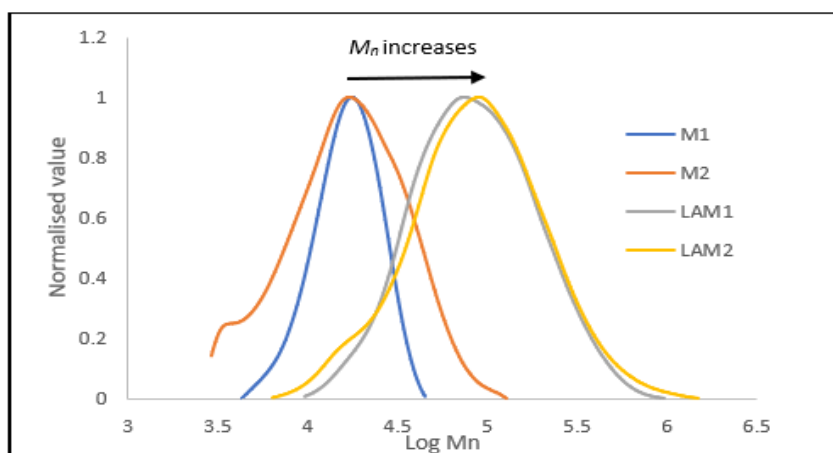


Figure 3.33. GPC traces of PMMA₁₅-*b*-P4VP₄₅ (Table 3.7 Entry 3 & 4) show non-significant difference between two replicates reaction. (Notes: M1= 1st block, PMMA (Entry 3), LAM1= BCP product (Entry 3), M2= 1st block, PMMA (Entry 4) , LAM2= BCP product (Entry 4)).

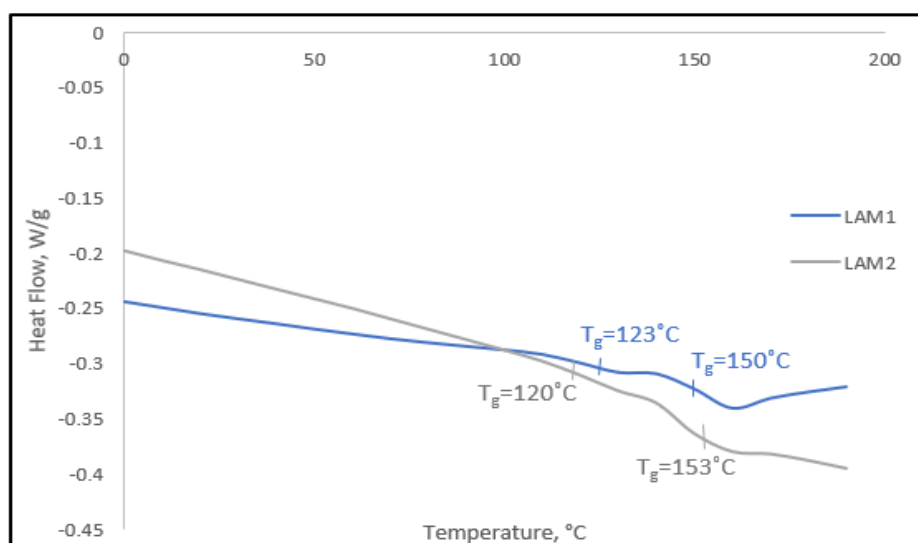


Figure 3.34. DSC traces of PMMA₁₅-*b*-P4VP₄₅ (Table 3.7 Entry 3 & 4) show a good agreement in T_g results between two replicates reaction. (Notes: LAM1= BCP product (Entry 3), LAM2= BCP product (Entry 4))

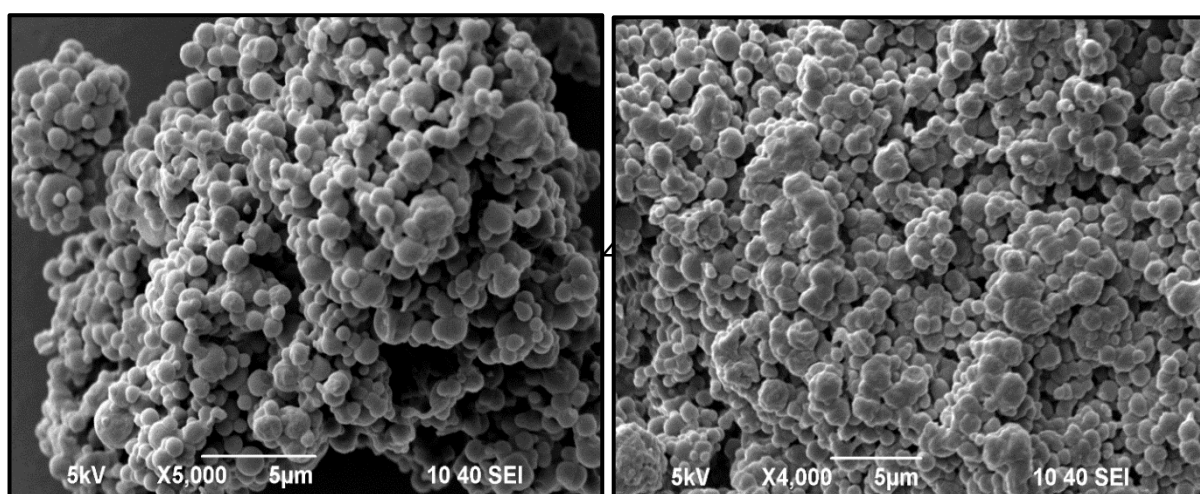


Figure 3.35. SEM Images of PMMA₁₅-P4VP₄₅ (Table 3.7 Entry 3 & 4) show discrete microparticles was obtained from both replicates reaction.

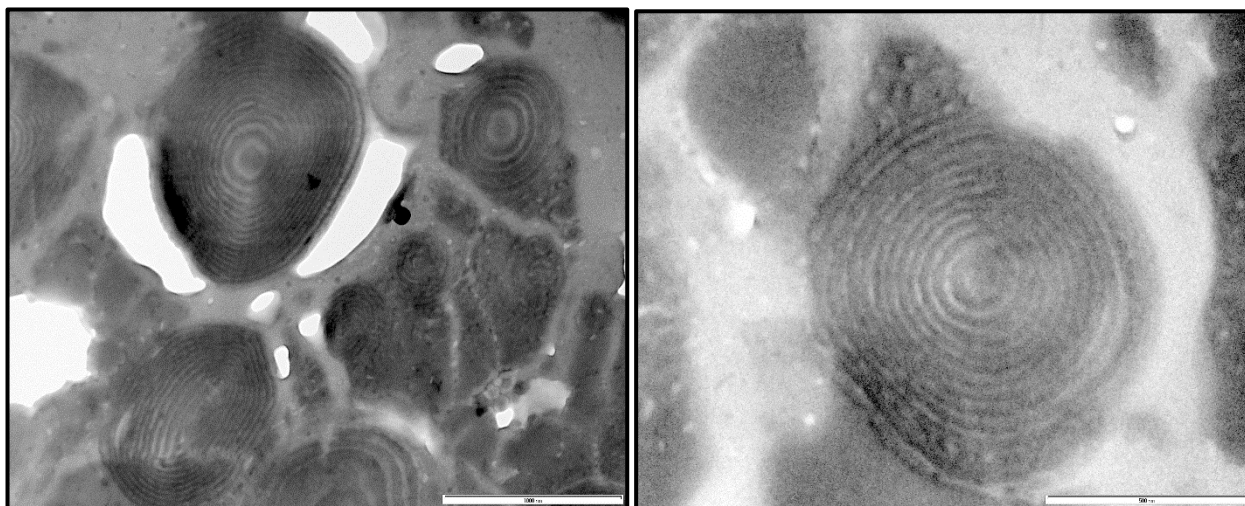


Figure 3.36. TEM Images of PMMA₁₅-P4VP₄₅ (Table 3.7 Entry 3 & 4) revealed that LAM morphology was successfully obtained from both replicates reaction.

3.5 Conclusions

This chapter has discussed the synthesis of the BCP PMMA-*b*-P4VP, using RAFT dispersion polymerisation in scCO₂. Initially, the first block of PMMA was synthesised using both FRP and CLRP to determine the differences of the products from both methods. Both techniques were investigated as both have benefits and which one is used often depends on end application of the polymer. Both methods produced white, fine, free-flowing powder, with a yield >85% and a conversion of >95%. The differences between the percent yield and percent conversion between reactions was attributed to human error during product collection from the autoclave, as some of the product sticks to parts of the autoclave such as the stirrer paddle and the large holes on the head of the autoclave that house the inlet and outlet pipes. Additionally, it is believed that some of the residual monomers were removed during the venting process, resulting in an artificially high conversion value.²⁵ The FRP products had average molecular weight (M_n) between 153,200 and 179,200 g/mol, with a dispersity of 1.4-1.5. In

comparison, the polymer produced by CLRP had a lower M_n with values ranging from 42,550 to 49,510 g/mol, which was closer to the target value of 50,000 g/mol, indicating good control by the RAFT agents used in this technique, namely DDMAT and CPDT. Due to the difference in M_n , the T_g of the PMMA produced by FRP was approximately 125–126 °C, this is higher than that of the PMMA synthesised by CLRP (100–116 °C); theoretically, the higher the M_n , the higher the T_g . Both techniques produced microparticles in the size range of 0.8 to 1.4 μm , which was found to be comparable to previous reports from the group that used 5% wt. PDMS-MA as a surfactant.^{11, 25, 38}

Subsequently, the primary goal of synthesising BCPs was accomplished by focusing on the PMMA-*b*-P4VP system. The polymerisation process was designed to produce BCPs with a range of sizes and a phase-separated morphologies. Initially attempts were made on both a small scale (20 mL) and on a medium scale (60 mL) at targeted M_n of 83,000 g/mol. The results obtained were generally comparable, and the successful synthesis of block copolymer was seen in the GPC results, which indicated chain extension of the PMMA by a shift in the peak to a higher M_n value in the final block copolymer, PMMA-*b*-P4VP. This is supported by an increase in the particle size, with the first PMMA block having a size of approximately 0.77 μm and the final block copolymers have a size of approximately 1.7 μm . In addition, the repeatability and reproducibility of the 60 mL reaction was determined, with satisfactory results obtained across replicates. The BCP, with a targeted molar block ratio of 60/40, produced a SPH internal phase separated morphology. However, the reaction targeting higher M_n ($M_{n\text{Target}} = 333,000$ g/mol) did not work very well and the M_n of BCP obtained was only 194,400 g/mol indicating that the RAFT agent was less effective at controlling polymerisation at higher molecular weights. Despite this, the molecular weight distribution remained unimodal, and the DSC showed two T_g s, giving an early indication that the

system had phase separated. However, TEM analysis was not performed because the SEM revealed that this higher molecular weight BCP had formed fused particles.

The next step focused on developing BCPs with a LAM internal morphology using the same BCP system, PMMA-*b*-P4VP, at a molar block ratio of 25/75. With a few modifications to a method previously developed in the group, BCPs, with a target molecular weight of $M_n = 60,000$ g/mol, could be successfully synthesised via a series of shorter independent steps, as described in Section 3.3.4.⁷ After the reaction, it was necessary to cool the autoclave to 10 °C in an ice bucket. This step was required when PMMA-CTA with low targeted M_n (15,000 g/mol) or low T_g were synthesised, as they tend to form softer polymer products as opposed to dry powder. The block copolymerisation was performed by re-dispersion of PMMA-CTA, that had previously been synthesised and stored for future use. This was subsequently chain extended through the addition of the second monomer, 4VP. To avoid the dissolution of the PMMA, the addition of 4VP to the living PMMA chains was carried out in two stages and the monomer was added under high pressure by an HPLC pump. The first addition induced phase separation within the formed particles giving rise to an internal morphology. The addition of the remaining monomer allowed for complete chain extension to occur and maintained the high quality of the microparticles.

SEM analysis showed that the synthesised products were well-defined microparticles, while the TEM analysis confirmed the formation of a LAM internal morphology. The DSC results supported this, with the trace showing two transitions, indicating the presences of each block, PMMA and P4VP. In addition, the block copolymerisation with a molecular weight of 60,000 g/mol demonstrated excellent repeatability and reproducibility across replicates.

The reactions targeting higher M_n ($M_{nTarget} = 100,000$ g/mol) did not work. The BCP product gave a SPH internal morphology instead the desired LAM. The GPC trace showed a high molecular weight shoulder which, as kinetics revealed, became more visible at high conversion.² This indicated that side reactions, such as chain transfer to polymer, which seemed to be enhanced in scCO₂, were most likely facilitated by the lower viscosity.⁴ However, the two-transitions observed in the DSC analysis show the presence of both blocks and was a clear indication that phase separation had occurred. Both microscopy analysis, SEM and TEM revealed that product contained fused particles and phase separated to form SPH morphology.

3.6 References

1. J. Jennings, Thesis (PhD)--University of Nottingham, 2013., 2007.
2. J. Jennings, M. Beija, A. P. Richez, S. D. Cooper, P. E. Mignot, K. J. Thurecht, K. S. Jack and S. M. Howdle, *Journal of the American Chemical Society*, 2012, **134**, 4772.
3. J. Jennings, M. Beija, J. T. Kennon, H. Willcock, R. K. Reilly, S. Rimmer and S. M. Howdle, *Macromolecules*, 2013, **46**, 6843-6851.
4. J. Jennings, S. Bassett, D. Hermida-Merino, G. Portale, W. Bras, L. Knight, J. J. Titman, T. Higuchi, H. Jinnari and S. M. Howdle, 2015.
5. J. Jennings, G. He, S. M. Howdle and P. B. Zetterlund, *Chem. Soc. Rev.*, 2016, **45**, 5055-5084.
6. S. P. Bassett, N. A. Birkin, J. Jennings, E. Chapman, R. K. O'Reilly, S. M. Howdle and H. Willcock, *Polym. Chem.*, 2017, **8**, 4557-4564.
7. M. Alauhdin, Thesis (PhD)--University of Nottingham, 2017., 2017.
8. M. Alauhdin, T. M. Bennett, G. He, S. P. Bassett, G. Portale, W. Bras, D. Hermida-Merino and S. M. Howdle, *Polym. Chem.*, 2019, **10**, 860-871.
9. G. He, T. M. Bennett, M. Alauhdin, M. W. Fay, X. Liu, S. T. Schwab, C.-G. Sun and S. M. Howdle, *Polym. Chem.*, 2018, **9**, 3808-3819.
10. G. He, T. M. Bennett, K. Alias, L. Jiang, S. T. Schwab, M. Alauhdin and S. M. Howdle, *Polymer Chemistry*, 2019, **10**, 3960-3972.
11. R. R. Larder, T. M. Bennett, L. S. Blankenship, J. A. Fernandes, B. K. Husband, R. L. Atkinson, M. J. Derry, D. T. W. Toolan, H. A. Centurion, P. D. Topham, R. V. Gonçalves, V. Taresco and S. M. Howdle, *Polymer chemistry*, 2021, **12**, 2904-2913.
12. F. Z. Benabid, F. Zouai, A. Silini and D. Benachour, *Iranian journal of science and technology. Transaction A, Science*, 2018, **42**, 245-249.
13. B. I. N. Zhao and X. Zhao, *Journal*, 2014.
14. P. Gilormini, L. Chevalier and G. Régnier, *Polymer engineering and science*, 2010, **50**, 2004-2012.

15. Y. Gao, Y. Wu, J. Liu and L. Zhang, *Journal of polymer science. Part B, Polymer physics*, 2017, **55**, 1005-1016.
16. E. Yoshida, *Colloid and polymer science*, 2012, **290**, 661-665.
17. A. M. Gregory, Thesis (PhD)--University of Nottingham, 2008.
18. P. Ramar, S. Jana, S. Chatterjee, S. N. Jaisankar and D. Samanta, *New journal of chemistry*, 2019, **43**, 15935-15945.
19. J. G. Kennemur, *Macromolecules*, 2019, **52**, 1354-1370.
20. C. Cummins and M. A. Morris, *Microelectronic engineering*, 2018, **195**, 74-85.
21. S.-W. Hsu, A. L. Rodarte, M. Som, G. Arya and A. R. Tao, *Chemical reviews*, 2018, **118**, 3100-3120.
22. M. B. Gawande, A. Goswami, T. Asefa, H. Guo, A. V. Biradar, D.-L. Peng, R. Zboril and R. S. Varma, *Chemical Society reviews*, 2015, **44**, 754-759.
23. B. H. Sohn and B. H. Seo, *Chemistry of materials*, 2001, **13**, 1752-1757.
24. P. Christian, S. M. Howdle and D. J. Irvine, *Macromolecules*, 2000, **33**, 237-239.
25. A. J. Haddleton, S. P. Bassett and S. M. Howdle, *The Journal of supercritical fluids*, 2020, **160**, 104785.
26. K. Kortsen, A. A. C. Pacheco, J. C. Lentz, V. Taresco and S. M. Howdle, *The Journal of supercritical fluids*, 2021, **167**.
27. J. Brandrup, E. H. Immergut and E. A. Grulke, *Polymer handbook / editors J. Brandrup, E. H. Immergut, and E. A. Grulke ; associate editors A. Abe, D. R. Bloch*, Hoboken, N.J. : John Wiley & Sons, Hoboken, N.J., 4th ed. edn., 1999.
28. G. Odian, *Principles of Polymerisation*, John Willey & Sons, Inc., 4th Edition edn., 2004.
29. A. A. C. Pacheco, A. F. Da Silva Filho, K. Kortsen, M. W. D. Hanson-Heine, V. Taresco, J. D. Hirst, M. Lansalot, F. D'Agosto and S. M. Howdle, *Chemical science (Cambridge)*, 2020.
30. K. Ute, N. Miyatake and K. Hatada, *Polymer*, 1995, **36**, 1415-1419.

31. J. Shin, W. Bae and H. Kim, *Kolloid-Zeitschrift und Zeitschrift für Polymere*, 2010, **288**, 271-282.
32. M. R. Giles, J. N. Hay, S. M. H. and R. J. Winder, *Polymer*, 2000, **41**, 6715 - 6721.
33. A. M. Gregory, PhD Thesis, University of Nottingham, 2007.
34. A. Arora, D. C. Morse, F. S. Bates and K. D. Dorfman, *Soft Matter*, 2015, **11**, 4862-4867.
35. M. Shoji, M. Eguchi, J. M. Layman, M. P. Cashion, T. E. Long and H. Nishide, *Macromolecular Chemistry and Physics*, 2009, **210**, 579-584.
36. N. P. Truong, M. V. Dussert, M. R. Whittaker, J. F. Quinn and T. P. Davis, 2015, **6**, 3865-3874.
37. M. Matsen and F. Bates, *Macromolecules*, 1996, **29**, 1091-1098.
38. T. D. McAllister, T. M. Bennett, C. Petrillo, C. Topping, L. D. Farrand, N. Smith and S. M. Howdle, *Journal of Materials Chemistry C*, 2019, **7**, 12194-12203.

Chapter 4

***In situ* crosslinking of nanostructured block copolymer microparticles in super critical carbon dioxide**

The main focus of this chapter is crosslinking, which is discussed in depth including its aims, a discussion of the methodologies, and benefits. It will describe a newly developed method for crosslinking microparticles, that successfully preserves their internal morphology at varying degrees of crosslinking. Initially, free radical polymerisation (FRP) was used to crosslink PMMA homopolymer. The characterisation of the PMMA products, with varied degrees of crosslinking, will be examined in depth. Subsequently, RAFT polymerisation will be employed to develop a novel and facile method for *in situ* crosslinking copolymerisation in scCO₂ dispersion. This will enable the fixing of the internal nanostructure of the BCP microparticles with either SPH or LAM internal morphology. The key discovery is the behaviour and performance of crosslinked microparticles, particularly the LAM, which is a novel characteristic of our work. Various analytical techniques, including a dissolution test in chloroform and THF, swelling/de-swelling by an ethanol-hexane mixture were used to determine the porosity control by degree of crosslinking. The overall conclusion of this chapter will be to demonstrate the effectiveness of the new crosslinking method to preserve the microstructure and internal morphology of SPH and LAM microparticles in the presence of good solvents.

4.1 Introduction

In spite of the numerous current developments in the synthesis of nanostructured BCP microparticles, as discussed in depth in the previous chapter, in particular heterogeneous controlled radical polymerisation,¹⁻⁴ there is an essential plight: the particle structure can be lost in some application conditions. Hence my approach is to develop a method to fix the problem by using the crosslinking approach.

The crosslinking of polymers has become an area of intense scientific investigation over the past few decades, because the resulting materials have many interesting properties, possess improved mechanical properties and/or resistance to external stimuli such as temperature, solvents and reactive species.⁵ Furthermore, crosslinking improves the capability of site-specific drug delivery, with no off-target effects that is a crucial feature for drug carriers for controlled release. It has also been demonstrated that the crosslinking of polymer materials enhances their resistance to fluids^{6, 7} and stress cracking.⁸⁻¹¹

In polymerisation, crosslinking is a process that forms a network, in which the molecules are linked to each other at points other than their ends. It is also referred to as covalent crosslinking. This is a common and robust strategy to stabilize block copolymer nano-assemblies prepared by reversible addition-fragmentation chain transfer mediated -induced self-assembly (RAFT-mediated PISA). Numerous compounds with unique reactive substituents have been explored for their potential to crosslink block copolymer nano assemblies. To summarise, the crosslinking concepts that are being used can be divided into two categories: *in situ* crosslinking and post-polymerization crosslinking. For discussion purposes, this chapter has focused on a specific family of crosslinked polymer compounds.

As a basis for this study, initial attempts were made to crosslink homopolymer PMMA particles, by dispersion polymerisation using FRP in

scCO₂. Even though this approach was not novel, it allowed for the set-up of optimised experimental conditions which could be used in subsequent cross linking reaction involving block copolymers. In 2002, Wang et al. were successful in preparing discrete, crosslinked micropolymer particles, with high monomer conversion in less than four hours in scCO₂. They found that the morphology of synthesised particles was dramatically affected by the reaction pressure and stabiliser concentration.¹² Later in 2010, Shin et al. also demonstrated the effect of reaction pressure on the morphology of crosslinked PMMA particles.¹³ It was found that the crosslinked PMMA particles became more agglomerated as the concentration of EGDMA increased and as the pressure decreased at constant temperature (Figure 4.1 and 4.2). However, the T_g of the crosslinked particles increased with increasing EGDMA concentration, pressure, and temperature, indicating that the morphology and properties of PMMA particles are well controlled by both the crosslinker content and CO₂ density.¹³

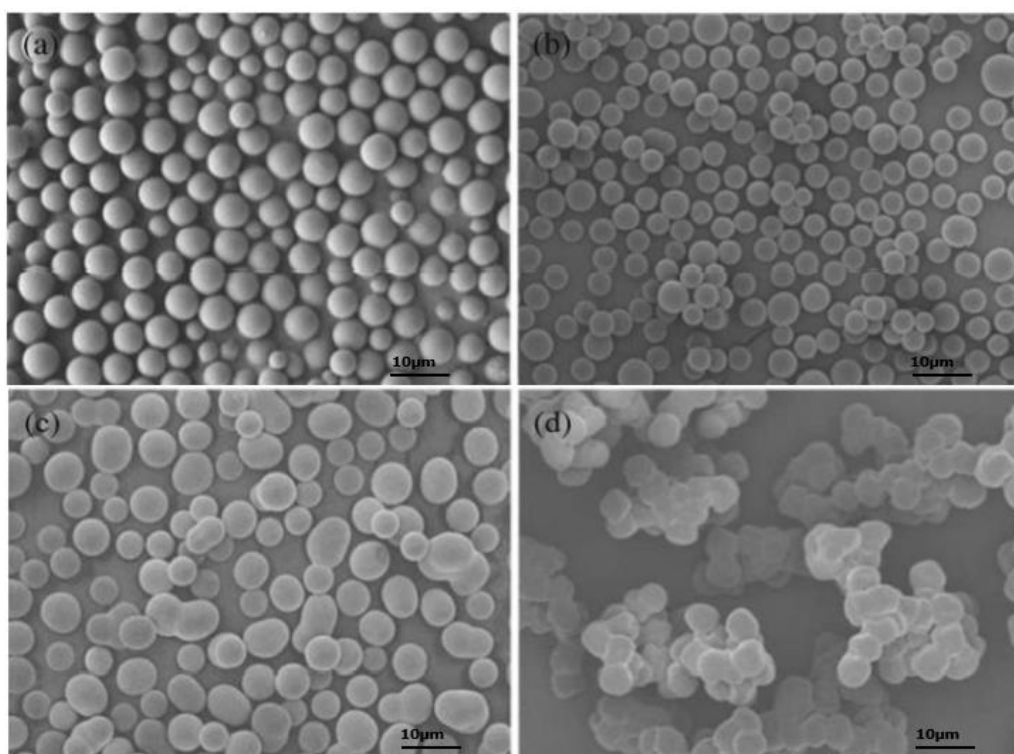


Figure 4.1. SEM pictures of PMMA particles with crosslinker amount of 0 wt% (a), 0.1 wt% (b), 0.2 wt% (c) and 0.4 wt% (d).¹³ All scale bars are 10 μm. The particles become more agglomerated as the crosslinker amount increased.

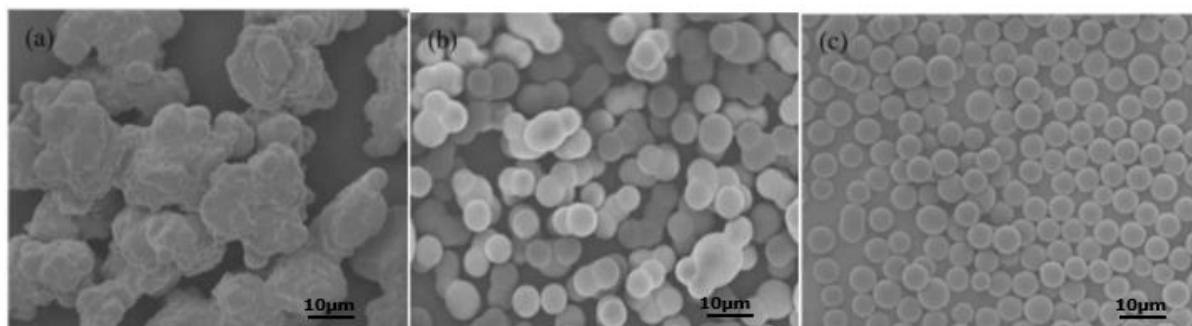


Figure 4.2. SEM pictures showing the effect of reaction pressure on the particle morphology, at 200 (a), 280 (b) and 350 bar (c).¹³ All scale bars are 10 μm .

Over the past decades, several experimental techniques have been developed in order to crosslink polymeric particles. As discussed in depth in chapter one, the techniques used were categorised into two methods i.e., post-polymerisation chemical reactions and *in situ* crosslinking. Hence, this chapter will bring the background of this study on how crosslinking approach was chosen.

The Howdle group have previously established a synthetic route to produce nanostructured microparticle BCPs on the multigram scale via a one pot RAFT dispersion polymerisation in scCO_2 (Figure 4.3).^{2, 14-17} In addition, the group has also optimised an approach to manipulate the microparticle size, by controlling both the initial monomer and stabiliser loadings. The diameters of the microparticles can be well controlled from 5 μm down to 300 nm (Figure 4.4).¹⁸

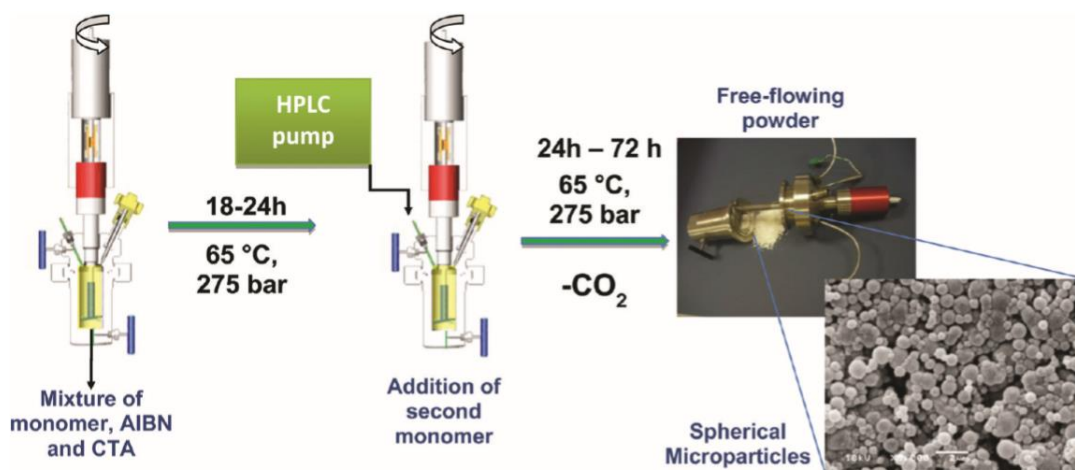


Figure 4.3. One-pot synthesis method for the clean preparation of nanostructured polymeric microparticles in scCO₂.¹⁴

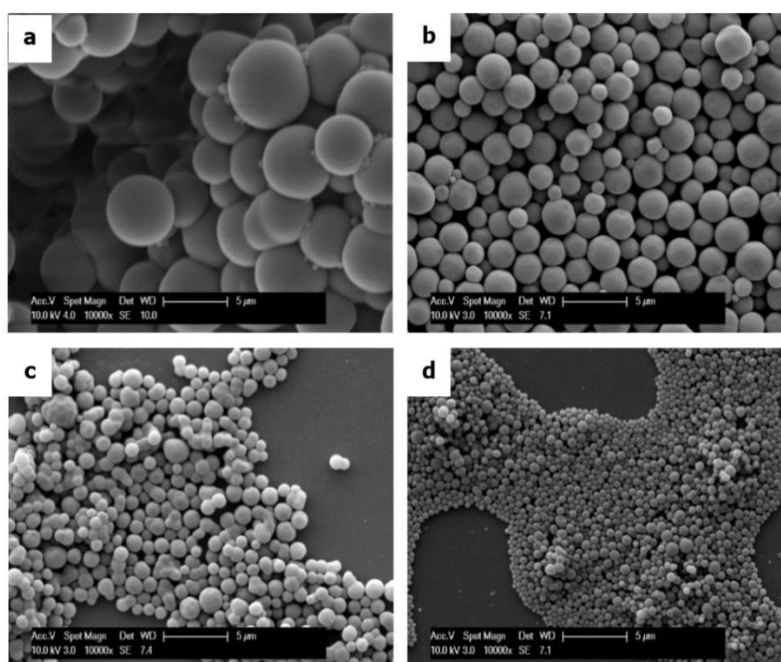


Figure 4.4. SEM images showing polymer particles synthesised with a) 1 wt%, b) 5 wt%, c) 10 wt% and d) 20 wt% PDMS-MA stabiliser. The number average diameters are 3966, 1815, 1047 and 508 nm respectively.¹⁸ All scale bars are 5 µm.

They recently published a versatile technique to transform these nanostructured microparticles into porous microparticles via a swelling/rapid deswelling process.¹⁶ It was demonstrated that the porosity can be customised over a wide size range from 20 to 200 nm, and diverse morphologies from isolated spherical pores, short porous channels, to interpenetrated pore networks, could be achieved by adjusting the block ratio and block length (Figure 4.5).¹⁶

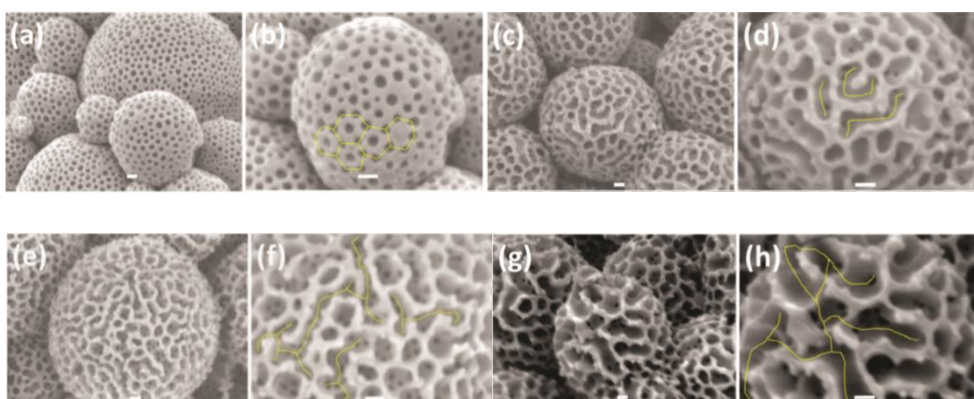


Figure 4.5. Controlled nanoporosity introduced into block copolymer microparticles by selective swelling/deswelling in ethanol with hexane. SEM images of PMMA-*b*-P4VP porous microparticles. (a) PMMA-P4VP13.3, (c) PMMA-P4VP19.9, (e) PMMA-P4VP27.8, (g) PMMA-P4VP30.9. (b, d, f, h) are higher magnification images of (a, c, e, g) respectively. The yellow lines in (b, d, f, h) mark the surface pore evolution from isolated spherical pores to short channels, and to interconnected channels.¹⁶

To make these materials more versatile for a wide range of applications, such as templates for materials synthesis, drug delivery, slow-release materials, etc., it is important to ensure that the particle structures and internal morphology can be sufficiently sustained when exposed to fluid (for example organic solvent) environment. To the best of our knowledge, little effort has been given to the internal crosslinking approach of such larger micron-sized particles, particularly those with hierarchical structures achieved *in situ* through polymerisation induced microphase separation.

Based on these arguments and the knowledge gap in this field, we now describe a technique for selectively crosslinking the internal phase separated domains of BCP microparticles during their one-pot polymerisation in scCO₂, therefore enhancing the integrity of the structure in the presence of solvents or, indeed, any other trigger. This technique permits *in situ* crosslinking of nanostructured BCP microparticles without impairing their polymerisation-induced phase separation morphologies.^{19,}

20

4.2 Materials

Methyl methacrylate (MMA, ProSciTech, 99%) and 4-vinylpyridine (4VP, Acros, 95%) were purified by passing through a neutral alumina column and stored at -20°C, 2,2'-azobis(isobutyronitrile) (AIBN, Sigma Aldrich, 98%) was re-crystallised in methanol, methacrylate terminated polydimethylsiloxane (PDMS-MA, M_n= 10,000 g mol⁻¹, ABCR GmbH & Co.), 2-(dodecylthiocarbonothioylthio)-2-methylpropionic acid (DDMAT, Sigma Aldrich, HPLC Grade, 98%), ethylene glycol dimethacrylate (EGDMA, Merck, 97.5%), divinylbenzene (DVB, Aldrich, Technical Grade 80%), CDCl₃ (Aldrich, 99.9%), HPLC grade THF (Acros), chloroform (Aldrich, 99.9%), ethanol, absolute (Fisher >99.8%), triethylamine (TEA), n-dodecane (Alfa Aesar, 99+%) and iodine (Fisher) were all used as received. Agar 100 resin (Agar Scientific) was used as received, and a formulation of medium hardness was used for embedding samples. All high-pressure reactions used high purity carbon dioxide (>99.99%, BOC Gases, SFC Grade) as received.

4.3 Methods

4.3.1 *In situ* crosslinking of PMMA homopolymer

The reaction was performed using the same high-pressure autoclave set-up and conditions described in the previous chapter (3.3.1) by batch reaction in one-pot, using FRP technique (Figure 4.6). Once satisfied that the equipment was leak free, the reactants were weighed into a glass vial accordingly as follows; monomer, MMA (3.33 mL), initiator, AIBN (1 wt% with respect to MMA), surfactant, PDMS-MA (5 wt% with respect to MMA) and crosslinker, EGDMA (0.1 wt% with respect to MMA). The mixture of reactants was then degassed with argon for about 20-30 minutes. In the meantime, the autoclave was also degassed with CO₂ at 15-40 psi prior to injection of the reactants mixture. The autoclave was then sealed, pressurised to 650 psi, heated to 65 °C and pressurised further to the reaction condition for about 4080 psi gradually, left stabilise and stirred at 300 rpm for 4 hours. Prior completion of the reaction, the temperature was set to 0°C and the autoclave was allowed to cool to room temperature before being depressurised. The resulting products were collected using spatula and filter paper before being kept in a suitable sized glass vial.

Stage 1

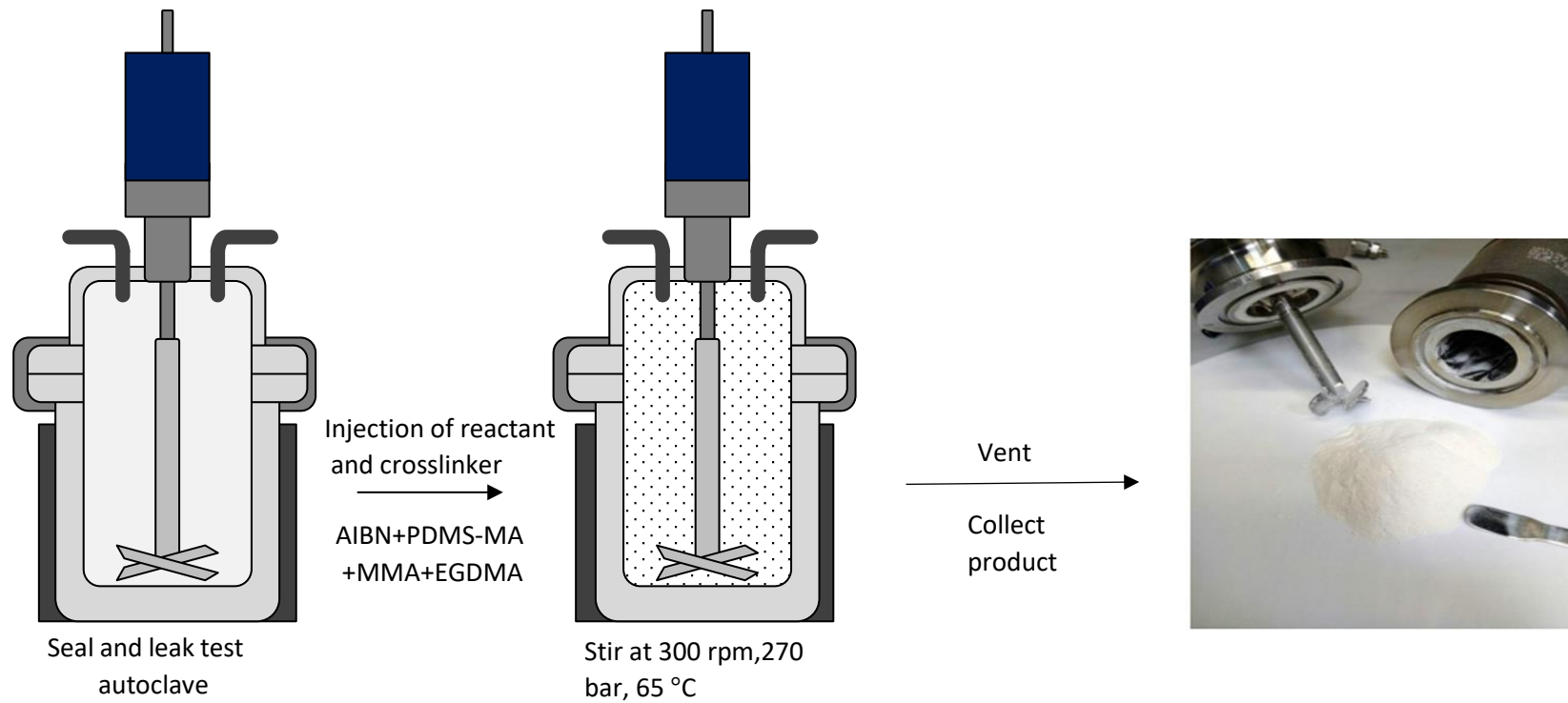


Figure 4.6. *In situ* crosslinking of PMMA homopolymer microparticles by FRP dispersion polymerisation in scCO_2 in a one-pot, batch method. It involves only 1 stage; all reactants needed for polymerisation of PMMA and crosslinking with EGDMA was injected into the autoclave at the start of reaction.

4.3.2 *In situ* crosslinking copolymerisation of PMMA-*b*-P4VP via RAFT

The following section will discuss two different approaches in adding 4VP by one-step addition method or two-step addition method which were applied to particles with a SPH and LAM internal morphology.

4.3.2.1 One-step addition -SPH morphology

The *in situ* crosslinking of PMMA-*b*-P4VP was first carried out in one-step addition of 4VP method, in which the crosslinker DVB was copolymerised along with 4VP once the first monomer, MMA was consumed.

A typical one pot, one-step addition of 4VP method is described below for 0.5 wt.% crosslinker relative to the total 4VP monomer, PMMA₅₀₀-*b*-P4VP₃₃₀/D0.5 (where D denotes the crosslinker and numbers following denote the amount of crosslinker in weight percentage relative to total 4VP) (Figure 4.7).

An autoclave was purged with CO₂ for approximately 20-30 minutes (~ 30 psi). The reactants needed to grow the first block, PMMA. MMA (7.5 g), DDMAT (55 mg), AIBN initiator (12.5 mg), and PDMS-MA surfactant (0.625 g) were pre-mixed in a glass vial and degassed with argon for 20-30 minutes before being transfer into the autoclave. The autoclave was then sealed, pressurised to 650 psi, heated to 65 °C and gradually pressurised further to the reaction condition, 3500 psi. The autoclave was left to stabilise and stirred at 300 rpm for 20 hours, to achieve full conversion of the MMA. Subsequently, the mixture containing the second monomer, 4VP (5 g), AIBN (6.3 mg) and crosslinker, DVB (0.025 g) was degassed with argon for 20-30 minutes and pumped-in through the inlet pipe dedicated for HPLC addition on the top of the autoclave at 1 mL/min.

The crosslinking copolymerisation of 4VP and DVB was allowed to react for a further 20 hours, at approximately 3500-4000 psi depending on the final pressure that the autoclave settled at after the injection process. Post reaction, the autoclave was cooled to room temperature and then depressurised to allow for collection of the final product, a fine, free-flowing white powder.

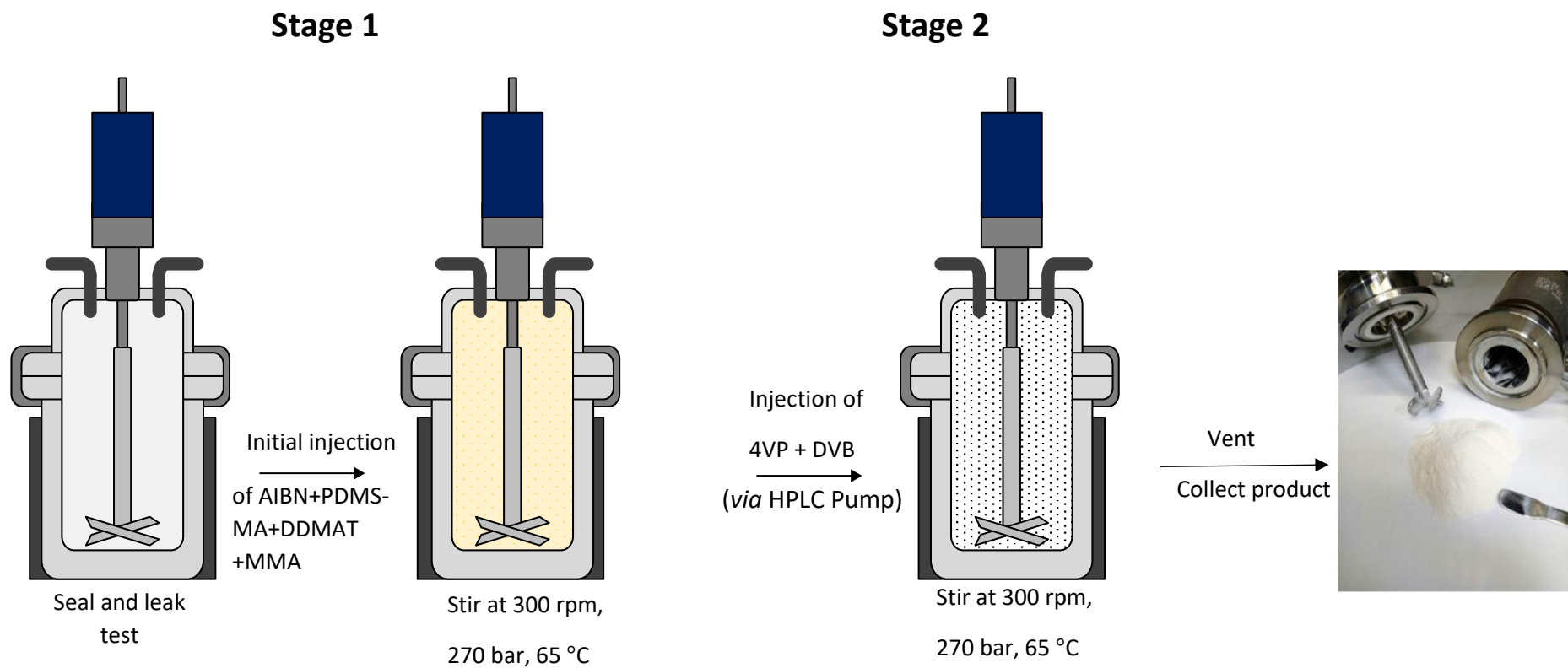


Figure 4.7. The *in situ* crosslinking of PMMA-*b*-P4VP microparticles by RAFT dispersion polymerisation in scCO₂ in a one-pot, one-step addition of 4VP method. It involves 2 stages; the initial injection to grow the 1st block PMMA particles (stage 1) and the injection of 4VP together with crosslinker (DVB) to crosslink 4VP domain in the microparticles while the 4VP chain was growing (stage 2).

4.3.2.2 Two-step addition -SPH morphology

In this method, the only difference was that the addition of 4VP was performed in two stages and the crosslinker was combined with the second portion of 4VP. It was developed based on modification of method stated earlier in Chapter 3 (Section 3.3.3) to crosslink microparticles with SPH nanostructure.

As before, a typical one-pot, two-step addition of 4VP method is described below for PMMA₅₀₀-*b*-P4VP₁₇₀-*b*-P4VP₁₆₀/D0.5, 0.5 wt.% of crosslinker relative to the total 4VP monomer (where D denotes the crosslinker and numbers following denote the amount of crosslinker in weight percentage relative to total 4VP) (Figure 4.8).

The first block polymerisation of PMMA, was conducted as described above in section 4.3.2, using MMA (7.5 g), DDMAT (55 mg), AIBN initiator (12.5 mg), and PDMS-MA surfactant (0.625 g). After a given polymerisation time of the first block, typically 20 hours, the second block (P4VP) was then grown by addition of the first portion of 4VP (2.55 g) and additional AIBN (6.3 mg), which had been purged with Argon for 20-30 minutes and added to the autoclave via a HPLC pump at 1 mL/min. The polymerisation of 4VP was left to proceed for another 20 hours, with continuous stirring at 300 rpm. Subsequently, the second portion of 4VP (2.45 g) and AIBN (6.3 mg) together with DVB (0.05 g), following the same procedure described above. The crosslinking copolymerisation of P4VP with DVB was allowed to proceed for a further 20 hours. The autoclave was then cooled to room temperature and vented to release the pressure, before the product was collected. The product obtained was typically a fine white powder.

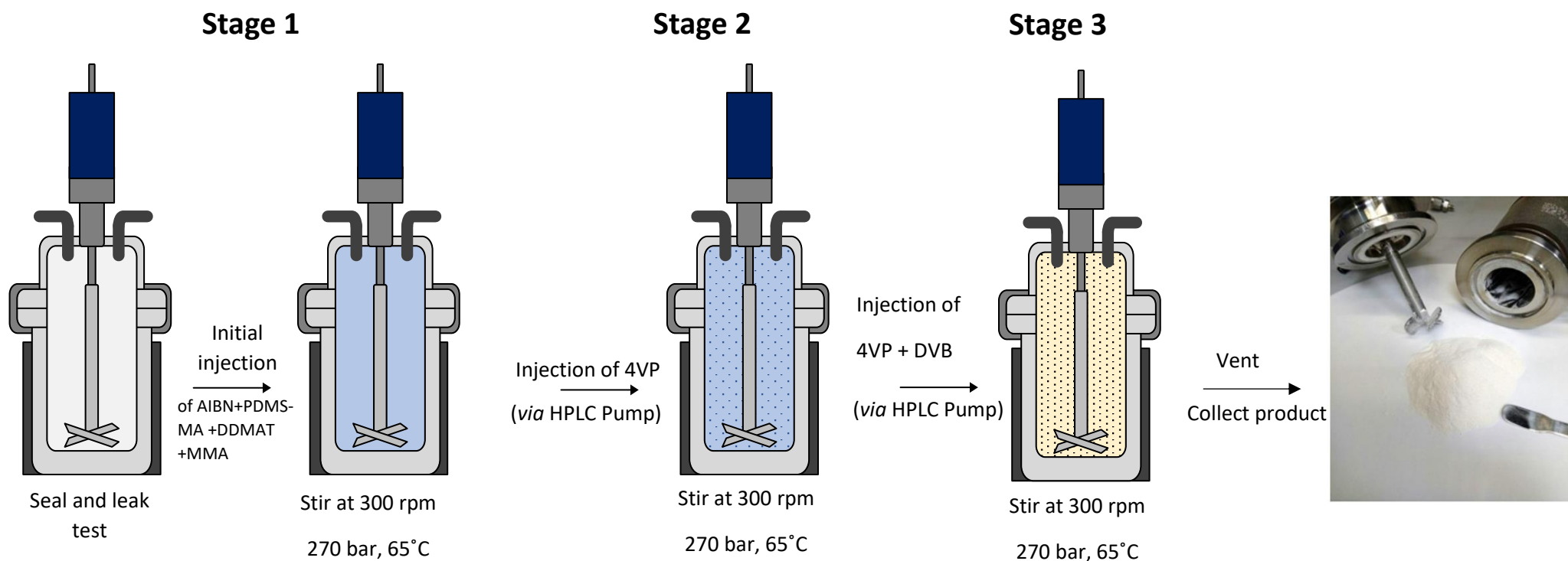


Figure 4.8. *In situ* crosslinking of PMMA-*b*-P4VP microparticles by RAFT dispersion polymerisation in scCO₂ in a one-pot, two-step addition of 4VP method.¹⁹ It involves 3 stages; the initial injection to grow the 1st block PMMA particles (stage 1), the injection of certain portion of 4VP for chain extension (stage 2) and then the injection of the remaining 4VP together with crosslinker (DVB) for crosslinking of 4VP domain (stage 3)

4.3.2.3 Two-step addition -LAM morphology.

This method was developed based on modification of the method described in section 3.3.4, to crosslink microparticles with LAM nanostructure. It also involved two step addition of 4VP in which DVB was copolymerised with the second portion of 4VP.

A method describes below for PMMA₁₅₀-*b*-P4VP₄₀₀-*b*-P4VP₅₀/D0.5, 0.5 wt.% of crosslinker relative to the total 4VP monomer (where D denote the crosslinker and numbers following denote the amount of crosslinker in weight percentage relative to total 4VP) (Figure 4.9)

A 60 mL autoclave was charged with pre-synthesised PMMA-RAFT (section 3.3.4) (3.76 g, assumed M_n PMMA = 15,000 Dalton) and PDMS-MA (0.562 mg, 5wt% w.r.t. 4VP) before it was clamped and purged with CO₂ (50-60 psi) for 15 minutes. The autoclave was sealed and pressurised with the addition of CO₂ to 800 psi. The stirrer was turned on and adjusted to 300 rpm to start the re-dispersion process. The heater was then set to 65 °C. Once 65 °C had been reached, additional CO₂ was added to reach a pressure of 3000 psi and the system was left for at least 4 hours (overnight is preferred) to allow for a good re-dispersion. Subsequently, the second block (P4VP) was grown by adding the first portion of 4VP (10.53 g) and additional AIBN (26.3 mg), which was purged with argon for 20-30 minutes prior to being added to the autoclave via a HPLC pump at 1 mL/min. The polymerisation of 4VP was left to proceed for another 20 hours, with continuous stirring at 300 rpm. Following this, the second portion of 4VP (1.32 g) and AIBN (3.3 mg) together with DVB (0.0562 g) was added, following the same procedure described above. The crosslinking copolymerisation of P4VP with DVB was allowed to proceed for a further 20 hours. Once the reaction was completed, the heating was removed, and autoclave was allowed to cool to room temperature before being depressurised. The resulting products were collected and kept at room temperature for characterisation.

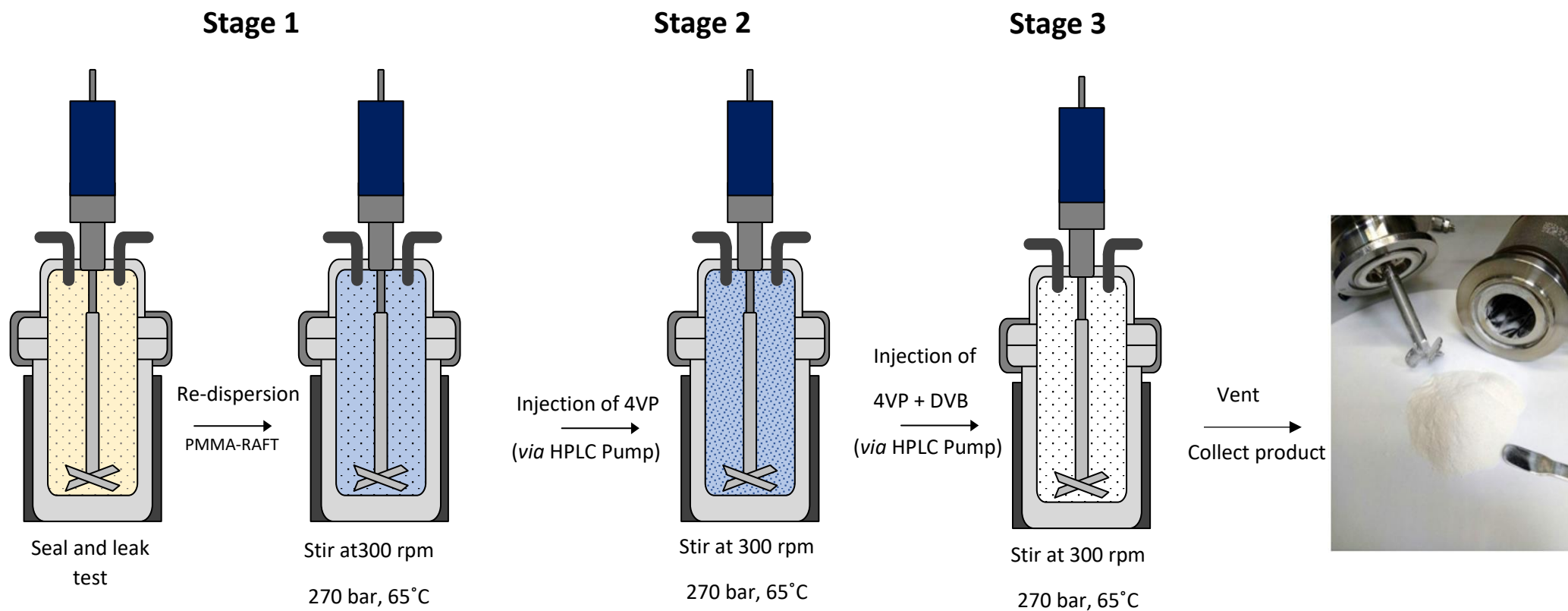


Figure 4.9. *In situ* crosslinking of PMMA-*b*-P4VP microparticles by RAFT dispersion polymerisation in scCO₂ in a series of shorter independent steps by two-step addition of 4VP method. It involves 3 stages; the re-dispersion of PMMA-RAFT microparticles (stage 1), the injection of a certain portion of 4VP for chain extension (stage 2) and the injection of remaining 4VP together with crosslinker (DVB) to crosslink the 4VP domain (stage 3).

4.3.3 Determination of crosslinking formation

The BCP samples, both non-crosslinked and crosslinked microparticles (30 mg) were dispersed into chloroform (3 mL) and shaken using a mechanical shaker to get sufficient homogenization of the resulting solutions or suspensions. Subsequently, the samples were left on the bench for 24 hours for observation. The same procedure was repeated using tetrahydrofuran (THF). The choice of solvent is based on a good solvent that can dissolve the targeted polymer materials.

4.3.4 Determination of Insoluble Fraction (Gel Content)



Figure 4.10. Procedure to determine the crosslinking density of PMMA-*b*-P4VP that was crosslinked by DVB. Dissolution of material in chloroform (1), Sample filtration (2) and soluble (in the tube) and insoluble (on the filter paper) components (3).

Analysis was performed by dissolving approximately 100 mg of materials (non crosslinked and crosslinked BCP microparticles) in 10 mL of chloroform (to get a concentration of ~ 10 mg/mL) (Figure 4.10). After allowing the material to settle overnight, it was frozen at $T = -20$ °C and centrifuged to obtain a satisfactory separation. Subsequently, the samples were filtered to separate the soluble from the insoluble components. Following this, the samples were dried in a vacuum oven, set to $T = 55$ °C, and weighed repeatedly until a consistent weight was obtained. The gel content was measured by weighing the dried fraction of insoluble particles, m_2 obtained

from chloroform layer over the initial weight of samples exposed, m_1 . Gel content was determined from the following equation:

$$\text{GF (\%)} = (m_2 / m_1) \times 100 \quad \text{(Equation 4.1)}$$

4.3.5 Porosity Control by Degree of Crosslinking

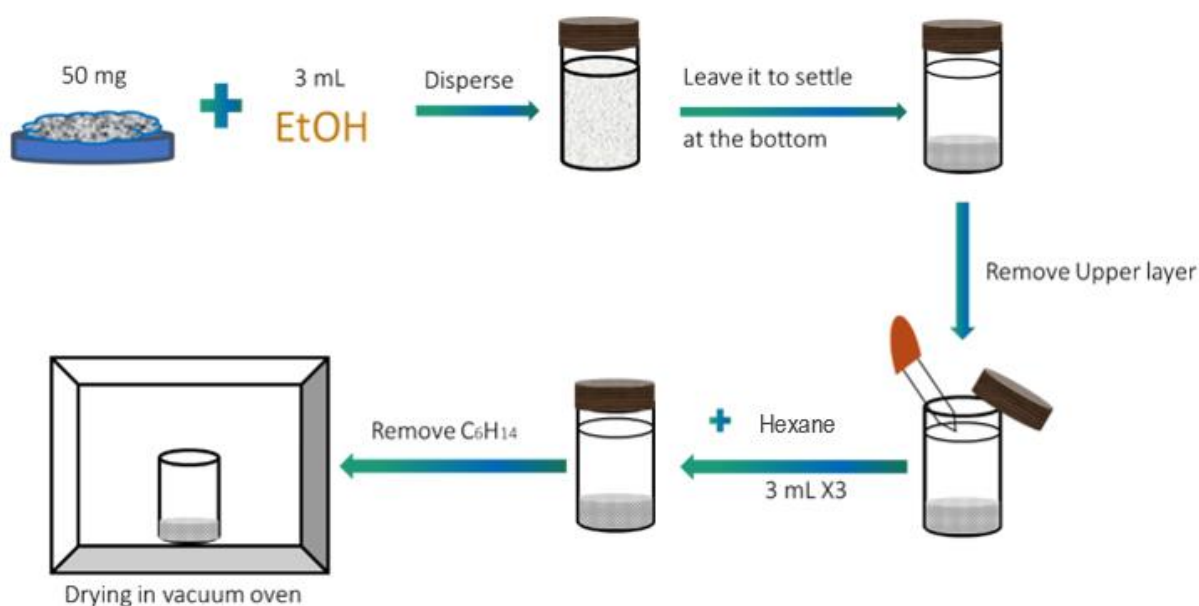


Figure 4.11. Swelling/ deswelling process of crosslinked particles in EtOH/hexane, to evaluate porosity control by degree of crosslinking.

The BCP microparticles (50 mg) were dispersed in ethanol (3 mL) in a glass vial and manually shaken three times over a two-hour period. The particles were then allowed to stand until they settled to the bottom of the vial. The upper layer of alcohol was removed and hexane (3 mL) was added and the particles were thoroughly rinsed with vigorous shaking by hand. After two hours, the particles were allowed to resettle before the hexane layer was removed. Three additional hexane rinses were performed to completely

remove the alcohol, and the polymer obtained was dried in a vacuum oven at 25 °C for > 2 hours prior to further analysis (Figure 4.11).

4.4 Results and Discussion

4.4.1 *In situ* crosslinking of PMMA homopolymer

Initial attempts to develop a crosslinking method for microparticles in scCO₂ were done via a simple one pot, batch method. This method investigated the effects of introducing a crosslinking agent during polymerisation of PMMA via free radical technique. The crosslinking agent used was EGDMA and it was added at systematically increasing concentrations, starting from 0 wt.%, 0.1 wt. %, 0.2 wt. %, 0.4 wt. % and 1.0 wt. % (Table 4.1, entry 1-5). All products were collected as a dried powder and the particle morphology was investigated by SEM. This analysis revealed that crosslinker loadings of 0.1 and 0.2 wt.% (Table 4.1, entry 2 and 3) resulted in discrete spherical particles (Figure 4.12a-b). In contrast, increasing the loading to 0.4 wt. % (Table 4.1, entry 4) saw the formation of agglomerated particles (Figure 4.12c), which were fused (Figure 4.12d) even further at the highest loading of 1.0 wt. % (Table 4.1, entry 5). These results agree with those reported by Shin et al. in 2010 for crosslinked PMMA synthesised via dispersion polymerisation in scCO₂,¹³ whilst Bassett et al. reported the same trend of results for crosslinked polybetaine.²¹ This data also indicates that the presence of the crosslinker (EGDMA) was disrupting the initial nucleation process of the reaction, at crosslinker loadings of 0.4 wt. % and above (Table 4.1, entry 4 and 5). Similar findings were also reported again by both Shin et al. and the Howdle group, showing that incorporation of as low as 0.4 wt. % (Table 4.1, entry 4) of crosslinker in the dispersion polymerisation of MMA interrupted the creation of distinct particles.¹³ The mean diameter (D_n) of the primary particles decreased as the concentration of crosslink agent increased and was not reported for higher loading of 0.4

wt. % and 1.0 wt. % (Table 4.1, entry 4 - 5) due to formation of significantly agglomerated particles.

However, Shin et al. noted that the crosslinked PMMA particles were less agglomerated and became more spherical as pressure increased up to 380 bar.¹³ Wang et al. reported a similar effect of higher reaction pressures during their preparation of crosslinked poly(glycidyl methacrylate) by dispersion polymerisation in scCO₂.¹² Based on this finding, the reaction pressure used for making these crosslinked polymers was increased higher than the standard FRP reaction that was used in making the PMMA in Section 3.3.1. However, it could not improve the particle morphology much, especially at 0.4 wt.% and above (Table 4.1, entry 4 - 5).

Table 4.1. Summary of results of crosslinked PMMA with various loadings of EGDMA by batch method via Free Radical Polymerisation (FRP).

Entry	Crosslinker (wt.%)	Solubility (CHCl ₃ /THF)	M_n^a (g/mole)	\bar{D}^a	T_g^b (°C)	D_n (µm) ^c	Morphology of powder ^d
1	0	Fully dissolved	238,100	1.4	128	2.5	Sphere
2	0.1	Cloudy & dissolved in 24 hours	235,800	1.7	125	2.4	Sphere
3	0.2	Cloudy & dissolved in 24 hours	189,700	1.6	124	2.3	Sphere
4	0.4	Precipitate	150,900	1.5	125	-	Slightly aggregated
5	1.0	Precipitate	1,375	2.8	122	-	Highly aggregated

The reactions were conducted at 65°C and 270 bars for 24 hrs, the reactants consist of MMA (3.33 mL), AIBN (1 wt.% w.r.t. MMA), PDMS-MA (5 wt.% w.r.t. MMA) and EGDMA (0.1-1.0 wt.% w.r.t. MMA). ^a -determined via GPC, ^b -determined by DSC, ^c -diameter of the primary particle, measured by ImageJ, ^d-determined by SEM.

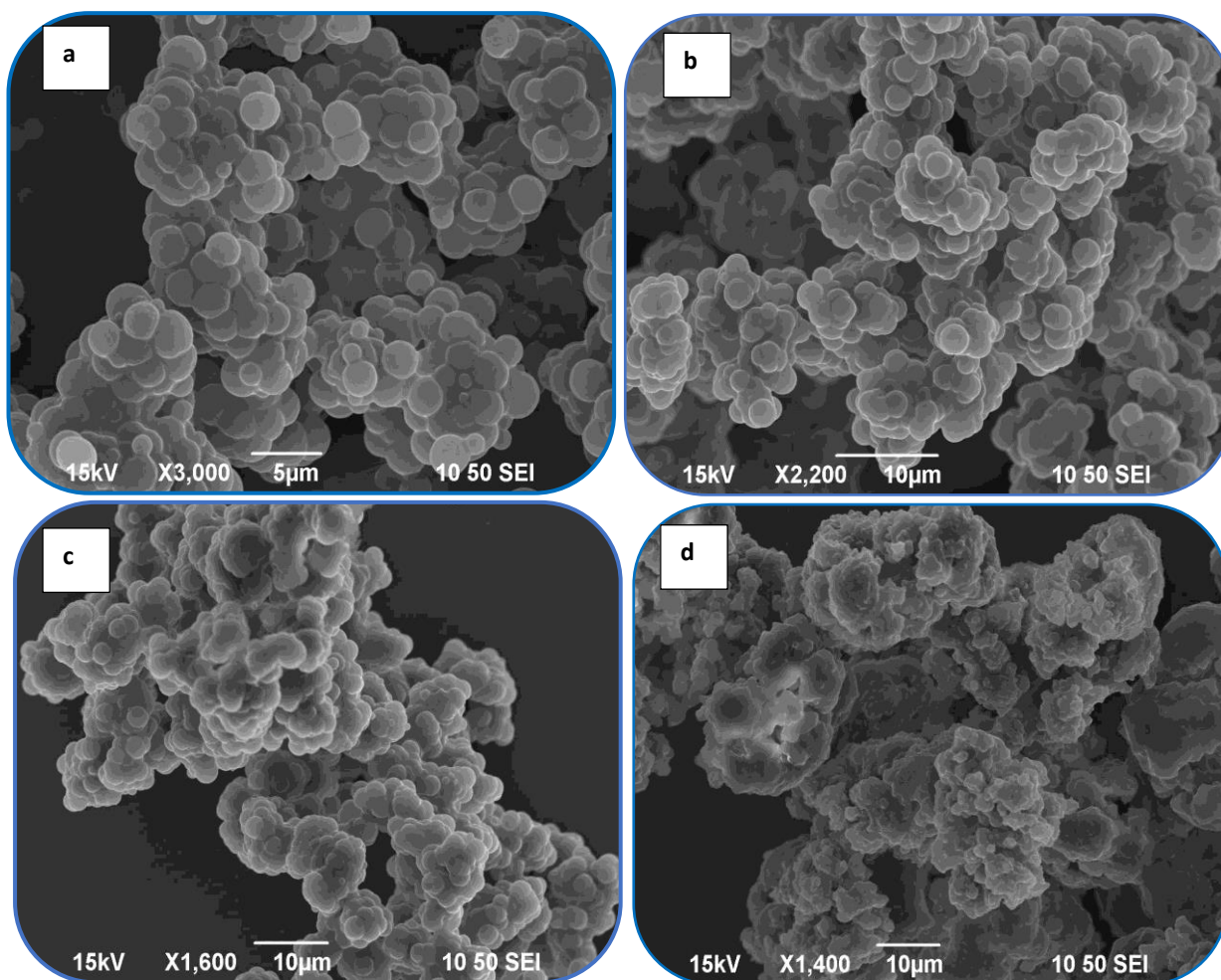


Figure 4.12. SEM images of crosslinked PMMA with various loadings of EGDMA by batch method free radical polymerisation, 0.1 wt.% (a), 0.2 wt.% (b), 0.4 wt.% (c), 1.0 wt.% (d) (Table 4.1, entry 2-5). The particles started to agglomerate at 0.4 wt.% (Table 4.1, entry 4).

When a crosslinking agent is introduced during polymerisation, it replaces some of the van der Waal's forces between polymer chains with stronger carbon-carbon (C-C) covalent bonds. This acts to reduce the mobility of each polymer segment and increase the system rigidity, thus increasing resistance to temperature, among other things.²² Consequently, an increase in the T_g of crosslinked polymers as a function of crosslinker incorporation is typically expected. However, the T_g values obtained from the DSC analysis of the series of crosslinked PMMA (Table 4.1, entry 1-5)

synthesised decreased as the concentration increased compared to the PMMA control (0 wt.% of EGDMA, Table 4.1, entry 1) as shown in Figure 4.13. The same trend obtained from the dynamic mechanical analysis (DMA) (Figure 4.14), which seems to support the DSC results. DMA plots (Figure 4.14) indicate a single distinctive peak at around 128 °C that is clearly assigned to the PMMA.

Shi et al. explained this behaviour was due to the formation of primarily branched polymers instead of fully crosslinked, because the material exhibits a lower T_g in comparison to their linear polymer counterparts.²³ Jerolimov et al. on the other hand discussed a further factor affecting the T_g is efficiency of the crosslinking reaction, which is always less than 100%. Unreacted monomers and partially reacted pendant methacrylate groups will be present, and act as plasticisers, which reduces T_g .²⁴ These observations clearly explain reducing trend of T_g of polymer obtained in the experiments with increasing loading of crosslinker, as shown in both Figure 4.13 and 4.14.

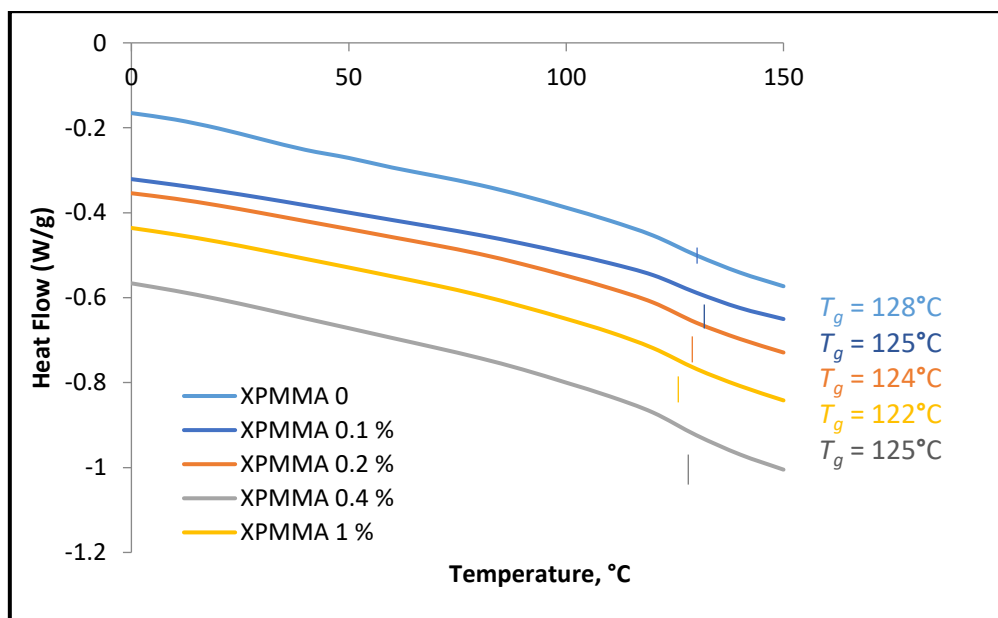


Figure 4.13. T_g (°C) of crosslinked PMMA with various loadings of EGDMA by batch method FRP using DSC (Table 4.1, entry 1-5). It shows a decreasing trend of T_g as the crosslinker amount increases.

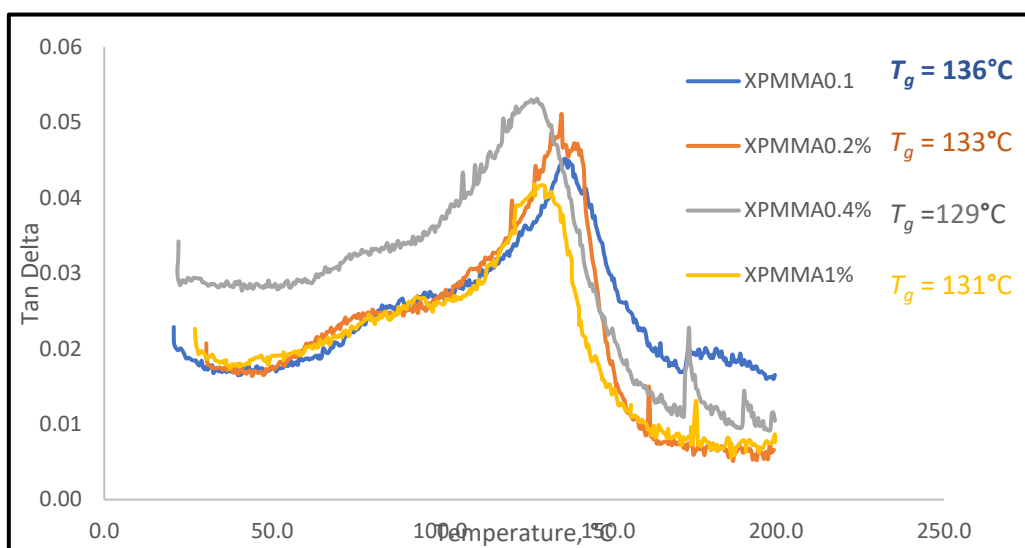


Figure 4.14. DMA of crosslinked PMMA with various loadings of EGDMA synthesis by batch method FRP (Table 4.1, entry 2-5). A trend of decreasing T_g as the crosslinker amount increases was observed.

A further experiment was carried out to confirm the presence of crosslinking within microparticles. The particles were dissolved in three different solvents namely chloroform, tetrahydrofuran and acetone. These were chosen as they are good solvents for PMMA particles, and they should fully dissolve if no crosslinking is present. The PMMA synthesised using loadings of 0.1 and 0.2 wt. % EGDMA fully dissolved in all of the solvents when left for 24 hours (Table 4.1, entry 2 and 3). In contrast, the polymer synthesised with loadings of 0.4 and 1.0 wt. % only partially dissolved (Table 4.1, entry 4 and 5). It is well known that crosslinked polymers cannot be dissolved in solvents because the crosslinks inhibit interaction between polymer chains and solvent molecules, thus preventing the polymer chains from being transported into solution.²⁵ These results thus support the formation of branched polymers at lower EGDMA loadings (0.1 and 0.2 wt. %, Table 4.1, entry 2 and 3) and only partially crosslinked polymers at increase EGDMA loading (0.4 and 1.0 wt. %, Table 4.1, entry 4 and 5).

In addition to the solubility tests, the samples were analysed using GPC to check their M_n values, which can be used as an indicator of polymer branching or (partial) crosslinking. A trend of decreasing M_n values as the amount of EGDMA increased was observed (Figures 4.15 and 4.16).

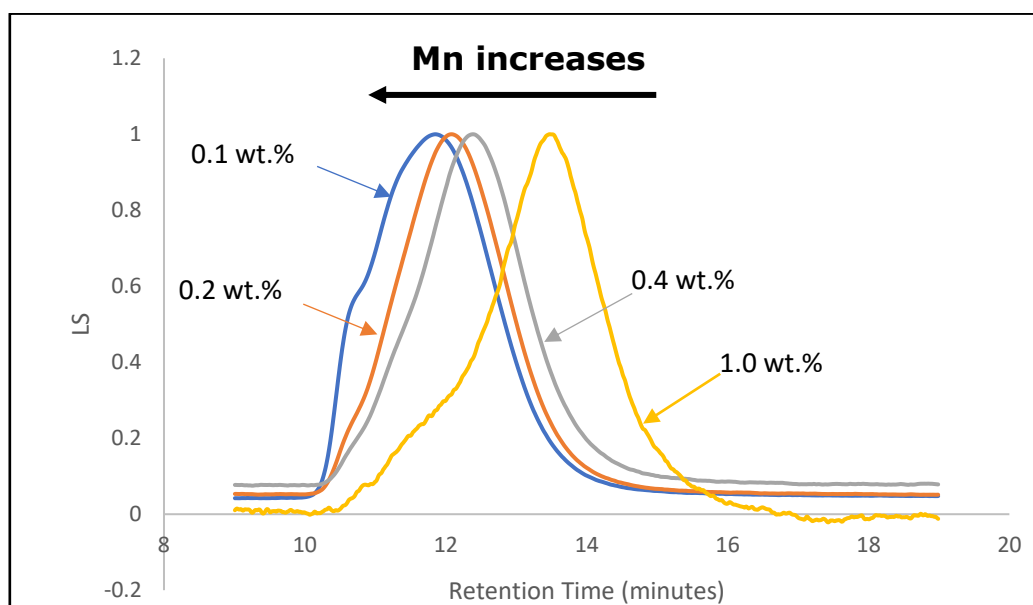


Figure 4.15. GPC traces of crosslinked PMMA with various loadings of EGDMA synthesised by batch method FRP (Table 4.1, entry 2-5). The M_n decreases as the amount of crosslinker increases.

This result is somewhat counterintuitive because according to theory, the molecular weight of a crosslinked polymer is expected to increase relative to its non-crosslinked equivalent. However, prior to the GPC analysis, every sample (dissolved in the respective solvent) was filtered through a 0.2 μm PTFE syringe filter prior to injection into the column. This would have the effect of removing the non-soluble and presumably much higher molecular weight crosslinked fraction of the sample. The analysed molecular weight of resulting sample would therefore be heavily skewed towards lower values as a function of the degree of crosslinking, potentially explaining the trends observed here (Figures 4.15 and 4.16).

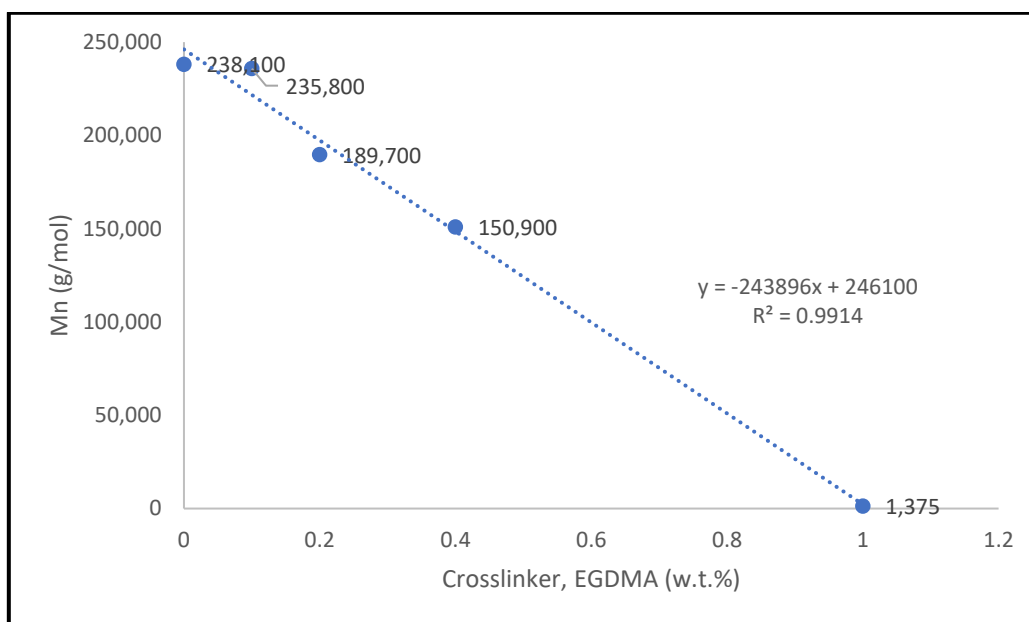


Figure 4.16. Effect of crosslinker (EGDMA) on molecular weight of PMMA obtained by one-stage batch method via FRP (Table 4.1, entry 1-5).

From these observations, it can be concluded that the one-stage batch reaction method produced only particles with branched polymer, at higher loadings the particles contained more crosslinked polymer. It has recently been reported that switching to a two-stage reaction method is a more effective way to synthesise distinct and highly spherical crosslinked microparticles, with the key adjustment being to introduce the crosslinking agent after the initial particle nucleation phase.^{26, 27}

4.4.2 *In situ* crosslinking copolymerisation of PMMA-*b*-P4VP via RAFT

4.4.2.1 One-step addition -SPH morphology

The next set of reactions introduced the crosslinker into the BCP, using a method discussed in Section 4.3.2. Preliminary *in situ* crosslinking reaction of PMMA-*b*-P4VP was performed in a one-pot and one-step addition of 4VP method, in which the crosslinker, divinyl benzene (DVB) was copolymerised along with 4VP once the first monomer, MMA, was consumed. The target block ratio of PMMA/P4VP was kept at a constant molar value of 60/40, while the crosslinking degree was varied from 0-2 wt.% (Table 4.2, entry 1-4).

Table 4.2. Crosslinked block copolymer, PMMA-*b*-P4VP microparticles synthesised by one-step *in situ* crosslinking via RAFT dispersion polymerisation in scCO₂.^a

Block Copolymers		Crosslinker	SEM	TEM	
Entry	PMMA ₅₀₀ - P4VP ₃₃₀ /D ^b	DVB (wt.%)	d _m ^c (µm)	Internal Morphology	d _{P4VP} ^d (nm)
1	PMMA ₅₀₀ - P4VP ₃₃₀	0	1.60±0.31	SPH ^h	^e 47±6 ^f 26±4
2	PMMA ₅₀₀ - P4VP ₃₃₀ /D0.5	0.5	1.42±0.29	SPH	28±5 15±3
3	PMMA ₅₀₀ - P4VP ₃₃₀ /D1	1	1.23 ^g	SPH	-
4	PMMA ₅₀₀ - P4VP ₃₃₀ /D2	2	-	-	-

^aThe reactions were conducted at 65°C and 270 bars, the reactants consist of MMA (7.5 g), DDMAT (55 mg), AIBN (12.5 mg) and PDMS-MA (5 wt.% w.r.t. MMA and 4VP) for the 1st block, PMMA; 4VP (5g), AIBN (6.25 mg) and DVB (0.5-2.0 wt.% w.r.t. 4VP) for the

chain extension and crosslinking of 2nd block (P4VP/DVB). The reaction time for PMMA is 18-24 h and 16-24 h for P4VP/DVB; ^b- D denote DVB, and the numbers following denote the weight percentage of DVB relative to total 4VP; ^c-the average particle diameter measured by ImageJ from SEM images ^d- the average domain size of P4VP (d_{P4VP}) was calculated by counting over 100 domains from TEM images by ImageJ; ^e- d_{P4VP} in the middle layer and ^f- d_{P4VP} in the core area; ^g-the microparticles are partially fused; ^h-SPH=spherical internal morphology.

The BCPs containing crosslinker amounts ranging from 0.5 wt.% to 2 wt.% of DVB relative to 4VP (PMMA₅₀₀-P4VP₃₃₀/D0.5, PMMA₅₀₀-P4VP₃₃₀/D1 and PMMA₅₀₀-P4VP₃₃₀/D2) (Table 4.2, entry 2 - 4), were analysed by SEM and compared to the resulting BCP particles synthesised without crosslinker (PMMA₅₀₀-P4VP₃₃₀) (Table 4.2, entry 1). It was found that both with or without addition of a small amount of crosslinker (0.5 wt.%) (Table 4.2, entry 1 and 2), discrete particles were formed, as illustrated by the SEM images (Figure. 4.17a-b). In contrast, the particles started to fuse, and high level of agglomeration was observed at 1 wt.% of crosslinker (Table 4.2, entry 3, Figure 4.17c). Complete architecture destruction was seen at 2 wt.% (Table 4.2, entry 4, Figure 4.17d).

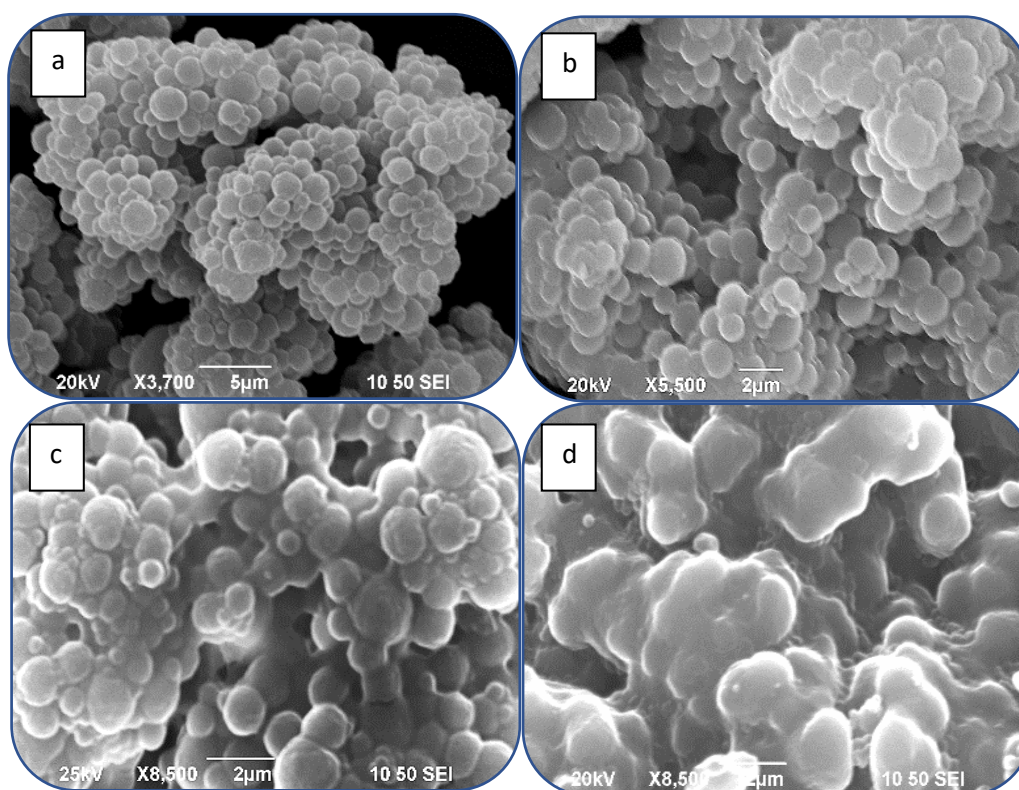


Figure 4.17. SEM images of non-crosslinked BCP corresponds to entry 1 (a) and crosslinked BCP containing 0.5 wt.% corresponds to entry 2 (b), 1 wt.% corresponds to entry 3 (c) and 2 wt.% corresponds to entry 4 (d) DVB by one-step addition method. The particles started to fuse at 1 wt.% (Table 4.2, entry 3).

The cross section imaged using TEM showed that the particles had an internal spherical nanostructure (Table 4.2, entry 1-4, Figure 4.18 a-c) and confirmed that the polymerisation induced phase separation was preserved up to 1 wt.% of DVB (PMMA₅₀₀-P4VP₃₀/D1) (Figure 4.18c, Table 4.2, entry 3). However, some smaller particles had formed in the reaction containing 1 wt.% DVB (Table 4.2, entry 3), which caused the particles to agglomerate (as seen on SEM image, Figure 4.17c). As these appear as darker areas and some are fully black spheres in bright field TEM (Figure 4.18c), this suggests that the small particles are mainly formed from homopolymer P4VP chains. Thus, suggesting that the crosslinking copolymerisation loses some control when 1 wt.% of DVB is added together with 4VP in one-step,

and the dispersion becomes unstable at the latter stages of the copolymerisation.¹⁹

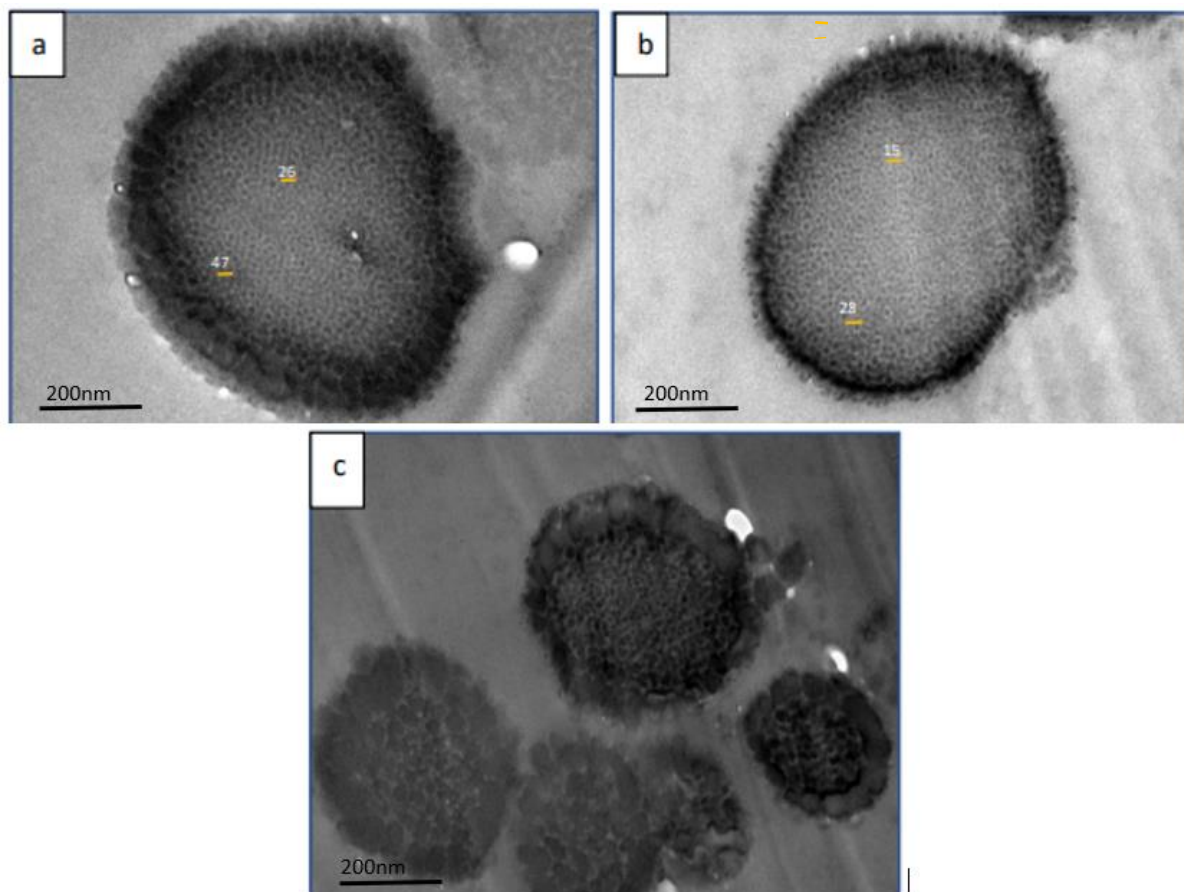


Figure 4.18. TEM images of BCP/D0% corresponds to entry 1 (a), BCP/D0.5% corresponds to entry 2 (b) and BCP/D1% corresponds to entry 3 (c). The decrease in domain size of the SPH domains shows the efficiency of the crosslinking process (Table 4.2, entry 1 and 2).

The internal domains of P4VP within the sample prepared with 0 wt.% DVB, PMMA₅₀₀-P4VP₃₃₀ ($dP4VP_{P.Layer} = 47$, $dP4VP_{Middle} = 26$) (Table 4.2, entry 1, Figure 4.18a), are much bigger than those of the sample prepared with 0.5 wt.% DVB, PMMA₅₀₀-P4VP₃₃₀/D0.5 ($dP4VP_{P.Layer} = 28$, $dP4VP_{Middle} = 15$) (Table 4.2, entry 2, Figure 4.18b). The spherical areas, recognised as the P4VP domains as they are darker than the PMMA domains in bright-field TEM,² are surrounded by a matrix of PMMA.

This size difference of the P4VP domains is a clear indication that they have become crosslinked, because this will restrict their capacity to be swollen by the residual monomer and/or scCO₂, on account of the additional covalent linkages between the adjacent polymer chains.²⁶ This information validates that the one-step crosslinking copolymerisation of 4VP with 0.5 wt.% DVB (Table 4.2, entry 2) proceeds under RAFT control while also maintaining a satisfactory dispersion.

4.4.2.2 Two-step addition -SPH morphology

The greatest challenge in this study has been to increase the amount of crosslinker while maintaining the microparticle structure and internal phase separation morphology of the crosslinked block copolymers. The best way to do this has been recognised by delaying the addition of crosslinker via the modification of an established method previously reported by our group, namely a two-stage addition method.¹⁹ This method works by allowing the chain extension of 4VP to proceed until an internal phase separation morphology has formed. Subsequently, the reaction is continued by addition of DVB together with the remaining 4VP. Our recent study revealed that the polymerisation induced microphase separation begins when P4VP = ~5 kDa and when the first PMMA-block has a length of ~50 kDa.¹⁶ Based on this finding, 4VP was added in two steps, where the first portion of 4VP was adequate to induce microphase separation when fully polymerised (Table 4.3). In this way, crosslinker quantities of up to 16 wt.% relative to the total 4VP monomer content (combined volume of the first and second additions) were added to the reaction, with the products being obtained as fine powders in each case, with the exception of the sample incorporating 16 wt.% that was collected as coarse powders instead (Table 4.3, entry 1-6).

Table 4.3. Crosslinked BCP, PMMA-*b*-P4VP microparticles synthesised by two-step *in situ* crosslinking via RAFT dispersion polymerisation in scCO₂.^a

Entry	Block Copolymers	Crosslinker (wt.%)	SEM (d_m^c) (μm)	TEM Morphology	TEM d_{P4VP}^d (nm)
1	PMMA ₅₀₀ -P4VP ₁₇₀ -P4VP ₁₆₀ /D ^b	0.5	1.50±0.20	SPH ^h	^e 26±7 ^f 26±6 ^g 25±5
2	PMMA ₅₀₀ -P4VP ₁₇₀ -P4VP ₁₆₀ /D1	1	1.30±0.30	SPH	52±8 38±8 25±5
3	PMMA ₅₀₀ -P4VP ₁₇₀ -P4VP ₁₆₀ /D2	2	1.20±0.30	SPH	43±7 29±6 20±4
4	PMMA ₅₀₀ -P4VP ₁₇₀ -P4VP ₁₆₀ /D4	4	0.99±0.40	SPH	37±4 21±4 19±3
5	PMMA ₅₀₀ -P4VP ₁₇₀ -P4VP ₁₆₀ /D8	8	0.89±0.30	SPH	28±5 18±3 16±3
6	PMMA ₅₀₀ -P4VP ₁₇₀ -P4VP ₁₆₀ /D16	16	0.93±0.30	SPH	51±9 31±6 20±3

^aThe reactions were conducted at 65°C and 270 bars, the reactants consist of MMA (7.5 g), DDMAT (55 mg), AIBN (12.5 mg) and PDMS-MA (5 wt.% w.r.t. MMA and 4VP) for the 1st block, PMMA; 4VP (5g), AIBN (6.25 mg) and DVB (0.5-16 wt.% w.r.t. 4VP) for the chain extension and crosslinking of 2nd block (P4VP/DVB), the addition of 4VP was made in 2 stages whilst DVB was added during the last stage. The reaction time for PMMA is 18-24 h and 16-24 h for P4VP/DVB; ^b D denote DVB, and the numbers following denote the weight percentage of DVB relative to total 4VP; ^cthe average of particle diameter measure by ImageJ from SEM images ^dthe average domain size of P4VP (d_{P4VP}) was calculated by counting over 100 domains from TEM images; ^e d_{P4VP} in the periphery layer, ^f d_{P4VP} in the middle layer and ^g d_{P4VP} in the core area; SPH^h = spherical internal morphology.

This method allowed the addition of DVB ranging from 0.5 -16 wt.% (Table 4.3, entry 1-6), while maintaining the particle structures as well as their internal morphology. SEM images confirmed that the products remained as discrete microparticles without agglomeration (Figure 4.19a-f). However, most of the SEM images obtained from the sample containing 16 wt. % DVB (Table 4.3, entry 6) showed agglomerated particles (Figure 4.20a-b), except for one area, (Figure 4.19f) which showed distinct microparticles. These distinct microparticles could be comprised of P4VP homopolymer only, as previously discussed, which indicate a lack of control of the crosslinking copolymerisation at this amount of DVB.

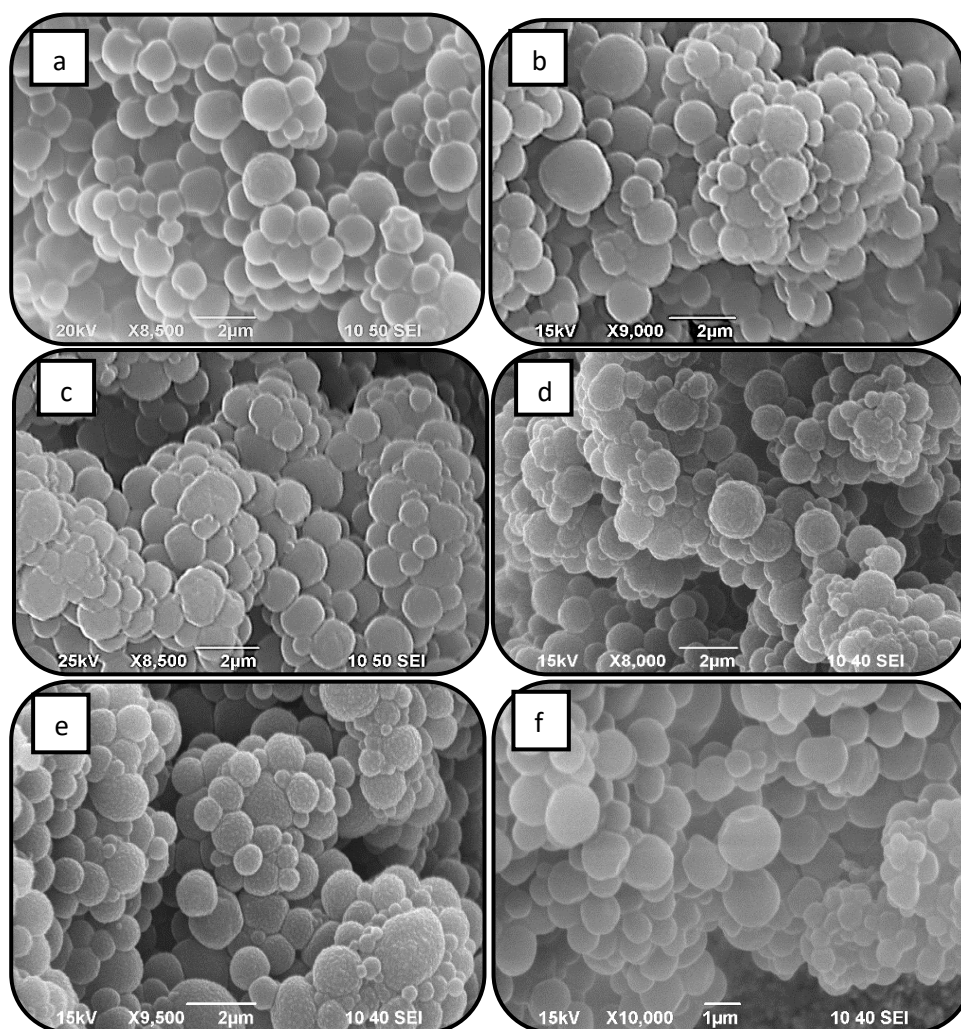


Figure 4.19. SEM images of crosslinked BCP incorporating 0.5 (a), 1 (b), 2 (c), 4 (d), 8 (e) and 16 (f) wt.% of DVB by two-step addition method presented distinct particles (Table 4.3, entry 1-6).

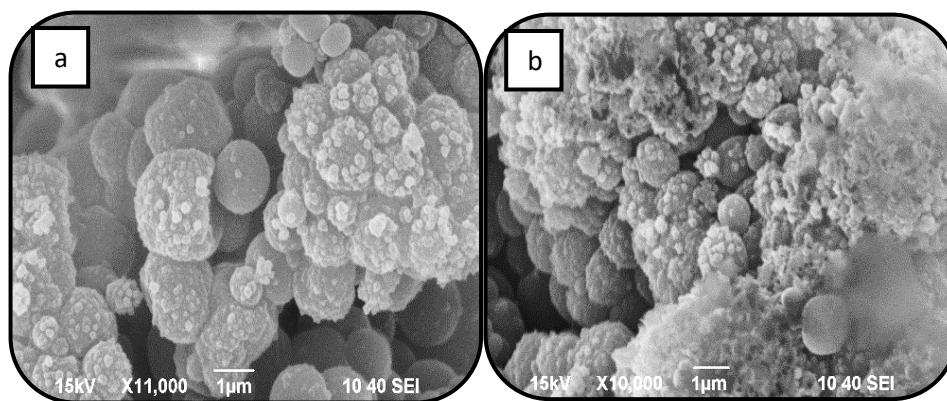


Figure 4.20. SEM images of crosslinked BCP incorporating 16 w.t.% DVB (Table 4.3, entry 6). This sample showed agglomerated particles (a & b).

Additionally, the size reduction of all the crosslinked microparticles (Table 4.3, entry 1-6) in comparison to non-crosslinked microparticles (Table 4.2, entry 1) indicated that the crosslinking process had occurred. Size measurements revealed a decreasing trend in the diameter of the microparticles as a function of crosslinker concentration (Figure 4.21a). As expected, the crosslinked particles synthesised with a concentration of 16 wt.% DVB (Table 4.3, entry 6) deviated from the trend because of a complete loss of control. The SEM images (Figure 4.20a-b) demonstrate the formation of particles of various sizes with agglomeration, as well as sub-100 nm particles. This resulted from the difference in reactivity between PMMA and P4VP, as well as the presence of unreacted DVB (crosslinker) during polymerisation. The amount of DVB was too high and that the unreacted portion formed the shortest oligomers visible as agglomerations and sub-particles in the SEM images.

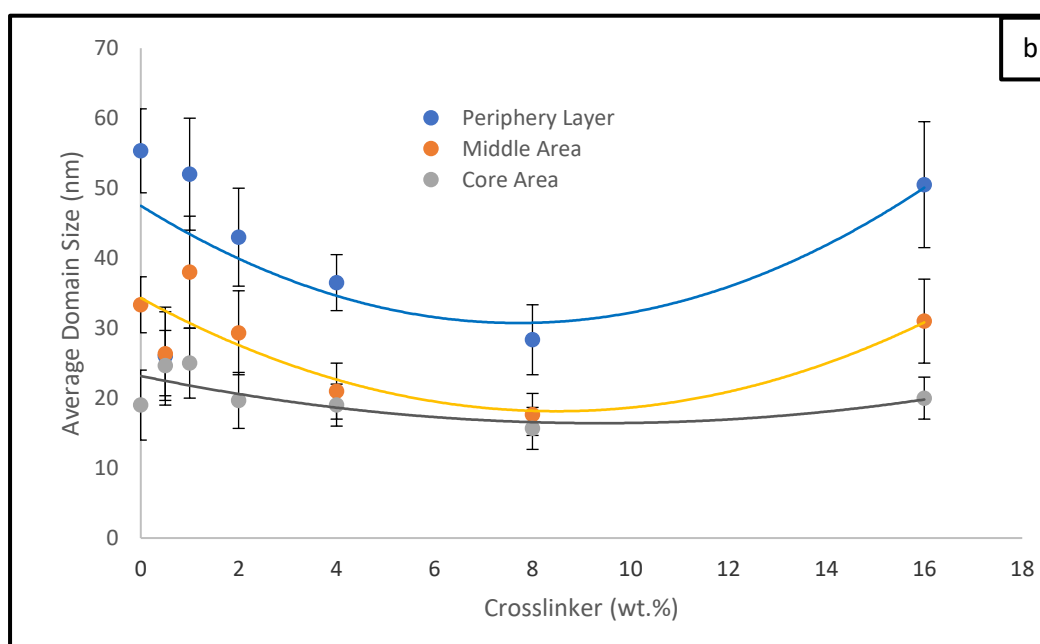
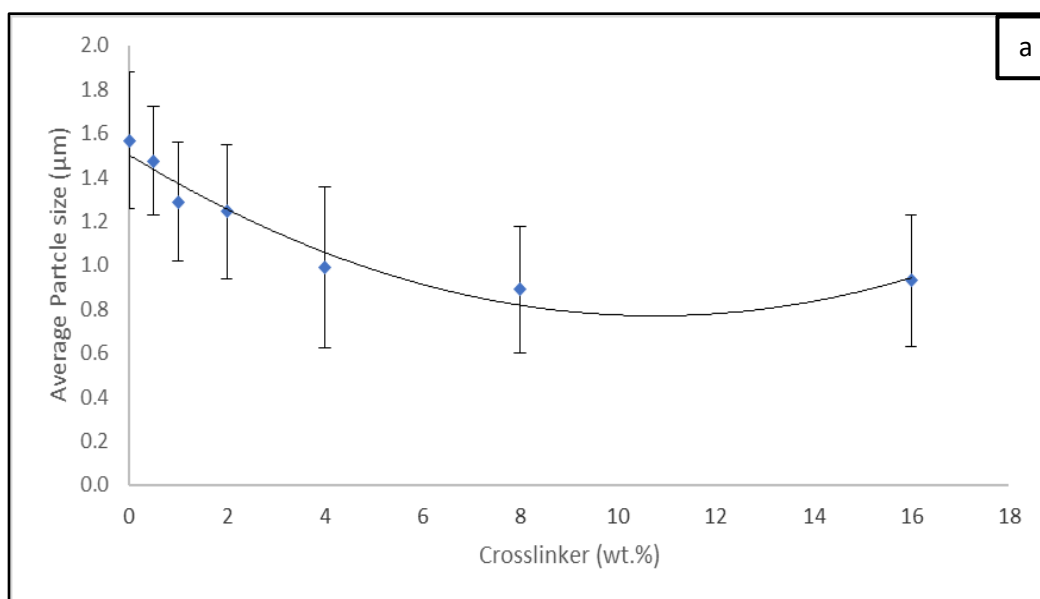


Figure 4.21. (a) Particle diameter trend of crosslinked BCP via two-step addition method (Table 4.3, entry 1-6). (b) The average internal domain size of crosslinked P4VP at three different area of the internal domain; periphery layer, middle area and core area via two-step addition method (Table 4.3, entry 1-6).

TEM analysis of the respective cross-sections was performed to investigate how the amount of crosslinker incorporated affected the internal morphology. The results showed that all of the crosslinked microparticles

synthesised using the two-step addition method retain the spherical morphology (Table 4.3, entry 1-6, Figure 4.22a-f) of internal phase separation agreeing with that of their non-crosslinked microparticles (Table 4.2, entry 1, Figure 4.18a). This was even observed for the agglomerated particles obtained from the reaction incorporating 16 wt.% of crosslinker (Table 4.3, entry 6, Figure 4.23a-b). The internal domain size for all crosslinked samples varied according to their position within the microparticles, following this sequence; periphery layer > middle area > core area. The periphery layer (outer layer) was seen to be the most swollen by residual monomers or scCO₂ in this high-pressure polymerisation system. However, in most cases the average domain size of the crosslinked P4VP is also smaller than those without crosslinker, for reasons discussed previously (Table 4.3, entry 1-6, Figure 4.21b). The domain size reduction in crosslinked samples led to a decrease of the diameter values, which reduced their capacity to be swollen by the remaining monomer or scCO₂ during polymerisation.

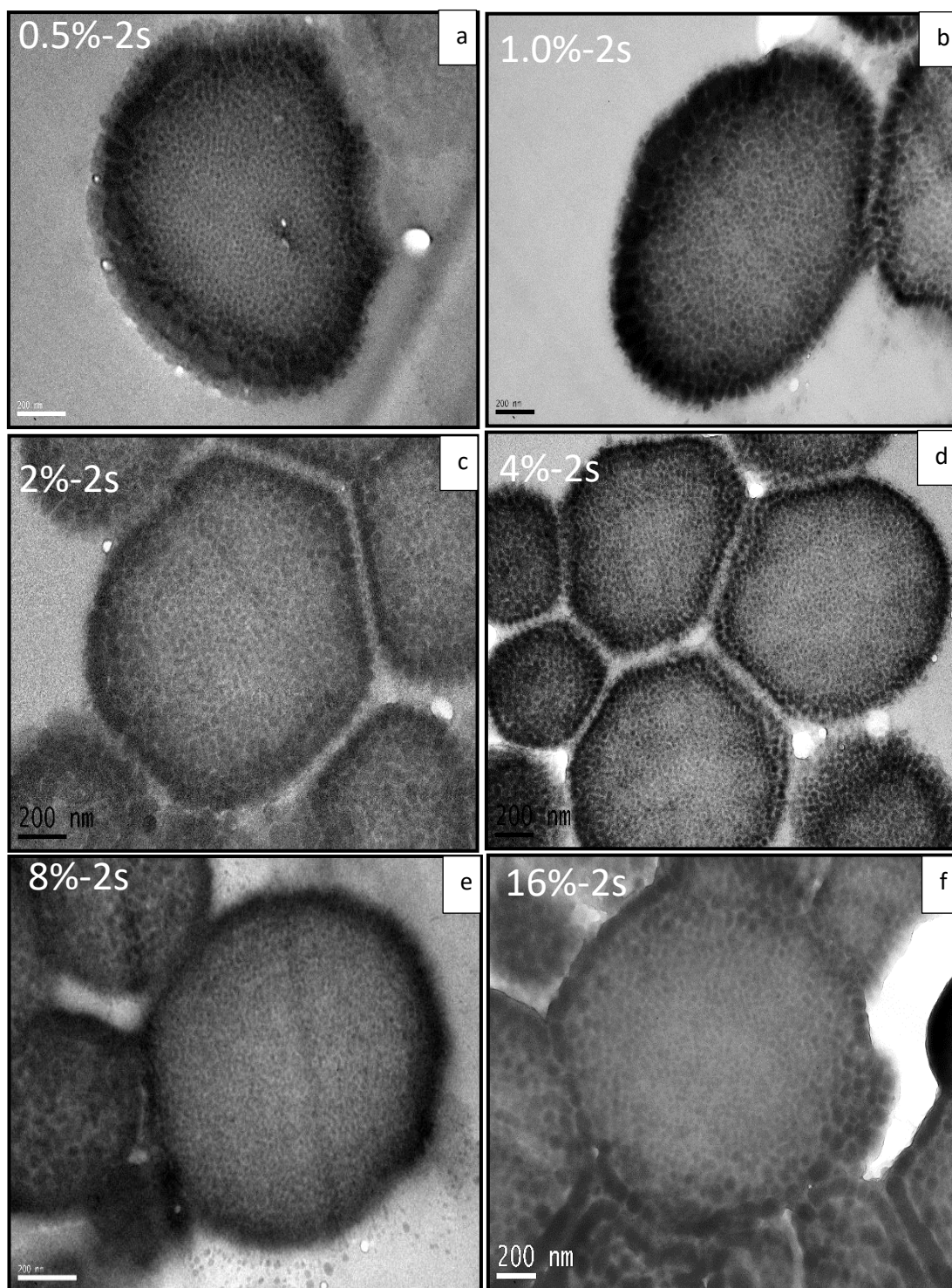


Figure 4.22. TEM images of the preserved internal phase separation morphology of crosslinked microparticles incorporating different levels of crosslinker (0.5 - 16 wt.%) added via two-stage addition method (Table 4.3, entry 1-6).

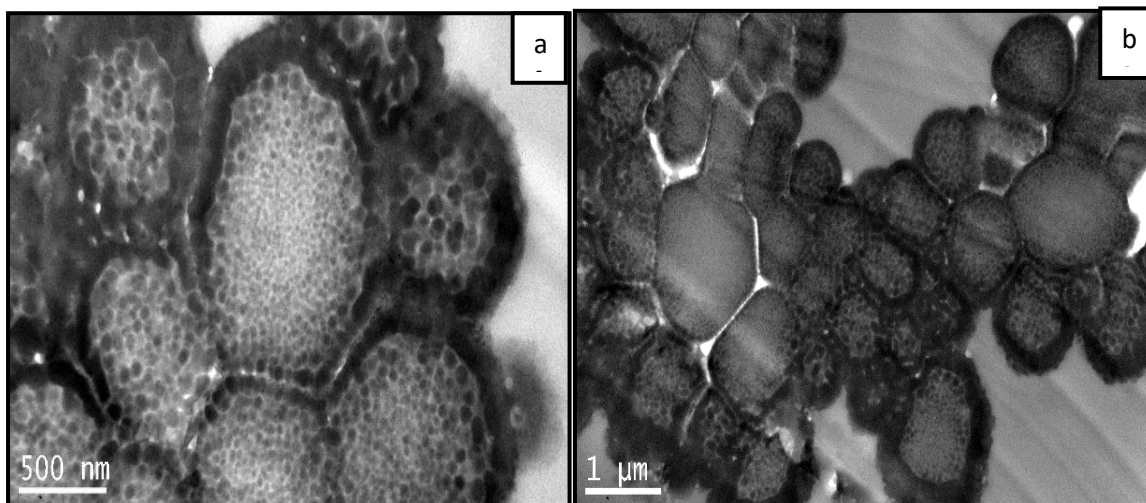


Figure 4.23. TEM images of the preserved internal phase separation morphology of microparticles synthesised with 16 wt.% DVB added via two-stage method (Table 4.3, entry 6) (a). Inhomogeneity of domain size formed with this amount of crosslinker (b).

4.4.2.3 Physical Properties - SPH morphology

4.4.2.3.1 Dissolution Test

The dissolution tests in chloroform were performed to further confirm the extent of crosslinking within the microparticles. Chloroform is a good solvent to dissolve both the PMMA and P4VP blocks. All samples from both the one-step (Table 4.2, entry 1-4) and two-step methods (Table 4.3, entry 1-6) were dissolved in chloroform, including the non-crosslinked samples (Figure 4.24). It was found that the non-crosslinked sample (PMMA₅₀₀-P4VP₃₃₀) (vial (a) in Figure 4.24) fully dissolved, forming a transparent solution, in less than 5 minutes. By contrast, the crosslinked samples synthesised using the one-step addition method (Table 4.2, entry 2-4), containing 0.5 - 2 wt.% (vial (b), (c), and (d) in Figure 4.24) formed a gel, with two distinct layers after 24 hours of contact with the solvent. This obvious insolubility of the particles in chloroform is a good indicator of crosslink formation.

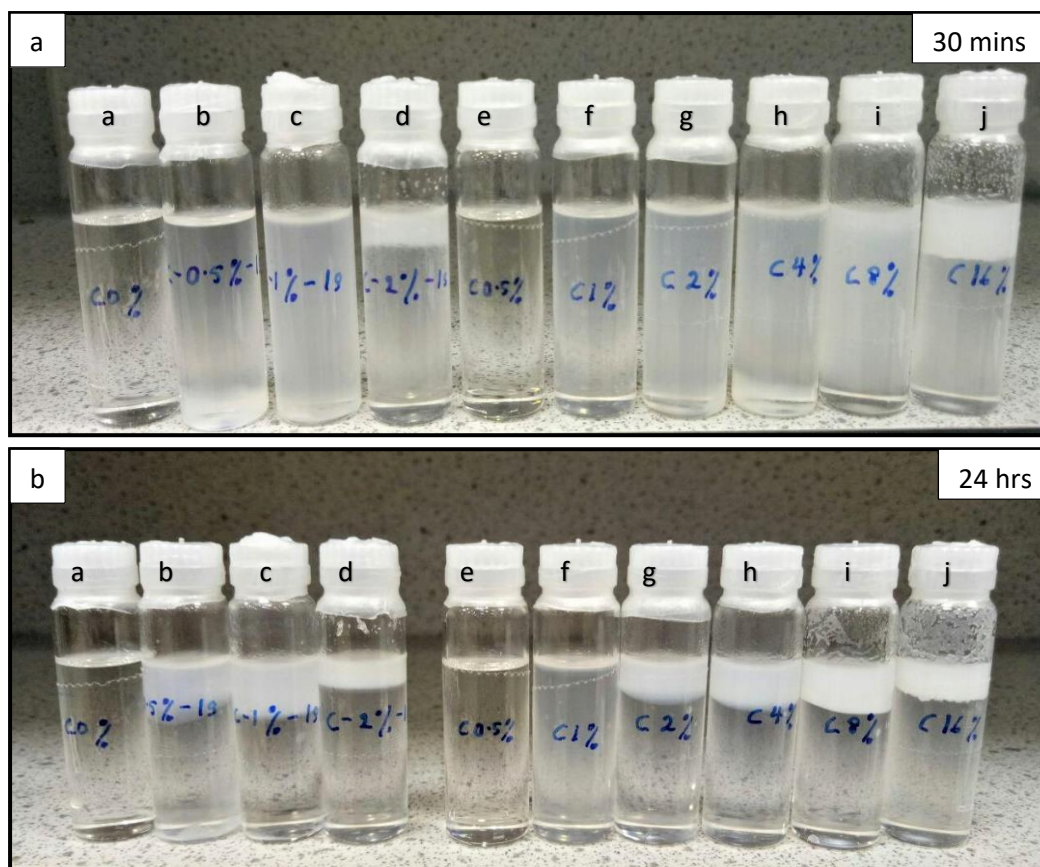


Figure 4.24. Photographic images of the samples dispersed in chloroform (dissolution test)- observation after 30 minutes (a) and 24 hours (b). From left to right: a)PMMA₅₀₀-P4VP₃₃₀, b)PMMA₅₀₀-P4VP₃₃₀/D0.5, c)PMMA₅₀₀-P4VP₃₃₀/D1, d)PMMA₅₀₀-P4VP₃₃₀/D2 (Table 4.2, entry 1-4) and e)PMMA₅₀₀-P4VP₁₇₀-P4VP₁₆₀/D0.5, f)PMMA₅₀₀-P4VP₁₇₀-P4VP₁₆₀/D1, g)PMMA₅₀₀-P4VP₁₇₀-P4VP₁₆₀/D2, h)PMMA₅₀₀-P4VP₁₇₀-P4VP₁₆₀/D4, i)PMMA₅₀₀-P4VP₁₇₀-P4VP₁₆₀/D8 and j)PMMA₅₀₀-P4VP₁₇₀-P4VP₁₆₀/D16 (Table 4.3, entry 1-6).

In the case of samples synthesised using the two-step addition method (Table 4.3, entry 1), the sample incorporating 0.5 wt.% DVB (PMMA₅₀₀-P4VP₁₇₀-P4VP₁₆₀/D0.5) (vial (e) in Figure 4.24) formed a clear solution when left 30 minutes and remained clear after 24 hours. The sample incorporating 1 wt.% DVB also remained as a cloudy dispersion (PMMA₅₀₀-P4VP₁₇₀-P4VP₁₆₀/D1) (vial (f) in Figure 4.24). In contrast, the samples incorporating 2-16 wt.% DVB (vial (g), (h), (i) and (j) in Figure 4.24) floated to the surface, forming a gel layer showing that the particles

were insoluble suggesting that some part of the particles is crosslinked. However, at low crosslinking concentrations, 0.5 wt.% DVB (PMMA₅₀₀-P4VP₁₇₀-P4VP₁₆₀/D0.5), the sample was not completely crosslinked but instead generated branched polymer and hence was soluble (vial (e) in Figure 4.24). All the samples were subjected to further analysis; the residue or gel formed was left to dry for SEM (Figure 4.25) and TEM (Figure 4.26b) analysis to obtain their particle morphology, whilst the soluble part, dissolved in chloroform were filtered for GPC analysis (Figure 4.27).

The SEM images of these chloroform residues showed that the discrete spherical particle was destroyed after dissolving (Figure 4.25). This observation suggests that the particle scaffolds collapse in chloroform, but the polymers were mainly insoluble due to the formation of crosslinking. However, TEM analysis of one of the crosslinked samples (PMMA₅₀₀-P4VP₁₇₀-P4VP₁₆₀/D1) revealed that the internal morphology of the crosslinked domain of P4VP was well preserved despite the collapse of the microparticle scaffold (Figure 4.26b). Nevertheless, the particles swelled and lost their spherical microstructure in comparison to before exposure to the chloroform (Figure 4.26a). The observation of some retained polymer phase separation might be due to the presence or mixture of both soluble and non-soluble part during sampling of both SEM and TEM.

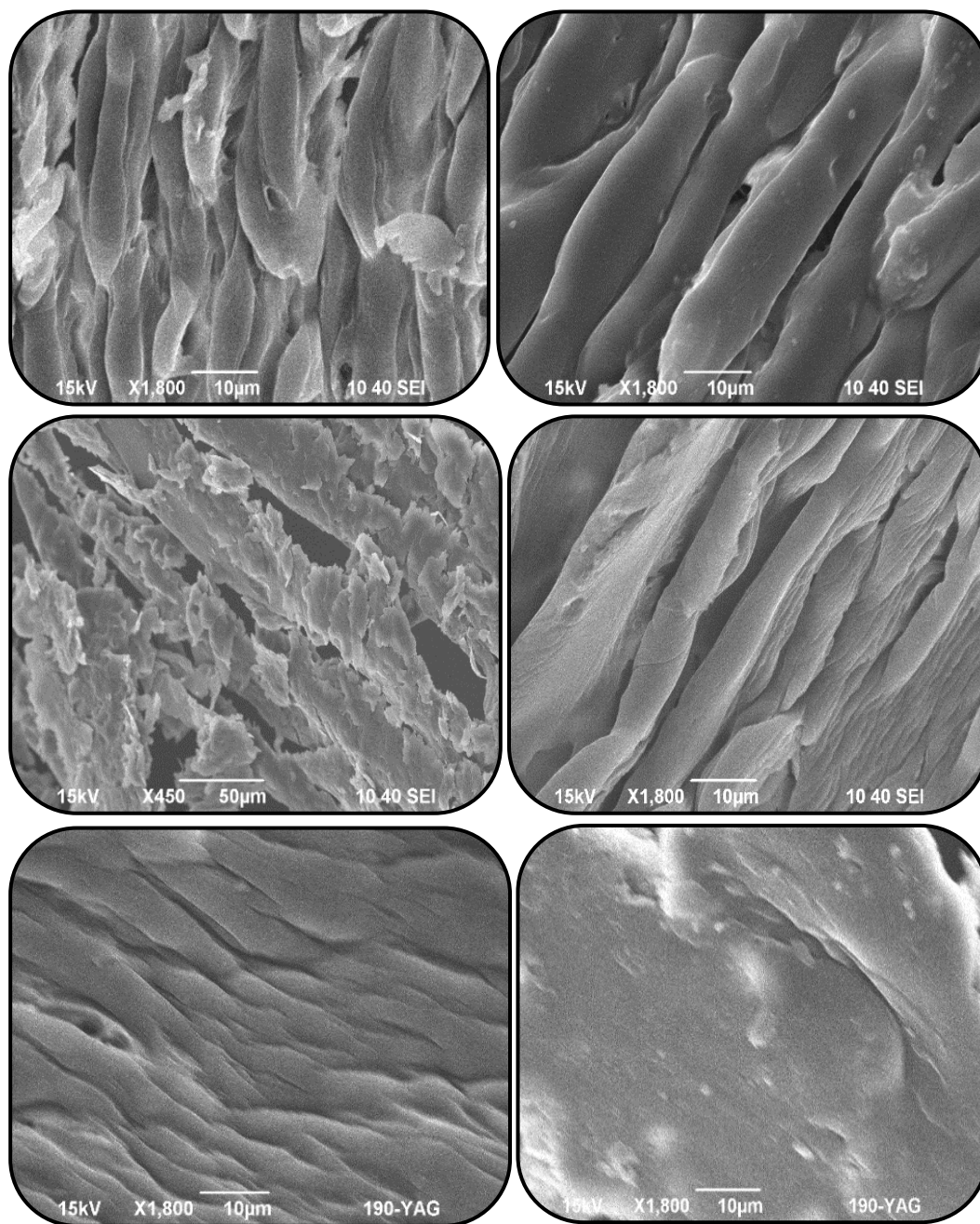


Figure 4.25. SEM images of chloroform residues of crosslinked BCP. PMMA₅₀₀-P4VP₃₃₀/D0.5 (a) (vial (b) in Figure 4.24), PMMA₅₀₀-P4VP₁₇₀-P4VP₁₆₀/D1 (b) (vial (f) in Figure 4.24), PMMA₅₀₀-P4VP₁₇₀-P4VP₁₆₀/D2 (c) (vial (g) in Figure 4.24), PMMA₅₀₀-P4VP₁₇₀-P4VP₁₆₀/D4 (d) (vial (h) in Figure 4.24), PMMA₅₀₀-P4VP₁₇₀-P4VP₁₆₀/D8 (e) (vial (i) in Figure 4.24) and PMMA₅₀₀-P4VP₁₇₀-P4VP₁₆₀/D16 (f) (vial (j) in Figure 4.24) showing collapse particles.

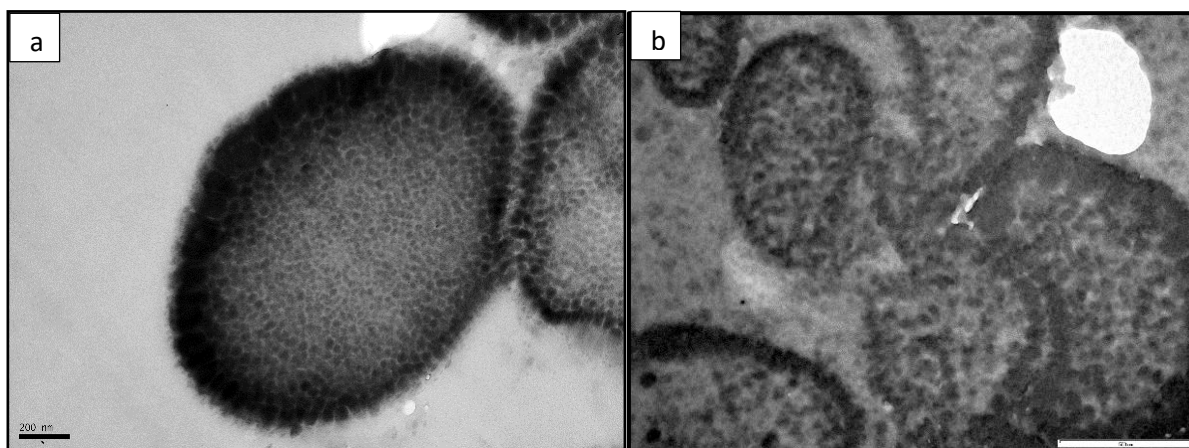


Figure 4.26. TEM images of crosslinked BCP, PMMA₅₀₀-P4VP₁₇₀-P4VP₁₆₀/D1 synthesised with 1 wt.% DVB before (a) (Table 4.3, entry 2) and after (b) exposure to chloroform (vial (f) in Figure 4.24), showing preserved internal morphology despite the swelling effect on the particles.

Further investigation was carried out by GPC analysis to check the nature of the soluble part, dissolved in the chloroform. The BCP sample at 0 wt.% DVB (PMMA₅₀₀-P4VP₃₃₀) gave $M_n = 86,250$ g/mol ($\bar{D} = 1.7$) (Figure 4.27, vial (a) in Figure 4.24), which confirmed that all particles were dissolved in the chloroform as it is close to the target M_n ($M_{n\text{Targetted}} = 83,000$ g/mol). All samples synthesised using the one-step addition method containing 0.5–2 wt.% DVB (vial (b)-(d) in Figure 4.24), gave M_n values ranging from 49,140 to 59,020 g/mol ($\bar{D} = 3.4\text{-}5.3$), indicating the M_n value of the non-crosslinked particles were lower compared to the samples synthesised using two-step addition method with values ranging from 53,140 to 77,850 g/mol ($\bar{D} = 1.9\text{-}4.5$) (Figure. 4.27, vial (e)-(j) in Figure 4.24).

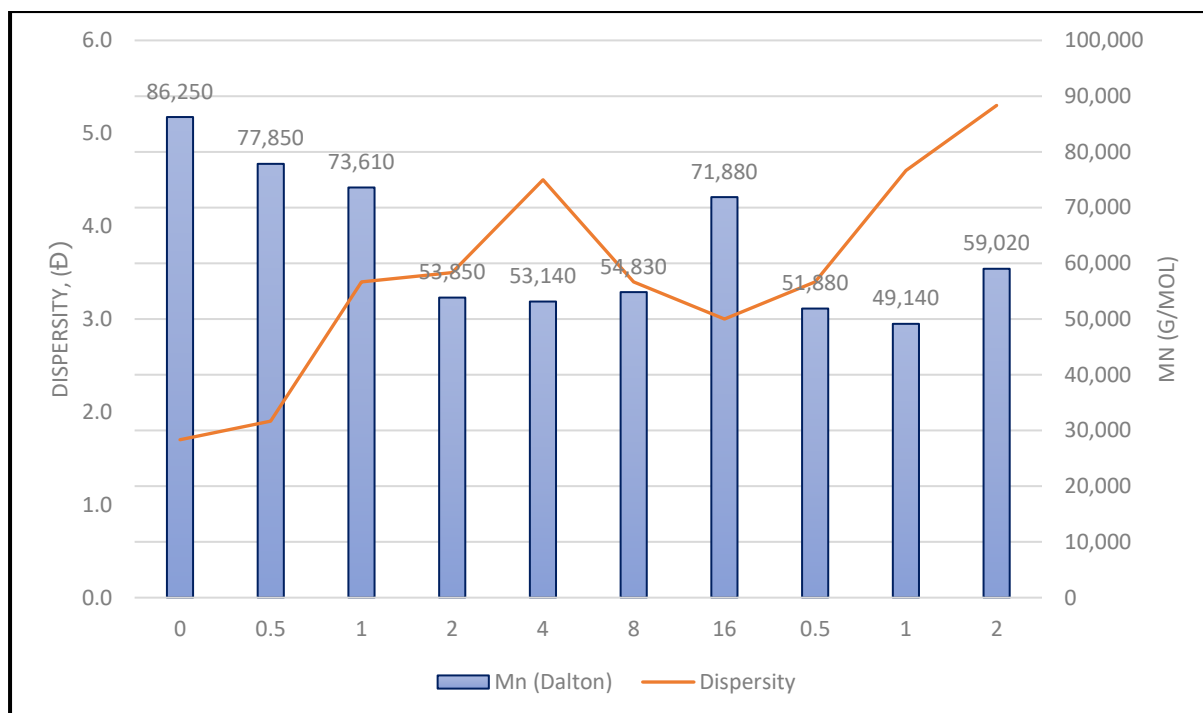


Figure 4.27. Average molecular weight, M_n and dispersity, \bar{D} of chloroform dissolution layers, which mainly contained non-crosslinked particles [From left to right: 0 : (vial (a) in Figure 4.24) , 0.5-16: (vial (e)-(j) in Figure 4.24) and 0.5-2: (vial (b)-(d) in Figure 4.24)].

In the case of the samples synthesised using the two-step addition method, the sample incorporating the lowest amount of crosslinker, PMMA₅₀₀-P4VP₁₇₀-P4VP₁₆₀/D0.5 (Table 4.3, entry 1), gave a $M_n = 77,850$ g/mol ($\bar{D} = 1.9$), indicating that almost all particles were dissolved ($M_{nTargetted} = 83,000$ g/mol). This result is consistent with the observation of the clear solution obtained (vial (a) in Figure 4.24), which showed that microparticles were dissolved because of the absence of crosslinking in the particles. This result also shows that the addition of crosslinker at 0.5 wt.% (vial (b) in Figure 4.24) worked well when done in a single step ($M_n = 51,880$ g/mol, $\bar{D} = 3.4$) of 4VP addition rather than a two steps addition ($M_n = 77,850$ g/mol, $\bar{D} = 1.9$, vial (e) in Figure 4.24).

The sample $M_n = 73,610$ g/mol ($\bar{D} = 3.4$) for PMMA₅₀₀-P4VP₁₇₀-P4VP₁₆₀/D1 (vial (f) in Figure 4.24) indicates the formation of crosslinking

at certain degree for the sample containing 1 wt.% DVB, this can be seen by the cloudy solution that formed after 30 minutes and 24 hours exposure to chloroform (vial (f) in Figure 4.24 a & b). When the amount of crosslinker increased to 2–8 wt.% (vial (g)-(i) in Figure 4.24), lower M_n was recorded, ranging from 53,140–54,830 g/mol ($\bar{D} = 3.4-4.5$). This showed that more of the particles had been crosslinked as the amount of DVB increased. However, at the highest level of crosslinking (16 wt.%) (vial (j) in Figure 4.24), the M_n increased again to 71,880 g/mol ($\bar{D} = 3.1$), this might be due to the fact that the crosslinking dispersion polymerisation process at 16 wt.% crosslinker loading has lost control. The results support the findings in both SEM (Figure 4.20) and TEM (Figure 4.23) of sample contained 16 wt.% of DVB and demonstrate loss of control of the dispersion polymerisation.

In summary, these GPC results (Figure 4.27) corroborate the observation in Figure 4.24, leading to the conclusion that the crosslinking process has taken place at certain degree by formation of cloudy solutions and gel layers, as shown in both Figure 4.24a and b.

The gel content (%) of the insoluble particles produced from the samples upon exposure to chloroform was measured gravimetrically (Figure 4.28). All samples synthesised using the two-step addition method (vial (e)-(j) in Figure 4.24), including one sample from one-step addition method containing 0.5 wt.% DVB (vial (b) in Figure 4.24), were measured.

The gel content increased linearly with increasing crosslinking, reaching a maximum of 73 % in the sample containing 2 wt. % DVB (vial (g) in Figure 4.24), before steadily decreasing to approximately 53% (vial (i) in Figure 4.24) as the amount of crosslinker doubled. These were samples synthesised using the two-step addition method and suggest that 2 wt. % DVB is the optimal concentration at which crosslinking prevails over chain scission of the BCP microparticles, resulting in the formation of crosslinked microparticles with the highest gel content. In comparison, the

addition of 0.5 wt.% DVB using the one-step addition method (vial (b) in Figure 4.24) resulted in the highest gel content (80 %) in the sample, indicating that one-step addition results in more crosslinking formation. These findings corroborated all of the observations made during the chloroform dissolution test.

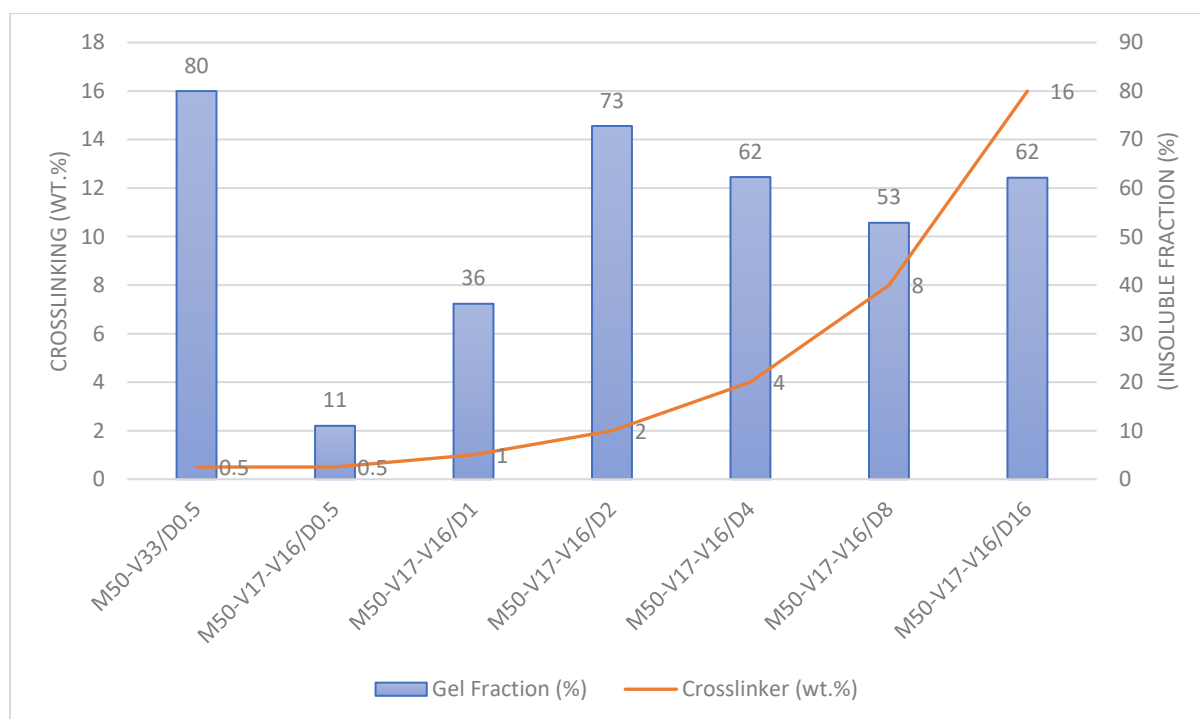


Figure 4.28. The insoluble fraction (%) recovered from the chloroform dissolution test of the crosslinked samples containing DVB ranging from 0.5 to 16 wt.% synthesised using one-step (vial (b) in Figure 4.24) and two-step (vial (e)-(j) in Figure 4.24) addition methods. The sample PMMA₅₀₀-P4VP₃₃₀/D0.5 (M50-V33/D0.5) synthesised by the one-step method contained the highest insoluble fraction.

The particles were also dispersed in THF, which is an excellent solvent for PMMA but only dissolves P4VP with shorter chain lengths (MW < 5000 g/mol, i.e repeating units <45). Microparticles without crosslinking (0 wt.% DVB) PMMA₅₀₀-P4VP₃₃₀ (vial (a) in Figure 4.29, Table 4.2, entry 1) formed a one phase, cloudy solution, which suggests that there is insoluble P4VP presence in this sample. Further analysis was carried out by GPC, to check

if there was any THF-soluble material present. The GPC traces indicated a unimodal peak with M_n value = 67,810 g/mol ($\bar{D}=1.2$) (Figure. 4.30a), confirming the presence of a THF-soluble material.

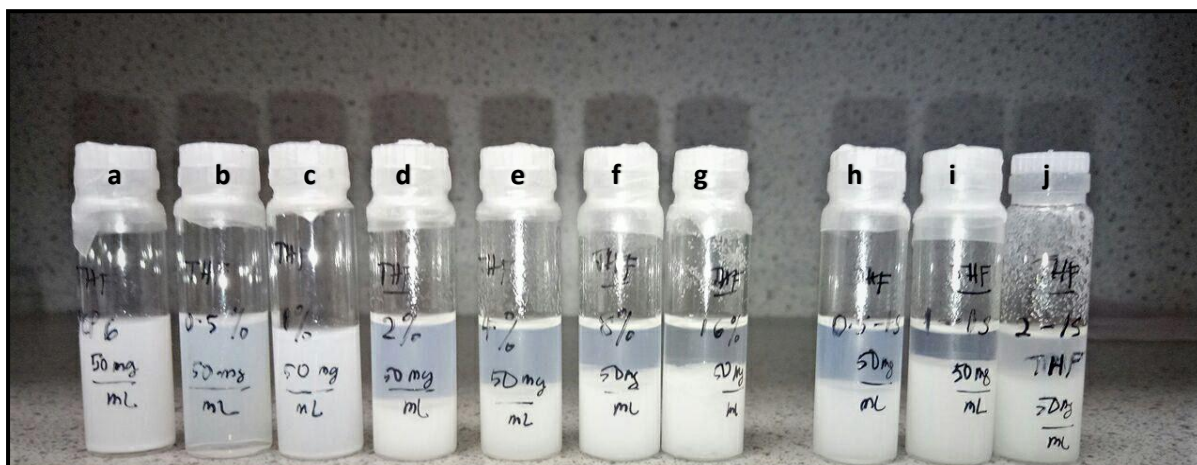


Figure 4.29. Photographic image of the samples dispersed in THF-observed after 24 hours. From left to right: PMMA₅₀₀-P4VP₃₃₀ (a), PMMA₅₀₀-P4VP₁₇₀-P4VP₁₆₀/D0.5 (b), PMMA₅₀₀-P4VP₁₇₀-P4VP₁₆₀/D1 (c), PMMA₅₀₀-P4VP₁₇₀-P4VP₁₆₀/D2 (d), PMMA₅₀₀-P4VP₁₇₀-P4VP₁₆₀/D4 (e), PMMA₅₀₀-P4VP₁₇₀-P4VP₁₆₀/D8 (f), PMMA₅₀₀-P4VP₁₇₀-P4VP₁₆₀/D16 (g) PMMA₅₀₀-P4VP₃₃₀/D0.5 (h), PMMA₅₀₀-P4VP₃₃₀/D1 (i), PMMA₅₀₀-P4VP₃₃₀/D2 (j). [(a): Table 4.2, entry 1, (b)-(g): Table 4.3, entry 1-6, (h)-(j): Table 4.2, entry 2-4].

In general, as the crosslinking increased in the samples synthesised using both methods (one step: vial (h)-(j) in Figure 4.29 and two steps: vial (b)-(g) in Figure 4.29) the solution became less cloudy and separated into two layers. The particles became denser than the THF and settled at the bottom of the vials. This demonstrates that the presence of the crosslinker increases the resistance of the microparticles to THF. This observation verified the GPC results for crosslinked particles, PMMA₅₀₀-P4VP₁₇₀-P4VP₁₆₀/D4 (Vial (e) in Figure 4.29) in which no peak was found due to the insoluble nature of the crosslinked particles in THF (Figure 4.30 (b)).

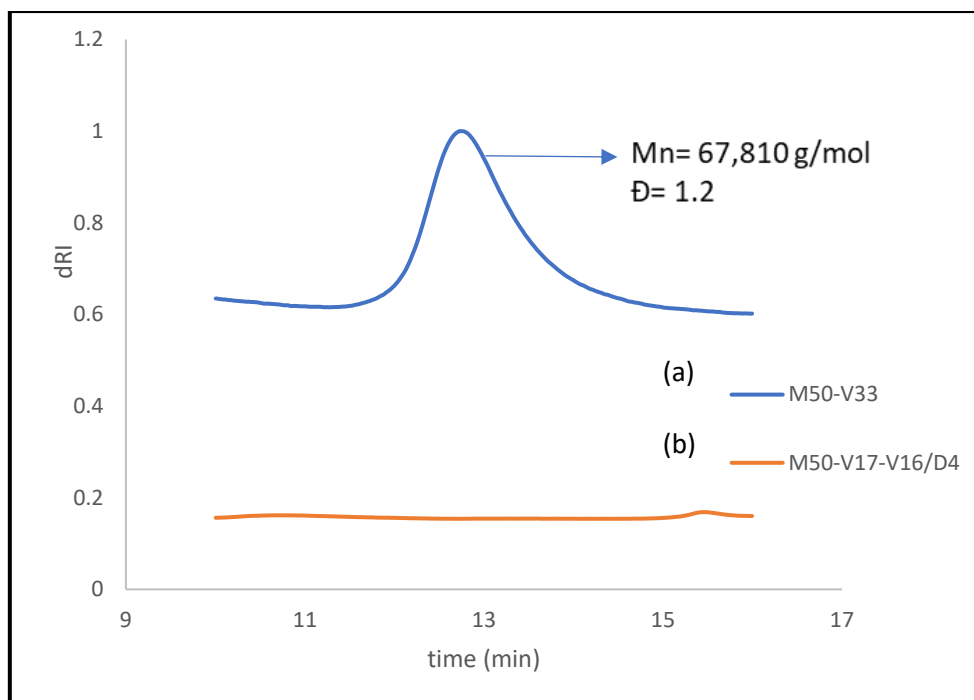


Figure 4.30. GPC traces of BCP contained 0 wt.% DVB (PMMA₅₀₀-P4VP₃₃₀, vial (a) in Figure 4.29), containing soluble particles (blue line (a)) and BCP containing 4 wt.% DVB (PMMA₅₀₀-P4VP₁₇₀-P4VP₁₆₀/D4, vial (e) in Figure 4.29) (orange line (b)) showing no peak obtained as crosslinked particles become resistance towards THF.

SEM and TEM imaging was also carried out to see how the microparticles and internal morphology behaved after being exposed to THF. The microparticles containing 4 wt. % DVB (PMMA₅₀₀-P4VP₁₇₀-P4VP₁₆₀/D4, vial (e) in Figure 4.29) lost their microparticle structure, as shown by the SEM image (Figure 4.31a), but the internal morphology is preserved well, as revealed by the TEM image (Figure 4.31b). However, the microparticle and the P4VP domain swelled after exposure to THF (Figure 4.31c). Even though 4VP and DVB crosslinking copolymerization occurs mostly within pre-formed P4VP domains within microparticles, these findings show that the ordinarily THF soluble PMMA matrix is also endowed with a high level of solvent resistance.

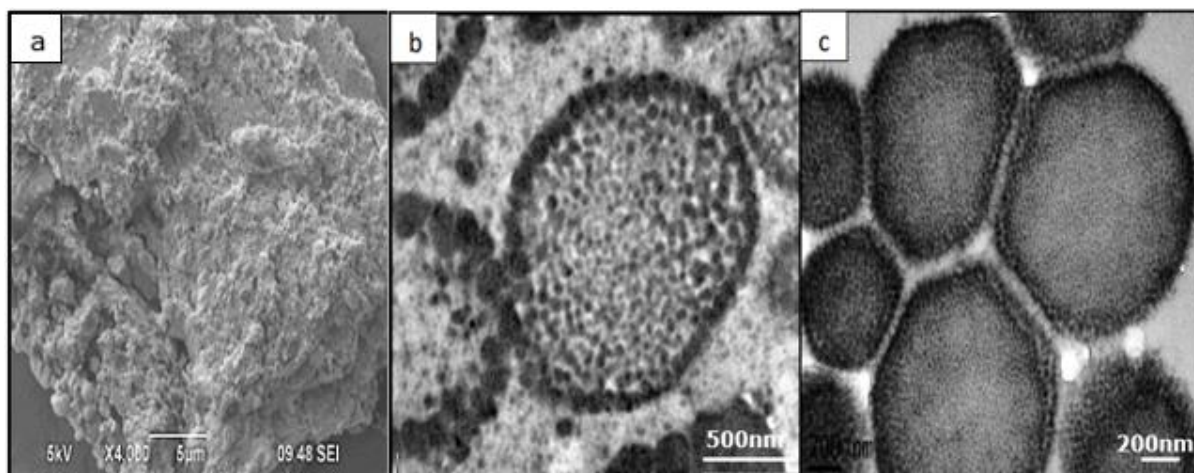


Figure 4.31. SEM (a) and TEM images of PMMA₅₀₀-P4VP₁₇₀-P4VP₁₆₀/D4 microparticles synthesised with 4 wt.% of DVB (vial (e) in Figure 4.29), after (b) and (c) before dispersion in THF overnight. The microparticles collapsed whilst the internal structure preserved well with some swelling effect.

4.4.2.4 Porosity control by a degree of crosslinking- SPH morphology

In 2018, the group successfully developed a simple method for converting nanostructured BCP microparticles to porous microparticles via swelling/deswelling in alcohol. It was demonstrated that by adjusting the block ratio and block length, the porosity can be custom-made across a range of different sizes and through a variety of morphologies. To achieve porous microparticles without causing inter-particle fusion, the swollen minority P4VP-block of PMMA-*b*-P4VP must be less than 35 mol%. This can be slightly improved by using a low swelling solvent, but even this eventually limits the types of BCP microparticles compatible with this process. Therefore, this study hypothesised that the swelling degree of the minority block could be used to tune the porosity in these systems during the swelling/deswelling process in response to the degree of crosslinking.

To investigate the effect of crosslinking on the porosity generated during solvent swelling, PMMA₅₀₀-*b*-P4VP₃₃₀ microparticles containing

varying concentrations of crosslinker synthesised using both methods were subjected to a swelling/deswelling process in ethanol and hexane (Table 4.4, entry 1-8). In this case, ethanol is an excellent solvent for P4VP, whereas hexane is non-solvent for both blocks. The microparticles with 0 wt.% DVB (PMMA₅₀₀-P4VP₃₃₀, Table 4.4, entry 1) developed large surface macropores with $d_w = >100$ nm, and numerous spherical pores merged into interconnected pore channels (Figure 4.32a). Additionally, the porous microparticles were significantly merged, as demonstrated in our recent report, due to swelling of the P4VP domains and collapse of the surrounding PMMA framework in microparticles with a high P4VP ratio.

Table 4.4. Effect of crosslinking on the porosity generated during solvent swelling of block copolymer PMMA₅₀₀-*b*-P4VP₃₃₀ synthesised using one-step addition^a and two-step addition^b method, at different loading of crosslinking (0-16 wt.% of DVB).

Entry	Sample	Crosslinker amount (w.t. %)	Pore width, d_w^c (nm)
1	PMMA ₅₀₀ -P4VP ₃₃₀	0	>100
2	PMMA ₅₀₀ -P4VP ₃₃₀ /D0.5	0.5	~20
3	PMMA ₅₀₀ -P4VP ₁₇₀ -P4VP ₁₆₀ /D0.5	0.5	40-140
4	PMMA ₅₀₀ -P4VP ₁₇₀ -P4VP ₁₆₀ /D1	1	~50
5	PMMA ₅₀₀ -P4VP ₁₇₀ -P4VP ₁₆₀ /D2	2	~20
6	PMMA ₅₀₀ -P4VP ₁₇₀ -P4VP ₁₆₀ /D4	4	<10
7	PMMA ₅₀₀ -P4VP ₁₇₀ -P4VP ₁₆₀ /D8	8	-
8	PMMA ₅₀₀ -P4VP ₁₇₀ -P4VP ₁₆₀ /D16	16	-

^a-entry 1-2, ^b-entry 3-8, ^c-measured by ImageJ

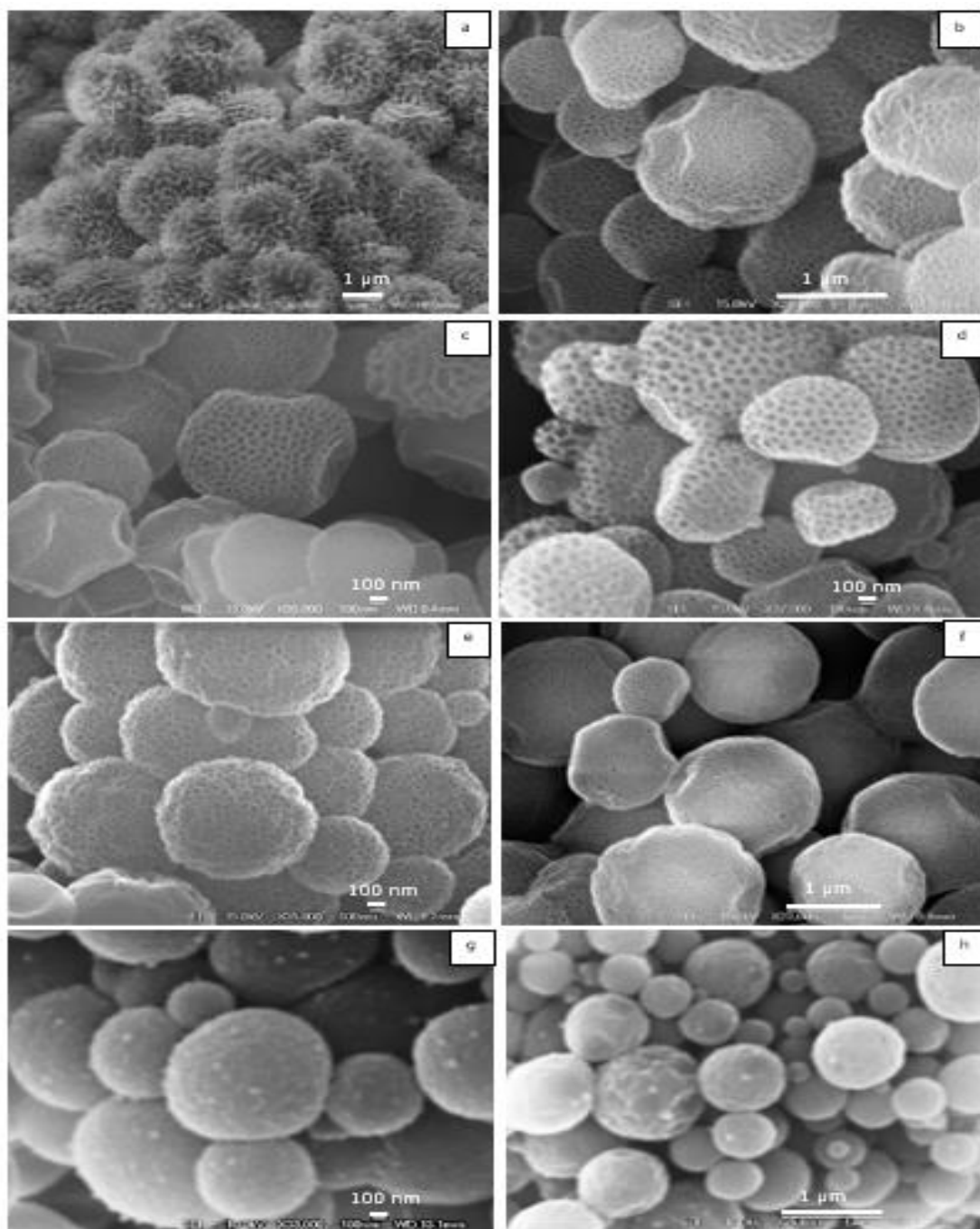


Figure 4.32. SEM images of BCP $\text{PMMA}_{500}\text{-}b\text{-P4VP}_{330}$ synthesised at different loadings of crosslinking (0.5–16 wt.% of DVB) after swelling in ethanol. The porosity decreased as the crosslinker amount increased in almost all of the samples- $\text{PMMA}_{500}\text{-P4VP}_{330}$ (a), $\text{PMMA}_{500}\text{-P4VP}_{330}/0.5$ (b) $\text{PMMA}_{500}\text{-P4VP}_{170}\text{-P4VP}_{160}/\text{D}0.5$ (c), $\text{PMMA}_{500}\text{-P4VP}_{170}\text{-P4VP}_{160}/\text{D}1$ (d), $\text{PMMA}_{500}\text{-P4VP}_{170}\text{-P4VP}_{160}/\text{D}2$ (e), $\text{PMMA}_{500}\text{-P4VP}_{170}\text{-P4VP}_{160}/\text{D}4$ (f), $\text{PMMA}_{500}\text{-P4VP}_{170}\text{-P4VP}_{160}/\text{D}8$ (g) and $\text{PMMA}_{500}\text{-P4VP}_{170}\text{-P4VP}_{160}/\text{D}16$ (h). [(a): Table 4.4, entry 1, (b): Table 4.4, entry 2, (c)-(h): Table 4.4, entry 3-8].

Following ethanol swelling, the sample prepared using the one-step addition method with the lowest DVB content (0.5 wt. %, PMMA₅₀₀-P4VP₃₃₀/D0.5) (Figure 4.32b, Table 4.4, entry 2) had a pore width $d_w \approx 20$ nm, which is significantly smaller than the non-crosslinked PMMA₅₀₀-P4VP₃₃₀ sample ($d_w > 100$ nm) (Figure 4.32a, Table 4.4, entry 1). In addition, in the absence of any inter-particle fusion, this sample developed into perfectly discrete porous microparticles (Figure 4.32b, Table 4.4, entry 2).

In contrast, the sample synthesised with the same amount of DVB via the two-step addition method (0.5 wt. %, PMMA₅₀₀-P4VP₁₇₀-P4VP₁₆₀/D0.5) was found to have a large range of pore width, ranging from 40-140 nm (Table 4.4, entry 3). In the SEM images (Figure 4.32c), a mixture of particles with different porosity was observed. This is expected due to the less crosslinked formation, which led to the branching formation instead. When the crosslinker amount was increased to 1 wt.% (PMMA₅₀₀-P4VP₁₇₀-P4VP₁₆₀/D1) the pore width become significantly smaller $d_w \approx 50$ nm (Table 4.4, entry 4) and the particles formed perfectly discrete porous microparticles without fusion between the particles (Figure 4.32d). When the crosslinking content was doubled to 2 wt.% (PMMA₅₀₀-P4VP₁₇₀-P4VP₁₆₀/D2), the pore width decreased even further to ~ 20 nm (Table 4.4, entry 5) and the microparticles shrank but maintained the discrete porosity (Figure 4.32e).

The porosity decreased to sub-10 nm when the amount of crosslinker was doubled further to 4 wt.% (PMMA₅₀₀-P4VP₁₇₀-P4VP₁₆₀/D4) (Table 4.4, entry 6), with some pores nearly closed (Figure 4.32f). Critically, both of the samples synthesised with 8 and 16 wt% of crosslinker (PMMA₅₀₀-P4VP₁₇₀-P4VP₁₆₀/D8 and PMMA₅₀₀-P4VP₁₇₀-P4VP₁₆₀/D16) (Table 4.4, entry 7 and 8) were almost completely lacking pores results and are essentially non-porous particles after ethanol swelling (Figure 4.32 g & h). Generally, these results demonstrate that swelling of the P4VP domains in ethanol can

be systematically controlled by increasing the amount of DVB added during polymerisation, specifically between 0.5 and 8 wt.% DVB.

When PMMA-*b*-P4VP microparticles swell and deswell, porosity forms in the regions normally occupied by the enlarged minority block, as was previously reported by He et al.²⁰ It has been shown that the volume of crosslinked microparticle P4VP domains increases as the DVB content lowers, decreasing voids caused by collapsing P4VP chains.²⁰

Byard et al. investigated the swelling of poly(*N,N*-dimethyl acrylamide)-*block*-poly(diacetone acrylamide) vesicles (PDMAM-*b*-PDAAm) crosslinked with adipic acid dihydrazide (ADH).²⁹ They discovered that in methanol, the mildly crosslinked vesicles swelled substantially. In comparison, swelling was significantly less severe with ADH/DAAM 0.050 due to the increased crosslinking produced under these conditions. Additionally, ADH/DAAM was covalently stabilised to a maximum of 0.075.

These findings are in line with our results. While BCP molecular weights and/or block ratios have previously been used to control porosity during swelling, these data now show that DVB crosslinker are a very good alternate way for achieving the same goal, which is to identify the maximum resistance point to swelling (non-porosity).

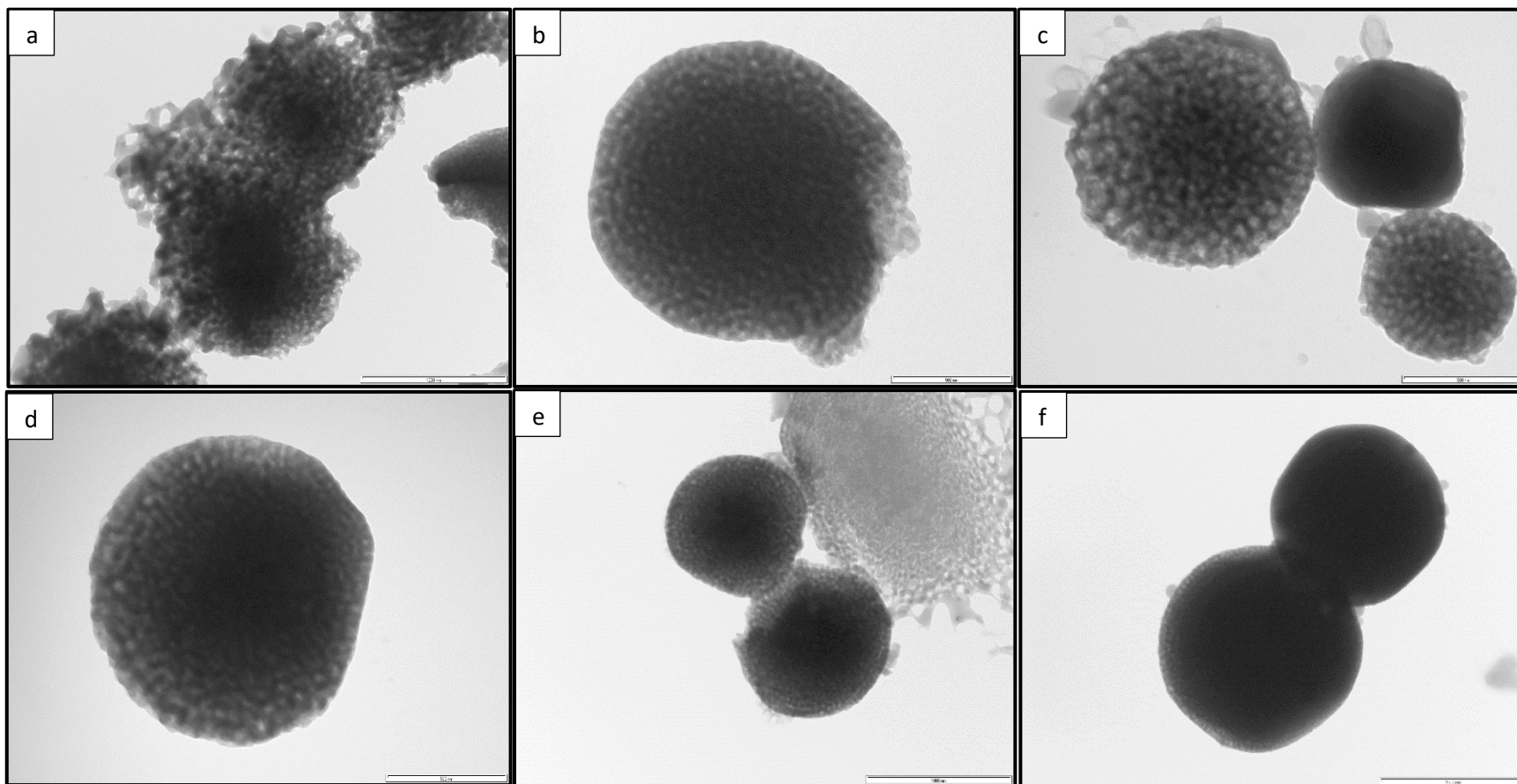


Figure 4.33. TEM images of crosslinked PMMA-*b*-P4VP microparticles after swelling in ethanol, which shows the porosity decreasing as crosslinker amount increased. PMMA₅₀₀-P4VP₃₃₀ with 0 wt% DVB (a), PMMA₅₀₀-P4VP₃₃₀/D0.5 with 0.5 wt% DVB (b), PMMA₅₀₀-P4VP₁₇₀-P4VP₁₆₀/D0.5 with 0.5 wt% DVB (c), PMMA₅₀₀-P4VP₁₇₀-P4VP₁₆₀/D1 with 1 wt% DVB (d), PMMA₅₀₀-P4VP₁₇₀-P4VP₁₆₀/D2 with 2 wt% DVB (e), PMMA₅₀₀-P4VP₁₇₀-P4VP₁₆₀/D4 with 4 wt% DVB (f). [(a): Table 4.4, entry 1, (b): Table 4.4, entry 2, (c)-(f): Table 4.4, entry 3-6].

The internal porosity of the crosslinked microparticles after swelling/deswelling was further investigated using TEM analysis. As shown in Figure 4.33a, the sample containing 0% DVB (Table 4.4, entry 1) has macropores larger than 50 nm and extensive inter-particle fusion, which is consistent with the SEM (Figure 4.32a) observations.

PMMA₅₀₀-P4VP₃₃₀/D0.5 (Table 4.4, entry 2) synthesised by the one step method, exhibits an intricate porous structure, with interconnected channels throughout the microparticle (Figure 4.33b). Additionally, the pore size is significantly reduced, with $d_w \sim 20$ nm, and inter-particle fusion is completely avoided. In comparison, when the same amount of crosslinker was added in two steps (Table 4.4, entry 3), the porosity size developed varied significantly between microparticles. There are particles with extremely small pore sizes, some of which appear to be non-porous at all, and there are also particles with larger pore sizes (Figure 4.33c).

The porosity of the samples synthesised with 1 wt.% DVB (PMMA₅₀₀-P4VP₁₇₀-P4VP₁₆₀/D1 (Table 4.4, entry 4) decreased further, the pore sizes reduced especially in the middle area of the particle (Figure 4.33d). When the DVB content is increased further to 2 wt.% (Table 4.4, entry 5), most of the porosity becomes even smaller throughout the particles (Figure 4.33e for PMMA₅₀₀-P4VP₁₇₀-P4VP₁₆₀/D2). PMMA₅₀₀-P4VP₁₇₀-P4VP₁₆₀/D4 (Table 4.4, entry 6) particles appear to lack porosity at 4 wt.% (Figure 4.33f). These non-porous particles are the only thing observed when the DVB content is increased to 8 wt.% (PMMA₅₀₀-P4VP₁₇₀-P4VP₁₆₀/D8, Table 4.4, entry 7). These findings support the SEM observations that pore size decreases dramatically as DVB content increases – from macropores (larger than 100 nm) to mesopores of 20 nm, sub-10 nm, and finally non-porous.

Interestingly, the swelling behaviour (or porosity) of crosslinked PMMA₅₀₀-P4VP₁₇₀-P4VP₁₆₀/D1 (Table 4.4, entry 4) in ethanol is similar to that of non-crosslinked M50-V12.4, whereas PMMA₅₀₀-P4VP₁₇₀-P4VP₁₆₀/D2 (Table 4.4, entry 5) is similar to M50-V7.6 (M50-V12.4 and M50-V7.6 are referred to as M-V19.9 and M-V13.3, respectively, in the recent group

report).¹⁶ It is reported that crosslinking has a similar effect on porosity control during the swelling/deswelling process as manipulating the block length. Smaller pores can thus be obtained by increasing crosslinking or decreasing block length.

4.4.2.4.1 Tilt-TEM Tomography

In order to inspect the internal porosity development throughout the whole microparticles, 3D structural analysis of the pores was carried out by using tilt TEM imaging with angle of up to 120°. To minimise distortion due to the missing wedge, pore size measurements were taken along the Z-axis of the tomographic reconstruction, which is parallel to the original zero tilt image. This analysis can minimise bias due to the missing section.¹⁶ All ten slices of the non-crosslinked sample PMMA₅₀₀-P4VP₃₃₀ (Table 4.4, entry 1) which contains 0% DVB, revealed the porous structure (Figure 4.34), as did the eight slices of the crosslinked sample PMMA₅₀₀-P4VP₁₇₀-P4VP₁₆₀/D1 (Table 4.4, entry 4), which contains 1% DVB (Figure 4.35)

The difference is readily apparent in the pore size and structure formed on the reconstructed slices; without crosslinking, large open ($d_w = >100$ nm) interconnected pores with uncontrollable sizes between the structure's surface (Figure 4.34, image 003, 045, 087) and the microparticles' middle (Figure 4.34, image 129, 171, 211, 253).

However, as a result of the crosslinker's effect on porosity control during solvation swelling, the crosslinked particles (Figure 4.35) at 1 wt.% formed discrete pores with smaller pore sizes throughout the particles. Reconstructed slices at the surface of the structure (Figure 4.35, image 009, 050, 090) reveal bigger open pores ($d_w = \sim 50$ nm). Slices in the middle of the reconstruction, passing through the centre of the particles, reveal much smaller pore widths, $d_w = \sim 20$ nm (Figure 4.35, image 135 and 180).

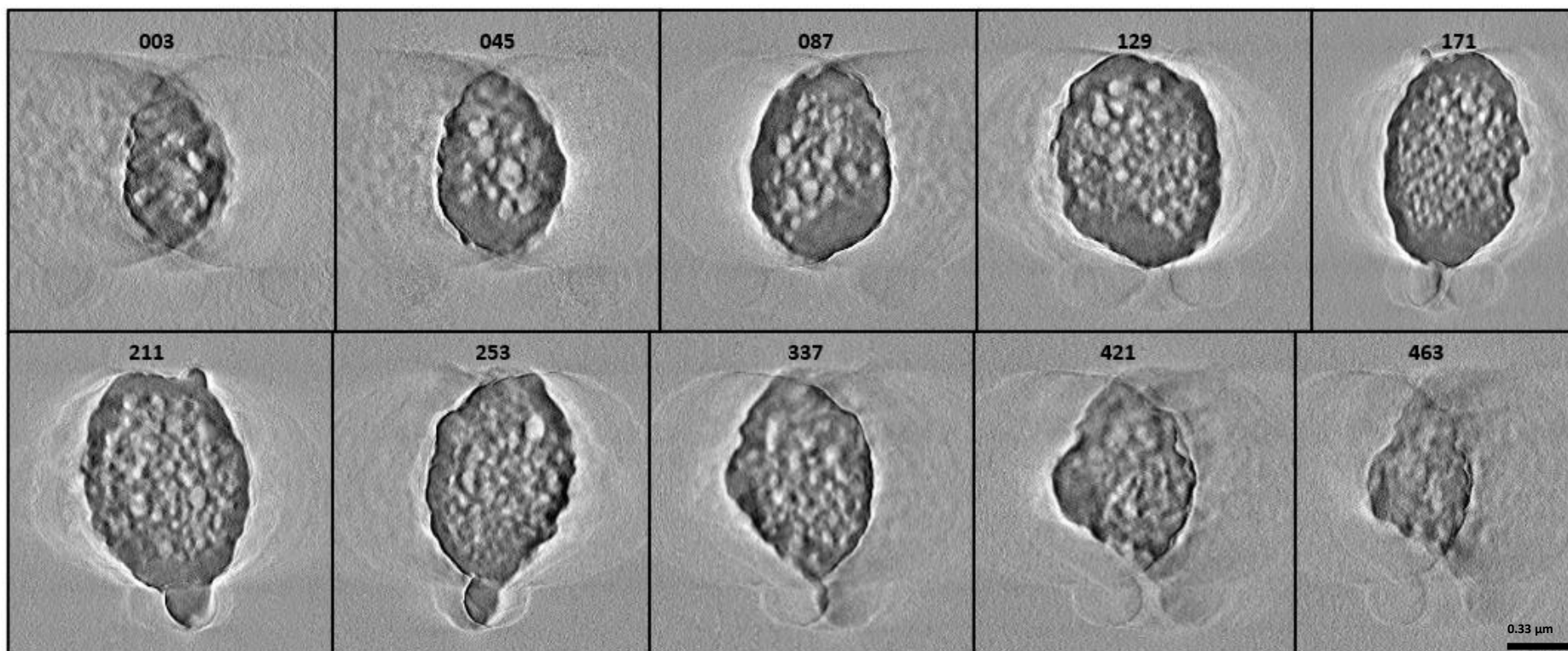


Figure 4.34. Selection of slices from the SIRT tomographic reconstruction of a non-crosslinked porous microparticle (PMMA₅₀₀-P4VP₃₃₀, Table 4.4, entry 1) showing 10 of 470 images (003, 045, 087, 129, 171, 211, 253, 337, 421 & 463) from the top surface to the bottom. The tilt series was taken at a 2550 electrons per nm² per s dose rate with 18 min and 41 s acquisition time.

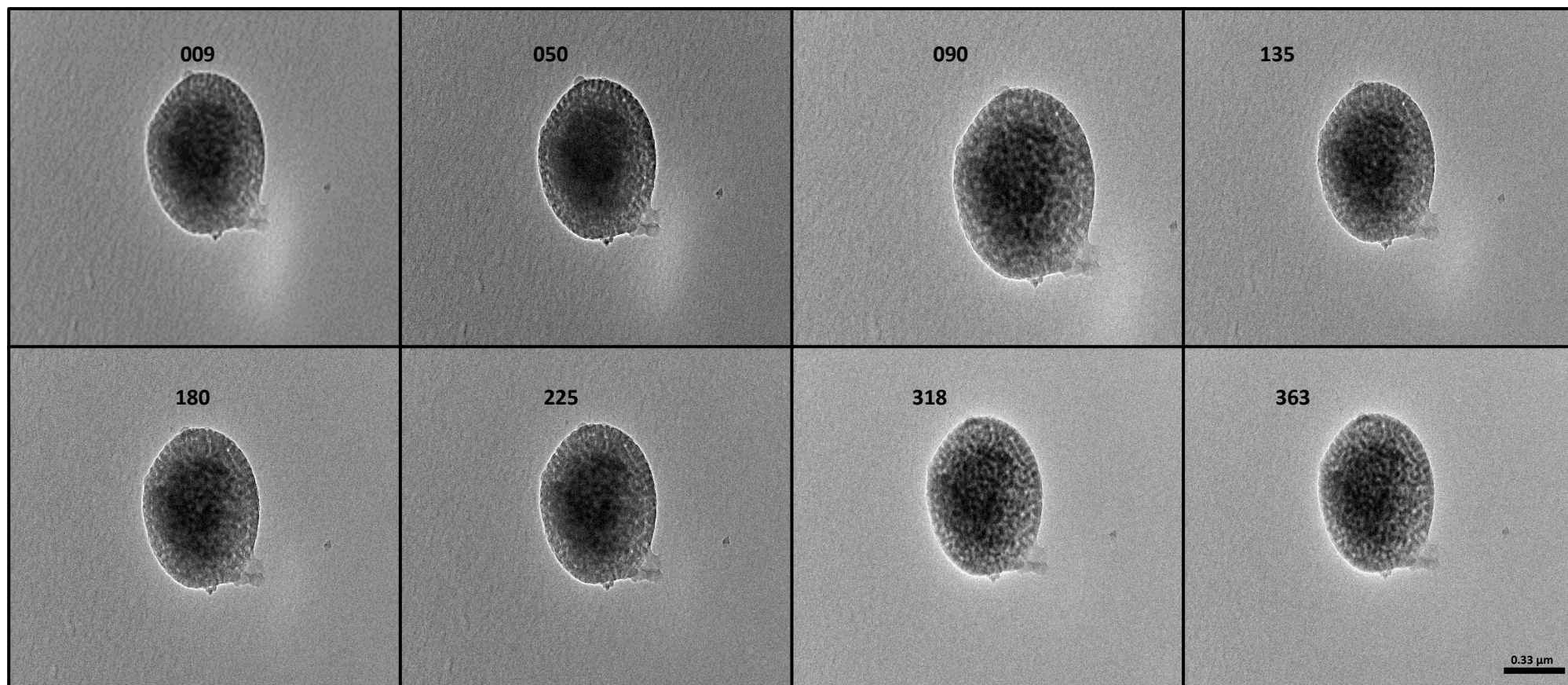


Figure 4.35. Selection of slices from the SIRT tomographic reconstruction of a crosslinked porous microparticle (PMMA₅₀₀-P4VP₁₇₀-P4VP₁₆₀/D1, Table 4.4, entry 4) showing 8 of 370 images (009, 050, 090, 135, 180, 225, 318 & 363) from the top surface to the bottom. The tilt series was taken at a 2550 electrons per nm² per s dose rate with 18 min and 41 s acquisition time.

These results support the pore width obtained by the standard TEM (Figure 4.33 a-f), as they were within the same range (Table 4.4). All slices from both non-crosslinked (Figure 4.34) and crosslinked (Figure 4.35) samples show the porosity structure, which further confirms that the pores are developed throughout the particle. The peripheral surface structure appears to be the result of progressive monomer exclusion towards the interior of the microparticles. As a result, in the later stages of polymerisation, the P4VP domains at the periphery are swollen with excess 4VP monomer, resulting in much larger domains than in the interior.²⁰

Overall, the ability to mix various techniques will expand the adaptability of this microparticle platform for generating hierarchically porous materials greatly.

4.4.2.5 Thermal Analysis- SPH morphology

The relationship between the T_g of each polymer block and the amount of crosslinker added to the polymerisation was studied using differential scanning calorimetry (DSC) (Figure 4.36 & 4.37). The products obtained from both synthesis methods exhibited two transitions, suggesting the existence of two blocks, PMMA (at approximately 125–128 °C) and P4VP (at approximately 150–158 °C). The T_g values of the PMMA were found to be stable around 125-128 °C regardless of the synthesis method, indicating that it was not affected crosslinking of the P4VP domain (Table 4.5 and Figure 4.38).

Table 4.5. The T_g ($^{\circ}\text{C}$) of block copolymer $\text{PMMA}_{500}\text{-}b\text{-P4VP}_{330}$ synthesised at different loading of crosslinking (0 wt.%-16 wt.% of DVB) by using one-step addition^a and two-step addition^b method.

Entry	Sample	Crosslinker amount (wt.%)	T_g ($^{\circ}\text{C}$)			
			PMMA	P4VP	PMMA (porous)	P4VP (porous)
1	$\text{PMMA}_{500}\text{-P4VP}_{330}$	0	127	152	129	154
2	$\text{PMMA}_{500}\text{-P4VP}_{330}/\text{D0.5}$	0.5	127	154	127	157
3	$\text{PMMA}_{500}\text{-P4VP}_{330}/\text{D1}$	1	128	154	- ^c	
4	$\text{PMMA}_{500}\text{-P4VP}_{330}/\text{D2}$	2	132	157	- ^c	
5	$\text{PMMA}_{500}\text{-P4VP}_{170}\text{-P4VP}_{160}/\text{D0.5}$	0.5	126	150	126	153
6	$\text{PMMA}_{500}\text{-P4VP}_{170}\text{-P4VP}_{160}/\text{D1}$	1	125	154	126	157
7	$\text{PMMA}_{500}\text{-P4VP}_{170}\text{-P4VP}_{160}/\text{D2}$	2	128	155	126	156
8	$\text{PMMA}_{500}\text{-P4VP}_{170}\text{-P4VP}_{160}/\text{D4}$	4	127	158	127	156
9	$\text{PMMA}_{500}\text{-P4VP}_{170}\text{-P4VP}_{160}/\text{D8}$	8	128	156	129	155
10	$\text{PMMA}_{500}\text{-P4VP}_{170}\text{-P4VP}_{160}/\text{D16}$	16	128	155	127	156

^a-entry 1-4, ^b-entry 5-10, ^c-Particle fused

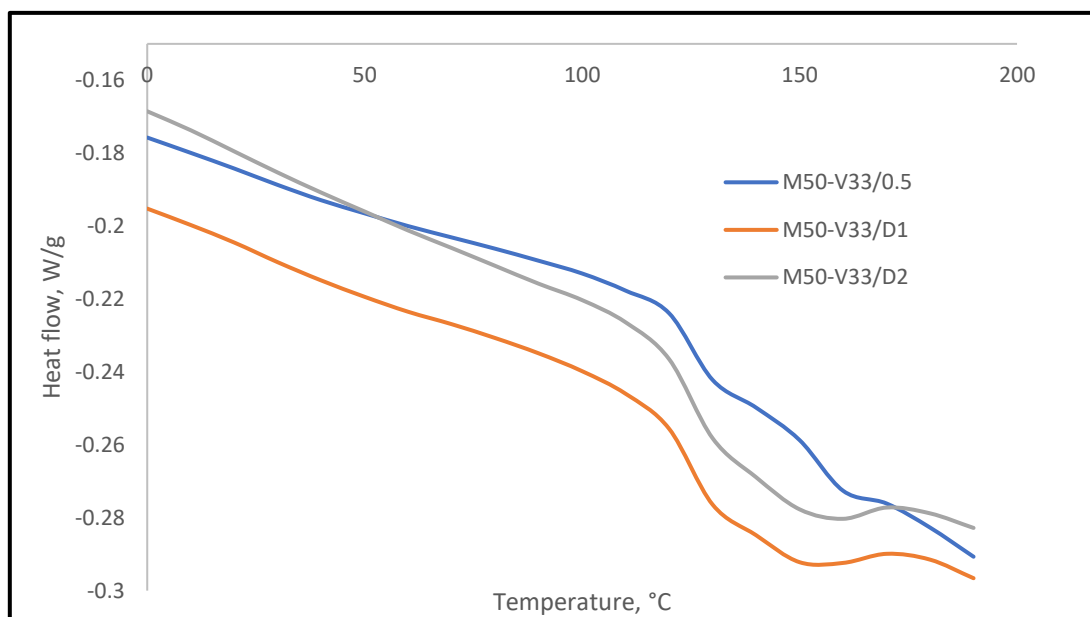


Figure 4.36. The T_g ($^{\circ}\text{C}$) measured by DSC of block copolymer $\text{PMMA}_{500}\text{-}b\text{-P4VP}_{330}$ synthesised using one-step addition method, at different loading of crosslinking (0.5-2 wt.% of DVB, Table 4.5, entry 1-4).

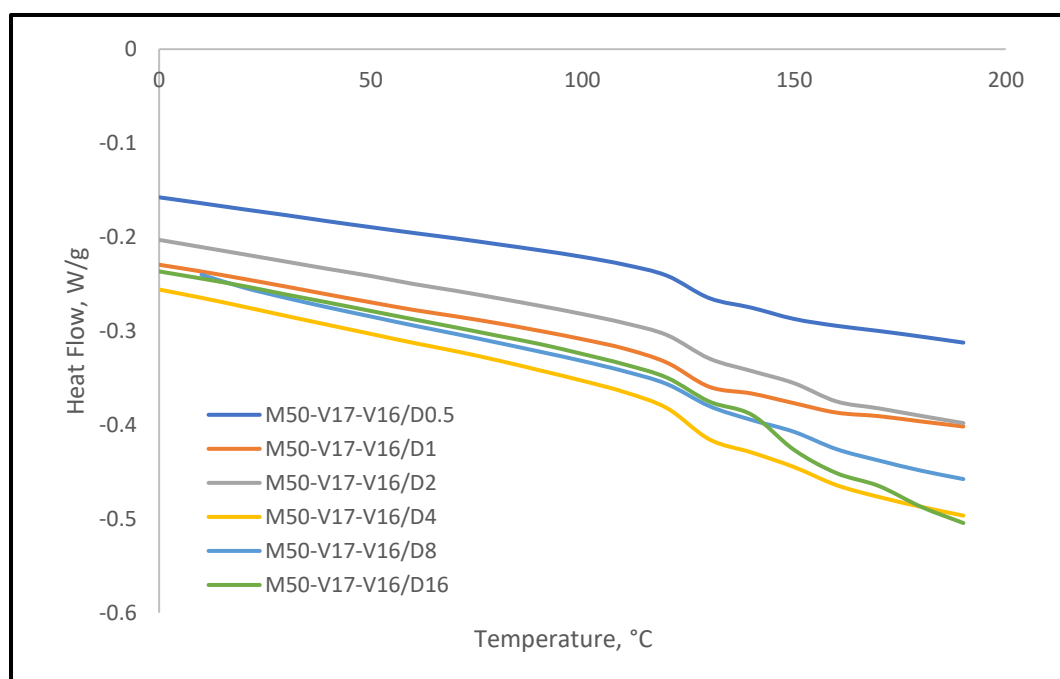


Figure 4.37. The T_g ($^{\circ}\text{C}$) measured by DSC of block copolymer $\text{PMMA}_{500}\text{-}b\text{-P4VP}_{330}$ synthesised using two-step addition method, at different loading of crosslinking (0.5-16 wt.% of DVB, Table 4.5, entry 5-10).

In the case of samples synthesised by the one-step addition method at 0.5 to 2 wt.% DVB ($\text{PMMA}_{500}\text{-P4VP}_{330}/\text{D0.5}$, $\text{PMMA}_{500}\text{-P4VP}_{330}/\text{D1}$ and

PMMA₅₀₀-P4VP₃₃₀/D2, Table 4.5, entry 2-4), the T_g of P4VP was higher in comparison to the sample with 0 wt.% (PMMA₅₀₀-P4VP₃₃₀, Table 4.5, entry 1). The T_g increased from 152 to 157 °C with an increasing trend as the amount of crosslinker increased. This result is expected, as all samples were found to be crosslinked, despite the fact that the particles agglomerated and fused upon addition at higher crosslinking amounts (1 and 2 wt. %, Table 4.5, entry 3 and 4).

On the other hand, the T_g of the P4VP domain from the two-stage addition method (Table 4.5, entry 5-10) was found to decrease below that of the 0 wt.% (PMMA₅₀₀-P4VP₃₃₀, Table 4.5, entry 1) when 0.5 wt.% DVB (PMMA₅₀₀-P4VP₁₇₀-P4VP₁₆₀/D0.5, Table 4.5, entry 5) was added, but it increased steadily about 5 °C between 1–4 wt. % DVB (Table 4.5, entry 6-8), peaking at 158 °C before reducing about 2 °C at 8 wt.% (Table 4.5, entry 9) and 16 wt.% (Table 4.5, entry 10). However, the reduction can be considered non-significant as it was still higher than the sample at 0 wt.% (Table 4.5, entry 1). This T_g trend was consistent with previous findings that the T_g values of polymers typically increased in response to the addition of crosslinking agents.¹³ This is strong evidence that the crosslinking reactions mainly affects the thermal properties of the P4VP domains. In the case of the PMMA₅₀₀-P4VP₁₇₀-P4VP₁₆₀/D0.5 (Table 4.5, entry 5) sample, it was determined that the branched polymer was formed rather than the crosslinked polymer, as the T_g was found to decrease upon the addition of crosslinker at a concentration of 0.5 wt.%t using this method. Reasons for this have previously been discussed by Shi et al.²³

Additionally, there is no significant difference recorded between T_g of non-porous and porous particles (Table 4.5 and Figure 4.38) from both methods showing a good sign of structural preservation.

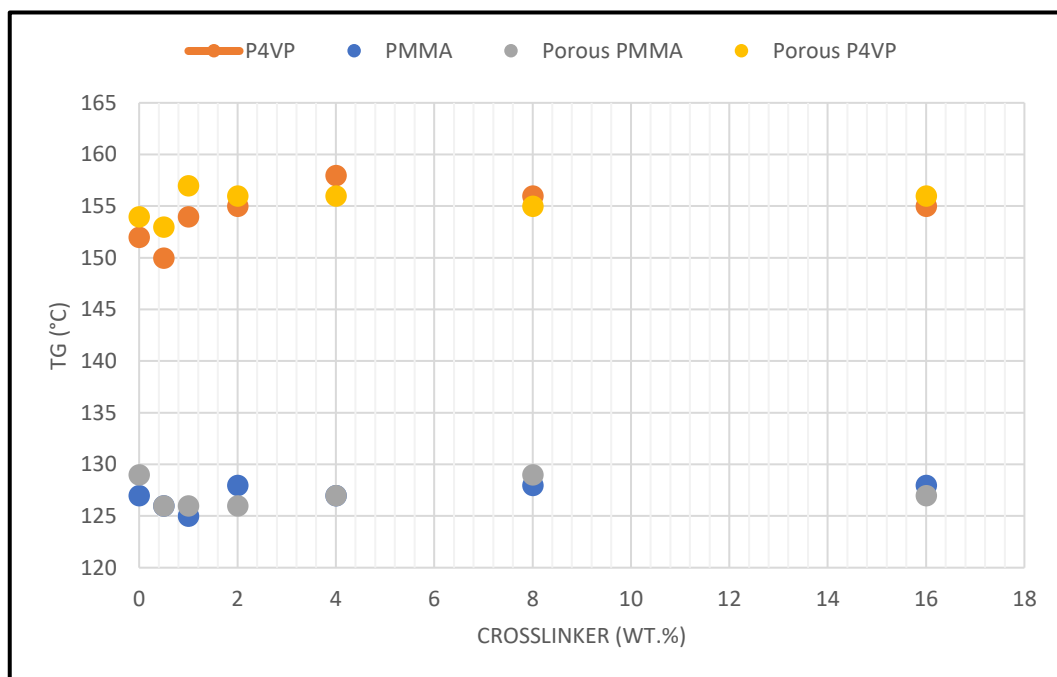


Figure 4.38. The T_g (°C) measured by DSC of block copolymer PMMA₅₀₀-*b*-P4VP₃₃₀ (porous and non-porous) synthesised using two-step addition method, at different loading of crosslinking (0-16 wt.% of DVB). There is no significant difference of T_g (°C) recorded for both porous and non-porous particles at 0 wt.% up to 16 wt.% crosslinker loading.

4.4.2.6 Two-step addition -LAM morphology

As discussed in-depth in chapter three (Section 3.4.5), this study has successfully synthesised LAM morphology using the same BCP system, PMMA-*b*-P4VP. This was achieved through the P4VP being the major block instead of PMMA. The SPH morphology was obtained by keeping the target block ratio of PMMA/P4VP at a molar value of 60/40 and the LAM was obtained when a molar value of 25/75 was used instead.

In order to evaluate the versatility of this crosslinking method, it was then applied to this LAM morphology. There were two amounts of crosslinking incorporated i.e. 0.5 wt.% and 2 wt.% respectively. The targeting molecular weight of the PMMA block was 15 kDa and for the P4VP block was 45 kDa. The sample with the lowest amount of DVB, 0.5 wt.% (PMMA₁₅₀-P4VP₄₀₀-P4VP₅₀/D0.5, Table 4.6, entry 2) was collected as a fine

free-flowing powder. In contrast, the PMMA₁₅₀-P4VP₄₀₀-P4VP₅₀/D2 sample (Table 4.6, entry 3) which contained 2 wt.% DVB, contained some agglomeration. However, the quality of the powder was improved by increasing the stirring speed to ~400 rpm and reducing the injection flow rate of the crosslinker injection to 0.1 mL min⁻¹ (instead of 1 mL min⁻¹). A higher speed of stirring caused a good homogenisation of the particle dispersion, which led to the formation of good quality microparticles when the DVB crosslinker was incorporated at a very slow flow rate of addition (0.1 mL min⁻¹).

All samples were characterised by multiple analytical techniques and the results obtained were compared to the non-crosslinked particles produced without any inclusion of DVB (PMMA₁₅₀-P4VP₄₀₀-P4VP₅₀, Table 4.6, entry 1). As presented in the SEM images (Fig. 4.39; a, c and e), the samples containing both 0.5 wt.% (PMMA₁₅₀-P4VP₄₀₀-P4VP₅₀/D0.5, Table 4.6, entry 2) and 2 wt.% (PMMA₁₅₀-P4VP₄₀₀-P4VP₅₀/D2, Table 4.6, entry 3) DVB produced spherical discrete particles, as fine powders. In terms of particle size, the sample with the lowest DVB content (at 0.5 wt.%, Table 4.6, entry 2) was similar to the sample prepared with no crosslinker (Table 4.6, entry 1). By contrast, the particles synthesised with 2wt.% DVB are much smaller (Table 4.6, entry 3) showing that the crosslinking process worked well at 2 wt.% DVB.

Table 4.6. Crosslinked BCP, PMMA₁₅₀-*b*-P4VP₄₅₀ microparticles with LAM morphology synthesised by two-step addition method and *in situ* crosslinking via RAFT dispersion polymerisation in scCO₂.

Entry	Block Copolymers	Crosslinker	SEM	TEM	DSC	
					<i>T_g</i> (°C) PMMA/P4VP	<i>T_g</i> (°C) PMMA/P4VP (porous)
1	PMMA ₁₅₀ -P4VP ₄₀₀ -P4VP ₅₀	0	1.00±0.23 (µm)	LAM ^c	121/153	125/154
2	PMMA ₁₅₀ -P4VP ₄₀₀ - P4VP ₅₀ /D0.5	0.5	1.30±0.49 (µm)	LAM	123/ 154	- ^d
3	PMMA ₁₅₀ -P4VP ₄₀₀ -P4VP ₅₀ / D2	2	0.68±0.30 (µm)	LAM	123/ 155	126/154

The reactions were conducted using pre-synthesised PMMA-RAFT with given M_n values at 65°C and 270 bars for 40 hrs at 3 stages: 1) redispersion of PMMA-RAFT (3.76 g) with PDMS-MA (5 wt.% w.r.t. 4VP), 2) chain extension, 4VP (10.53 g) and AIBN (39 mg) and 3) crosslinking, 4VP (1.316 g), AIBN (15.8 mg) and DVB (0.5-2.0 wt.% w.r.t. total 4VP in 2nd and 3rd stage). ^aD denote DVB, and the numbers following denote the weight percentage of DVB relative to total 4VP; ^bthe average of particle diameter measure by ImageJ was calculated by counting over 100 domains from SEM images; LAM^c = lamellar internal morphology determined by TEM; ^{-d}non-crosslinked/branched polymer.

In addition, both amounts of crosslinker added using this method successfully preserved the phase separation morphology (LAM), even at 2 wt.% which is a considerably high amount of crosslinker (Figure 4.39 b, d and f).

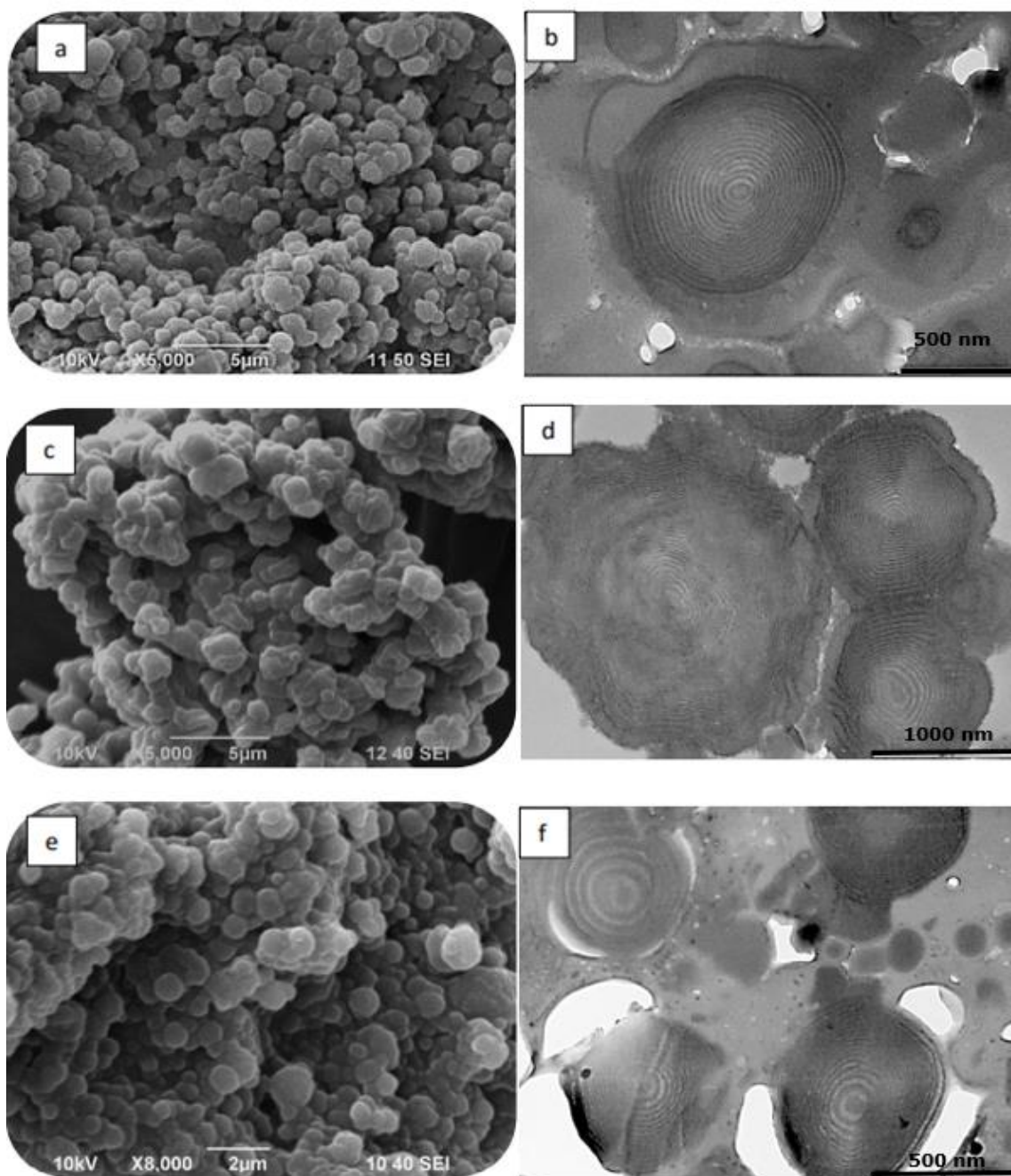


Figure 4.39. SEM and TEM images of BCP microparticles, PMMA₁₅₀-*b*-P4VP₄₅₀ (Table 4.6) incorporating 0 (a) & (b) (entry 1) , 0.5 (c) & (d) (entry 2) and 2 (e) & (f) wt.% DVB (entry 3). The microstructure and internal nanostructure of all the particles, synthesised using the two-step addition method in scCO₂, with or without crosslinker was successfully preserved.

The T_g of both samples that contained DVB were found to be higher in comparison to the non-crosslinked samples, but the difference was not significant (Table 4.6 and Figure 4.40). The same T_g trends of crosslinked polymer in $scCO_2$ has been previously reported in the group.^{20, 29} The difference in T_g recorded for the porous samples after swelling / deswelling treatment in ethanol/hexane was also found to be insignificant compared to the non-porous samples (Table 4.6).

As before, the dissolution test in chloroform (a good solvent for both PMMA and P4VP) was done to further confirm the crosslinking within the particles. The result showed formation of a cloudy solution that gradually disappeared over time with the sample containing 0.5 wt.% DVB (PMMA₁₅₀-P4VP₄₀₀-P4VP₅₀/D0.5). This indicated that this sample was branched as opposed to fully crosslinked. By contrast, a gel layer formed for the sample containing 2 wt.% DVB, indicating that there was some degree of crosslinking present. Whilst the non-crosslinked samples were fully solubilised, forming a clear solution, confirming that no crosslinking was present (Figure 4.41).

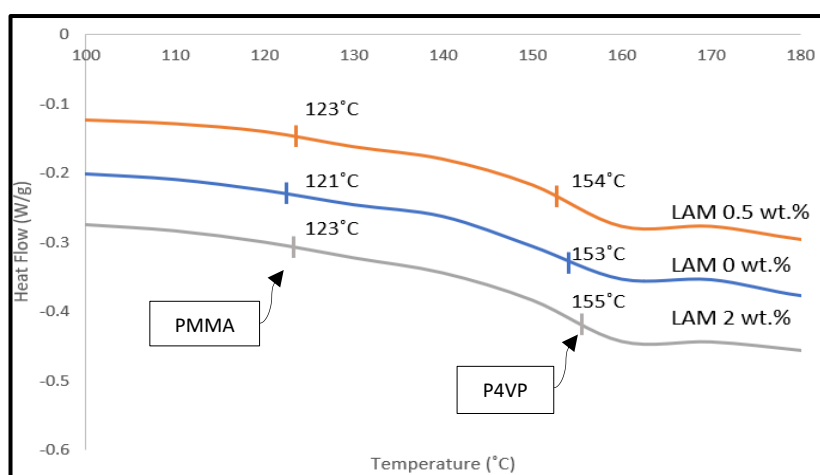


Figure 4.40. DSC traces of BCP, PMMA₁₅₀-P4VP₄₀₀-P4VP₅₀ contained DVB at 0 wt.%, 0.5 wt.% and 2 wt.%. The T_g increased as the crosslinker content increased (Table 4.6, entry 1-3).

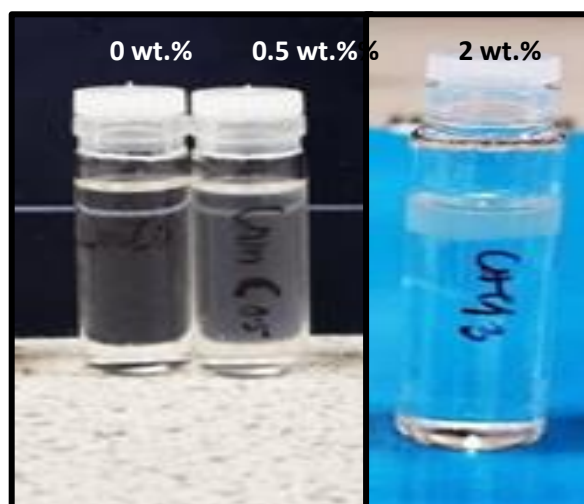


Figure 4.41. Photographs showing the solubility of the LAM particles contained DVB at 0 wt.%, 0.5 wt.% and 2 wt.% in chloroform. The LAM particles were fully dissolved at 0 wt.%, a slightly cloudy solution was formed for the 0.5 wt.% sample and a gel layer was formed for the 2 wt.% sample, indicating the presence of crosslinking (Table 4.6, entry 1-3).

4.4.2.6.1 Porosity control by a degree of crosslinking

The same procedure to investigate the porosity control by a degree of crosslinking, as discussed above in section 4.4.2.4 for SPH, was applied to both the non-crosslinked (PMMA₁₅₀-P4VP₄₀₀-P4VP₅₀, Table 4.6, entry 1) and crosslinked (PMMA₁₅₀-P4VP₄₀₀-P4VP₅₀/D2, Table 4.6, entry 3) LAM particles.

In ethanol, the non-crosslinked particles (PMMA₁₅₀-P4VP₄₀₀-P4VP₅₀) swelled a lot and became a gel-like solution (Figure 4.42a(i)) and only some particles were recovered after a hexane wash. The rest remained in gel form, as shown by the formation of a cloudy layer in the hexane (Figure 4.42b(i)).

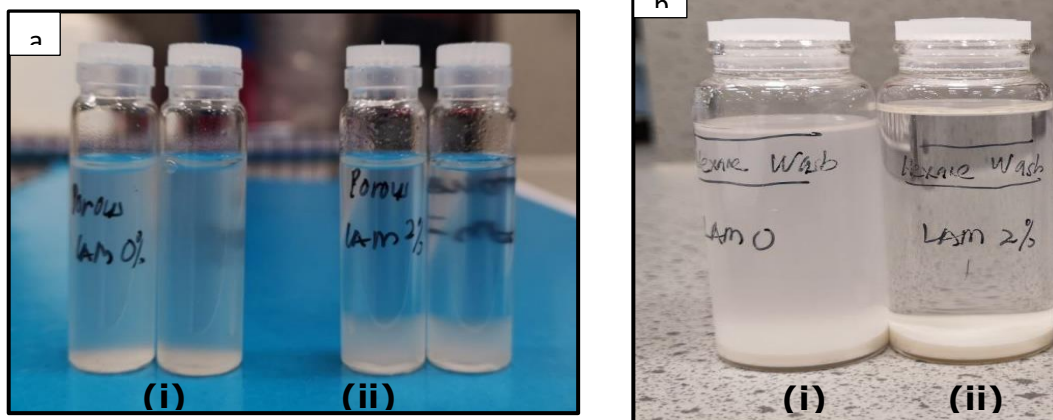


Figure 4.42. a) Photographic image of LAM particles without DVB crosslinking (i) (Table 4.6, entry 1) and with 2 wt.% DVB (ii) (Table 4.6, entry 3) dispersed in EtOH and b) the particles collected after the hexane washing process.

As expected, the non-crosslinked microparticle structure deformed, as shown by SEM images (Figure 4.43b). The TEM analysis showed that the internal LAM morphology of the microparticles had collapsed (Figure 4.44b), the image obtained after the samples had been stained with iodine clearly shows the contrast between the PMMA (lighter) and P4VP (darker) domains, as if the P4VP domain had erupted due to the swelling effect.

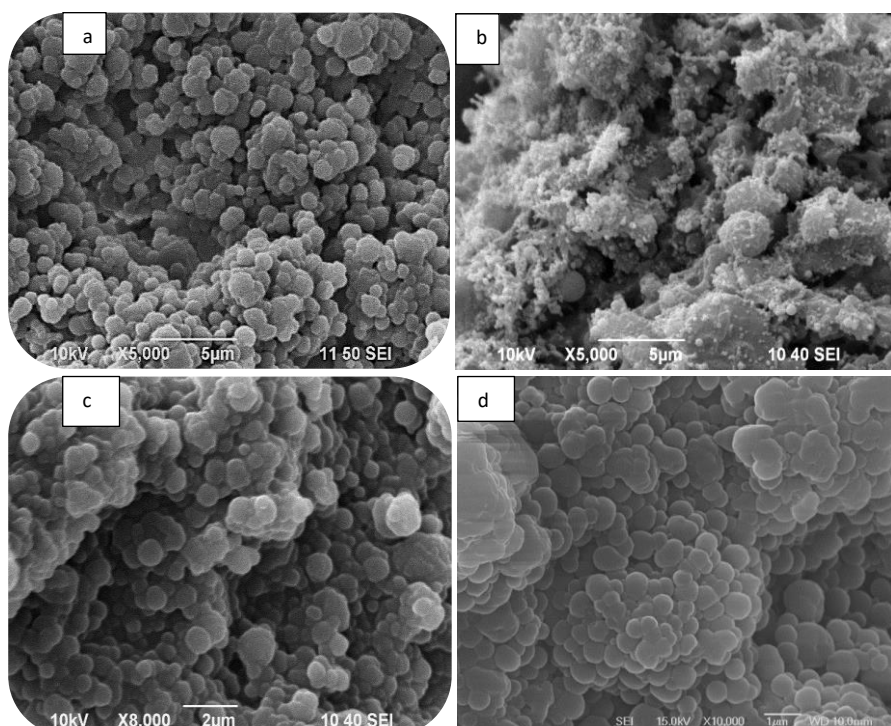


Figure 4.43. SEM images of LAM particles: non-crosslinked (PMMA₁₅₀-P4VP₄₀₀-P4VP₅₀) (a & b) and crosslinked with 2wt.% DVB (PMMA₁₅₀-P4VP₄₀₀-P4VP₅₀/D2) (c & d) before and after swelling/deswelling process in EtOH and hexane. The images show that the non-crosslinked (Table 4.6, entry 1) microparticles deformed and collapsed after the process (b) in comparison to discrete particles observed before the process (a). However, with the addition of crosslinker, the microparticle structure was preserved despite some swelling effect observed (d) compared to before process (c). The size of crosslinked particles (PMMA₁₅₀-P4VP₄₀₀-P4VP₅₀/D2) ($d_{mEtOH} = 0.81 \pm 0.25$ μm , (d)) was bigger after swelling compared to the original particle ($d_m = 0.68 \pm 0.30$ μm , (c), Table 4.6, entry 3).

In contrast, with the addition of 2 wt.% crosslinker (PMMA₁₅₀-P4VP₄₀₀-P4VP₅₀/D2), even though the particles were swollen, they settled at the bottom to form a gel layer in the ethanol (Figure 4.42a(ii)). The insoluble fraction was then recovered as particles after washing with hexane, a clear solution remained once the particles had fully segregated to the bottom (Figure 4.42b(ii)). This observation was corroborated by the SEM images, which revealed the preserved microparticle structure (Figure 4.43d). However, the particle size ($d_{mEtOH} = 0.81 \pm 0.25$) increased slightly as the particles absorbed some of the ethanol which caused the swollen

P4VP volume to increase. Overall, the crosslinked approach has successfully preserved the microparticles and the swelling degree of the particles containing 2 wt.% DVB and is considered controllable. This was supported by the particle size obtained after EtOH exposure ($d_{mEtOH} = 0.81 \pm 0.25$) which remains within the range of size before exposure ($d_m = 0.68 \pm 0.30$). The TEM images confirmed these findings, showing that the darker areas, which represents the P4VP domain, had been swollen by the solvent. As a result, the darker areas appear to dominate the particles at lower magnification while maintaining the microparticulate integrity (Figure 4.44d). The LAM nanostructure was also successfully preserved and is clearly visible at higher magnification (Figures 4.44e–4.44f).

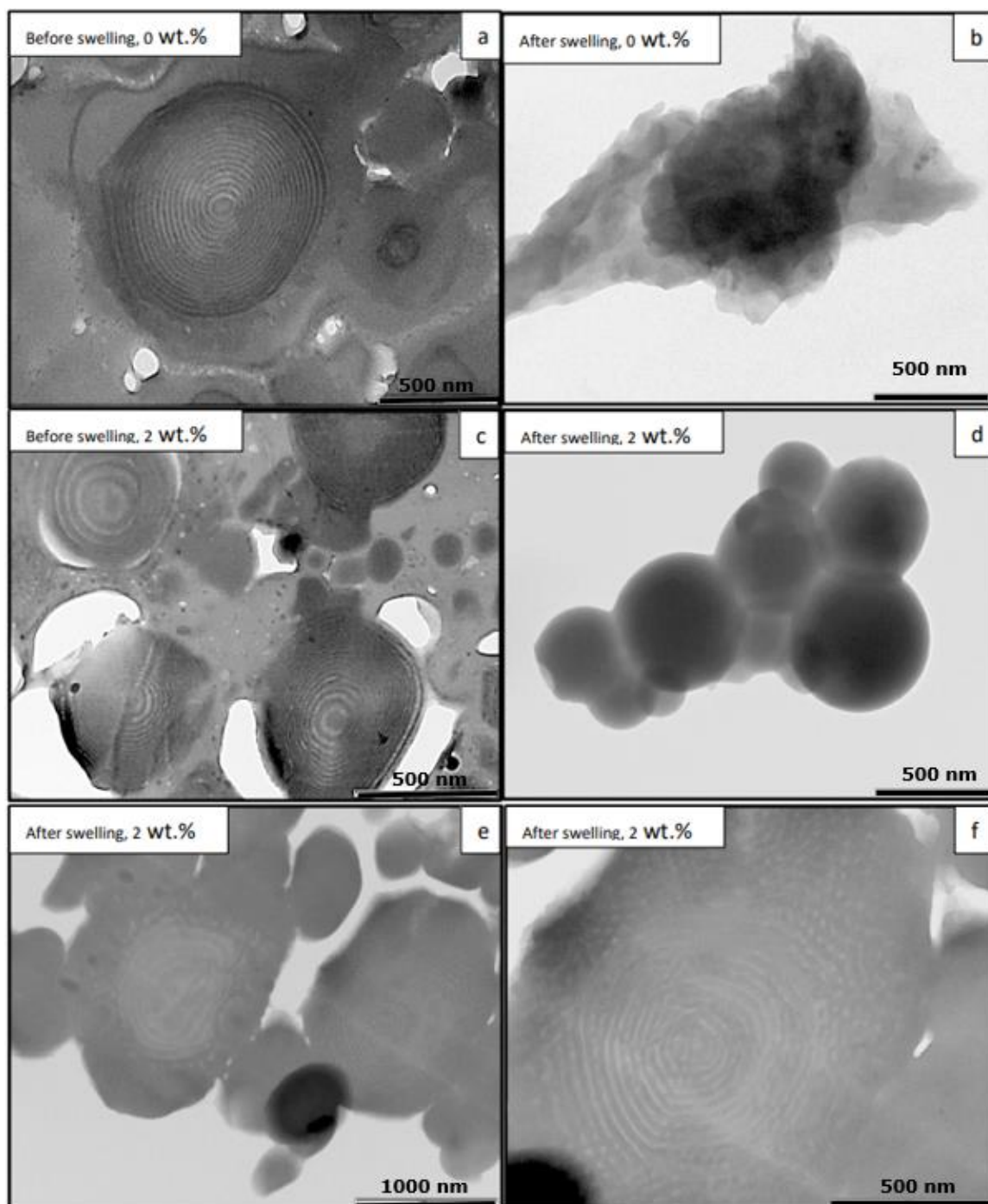


Figure 4.44. TEM images of LAM particles: non-crosslinked (PMMA150-P4VP400-P4VP50, Table 4.6, entry 1) (a & b) and crosslinked with 2wt.% DVB (PMMA150-P4VP400-P4VP50/D2, (Table 4.6, entry 3) (c & d) before and after swelling/deswelling process in EtOH and hexane. The microstructure of the non-crosslinked (0 wt. % DVB) particles had collapsed (b), whilst the presence of DVB at 2 wt.% has preserved the microparticles (d). The LAM morphology was preserved well after swelling and can be clearly seen in the higher magnification images (e) and (f). The particles after swelling were cryo-ultra-microtome at -60°C . All grids were stained with iodine prior imaging with TEM.

Further investigation of the particles after the swelling/deswelling process was performed by analysing them using adsorption isotherm measurement at -196°C (Figure 4.45). Both LAM samples with and without crosslinker recorded the Reversible Type II isotherms, identified by the shape resulting from unrestricted monolayer-multilayer adsorption up to high p/p° .³⁰ This indicated that the materials are entirely nonporous or macroporous. There is a significant change in the adsorption behaviour at high p/p° values, contributing to the higher amount of gas adsorbed, and that an abrupt change takes place at p/p° values between 0.9 and 1.

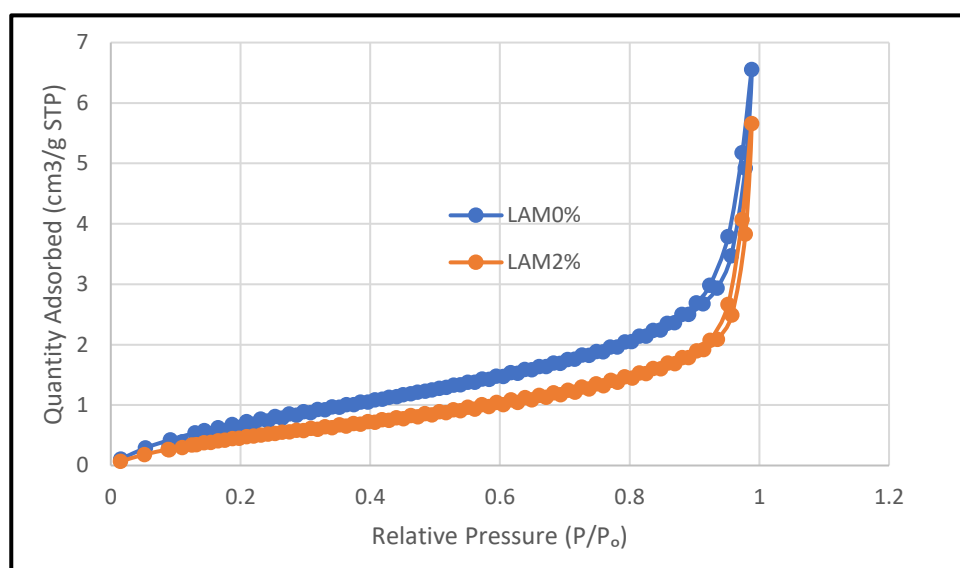


Figure 4.45. Nitrogen adsorption analysis of LAM microparticles after swelling/deswelling process in EtOH/Acetone. The graph shows the hysteresis loop of quantity adsorbed versus relative pressure of PMMA₁₅₀-P4VP₄₀₀-P4VP₅₀, LAM particle without crosslinker (LAM0%, Table 4.7, entry 1) and PMMA₁₅₀-P4VP₄₀₀-P4VP₅₀/ D2, LAM particle with 2 wt.% of crosslinker (LAM2%, Table 4.7, entry 2).

The polymer samples, which were mostly nonporous exhibit very low surface area and pore volume. The LAM0% (Table 4.7, entry 1) sample had a surface area of $3.28\text{ m}^2/\text{g}$, whilst LAM2% (Table 4.7, entry 2) was $2.13\text{ m}^2/\text{g}$, with pore volumes of 0.010 and $0.008\text{ cm}^3/\text{g}$ for LAM0% and LAM2% respectively. The pore diameter was 12.4 nm for LAM0% and 16.5

nm for LAM2%. As a results, a low value of total quantity of nitrogen was adsorbed by both samples, ranging from 5.66 to 6.56 cm³/g STP (Table 4.7). Theoretically, the surface area and pore volume play a fundamental role in the adsorption ability of polymer materials, in such a way that the lower the pore volume and surface area, the lower the adsorption capacity (Figure 4.45 and Table 4.7). However, it can be seen that the crosslinked LAM (LAM2%) has lower adsorption capacity in comparison to the non-crosslinked LAM (LAM0%), showing an effect of crosslinking in controlling the swelling/deswelling process in solvated condition.

Table 4.7 Summary of porosity information for the samples with LAM internal nanostructure analysed by nitrogen adsorption isotherms.

Entry	Sample	Crosslinker, DVB (wt.%)	Surface area^a (m²/g)	Pore Volume^b (cm³/g)	Pore Diameter^c (nm)	Total Quantity Adsorbed (cm³/g STP)
1	PMMA ₁₅₀ - P4VP ₄₀₀ - P4VP ₅₀	0.0	3.28	0.010	12.4	6.56
2	PMMA ₁₅₀ - P4VP ₄₀₀ - P4VP ₅₀ / D2	2.0	2.13	0.008	16.5	5.66

^a BET Surface Area.

^b BJH Adsorption cumulative volume of pores between 1.7 nm and 300 nm.

^c Adsorption average pore diameter (4V/A by BET).

As previously mentioned, this method is tailored to suit the PMMA-b-P4VP BCP which contains a minority of the swollen P4VP-block, (less than 35 mol%) to achieve porous microparticles without causing inter-particle fusion. We also hypothesised that the swelling process for the 3D microparticles is time dependent. This is in line with what was reported by Wang et al. who found varied pore morphologies were achieved by increasing swelling time from 10 minutes to 66 hours for a very dilute suspension of nanorods.³¹ In our previous study, the samples tested were in the form of dry powder and a substantial contact time >1 h was required to fully suspend the BCP microparticle powder in ethanol. In addition to this >12h was required for full solvent penetration and to fully swell gram quantities of our microparticles.²⁰

In conclusion, when the swollen P4VP-block was the majority of the BCP (molar ratio PMMA/P4VP = 25/75), and the swelling agent was ethanol, a good solvent for P4VP, the particles swelled and formed a gel layer before shrinking into particles after a hexane wash. More information could be gained about the porosity control by degree of crosslinking in the LAM particles tested in this study, with regards to both non-crosslinked and crosslinked particles containing 2 wt.% of DVB, with a number of improvements, for example, with different swelling agents, such as alcohols with different chain lengths (different polarity). In addition, testing a variable crosslinking degree of BCP samples might result in better morphology changes due to porosity generation.

In 2015, Yan et al. studied the role of swelling agents in selective swelling induced pore generation of cylinder-forming diblock copolymer, PS-b-P2VP (S2VP).³² The authors reported that high-carbon alcohols, including n-propanol, n-butanol and n-hexanol, produced cylindrical micelles because of their strong affinity toward the PS matrix. When high-carbon alcohols are employed as the swelling agents, the S2VP films experienced a much more drastic swelling effect compared to that of low-carbon alcohols (methanol and ethanol) (Figure 4.46).

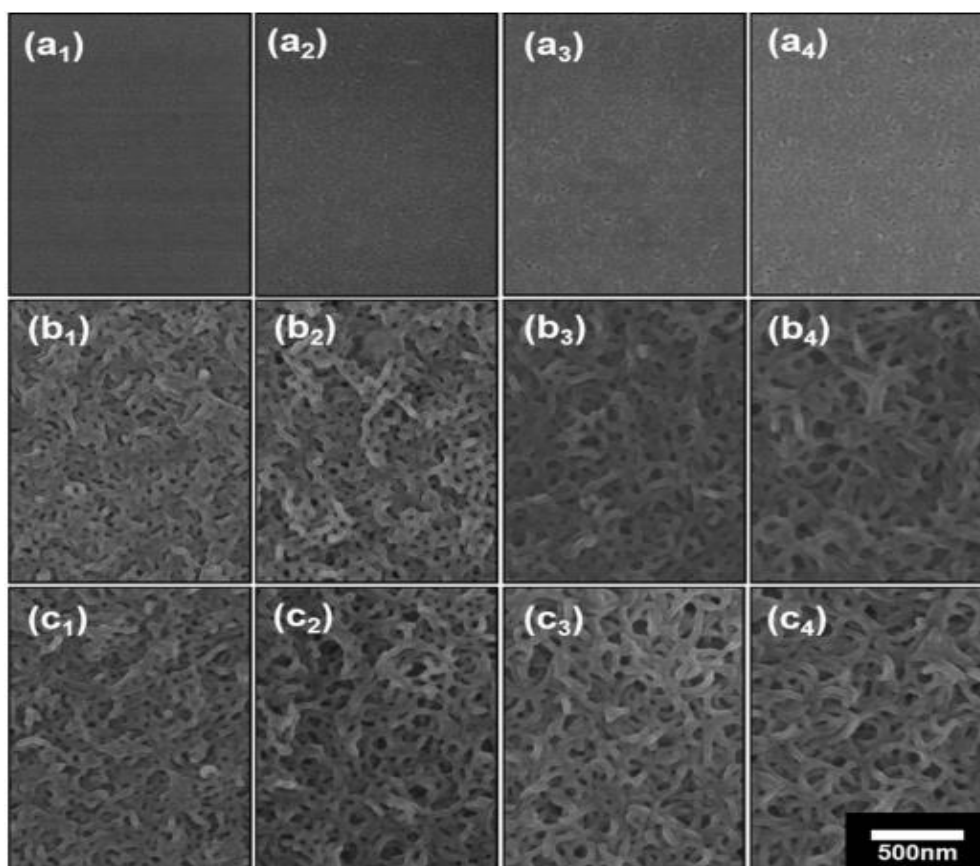


Figure 4.46. Surface SEM images of S2VP films soaked in (a) methanol, (b) n-propanol, and (c) n-butanol for (a₁, b₁, c₁) 10 min, (a₂, b₂, c₂) 1 h, (a₃, b₃, c₃) 4 h and (a₄, b₄, c₄) 15 h, respectively. All the images have the same magnification, and the scale bar is 500 nm.³²

Wang et al. investigated the topography of thin BCP films by surface reconstruction associated with selective swelling of one of the blocks.³¹ The collapse of the swollen chains upon drying yielded polymeric nanorods, exhibiting complex nanoscopic architectures characterized by a variety of mesopore structures and surface topographies, including channels along the nanorods, bunches of partially interconnected strands, and strings of spheres (Figure 4.47).³¹

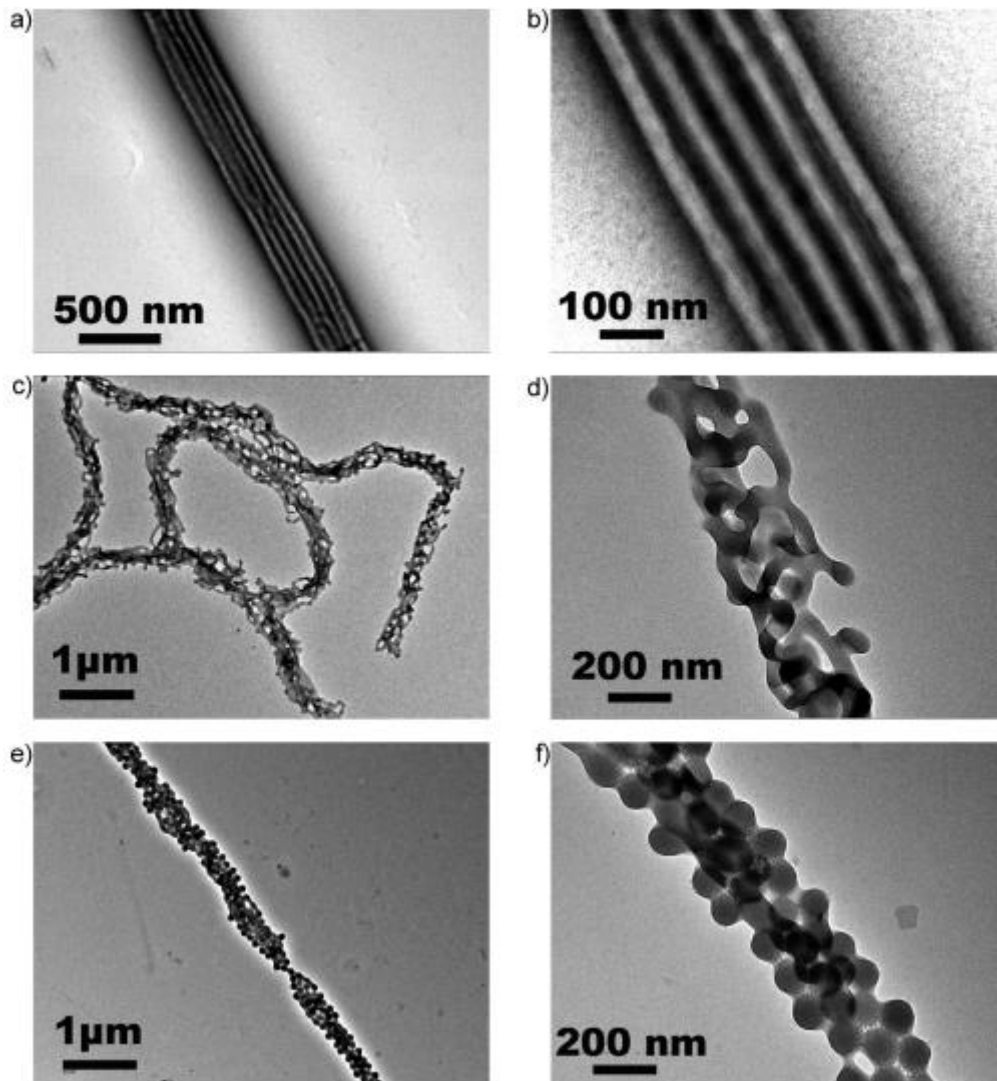


Figure 4.47 TEM images of nanorods consisting of cylinder-forming PS-*b*-P2VP at different stages of morphology reconstruction after exposure to an acidic environment. (a) Large-field view and (b) detail of nanorods with stage 1 morphology (cylindrical channels in solid matrix) obtained by heating them to 80 °C for 2 h while suspended in a 1:4 ethanol/0.01 M HCl(aq) mixture; (c) large-field view and (d) detail of nanorods with stage 2 morphology (interconnected strands) obtained by heating to 95 °C for 10 minutes while suspended in a 1:4 ethanol/ 0.01 M HCl(aq) mixture; (e) and (f) nanorods with stage 3 morphology (strings of spheres) obtained by heating to 95 °C for 15 h while suspended in a 1:4 ethanol/0.01 M HCl(aq) mixture.³¹

4.4.2.6.2 Dissolution Test

Solubility testing was also performed in a wider range of solvents to investigate the swelling performance and to evaluate the solubility information for certain application. All particles without or with DVB content were found to be hydrophobic, indicated by the fact that they floated to the surface when dispersed in water (Figure 4.48).

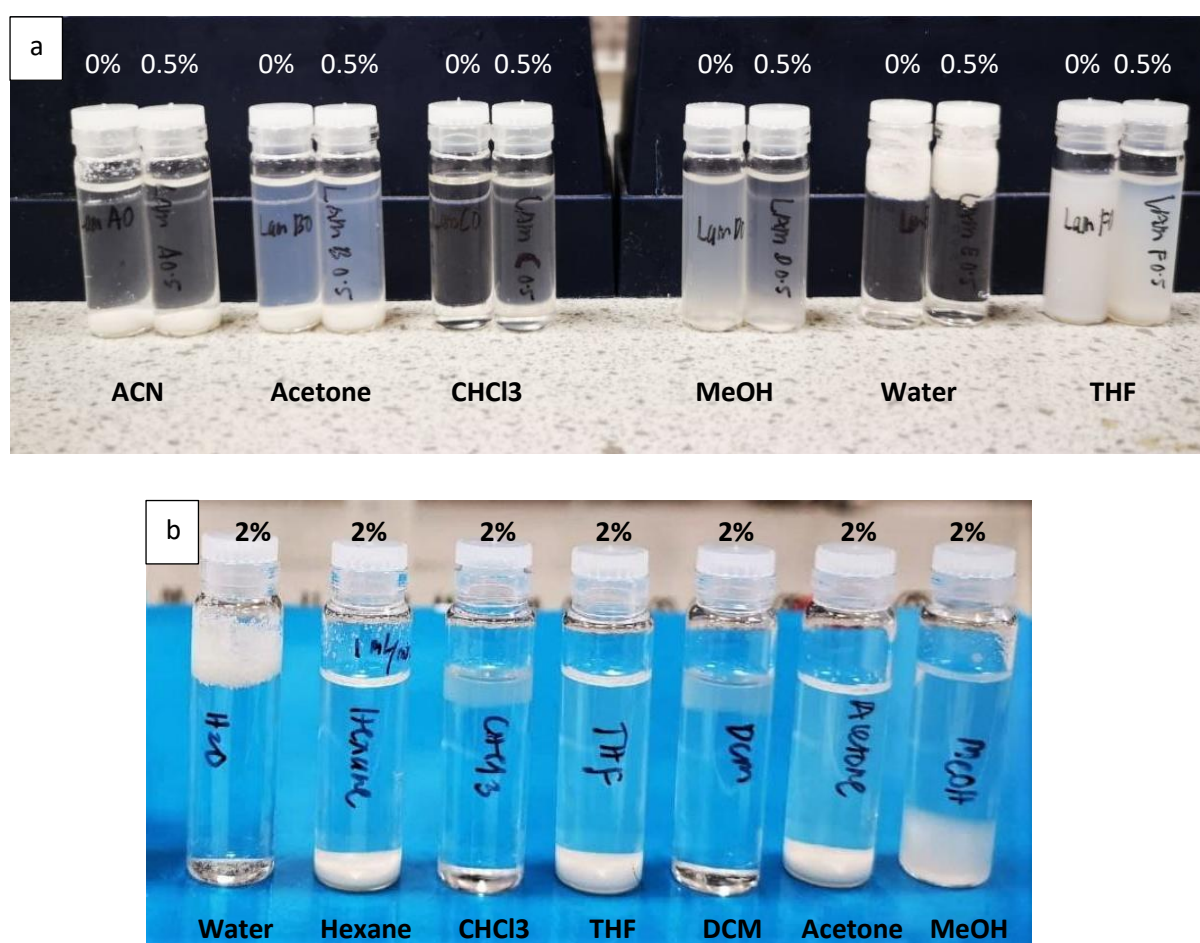


Figure 4.48. Solubility tests of (a) LAM0% (non-crosslinked) and LAM0.5% (branched) polymer samples and (b) LAM2% in various solvents to show the improvement in particle resistance to dissolution after being crosslinked with 2 wt.% of DVB (Table 4.8, entry 1-3).

Table 4.8 Summary of the solubility performance of LAM particles with 0, 0.5 and 2 wt.% DVB in various types of solvents.

Entry	DVB (wt.%)	Solubility					
		ACN	Acetone	THF	MeOH	Water	CHCl ₃
1	0	X	X	C	G	H	√
2	0.5	X	X	C	G	H	√
3	2	-	X	X	G	H	G

*X= insoluble, C=cloudy, √=soluble, G=swell, H=hydrophobic, - =no data

The particles without any crosslinker (0 wt.%, Table 4.8, entry 1) were not fully soluble in acetonitrile (ACN), acetone, tetrahydrofuran (THF) and methanol (MeOH), they either settled at the bottom of the vial in a few seconds (in ACN), formed a cloudy solution and settled at the bottom overnight (Acetone) or remained cloudy (THF) or swelled and turned into a gel solution (MeOH) (Figure 4.48a, 0%). The same observation was found for the particles that contained 0.5 wt.% DVB (Figure 4.48a, 0.5% and Table 4.8, entry 2). It is suspected that these particles contained branching as opposed to full crosslinking as previously discussed. The particles were then dried and analysed by SEM to investigate the particle morphology. The spherical microparticles structure no longer remained with the samples that had been previously dispersed in ACN, acetone, THF and MeOH (Figure 4.49, LAM0%). This is as expected since ACN, acetone and THF are good solvents of PMMA, whilst MeOH is a good solvent for P4VP.

The particles containing 2 wt.% DVB (Figure. 4.48b, 2% and Table 4.8, entry 3), were not soluble in all of the solvents tested including hexane, CHCl₃, THF, DCM, acetone and MeOH. They remained as particles and settled at the bottom of the vial when dispersed in hexane, THF and acetone. In contrast, they swelled and formed a gel layer in CHCl₃, DCM and MeOH. The gel layer formed either floated on the surface of the solvent

tested or sank to the bottom, depending on the density difference between the polymer and the solvent.

However, the SEM images of the particles after they had been exposed to all of the solvents tested indicated that the particles without crosslinker (LAM0%) had collapsed (Figure 4.49). The particles formed a thin layer on the surface in ACN and acetone, dried as a clear thin layer in THF and as a swollen thin layer in MeOH. Nevertheless, some particles' scaffold can be seen for samples containing 2 wt.% crosslinker (Figure 4.49, LAM2%). Thus, the addition of crosslinking could possibly increase the resistance of the LAM particles towards the solvents tested. Further analysis, such as TEM, to investigate the changes of the internal nanostructure of these particles after solvent exposure are needed in the future.

In summary, the in-situ crosslinking method was found to be suitable for crosslinking a different morphology of particles (LAM). It enabled the preservation of the integrity of both microstructure and internal nanostructure of LAM particles with up to 2 wt.% crosslinking degree. The microstructure and internal nanostructure of this crosslinked LAM was successfully fixed in the presence of good solvents such as EtOH followed by hexane swelling.

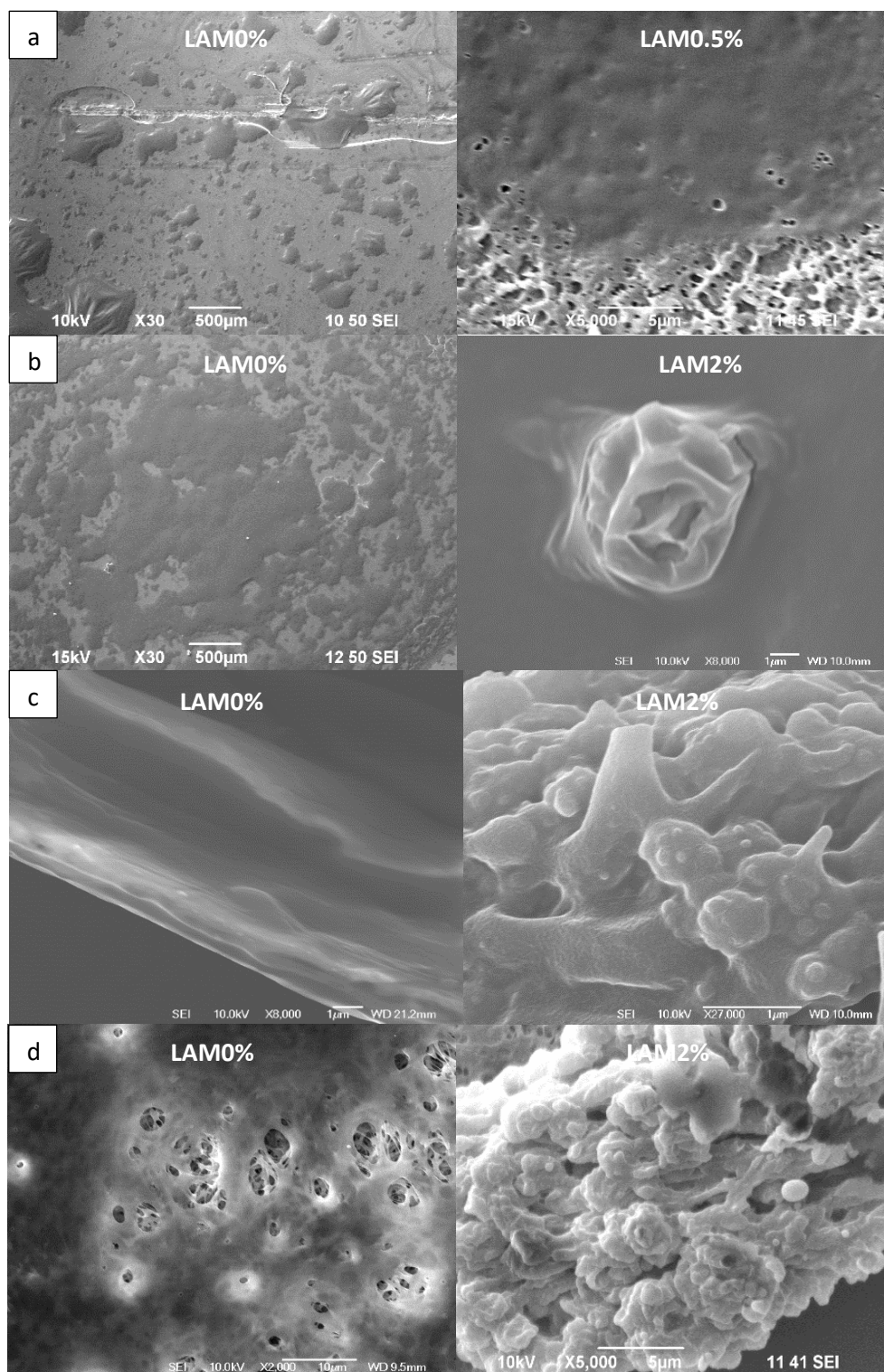


Figure 4.49. SEM images of LAM particles at 0 wt.%, 0.5 wt.% and 2 wt.% of DVB in various types of solvent: a) ACN b) Acetone c) THF and d) MeOH. It shows some particles' scaffold formed in crosslinked LAM at 2 wt.% which could enhance the resistance of the particle in comparison to the non-crosslinked LAM (LAM0%) (Table 4.8, entry 1-3).

4.5 Conclusion

In conclusion, this chapter discusses a novel approach to introducing crosslinking into nanostructured BCP microparticles via in situ crosslinking copolymerisation. The method allowed for retention of structural integrity under solvated conditions.

The initial work focused on the crosslinking of PMMA homopolymer in $scCO_2$ and was carried out by dispersion FRP in a one pot method. The agglomeration of PMMA particles synthesised incorporated EGDMA at 0 - 1 wt.% increased as the amount of crosslinker (EGDMA) increased. In addition, a trend of decreasing T_g as a function of cross-linker loading was observed in comparison to the linear PMMA particles, suggesting that the polymer microparticles formed during these experiments were more branched as opposed to fully crosslinked. The M_n values of these branched polymers, which also decreased proportionally, also agreed with this T_g trend when considering the sample preparation methods used prior to undertaking the analysis.

The development of a novel and facile method for "fixing" the internal nanostructure of BCP microparticles in dispersion in $scCO_2$ has been accomplished. Using a delayed addition of the crosslinker and a portion of the second monomer, it was possible to maintain the polymerisation-induced microphase separation within the microparticles, while simultaneously crosslinking the growing chains of the precursor, PMMA-*b*-P4VP microparticles with spherical (SPH) morphology. Moreover, a high crosslinker concentration of 16 wt.% DVB can be incorporated into the reaction using this method to generate microparticles with extensively crosslinked nanopatterns. It was also demonstrated that this synthetic procedure can be used to crosslink PMMA-*b*-P4VP microparticles with an internal lamellar (LAM) morphology.

The structural stability of the crosslinked PMMA-*b*-P4VP microparticles (with SPH morphology) was initially verified by dispersing them in suitable solvents, which preserved both the interior nanostructures and microparticulate scaffolds. Remarkably, it was discovered that the amount of porosity formed by swelling in ethanol is efficiently controlled by the amount of crosslinker supplied during the polymerisation. Macropores greater than 100 nm, mesopores 20 nm, sub-10 nm pores, and finally non-porous structures were all obtained by increasing the DVB concentration from 0 to 0.5, 1, and 4 wt.%, respectively. The T_g values of the crosslinked P4VP domains increased as a function of the amount of DVB incorporated, which matched with a decrease in the diameters of the microparticles.

In the case of LAM microparticles, both interior nanostructures and microparticulate scaffolds were well-preserved when up to 2 wt.% of crosslinking was incorporated. The size of crosslinked particles was found to decrease in comparison to the non-crosslinked particles and the T_g of the P4VP domain increased as an effect of crosslinking. The structural integrity of microparticles and the internal LAM morphology were also well preserved under solvated condition at this degree of crosslinking.

This adaptable technique significantly broadens the available range for synthesising porous BCP microparticles with customizable properties, morphologies, and pore sizes, hence significantly expanding their application potential in a variety of disciplines.

4.6 References

1. M. J. Monteiro and J. De Barbeyrac, *Macromolecules*, 2001, **34**, 4416-4423.
2. J. Jennings, M. Beija, J. T. Kennon, H. Willcock, R. K. Reilly, S. Rimmer and S. M. Howdle, *Macromolecules*, 2013, **46**, 6843-6851.
3. T. R. Guimarães, M. Khan, R. P. Kuchel, I. C. Morrow, H. Minami, G. Moad, S. b. Perrier and P. B. Zetterlund, *Macromolecules*, 2019, **52**, 2965-2974.
4. R. R. Larder, T. M. Bennett, L. S. Blankenship, J. A. Fernandes, B. K. Husband, R. L. Atkinson, M. J. Derry, D. T. W. Toolan, H. A. Centurion, P. D. Topham, R. V. Gonçalves, V. Taresco and S. M. Howdle, *Polymer chemistry*, 2021, **12**, 2904-2913.
5. J. Sedó, J. Saiz-Poseu, F. Busqué and D. Ruiz-Molina, *Advanced materials (Deerfield Beach, Fla.)*, 2013, **25**, 653.
6. J. D. F. Xuewei Xu, ‡ and Charles L. McCormick, *Macromolecules*, 2011, **44**, 1327-1334, 1327-1334.
7. L. Qiu, C. R. Xu, F. Zhong, C. Y. Hong and C. Y. Pan, *Macromolecular Chemistry and Physics*, 2016, **217**, 1047-1056.
8. A. Zhang, A. Li, Y. Wang, M. Liu, H. Ma, Z. Song and J. Liu, *RSC Adv.*, 2016, **6**, 103843-103850.
9. H. Li, L. Sui and Y. Niu, *Full Set - Includes 'Journal of Materials Science Letters'*, 2018, **53**, 12718-12730.
10. M. Chen, C. Zhou, Z. Liu, C. Cao, Z. Liu, H. Yang and H. Zhang, *Polymer International*, 2010, **59**, 980-985.
11. C. Zhou, H. Liu, M. Chen, G. Wu and H. Zhang, *Polymer Engineering & Science*, 2012, **52**, 2523-2529.
12. W. Wang, R. M. T. Griffiths, A. Naylor, M. R. Giles, D. J. Irvine and S. M. Howdle, *Polymer*, 2002, **43**, 6653-6659.
13. J. Shin, W. Bae and H. Kim, *Kolloid-Zeitschrift und Zeitschrift für Polymere*, 2010, **288**, 271-282.

14. J. Jennings, M. Beija, A. P. Richez, S. D. Cooper, P. E. Mignot, K. J. Thurecht, K. S. Jack and S. M. Howdle, *Journal of the American Chemical Society*, 2012, **134**, 4772.
15. J. Jennings, G. He, S. M. Howdle and P. B. Zetterlund, *Chem. Soc. Rev.*, 2016, **45**, 5055-5084.
16. G. He, T. M. Bennett, M. Alauhdin, M. W. Fay, X. Liu, S. T. Schwab, C.-G. Sun and S. M. Howdle, *Polym. Chem.*, 2018, **9**, 3808-3819.
17. M. Alauhdin, T. M. Bennett, G. He, S. P. Bassett, G. Portale, W. Bras, D. Hermida-Merino and S. M. Howdle, *Polym. Chem.*, 2019, **10**, 860-871.
18. T. D. McAllister, L. D. Farrand and S. M. Howdle, *Macromolecular Chemistry and Physics*, 2016, **217**, 2294-2301.
20. G. He, T. M. Bennett, K. Alias, L. Jiang, S. T. Schwab, M. Alauhdin and S. M. Howdle, *Polymer chemistry*, 2019, **10**, 3960-3972.
21. S. P. Bassett, N. A. Birkin, J. Jennings, E. Champman, R. K. O'Reilly, S. M. Howdle and H. Willcock, 2017.
22. P. W. BILLMEYER, *Textbook of polymer science.*, John Wiley and Sons Inc, New York and London , 1962.
23. Y. Shi, X. Cao, S. J. Luo, X. Wang, R. W. Graff, D. Hu, R. Guo and H. Gao, *Macromolecules*, 2016, **49**, 4416-4422.
24. V. Jerolimov, R. G. Jagger and P. J. Millward, *Acta Stomatol. Croat.* , 1994, **28**, 3-9.
25. B. A. Miller-Chou and J. L. Koenig, *Progress in Polymer Science*, 2003, **28**, 1223-1270.
26. J. S. Song and M. A. Winnik, *Macromolecules*, 2005, **38**, 8300-8307.
27. M. Benedetti, T. R. Congdon, S. P. Bassett, M. Alauhdin, S. M. Howdle, D. M. Haddleton, R. Pisano, M. Sangermano and T. L. Schiller, *Polym. Chem.*, 2017, **8**, 972-975.
28. R. Parilti, A. Castañon, M. Lansalot, F. D'Agosto, C. Jérôme and S. M. Howdle, *Polymer Chemistry*, 2019, **10**, 5760-5770.

29. S. J. Byard, M. Williams, B.E. McKenzie, A. Blanzs and S.P. Armes, *Macromolecules*, 2017, **50**, 1482.
30. M.Thommes, K. Kaneko, A.V. Neimark, J.P. Oliver, F. Rodriguez-Reinoso, J. Rouquerol and K. S. W. Sing, *Pure and applied chemistry*, 2015, **87**, 1051-1069.
31. Y. Wang, U. Gosele and M. Steinhart, *Nano letters*, 2008, **8**, 3548-3553.
32. N. Yan and physics, Y. Wang, *Journal of polymer science. Part B, Polymer*, 2016, **54**, 926-933.

Chapter 5

Testing for Potential Applications

This chapter details the testing of the crosslinked block copolymers made in this study, PMMA-*b*-P4VP, for possible use as enzyme supports, drug delivery agents and solid phase extraction packaging. There are three types of testing involved: immobilisation of enzymes such as lipase, adsorption and release of drugs for instance usnic acid, and a stationary phase for sample preparation. In order to meet the above-mentioned application requirements in terms of particle size and porosity, we first synthesised crosslinked microparticles of varying sizes in comparison to those previously synthesised (Chapter 4). The polymers obtained then were characterised and tested together with other synthesised polymers for potential application. The enzyme immobilisation study addressed a number of issues, including enzyme (lipase) stability, polymer support miscibility, and finally, lipase adsorption onto hydrophobic polymer support. While usnic acid (UA) is the adsorbed drug used in drug adsorption and release tests, in which the performance of both non-porous and porous samples will be highlighted. Finally, the ability of the polymer to act as a stationary phase for sample preparation- solid phase extraction (SPE) will be demonstrated by pollutant adsorption analysis.

5.1 Introduction

The results of a newly discovered method for preserving particle microstructure and internal nanostructure in a solvated environment by *in-situ* crosslinking copolymerisation by RAFT dispersion in scCO₂ have been reviewed in detail in Chapter 4. The polymer products, BCP PMMA₅₀₀-*b*-P4VP₃₃₀ microparticles with varying degrees of crosslinking ranging from 0 to 16 wt.%, produced discrete microparticles with narrow particle size distribution and average diameters ranging from 0.9 to 1.6 μm and were found to be well preserved in the particular solvation conditions. It was previously reported that adjusting the amount of surfactant, PDMS-MA, employed in the dispersion polymerisation process may effectively control the particle size. When the amount of surfactant was reduced, the particle size reportedly rose.¹ In order to demonstrate the versatility of the method developed, the amount of PDMS-MA was reduced to 2.5 wt.%, half of the amount used previously (5 wt.%), in order to synthesise a new batch of the same BCP, PMMA₅₀₀-*b*-P4VP₃₃₀ with a larger particle size at different crosslinking degree, varying from 0 - 4 wt.% DVB. Larger particle sizes may be useful in some applications, such as polymer stationary phase materials to avoid high back pressure when the solvent flows between the particles packing materials inside the chromatography column.^{2, 3} In addition, the synthesised product was treated further to make porous materials via swelling/deswelling in ethanol/ hexane to target a diverse range of applications. In order to prepare these microparticles for suitable application, a total of three tests were conducted for evaluation including enzyme immobilisation test, usnic acid adsorption and desorption and pollutant adsorption test.

Enzyme immobilisation can be defined as the confinement of enzyme molecules onto/ within a support / matrix physically and / or chemically, in such a way that it retains its full activity or most of its activity.⁴ Enzyme

immobilisation for use in biocatalysis is one of the foreseen potential applications for these porous block copolymer materials. It is often necessary to apply enzyme immobilisation in enzymatic activities in a wide range of industrial processes.⁵ In the 1960s, researchers began investigating enzyme immobilisation as a way to improve enzyme stability and reusability in industrial settings.⁶ Enzyme immobilisation within block copolymer particles and mesoporous materials have been reported and below are some examples.

The use of oleic acid-Pluronic block copolymer coated iron oxide as an enzyme immobilisation support was reported by Mahmood et al. for the hydrolysis of olive oil. The authors claimed that the lipase activities were sustained at levels of >90% of their original activities after seven recycles.⁷ In addition, polystyrene-*b*-poly(acrylic acid) demonstrated efficient catalytic turnover as nanoreactors for enzymatic reactions.⁸

Porous particles with their known excellent properties like high surface area and stability, have more advantages for this kind of application. Silicates, for example, have been tailor made by changing their surface functionalization to suit the criteria of enzyme supports. This was detailed in Magner's review.⁹ Plieva et al. have reported the use of immobilised lipase of hog pancreas in a macroporous poly(vinyl alcohol)-cryogel carrier. The resulting immobilised enzyme biocatalyst can last more than six months when stored in a fridge, in water-poor media.¹⁰

A readily available, lipase enzyme was used in this proof-of-concept trial. Triglyceride and other esterified substrates are converted by lipases. Lipases can be found in a wide variety of organisms, ranging from bacteria to humans, and they play an important role in basic metabolic processes. Some of the most notable industrial applications of lipases are in the manufacturing of cleaning agents and pharmaceuticals. In analytical chemistry, lipases are becoming increasingly popular as they can be used in biosensors and bioassays.¹¹ Standard tests of lipase activity in biochemistry are based on changes in the physio-chemical properties of the

medium which are recorded as colour changes.¹¹ A simple and rapid detection tool like UV-vis, that is readily available in most basic laboratories, would be enough to measure this colour change. Hence, the choice of lipase in this test was ideal and economical from the perspective of a proof-of-concept trial.

The next test for proof-of-concept was drug adsorption and desorption. The adsorbed drug was usnic acid (UA), a dibenzofuran natural extract known for its antimicrobial properties.¹² It is a bioactive compound mainly found as a secondary metabolite in lichens. It is a hydrophobic, weakly acidic compound (-OH position 3 pKa 4.4, (ii) -OH position 7 and 9 pKa 8.8 and 10.7) and a chiral molecule (stereogenic center is 9 b) (Figure 5.1). These properties suit the synthesised polymer in this study, PMMA-*b*-P4VP. The first polymer block, PMMA could cooperate with UA by hydrophobic interactions, while nitrogen within the aromatic pendants acts as a basic and coordinative agent for P4VP, hence offering a landscape for chemical alteration to interact with UA. The toxicity issues of UA are the only main concerns that limit the use of UA, for example in therapeutic applications.

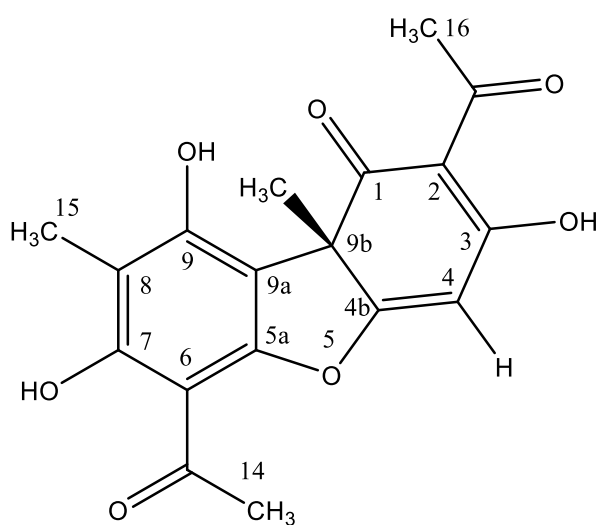


Figure 5.1 Usnic acid structure exhibits the features of weakly acidic compound.

Despite its toxicity, UA has been widely used in drug sorption and desorption applications by imparting the necessary properties and functional groups to the synthesised polymer that interacts with the antimicrobial drug. The development of an antimicrobial usnic acid-loaded core shell magnetic nanoparticle for use in the prevention and treatment of infections associated with medical devices was reported elsewhere.¹² As described by Taresco and co-authors, magnetic nanoparticles (MNPs) were coated with two different polymers with varying physicochemical properties. The MNPs contained either a hydrophobic star-branched polycarbonate (sbPCL₅₀) bearing hydroxyl groups or an intrinsically antimicrobial hydrophilic cationic polyacrylamide (pAcDED). It was reported that the hydrophilic pAcDED served as the best coating in that it enhanced the ability to load and release UA, as well as providing good antimicrobial properties.

In another publication, Grumezescu et al. have investigated the ability of UA to prevent biofilm formation by adsorption onto the surface of oleic acid coated-magnetite.¹³ The results indicated that oleic acid-surface modified Fe₃O₄/Oleic nanoparticles could be successfully used as coating agents for the formation of antibiofilm pellicles on a variety of medical devices. Subsequently, they loaded the magnetic coated polymer, poly(lactic-co-glycolic acid)-poly(vinyl alcohol) (PLGA-PVA), with UA for the same purposes, i.e., to quantify the ability of the bio-nano-active modified surface to control biofilm formation. In a series of steps, an antibiofilm, biocompatible thin coating was attained and deposited using the matrix-assisted pulsed laser evaporation (MAPLE) technique.¹⁴

Finally, the synthesised microparticles were tested for their suitability as stationary phase materials for sample preparation. The development of compact chromatographic techniques is critical in the analytical industry.

This can be attributed to properties including minimal sample volume injection and low mobile phase consumption, as well as great efficiency, high resolution, and quick analysis times. Low flow rates provide additional benefits due to the use of columns with a smaller internal diameter (I.D.), such as increased mass sensitivity, ease of coupling with mass spectrometer, lower costs, and the ability to adopt an environmentally friendly approach by reducing a lot of solvent waste and energy consumption.

In chromatography analysis, solid phase extraction (SPE) is a typical sample preparation method. For evaluating column selectivity and experimental conditions for attaining the best analyte separation, it is critical to choose the right stationary phase material. D’Orazio et al. studied capillaries packed with three types of particles (phenyl, C₁₈ porous silica and C₁₈ core-shell) as stationary phase for simultaneous determination of eighteen sulfonamides. They discovered that a capillary column (100 µm I.D.) packed in-house using a recently commercialised stationary phase, Kinetex® C18 core-shell, had the best selectivity.³

The incorporation of different materials, such as metal-organic frameworks, or other types of nanostructured materials (e.g. carbon nanohorns) has improved the selectivity and performance of organic polymer monoliths. Hypercrosslinked polymers have significantly increased the surface area of polymer monoliths, resulting in increased efficiency when applied to the separation of small molecules.¹⁵ Kibar and Tuncel demonstrated that using a hydrophobic crosslinking agent in the production of poly(1-(3-sulfopropyl)-2-vinylpyridinium hydroxide-co-glycerol dimethacrylate) poly(SVP-co-GDMA) and poly(1-(3-sulfopropyl)-2-vinylpyridinium hydroxide-co-ethylene glycerol dimethacrylate) poly(SVP-co-EDMA) microbeads increased the specific surface area nearly tenfold over the hydrophilic crosslinker. The performance of the microbeads as a

stationary phase in hydrophilic interaction liquid chromatography (HILIC) was found satisfactory.¹⁶

All the criteria described in the literature for these three applications have been found in the synthesised BCP microparticles that have been synthesised in this study. As a proof of concept, they were put through various tests that would show how suitable they would be for these applications.

5.2 Experimental

5.2.1 Synthesis of bigger crosslinked block copolymer PMMA₅₀₀-*b*-P4VP₃₃₀ particles

This set of reactions used *in-situ* crosslinking in a one-pot, two-step addition of 4VP method similar to what was previously described in Chapter 4.3.2.2. The only variation was in the amount of surfactant used. The concentration of PDMS-MA was reduced by half, from 5.0 to 2.5 wt.%. The amount of crosslinker used ranged from 0 to 4 wt.%.

5.2.2 Porosity Control by Degree of Crosslinking

The method used has previously been described in Chapter 4, Section 4.3.5

5.2.3 Lipase Immobilisation

5.2.3.1 Materials, Chemicals and Enzyme Preparation

The phosphate buffer (PO₄) was prepared at 25 mM at pH=7 for assay and 10 mM at pH=7 for lipase immobilisation. The substrate used namely p-nitrophenyl butyrate (PNB) was acquired from Sigma-Aldrich and was prepared at 4 mM in 25mM phosphate buffer (PO₄) (pH=7 at room temperature). Hog pancreas lipase was purchased from Fluka; spec. act. 23.9 U/mg prepared at 5 mg/mL in 10 mM phosphate buffer (PO₄) with addition of 0.5 wt.% surfactant (PGA and Tween-20) (pH=7 at room temperature) for immobilisation purposes. The block copolymer microparticles PMMA-*b*-P4VP synthesised in scCO₂: non-porous (PM1, LAM0

and LAM2) and porous particles (PorPM0 and PorPM1) with two different internal morphology, spherical (SPH) and lamellar (LAM) were used in the lipase immobilisation test.

5.2.3.2 Determination of Enzyme Activity

The enzyme activity was determined spectrophotometrically, using a microplate reader (EPOCH2 from BioTek®). Lipase Enzymatic assay was carried out by measuring the release of p-nitrophenol from catalysis of p-nitrophenyl butyrate (PNB) at an absorbance value of $A=348$ nm ($\epsilon = 5150$ M⁻¹ cm⁻¹). The assay was performed in the 96-wells plate in triplicate together with the control assay by measuring the change of absorbance (A) per unit of time (miliAbs/min) of each well. One unit of enzyme per milligram of enzyme (U/mg_{Enzyme}) was defined as the μ mol of p-nitrophenol released per minute per miligram of enzyme. The calculation was performed as follows:

$$A = \epsilon \times l \times C \quad \text{(Equation 5.1)}$$

$\epsilon = 5150$ M⁻¹cm⁻¹, Molar extinction coefficient for p-nitrophenol

$l = 0.733$ cm, lambda value of microplate for 250 μ L volume (from manufacturer)

A= Absorbance, Mean value recorded by the microplate reader (miliAbs/min)

$$\text{Enzyme Activity} = \frac{(\text{Mean Value}/1000) \times \text{Total Volume in L} \times 1000000}{(\epsilon \times l) \times (V_{\text{Enzyme}}) \times (C_{\text{Enzyme}})} \quad \text{(Equation 5.2)}$$

(U/mg_{Enzyme})

$L = 0.00025$, Total volume in each well on microplate i.e. 250 μ L

$V_{\text{Enzym}} = 0.01$ mL, Vol. of enzyme added into each well is 10 μ L

$C_{\text{Enzym}} = 5$ mg/mL, Concentration of enzyme prepared for immobilisation

5.2.3.3 Enzyme Stability Study

The stability study was carried out at the start of the study. The lipase enzyme solution was prepared at three different concentrations: 5 mg/mL, 2.5 mg/mL and 1 mg/mL. The enzyme activity of the freshly prepared lipase solution ($U/mg_{t=0}$) of each concentration was measured. All the enzyme solution were then stored at 4 °C over the weekend and the activity of the enzyme was measured ($U/mg_{t=0w}$). The stability of enzyme activity was measured by calculating the percentage of enzyme reduction with respect to the initial as follows:

$$\% \text{ Enzyme reduction} = \frac{(U/mg_{t=0}) - (U/mg_{t=0w})}{(U/mg_{t=0})} \times 100 \quad (\text{Equation 5.3})$$

5.2.3.4 Sample Miscibility Study

Approximately 10 mg of sample was dispersed in 1 mL of 10 mM phosphate buffer pH=7, shaken, and found to be quite hydrophobic, floating on the surface. Tween-20, which is readily available in the lab, and PGA, which was synthesised by a colleague in the group, were the two types of surfactants investigated. The same solution was then made in two vials, one with 0.5 wt. % PGA and the other with a mixture of 0.5 wt. % PGA and Tween-20. The effect of these two surfactants on lipase activity was then investigated. In a 10mM phosphate buffer with 0.5 wt.% PGA at pH = 7, and in a 10 mM phosphate buffer with a mixture of 0.5 wt.% PGA and Tween-20, a lipase solution of 5 mg/mL was made in two methods. Lipase activity was assessed at $t=0$ and upon completion of reaction, $t=2$ as a control.

5.2.3.5 Immobilisation of the enzyme

The enzyme immobilisation was carried out by adding copolymer samples (ca. 1 mg) to a lipase enzyme solution (5 mg/mL in 10 mM phosphate buffer with addition of 0.5 wt.% surfactant (PGA and Tween-20) at pH=7). In addition to the immobilisation preparations, the same lipase enzyme solution prepared without any copolymer sample was used as a control (U/mg_{Control}). The procedure was performed on ice (Figure 5.2) under mild agitation for 2 hours. The initial enzyme activity at $t=0$ (before with the addition of the polymer) was measured ($U/mg_{t=0}$). After 2 hours, the sample was filtered and recovered to determine the remaining enzyme activity in the liquid phase ($U/mg_{t=2\text{hrs}}$).

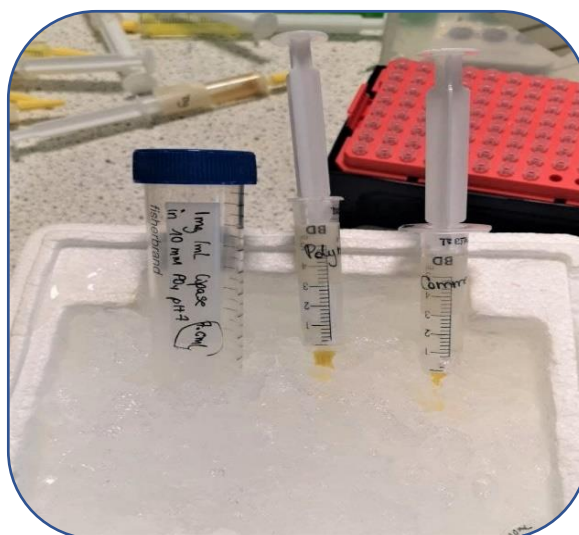


Figure 5.2. Lipase immobilisation.

The calculation of immobilisation yield (the percentage of immobilised activity with respect to the initial) was calculated as follows:

$$\% \text{ Remaining activity} = \frac{(U/mg_{t=0}) - (U/mg_{t=2\text{hrs}})}{(U/mg_{t=0})} \times 100 \quad (\text{Equation 5.4})$$

$$\% \text{ Immobilisation yield} = 100 - \% \text{ Remaining activity} \quad (\text{Equation 5.5})$$

5.2.4 Usnic Acid adsorption

Either the porous or the non-porous particles (ca. 2 mg) were put in contact with a UA solution in methanol at different concentrations (0.5, 1 and 2 mg/mL). The UA/particle weight ratio was set at 1/1 and kept constant. The UA amount put in contact with the particles was referred as $mg_{initial}$. After 24 hr under magnetic stirring at room temperature, the suspension was centrifugated at 3500 rpm for 15 minutes. The supernatant was collected and submitted to UV-vis analysis, to determine the amount of UA that remained in solution after contact with particles (mg_{post}). To do so, an Abs vs. UA concentration calibration curve at 290 nm was previously obtained. Subsequently, 1 mL of methanol was added to the particles and they were centrifugated again for 15 minutes. The supernatant was collected and analyzed by UV-vis spectroscopy to determine the drug amount weakly adsorbed drug and thus released in methanol (mg_{wash}). Following this, the particles were collected, lyophilized and stored at 4 °C.

The amount of adsorbed drug per mg of particles was obtained from the following equation:

$$\text{Adsorbed UA (mg/mg)} = \frac{mg_{initial} - mg_{post} - mg_{wash}}{mg_{particles}} \quad (\text{Equation 5.6})$$

The adsorption yield (%), was defined as the amount of UA adsorbed with respect to the initial drug amount:

$$\text{Adsorption Yield (\%)} = \frac{mg_{initial} - mg_{post} - mg_{wash}}{Mg_{initial}} \quad (\text{Equation 5.7})$$

5.2.5 Polymer Stationary Phase for Sample Preparation

5.2.5.1 Chemicals and Reagents

All chemicals used were of analytical reagent grade. Methanol (MeOH) and formic acid (99.0%, w/v) were purchased from Carlo Erba (Rodano, Milan, Italy) while acetonitrile of HPLC grade (ACN) and ultrapure water for HPLC were from VWR (International PBI S.R.l. Milan, Italy). Different analytical standard were used as target compounds including: sulfabenzamide (1) (antimicrobial agent), oxazepam (2) (benzodiazepine), Coumachlor (3) (anticoagulant), flavanone (4) (natural compound) were obtained from Sigma-Aldrich; Mecoprop (6), Diclofop (7) (herbicides in the free acidic form) were purchased from Dr. Ehrenstorfer GmbH (Augsburg, Germany); the nonsteroidal anti-inflammatory drugs (NSAIDs) cicloprofen (5) were kindly provided by Dr. Cecilia Bartolucci (Institute of Crystallography, CNR, Monterotondo, Roma, Italy).

A stock standard solutions of each (1 mg/mL) was prepared by dissolving the appropriate weight of each analyte in MeOH. These were stored at $-18\text{ }^{\circ}\text{C}$. The working solutions were prepared by diluting the stock solution to 100 $\mu\text{g/mL}$ with MeOH and then to the desired concentration $\text{H}_2\text{O/MeOH}$ (65:35, v/v). All solutions were stored at $4\text{ }^{\circ}\text{C}$ and kept away from direct light.

5.2.5.2 Instrumentation

Model FS 100b Decon (Hove, UK) was used as ultrasonic bath to sonicate the mobile phase, to dissolve analytes, to generate a homogeneous packing bed and stable stationary phase-slurry during the packing procedure. A Stereozoom 4 optical microscope (Cambridge Instruments, Vienna, Austria) with illuminator was used to inspect the status of the capillary columns and checking the fused silica capillary during the packing

procedure. An HPLC pump (Perkin Elmer Series 10, Palo Alto, CA, USA) was used for packing capillary column.

An outside polyimide-coated fused silica capillary (Polymicro TechnologiesTM, Silsden, UK), with 375 μm O.D. and 100 μm I.D. was used for preparation capillary columns. The stationary phase was XBridge C₁₈ (3.5 μm , 130 Å, carbon load 18%) was obtained unpacking a prep-guard cartridge from Water (Milford, USA) (gently provided by Prof. M.Á. Rodríguez Delgado, Unidad Departamental de Química Analítica, Facultad de Ciencias, Universidad de La Laguna (ULL), San Cristóbal de La Laguna, Spain). The columns were prepared in our laboratory following a slurry packing method and packed for 25 cm.² The detection window (on column detection) was obtained by carefully removing at 1.5 cm from the outlet frit a width of 5 mm of polyimide layer.

The nano-LC analyses were performed by using a UltimateTM Capillary HPLC unit from LC Packing Dionex (Amsterdam, The Netherlands). The instrument was equipped with a low dispersion six-port valve, with an external 15 μL loop (VICI VALCO Instruments, Houston, TX, USA) for injections and a UV detector. The lab-made flow cell detection was made in our laboratory. An aluminium block, of the same dimensions of the standard flow cell, was machined in order to accommodate the capillary column for on-column detection. The following parameters were set: wavelength at 200 nm, the constant time and data acquisition rate were 1.0 s and 10 Hz, respectively. In order to reduce dead volumes, minimizing band broadening effect, the capillary columns were directly connected to the injection valve.

The injection volume was 110 nL and the samples eluted in isocratic mode with a mobile phase consisting 0.1% (v/v) HFO in 60/40 ACN/H₂O (v/v) at 210 nL/min. The pump and detector were controlled by ChromeleonTM Chromatography Management System Software (version 6.6, LC Packings).

5.2.5.3 Dispersive solid-phase extraction procedure

The studied polymer phases were used in the d-SPE (dispersive solid phase microextraction) procedure to extract the target compounds from Milli-Q water sample.

The sorbent material was previously treated with a non-aggressive washing step in order to remove any contaminant trace of polymeric organic synthesis. In a 2 mL polypropylene vial, 10 mg of the sorbent material was weighed and was dispersed in 500 μ L of MeOH. After 2 min of strong vortex shaking, the suspension was centrifuged at 12,000 rpm for 5 min (Eppendorf MiniSpin Plus 5453 Centrifuge, Eppendorf AG, Hamburg, Germany). After removing the MeOH layer, the washing step was repeated twice (Figure 5.3).

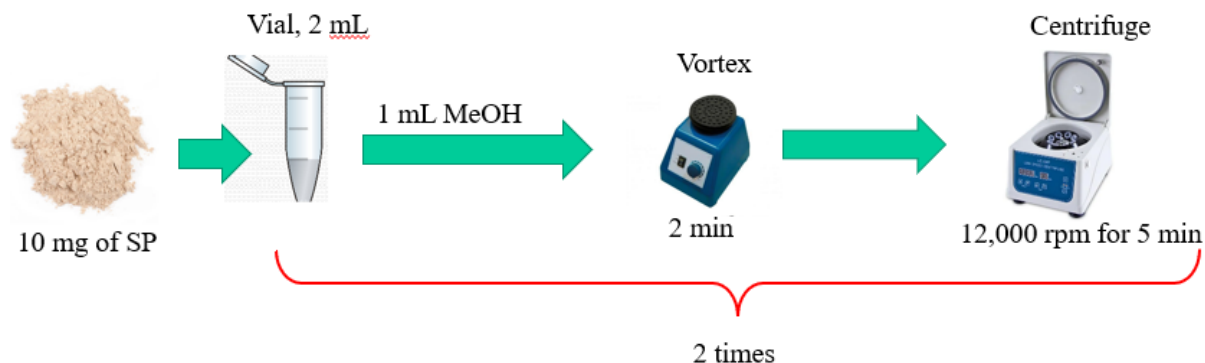


Figure 5.3. Washing step to remove any contaminant trace of polymeric organic synthesis

One mL of spiked or non-spiked Milli-Q was put together in the same vial containing polymer material. After two minutes of strong vortex shaking (2 min), the dispersion was centrifuged (12,000 rpm for 5 min). The polymer phase was washed with 500 μ L of Milli-Q water following the washing procedure previously outlined. Target analytes were extracted in

500 μL MeOH. After vortex shaking (2min) and centrifugation (12,000 rpm for 5 min), 100 μL of the methanolic extract was diluted 200 μL in Milli-Q water and injected into the nano-LC system (Figure 5.4)

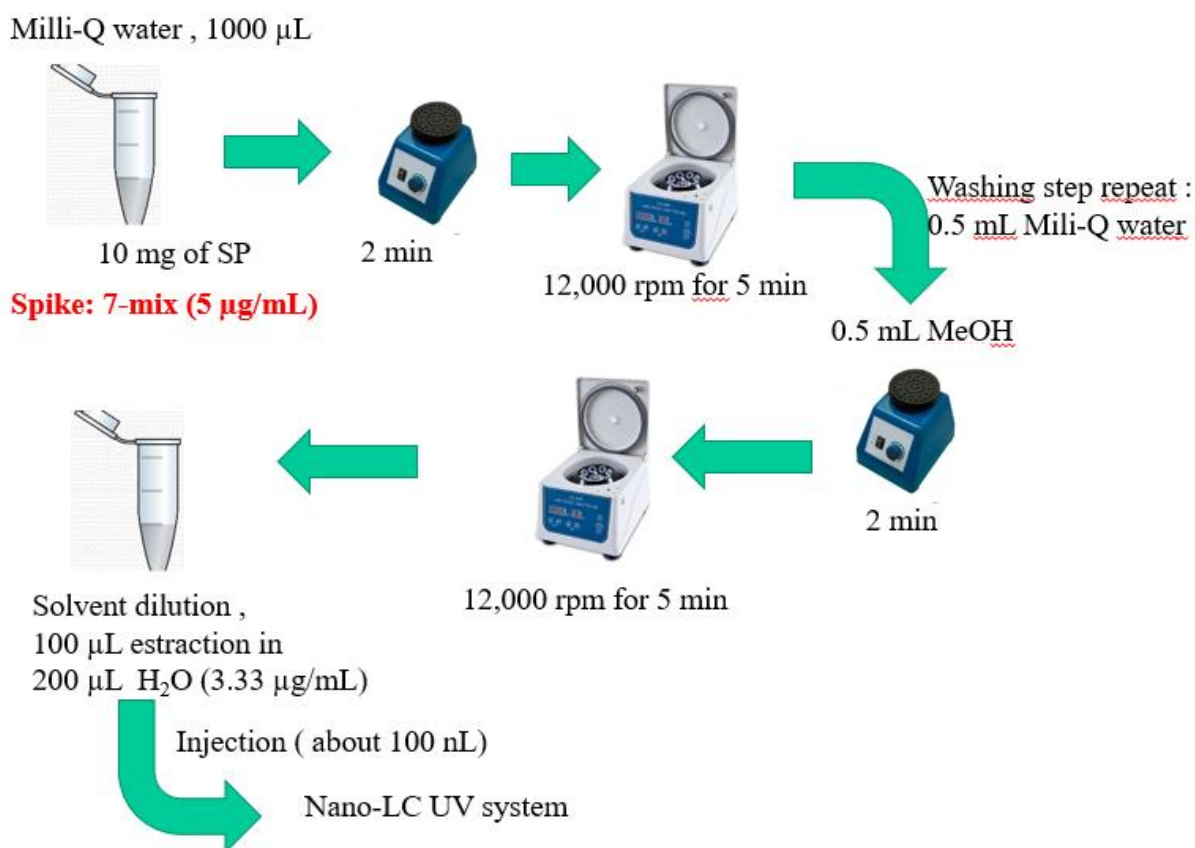


Figure 5.4 Extraction procedure before injection into the nano-LC system.

5.3 Results & Discussion

5.3.1 Synthesis of bigger PMMA-*b*-P4VP particles by two-step addition method – SPH

The BCP microparticles synthesised with 2.5 wt.% PDMS-MA (Table 5.1, entry 2-6) were fully characterised and compared with the microparticles synthesised with 5 wt.% PDMS-MA detailed in Chapter 4. The NMR characterization on sample with 0 wt.% DVB (2.5PMMA₅₀₀-P4VP₃₃₀, Table 5.1, entry 2) confirmed the monomer's polymerisation, and the molar block ratio obtained was 61/39. This was comparable to the 0 wt.% DVB sample synthesised with 5% PDMS-MA (5PMMA₅₀₀-P4VP₃₃₀, Table 5.1, entry 1) in Chapter 4. In addition, this value was within the target range (PMMA/P4VP=60/40). The number average molecular weight, M_n , of the non-crosslinked particles obtained from both PDMS-MA concentrations was comparable to one another and to the target value, $M_{nTargeted} = 83,000$ g/mol (Figure 5.5).

In the case of glass transition temperature, T_g , they were fairly close and in agreement with one another. The first block, PMMA, had a T_g of 126 -127 °C, while the second block, P4VP, had a T_g of 152 – 153 °C. These two distinct transitions are an indicator of microphase separation (Figure 5.6). In general, there was not much difference in the T_g s recorded for all samples containing 0.5 – 4.0 wt.% DVB (Table 5.1, entry 3-6) in comparison to the sample that contained 0 wt.% (Table 5.1, entry 2).

Table 5.1. BCP, PMMA₅₀₀-*b*-P4VP₃₃₀ synthesised at 2.5 wt.% and 5.0 wt.% of PDMS-MA with different concentrations of crosslinker by *in situ* crosslinking via RAFT dispersion polymerisation in scCO₂.

Entry	Block Copolymers ^a PMMA ₅₀₀ -V ₁₇₀ -V ₁₆₀ /D ^b	PDMS-MA (wt.%)	Crosslinker DVB (wt.%)	T_g PMMA/P4VP (°C)^c	SEM d_m^d (µm)	TEM Morphology^e	d_{P4VP}^f(nm)
1	5PMMA ₅₀₀ -P4VP ₃₃₀	5.0	0.0	127/153	1.6±0.35	SPH	47 ^g ±6 26 ^h ±4
2	2.5PMMA ₅₀₀ -P4VP ₃₃₀	2.5	0.0	126/152	2.4±0.31	SPH	69±5 46±3
3	2.5PMMA ₅₀₀ -V ₁₇₀ -V ₁₆₀ /0.5	2.5	0.5	125/155	2.3±0.40	SPH	62±7 43±4
4	2.5PMMA ₅₀₀ -V ₁₇₀ -V ₁₆₀ /1	2.5	1.0	125/154	1.9±0.31	SPH	60±7 40±4
5	2.5PMMA ₅₀₀ -V ₁₇₀ -V ₁₆₀ /2	2.5	2.0	125/152	1.8±0.32	SPH	55±7 38±3
6	2.5PMMA ₅₀₀ -V ₁₇₀ -V ₁₆₀ /4	2.5	4.0	125/153	1.7±0.29	SPH	46±6 32±4

The reactions were conducted at 65°C and 270 bars, the reactants consist of MMA (7.5 g), DDMAT (55 mg), AIBN (12.5 mg) and PDMS-MA (5 or 2.5 wt.% w.r.t. MMA and 4VP) for the 1st block, PMMA; 4VP (5g), AIBN (6.25 mg) and DVB (0.5-4.0 wt.% w.r.t. 4VP) for the chain extension and crosslinking of 2nd block (P4VP/DVB), the addition of 4VP was made in 2 stages whilst DVB was added during the last stage.

The reaction time for PMMA is 18-24 h and 16-24 h for P4VP/DVB; ^a- The numbers at the beginning of PMMA denote the weight percentage of PDMS-MA relative to total MMA and 4VP, ^b- D denote the weight percentage of DVB relative to total 4VP, ^c- determined by DSC, ^d- the average of particle diameter, measured by ImageJ, ^e-phase separation morphology. ^f- the average domain size of P4VP, measured by imageJ; ^g- in the periphery layer and ^h- in the core area.

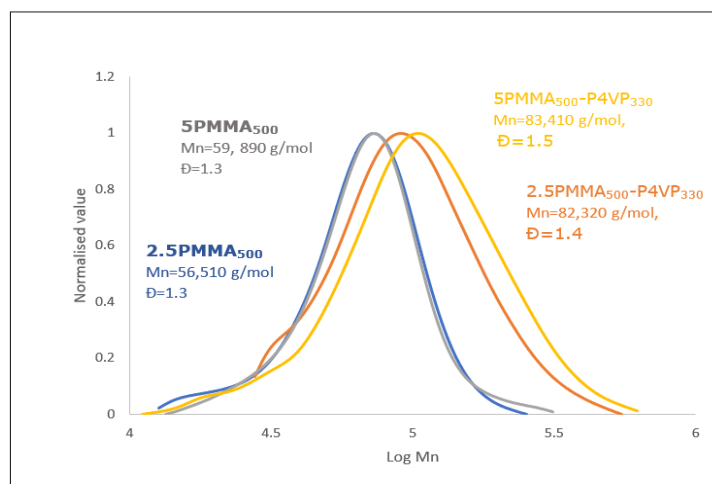


Figure 5.5. Molecular weight distribution of non-crosslinked particles 5PMMA₅₀₀-P4VP₃₃₀ and 2.5PMMA₅₀₀-P4VP₃₃₀ (Table 5.1, entry 1 and 2) synthesised at 5.0 and 2.5wt.% of PDMS-MA showing the M_n obtained of both samples are approximately the same, regardless of different amount of PDMS-MA used.

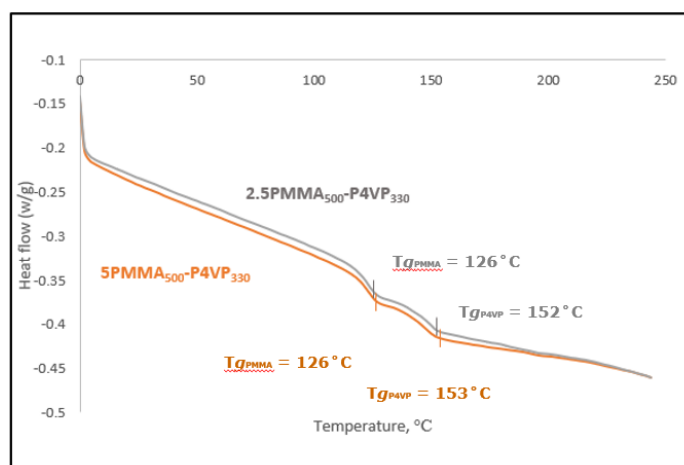


Figure 5.6. DSC traces showing the T_g of non-crosslinked block copolymer (Table 5.1, entry 1 and 2) synthesised with 5.0 (orange) and 2.5 wt.% PDMS-MA (grey) showing a comparable trend.

When these two-block phases separated, the SPH morphology was obtained as an internal nanostructure, as shown in the TEM images, shown in the inserts in Figure 5.7 (a and b). In addition, the SEM images revealed that the fine powders obtained were discrete, with an increase in particle size due to the effect of reducing the PDMS-MA to 2.5 wt.% (Table 5.1, entry 1 and 2 and Figure 5.7a and b).

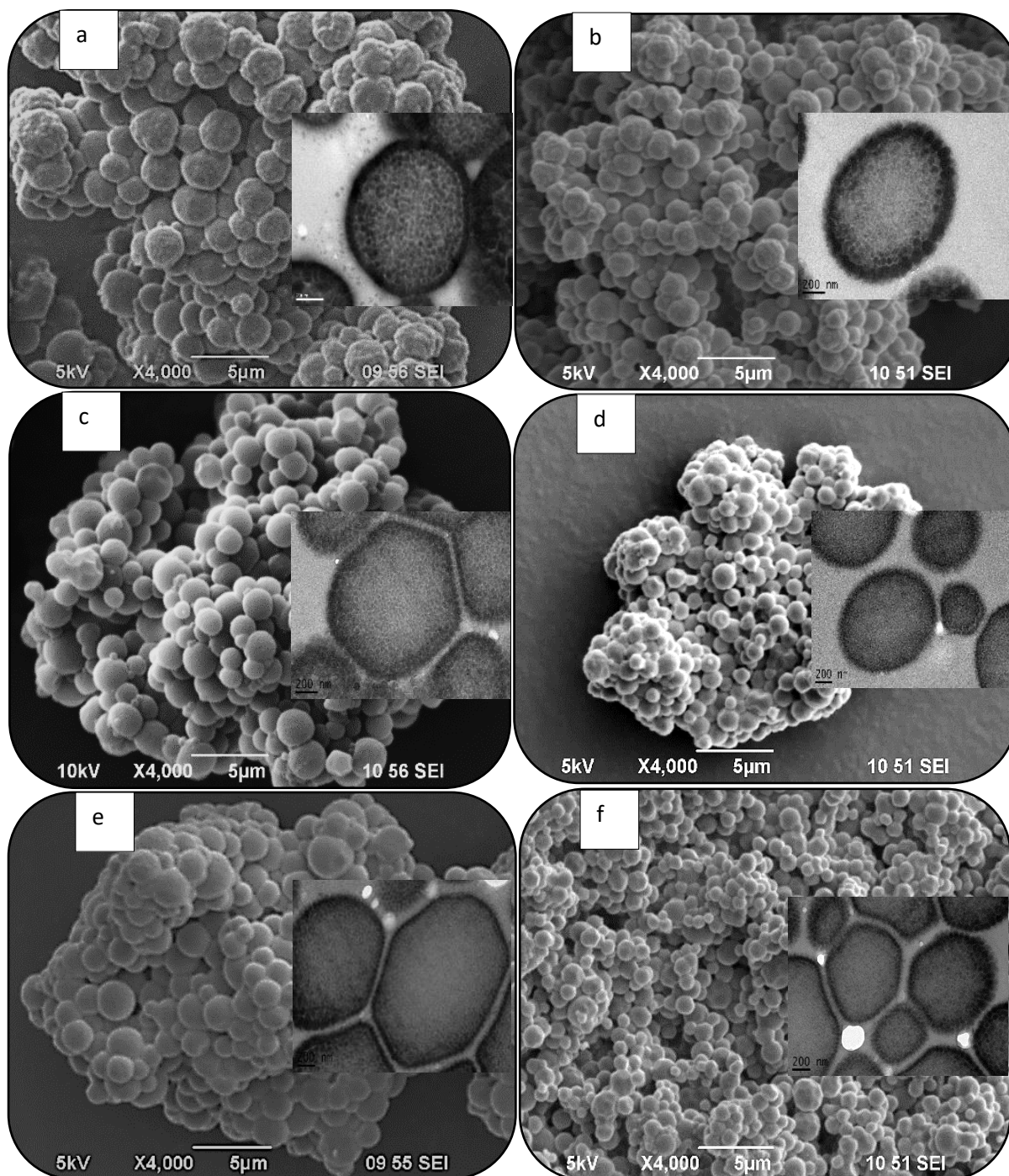


Figure 5.7. SEM images showing the difference in particle sizes obtained by varying the amount of surfactant; 2.5 (a, c & e) and 5 (b, d & f) wt.% PDMS-MA. The particles were also crosslinked at 0 (a & b), 2 (c & d) and 4 wt.% (e & f). The inserts show the TEM images of phase separation morphology of the microparticles remain the same (SPH) even though the domain size increased. (Table 5.1, entry 1, 2, 5 and 6 and Figure 5.8)

In the case of crosslinked BCP containing DVB at 0.5-4.0 wt.%, as anticipated, the particle size increased as the amount of PDMS-MA was reduced to 2.5 wt.% (Figures 5.7 and 5.8). As a result, the diameter of the new batch of crosslinked microparticles has been successfully increased to about 1.7-2.4 μm (Table 5.1, entry 2-6 and Figure 5.8) in comparison to the 5 wt.% with particle size ranged from 0.99 – 1.6 μm (Figure 5.8). The TEM images confirmed the phase separated morphology remained the same (SPH) even though the domain size increased (Figure 5.7 and Table 5.1).

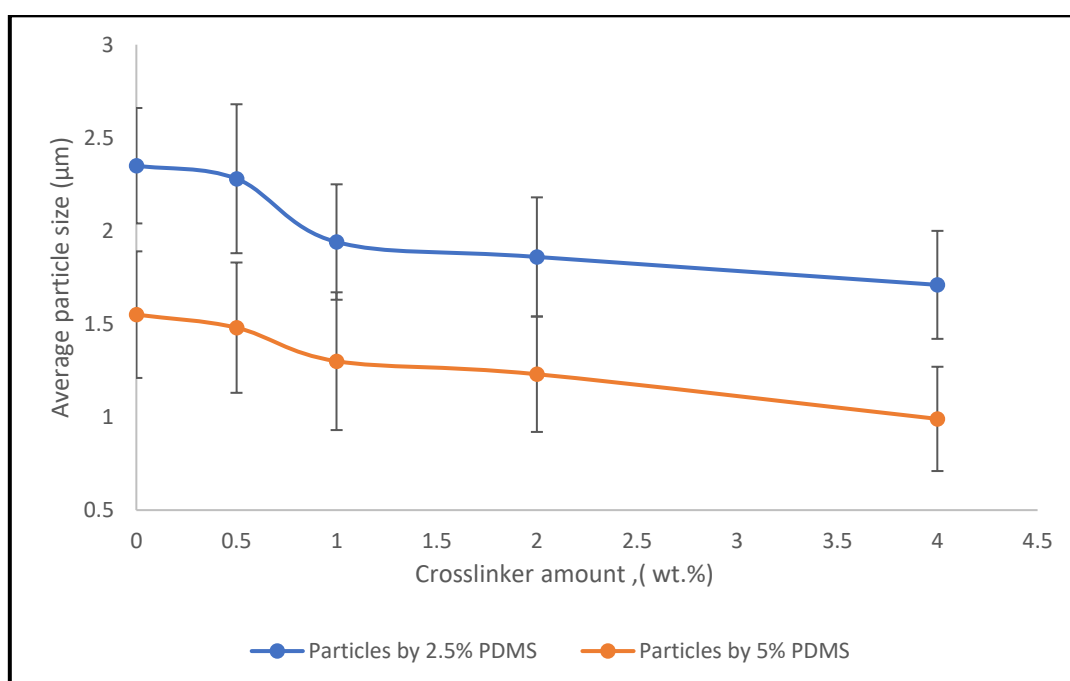


Figure 5.8. The particle size difference between block copolymer synthesised with 2.5 and 5.0 wt.% PDMS-MA at different crosslinking degree. (Table 5.1 and Figure 5.7)

5.3.1.1 Solubility Test

The solubility performance of particles in solvents is an important parameter for stationary phase or column packing material applications. The suitability of column packing materials with the polarity of mobile phase or eluent use must be compatible to suit the targeted compound. This test was also carried out to evaluate the performance of the crosslinking system developed in solvated conditions. Hence, a few types of solvent, which are a good solvent for either one of the blocks or both, including water, were chosen for testing.

From the observation, the particles containing 0 wt.% DVB (Table 5.2, entry 1) were solubilised in chloroform (CHCl_3), forming a clear solution. In contrast the particles swelled in acetonitrile (ACN), acetone and tetrahydrofuran (THF), forming a cloudy solution with some particles settling at the bottom of the vial. The particles were insoluble in methanol (MeOH) and hydrophobic (insoluble) in deionised water (D.I. H_2O) (Figure 5.9).

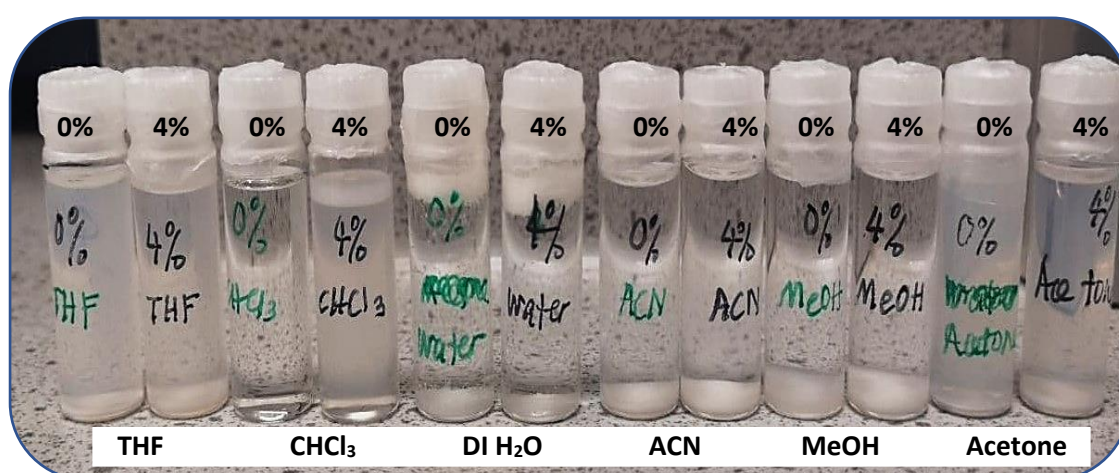


Figure 5.9. Photographic image of solubility behaviour of particles synthesised with 2.5 wt.% PDMS-MA, which contained 0 or 4 wt.% DVB in various solvents (Table 5.1, entry 2 and 6).

On the other hand, the particles containing 4 wt.% DVB (Table 5.2, entry 2) formed clear solutions, with particles settled at the bottom, in all solvents tested except in chloroform. This indicated that the crosslinking at 4 wt. % has reduced the solubility of particles in the solvents tested. The particles formed both a cloudy solution and a gel layer in chloroform, showing that they swelled in this solvent (Figure 5.9). The same result was observed even with samples at a lower degree of crosslinking (0.5 and 1 wt.% of DVB) (Figure 5.10 and Table 5.1, entry 3 and 4). Interestingly, in comparison to the particles synthesised with 5 wt.% PDMS-MA, both the 0.5 and 1 wt.% DVB samples formed clearer solutions, without the formation of any gel layer, indicating that the smaller particles are more soluble in chloroform even when they contained the same amount of DVB (Figure 5.10a) due to the higher surface area. These results corroborated the findings observed after the chloroform evaporated; the dried soluble part formed a thin layer at the bottom of the vials, whilst the gel layer, formed in the 2.5 wt. % PDMS-MA, samples were stuck to the vial's wall (Figure 5.10b).

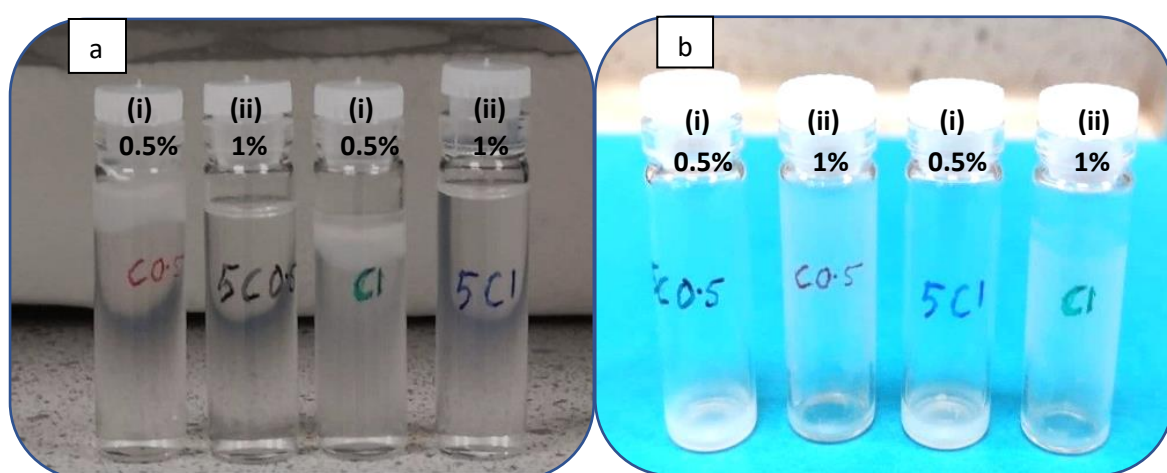


Figure 5.10. Photographic images of solubility behaviour of particles synthesised with 2.5 and 5 wt.% PDMS-MA, which contained either 0.5 or 1 wt.% DVB in chloroform. a) Particles at (i) 2.5 wt.% PDMS-MA formed a cloudy solution and a gel layer, whilst at (ii) 5 wt.% PDMS-MA a clearer solution was formed. b) The non-soluble gel layer stuck around the vial's wall at (i) 2.5 wt.% PDMS-MA but at (ii) 5 wt.% PDMS-MA the dried soluble fraction formed at the bottom after chloroform evaporated.

Table 5.2. Solubility behaviour of particles containing 0 and 4 wt.%

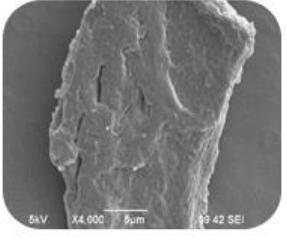
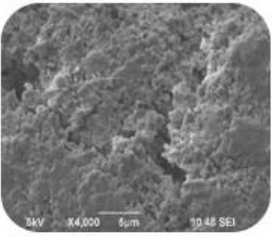
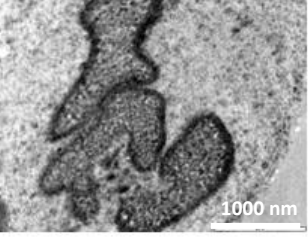
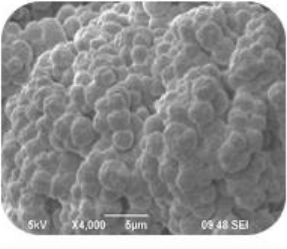
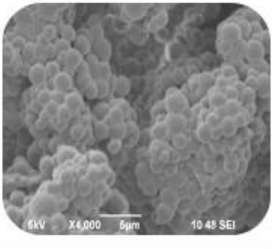
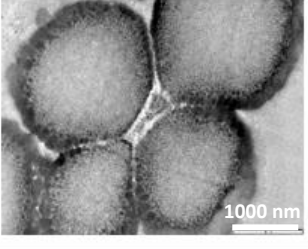
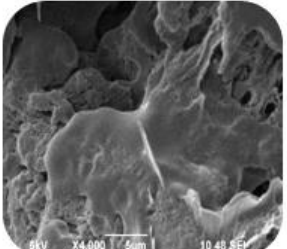
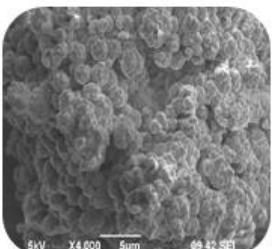
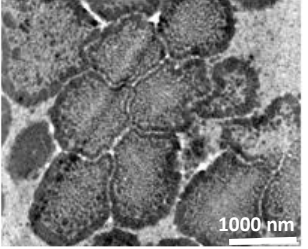
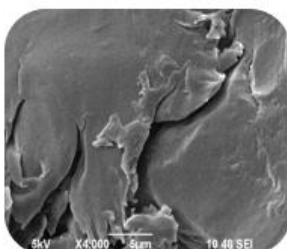
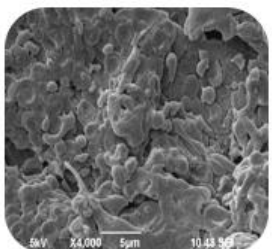
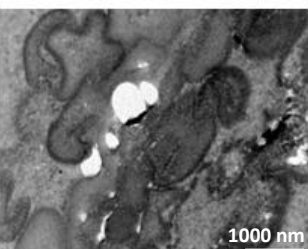
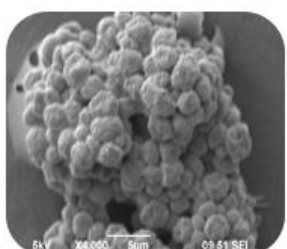
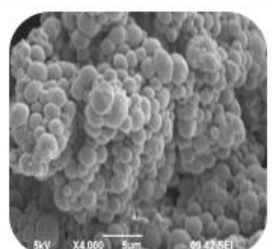
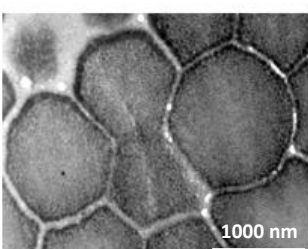
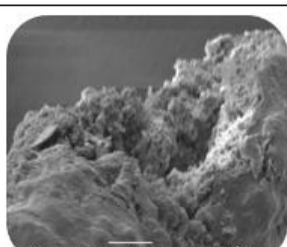
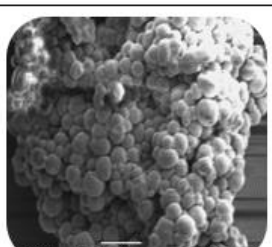
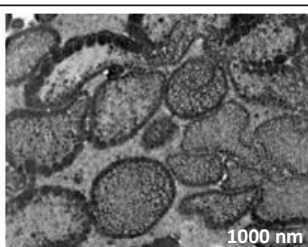
Entry	Samples	DVB (wt. %)	Physical Observation					
			CHCl ₃	H ₂ O	ACN	Acetone	MeOH	THF
1	2.5PMMA ₅₀₀ - P4VP ₃₃₀	0	Soluble	H ^a	Swell	Swell	I-S ^b	Swell
2	2.5PMMA ₅₀₀ -V ₁₇₀ - V ₁₆₀ /4	4	Swell	H ^a	I-S ^b	Swell	I-S ^b	I-S ^b

^aHydrophobic, ^bInsoluble

From SEM analysis, the microstructure of the particles containing 4 wt.% DVB was preserved after being exposed to all solvents tested except chloroform and acetone where the particles collapsed (Table 5.3). TEM analysis revealed that the internal structure was preserved in all solvents tested (Table 5.3). Both the SEM and TEM results suggested that the particle scaffolds collapse at 4 wt.% DVB in chloroform and acetone, but the polymers were mainly insoluble due to crosslinking formation in the P4VP domains. In comparison, the crosslinking enhanced the resistance of particles towards ACN and THF in comparison to the 0 wt.% DVB sample.

The solubility of the PMMA or P4VP block in these solvents is an important parameter to be considered. Chloroform is a good solvent for both blocks, whereas ACN, acetone, and THF are good solvents for the PMMA block. In addition, MeOH is only good for P4VP, and water is not good for either block. However, in all cases the TEM revealed the preservation of internal structure after solvent exposure. These results corroborated that the crosslinking process has worked well in crosslinking the P4VP domain.

Table 5.3. SEM and TEM images showing the solubility behaviour of non-crosslink (0 wt.% DVB) and cross-linked (4 wt.% DVB) samples.

Solvent	0 wt. %	4 wt. %	TEM of 4 wt. %
CHCl₃			
D.I. Water			
AC			
Acetone			
MeOH			
THF			

5.3.1.2 Porosity Control by Crosslinking

The effect of crosslinking on the porosity generated during solvent swelling of the BCP microparticles with different crosslinking degrees (0 - 4 wt.%) was performed by the swelling and deswelling method in ethanol and hexane as discussed previously in Chapter 4.

After being subjected to the swelling/deswelling process (2.5PMMA₅₀₀-P4VP₃₃₀), the SEM images showed the sample that contained 0 wt.% DVB formed interconnected porous channels that disrupted the phase separated morphology (Figure 5.11a). Particle fusion was also observed. The sample containing a higher crosslinker concentration, 4 wt.% DVB (2.5PMMA₅₀₀-V₁₇₀-V₁₆₀/4) (Figure 5.11c) created smaller pores in comparison to the 2 wt.% of crosslinker sample (2.5PMMA₅₀₀-V₁₇₀-V₁₆₀/2) (Figure 5.11b). These results show that crosslinking has taken place to control the swelling of P4VP domain, a source of swollen matrix in ethanol creating distinct porous structures and avoiding any particle fusion.¹⁷ These results agree with the outcome observed for the smaller particles size (with 5 wt.% PDMS-MA) as discussed in chapter 4.¹⁸

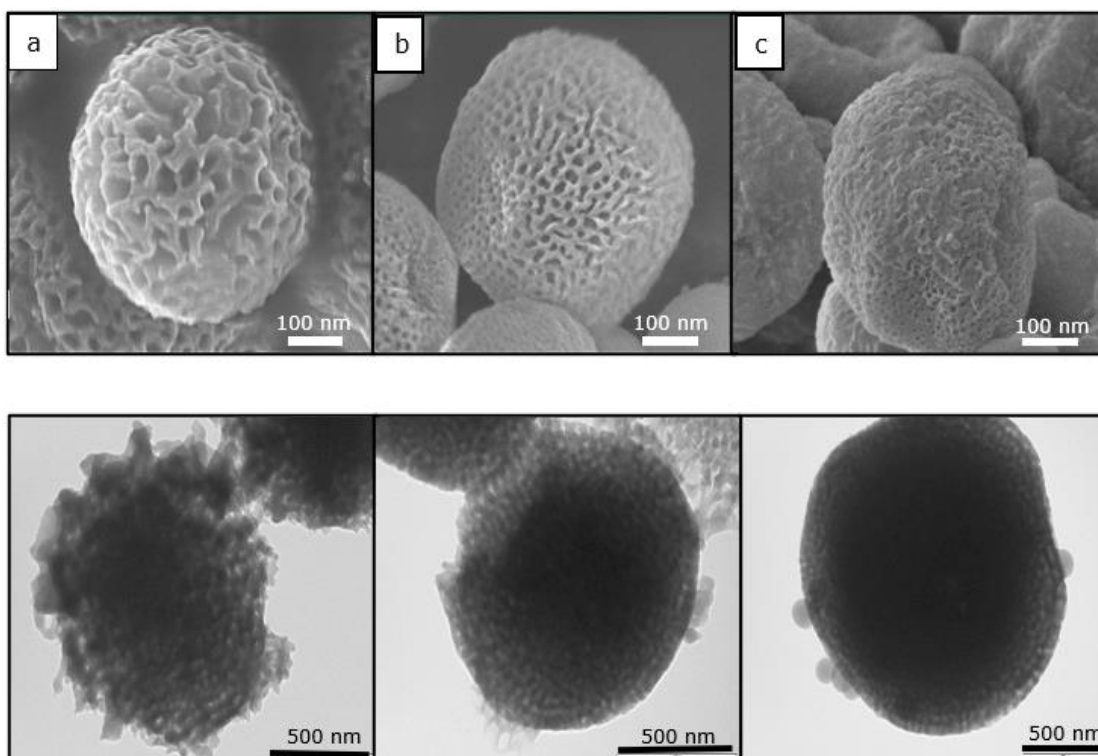


Figure 5.11. SEM (top row) and TEM (bottom row) images of (a) 2.5PMMA₅₀₀-P4VP₃₃₀, (b) 2.5PMMA₅₀₀-V₁₇₀-V₁₆₀/2 and (c) 2.5PMMA₅₀₀-V₁₇₀-V₁₆₀/4 porous particles (Table 5.1, entry 2, 5 and 6).

The TEM images (Figure 5.11, bottom row) also show that the internal morphology changes when the crosslinking concentration increased. The TEM images in Figure 5.12 show the controlled swelling of the entire samples (0- 4 wt.%) for the bigger particles (synthesised with 2.5 wt.% PDMS-MA). Extensive swelling can be clearly seen in the non-crosslinked samples (0 wt.% DVB) (Figure 5.12a). Whereas, the crosslinked samples have swollen slowly, keeping the pores intact, with decreases in pore size that eventually are seen to be nearly closed when the amount of crosslinker increased (Figure 5.12b-12e). These results demonstrated a comparable outcome to the smaller particles samples (containing 5 wt.% PDMS-MA) that were reported in chapter 4. Both sets of results are also in agreement with finding reported by Byard et al.^{18, 19}

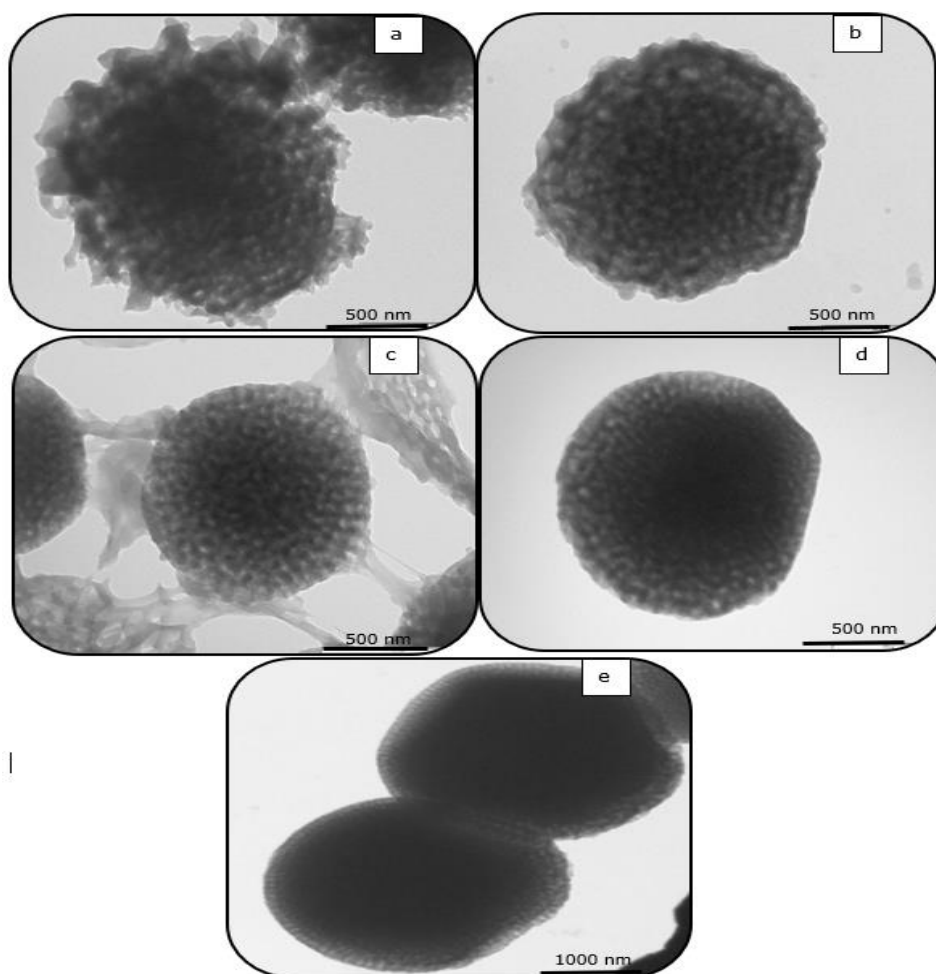


Figure 5.12. TEM images of (a) 2.5PMMA₅₀₀-P4VP₃₃₀ , (b) 2.5PMMA₅₀₀-V₁₇₀-V₁₆₀/0.5, (c) 2.5PMMA₅₀₀-V₁₇₀-V₁₆₀/1 (d) 2.5PMMA₅₀₀-V₁₇₀-V₁₆₀/2 and (e) 2.5PMMA₅₀₀-V₁₇₀-V₁₆₀/4 porous particles (Table 5.1, entry 2- 6).

5.3.1.2.1 Tilt- TEM Tomography

The porosity development throughout the particles was investigated by the tomographic reconstruction in the Z-axis, which is parallel with the original zero tilt image. In Figure 5.13, all slices revealed the porous structure in the non-crosslinked microparticle, 2.5PMMA₅₀₀-P4VP₃₃₀ (0 wt.% DVB). The crosslinked particle, 2.5PMMA₅₀₀-V₁₇₀-V₁₆₀/4 (4 wt.% DVB) is presented in Figure 5.14. The non-crosslinked microparticle, formed large open pores that interconnected with various sizes between the surface (Figure 5.13, images 427 and 442) and the middle of the microparticle (Figure 5.13, images 469 and 481).

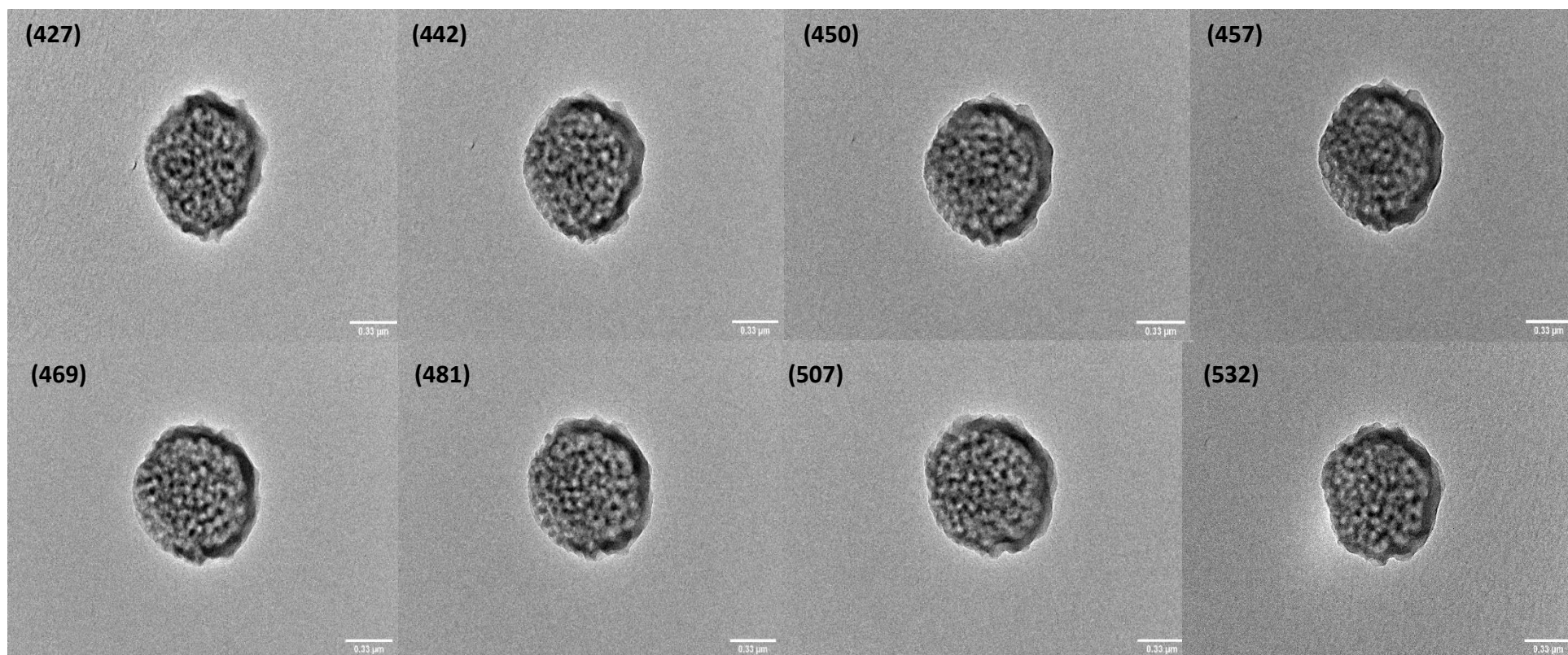


Figure 5.13 Selection of slices from the SIRT tomographic reconstruction of a non-crosslink porous microparticle, 0 wt.% DVB (2.5PMMA₅₀₀-P4VP₃₃₀, Table 5.1, entry 2) showing 8 of 111 (427, 442, 450, 457, 469, 481, 507 & 532) from the top surface to the bottom. The tilt series was taken at a 2550 electrons per nm² per s dose rate with 18 min and 41 s acquisition time.

In contrast, images produced from the crosslinked microparticles at the highest concentration of DVB (4 wt.%) did not show any porosity formation (Figure 5.14). It is believed that this lack of porosity in the imaging is actually due to the instrument limitation. The limit for tomography is the volume of polymer the beam can pass through; a 300 nm wide particle that is 50% porous will work well, as the beam only needs to travel through approximately 150 nm of material at most. If the same 300 nm particle is only 10% porous, then the beam needs to travel through over 250 nm of material, which may lead to a significant loss of information for the centre of the particle. The effect of crosslinking at a high degree (4 wt.%) to control the porosity formation during solvent swelling should also be considered. These two factors were found to confirm that the majority of the porosity formed on the surface of particles rather than at the centre part of the particles, as revealed by the typical 2D TEM results as presented in Figure 5.12e (2.5PMMA₅₀₀-V₁₇₀-V₁₆₀/4). To support this finding, results recorded of the microparticles synthesised using 5 wt.% PDMS-MA in chapter 4 can also be referred to. The sample containing 4 wt.% DVB (5PMMA₅₀₀-P4VP₁₇₀-P4VP₁₆₀/D4) also showed the same porosity distribution, as shown in Figure 5.15.

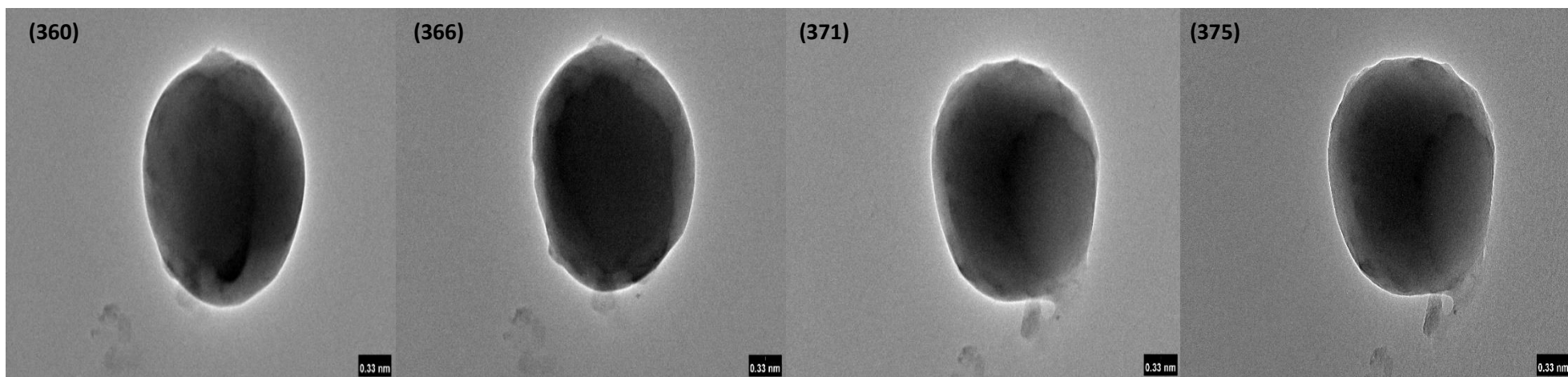


Figure 5.14. Selection of slices from the SIRT tomographic reconstruction of a crosslinked porous microparticle at 4 wt.% (2.5PMMA₅₀₀-V₁₇₀-V₁₆₀/4, Table 5.1, entry 6) showing 4 of 21 (360, 366, 371 & 375) from the top surface to the bottom. The tilt series was taken at a 2550 electrons per nm² per s dose rate with 18 min and 41 s acquisition time.

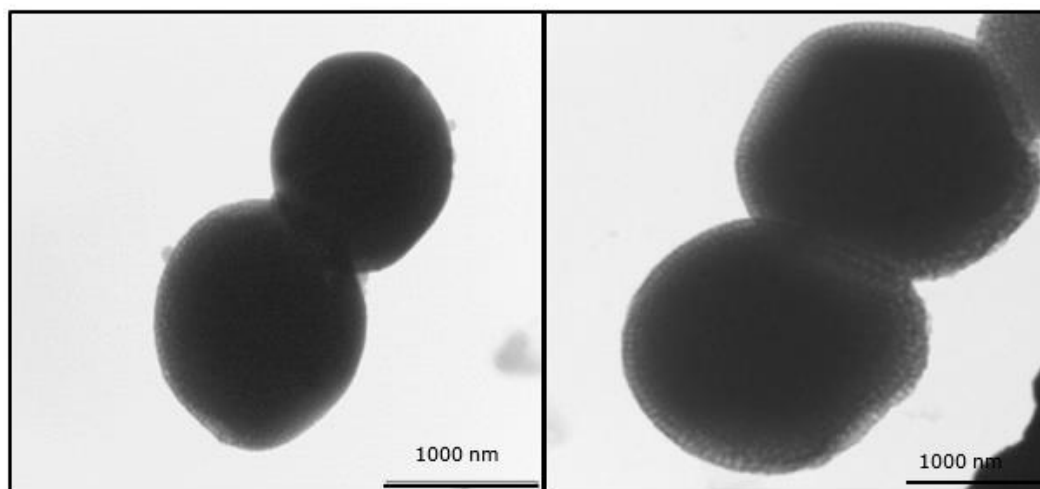
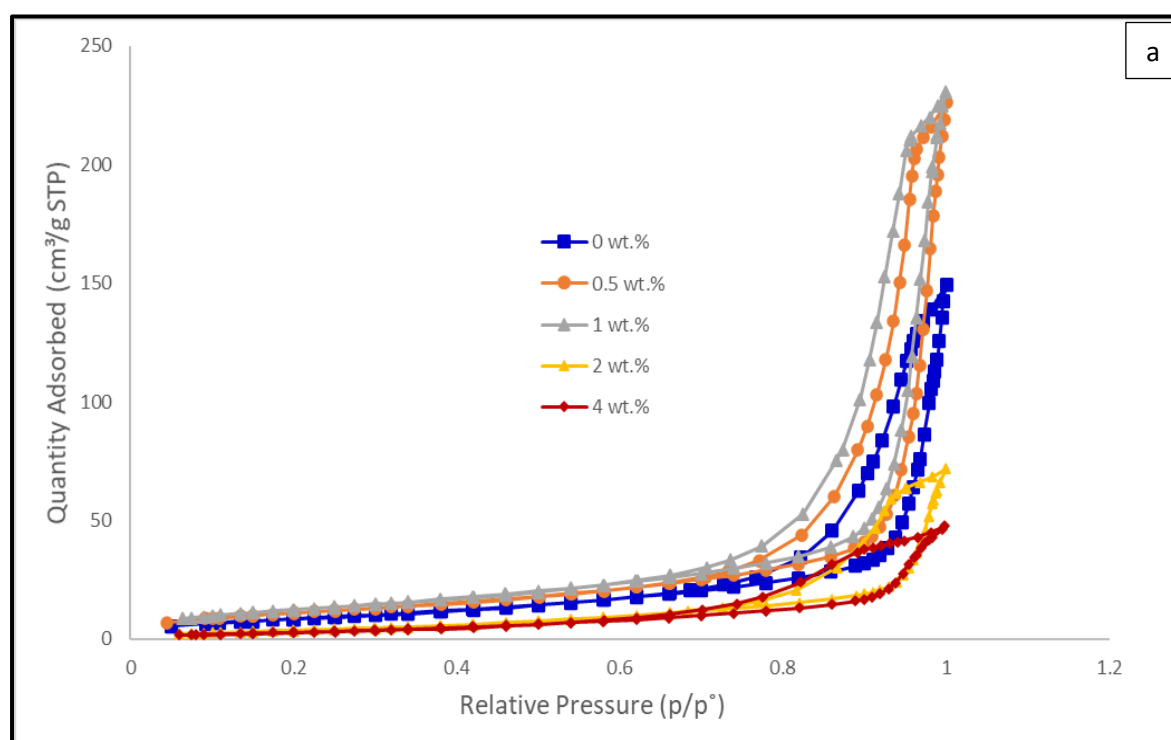


Figure 5.15. The TEM images of BCP microparticles synthesised at (a) 5 wt.% (5PMMA₅₀₀-P4VP₁₇₀-P4VP₁₆₀/D4) and (b) 2.5 wt.% (2.5PMMA₅₀₀-P4VP₁₇₀-P4VP₁₆₀/D4, Table 5.1, entry 6) PDMS-MA. Both samples contained the same amount of DVB (4 wt.%). The porosity distribution shows the majority on the surface of the particles rather than at the centre.

5.3.1.2.2 Nitrogen Adsorption Isotherms

The porous materials were further investigated using nitrogen adsorption isotherms at $-196\text{ }^{\circ}\text{C}$ (Figure 5.16). All of the samples tested recorded the typical type V isotherms.²⁰ The adsorption capacity of nitrogen was negligible for virtually all the samples analysed at pressures up to 0.8. This indicated that the materials are almost entirely mesoporous, with some macropores presence. The quasi-linear behaviour from p/p° values in the range of approximately 0.05 to 0.8 can be associated with the formation of a multilayer of gas on the surface of the polymer samples. The polymer samples, formed by interconnected pores, exhibit surface area between 12.8 to 47.31 m^2/g , the pore volume ranged from 0.07 – 0.34 cm^3/g and the pore diameter from 9.73 - 14.14 nm (Table 5.4, entry 1-6). As a main feature, the polymer samples present a broad bimodal pore size distribution (Figure 5.16b).



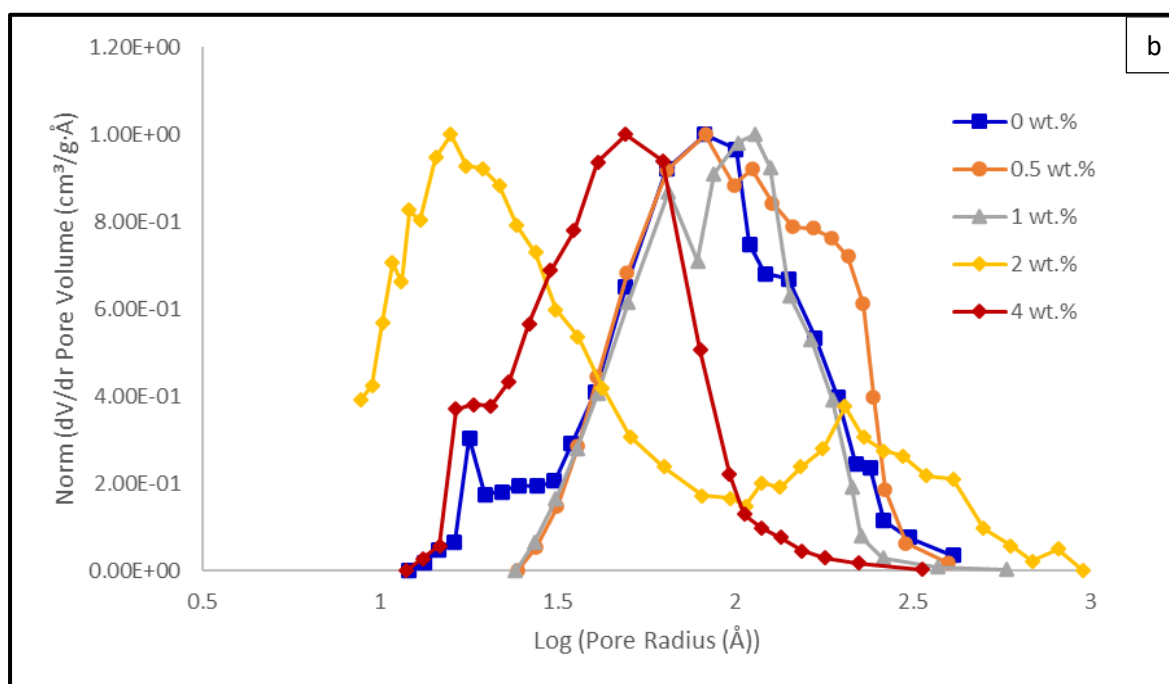


Figure 5.16. Nitrogen adsorption analysis of porous microparticles synthesised using 2.5 wt.% PDMS-MA, at various crosslinker levels (0 – 4 wt.%). (a) Hysteresis loop of quantity adsorbed versus relative pressure and (b) Pore size distribution (BJH Desorption dV/dr Pore Volume).

Table 5.4. Porosity information of samples analysed by Nitrogen Adsorption Isotherms.

Entry	Sample	Crosslinker, DVB (wt.%)	Surface area ^a (m ² /g)	Pore Volume ^b (cm ³ /g)	Pore Diameter ^c (nm)	Total Quantity Adsorbed (cm ³ /g STP)
1	2.5PMMA ₅₀₀ -P4VP ₃₃₀	0.0	33.42	0.21	9.7	149.24
2	2.5PMMA ₅₀₀ -V ₁₇₀ -V ₁₆₀ /D0.5	0.5	42.48	0.33	11.5	226.25
3	2.5PMMA ₅₀₀ -V ₁₇₀ -V ₁₆₀ /D1	1.0	47.31	0.34	12.8	230.65
4	2.5PMMA ₅₀₀ -V ₁₇₀ -V ₁₆₀ /D2	2.0	15.92	0.10	10.8	71.84
5	2.5PMMA ₅₀₀ -V ₁₇₀ -V ₁₆₀ /D4	4.0	12.80	0.07	14.1	46.19
6	5PMMA ₅₀₀ -V ₁₇₀ -V ₁₆₀ /D1	1.0 ^d	33.28	0.27	11.3	180.19

^aBET Surface Area

^bBJH Adsorption cumulative volume of pores between 0.85 nm and 150 nm

^cAdsorption average pore diameter (4V/A by BET)

^dSynthesised with 5 wt.% PDMS-MA

The sample synthesised with 2.5 wt.% of PDMS-MA that contained 1 wt.% DVB (2.5PMMA₅₀₀-V₁₇₀-V₁₆₀/D1, Table 5.4, entry 3) adsorbed the highest amount of nitrogen (230.65 cm³/g STP). In contrast, the sample containing the highest DVB content, 4 wt.% (2.5PMMA₅₀₀-V₁₇₀-V₁₆₀/D4, Table 5.4, entry 5) adsorbed the lowest amount (46.19 cm³/g STP). The amount of adsorbed gas can be closely correlated to the surface area and

pore volume of the sample tested. In this case, the sample with the highest surface area (47.31 m²/g) and pore volume (0.34 cm³/g) adsorbed the highest amount of nitrogen (2.5PMMA₅₀₀-V₁₇₀-V₁₆₀/D1, Table 5.4, entry 3) and vice versa. At the highest DVB content, 4 wt. (2.5PMMA₅₀₀-V₁₇₀-V₁₆₀/D4, Table 5.4, entry 5) a characteristic H2 hysteresis loop was observed, which is related to the presence of 'ink-bottle like' pores. It also had the lowest porosity amongst tested sample, which corroborated with the result from the TEM and SEM as discussed earlier.

The samples (2.5PMMA₅₀₀-V₁₇₀-V₁₆₀/D0.5, Table 5.4, entry 2) containing 0.5 wt.% DVB showed a similar trend of H2 hysteresis loop of quantity adsorbed versus relative pressure with sample 2.5PMMA₅₀₀-V₁₇₀-V₁₆₀/D1 (Table 5.4, entry 3). From the results obtained, both samples recorded non-significant different values of all parameters measured during the analysis. However, the pore size distribution for the sample containing 0.5 wt.% DVB was slightly distributed towards the bigger size region in comparison to the sample synthesised with 1.0 wt.% crosslinker.

The pore structure (size and volume) plays a fundamental role in the adsorption ability of polymer materials, in such a way that the bigger the pore size, the higher the adsorption capacity (Figure 5.16 and Table 5.4). The trend of crosslinking concentration on nitrogen adsorption behaviour can be seen from the samples synthesised with 0, 2 and 4 wt. % (Table 5.4, entry 1, 4 and 5). As the amount of crosslinking increased, the amount of nitrogen adsorbed decreased (Figure 5.16a), due to the decreased value of associated parameters, e.g. surface area and pore volume (Table 5.4). In terms of the pore size distribution, the sample that contained 0 wt.% (Table 5.4, entry 1) was located at the bigger size region, the sample with 2 wt.% (Table 5.4, entry 4) had a broad pore size distribution, which covered both the smaller and bigger size region. The non-crosslinked sample (2.5PMMA₅₀₀-P4VP₃₃₀, Table 5.4, entry 1) exhibited a very broad bimodal pore size distribution, containing pores size in the range from approximately 1 to 100 nm. Despite this, it seems that the adsorption

capacity is determined by the pores with size distributed in the region between 10 and 100 nm, which can explain why the sample 2.5PMMA₅₀₀-P4VP₃₃₀ was able to adsorb more nitrogen than the sample synthesised with 4 wt.% (Table 5.4, entry 5) crosslinker.

Figure 5.17 shows the comparative adsorption behaviour of samples 2.5PMMA₅₀₀-V₁₇₀-V₁₆₀/D1 and 5PMMA₅₀₀-V₁₇₀-V₁₆₀/D1 (Table 5.4, entry 3 and 6). The aim was to evaluate whether the concentration of PDMS-MA determined the average particle size of the crosslinked microparticles, and ultimately this correlates the particle size with the pore features, which determines the overall adsorption capacity of the polymer samples. In terms of particle size, the smaller particles synthesised with 5 wt.% PDMS-MA, with average particle size of 1.30 μm (5PMMA₅₀₀-V₁₇₀-V₁₆₀/D1, Table 5.4, entry 6), gave a lower quantity of nitrogen absorbed in comparison to the bigger particles (average particle size equal to 1.94 μm), 2.5PMMA₅₀₀-V₁₇₀-V₁₆₀/D1 (Table 5.4, entry 3) at the same amount of crosslinking (1 wt.%). (Figure 5.17a). The pore size distribution for these samples were significantly different: the smaller particle size (sample synthesised with 5 wt.% PDMS-MA) had a broader pore size distribution in comparison to the bigger particle (2.5 wt.% PDMS-MA) synthesised with the same crosslinker concentration (Figure 5.17b).

It is reasonable to assume that in general, the pore volume has the biggest impact on the adsorption capacity of the polymer samples, which can explain why porous particles with similar pore diameter have different ability to adsorb nitrogen. For samples with similar pore diameter, it can be assumed that the higher the pore volume (or the higher the pore length) the higher the surface area and consequently the higher the amount of gas that can be adsorbed (Table 5.4).

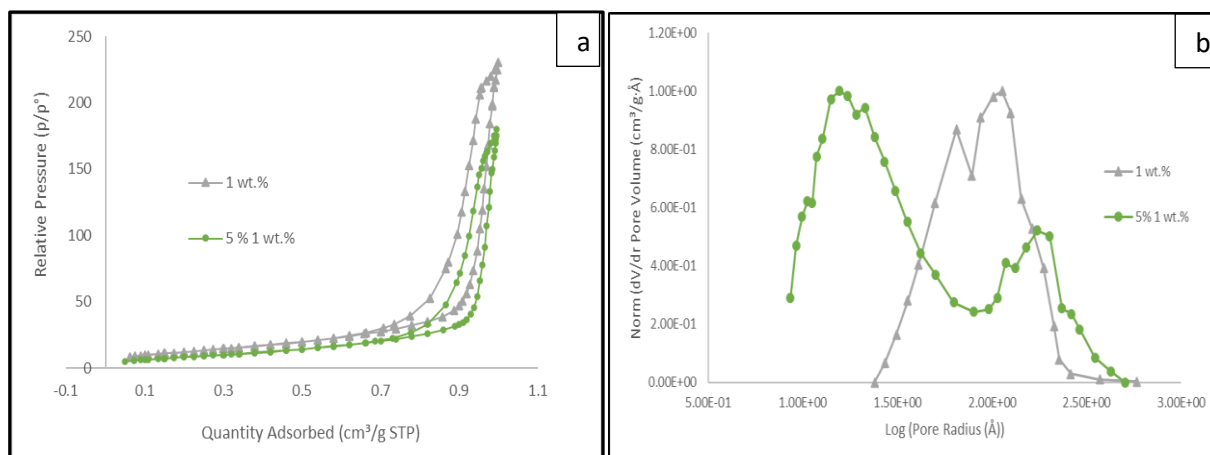


Figure 5.17. Nitrogen adsorption analysis of porous microparticles synthesised with 2.5 and 5 wt.% PDMS-MA with 1 wt.% of DVB (Table 5.4, entry 3 and 6). (a) Hysteresis loop of quantity adsorbed versus relative pressure; (b) Pore size distribution (BJH Desorption dV/dr Pore Volume).

The T_g of the porous particles have been studied and compared to the non-porous particles. It was found that both porous and non-porous particles have no significant difference of T_g at all crosslinking contents (Figure 5.18). This is a good indicator that there are no changes in particle structure after the swelling procedure.

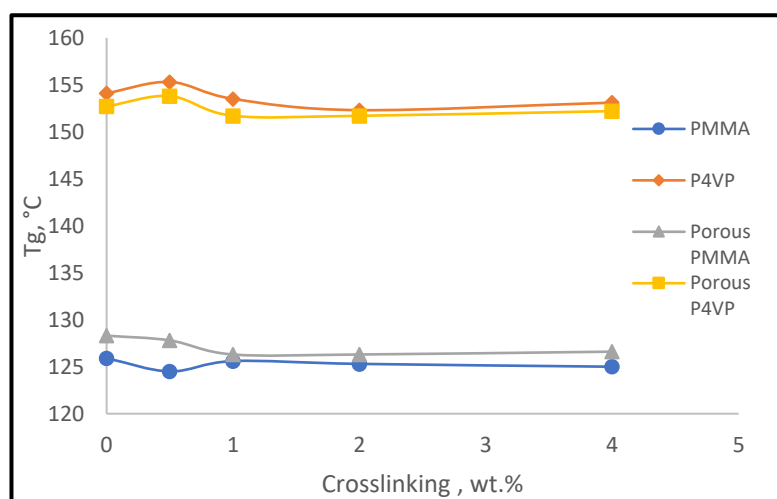


Figure 5.18. T_g of porous and non-porous particles by DSC analysis. There are no significant changes in T_g value for both sample before and after swelling/deswelling procedure.

Generally, the SEM, TEM/ tilt TEM and nitrogen adsorption isotherms results have shown that we have good of crosslinking control, regardless of particle size ranging from 0.6 -2.5 μm synthesised at 2.5 and 5 wt.% PDMS-MA.

5.3.2 Enzyme Immobilisation

5.3.2.1 Enzyme Stability Study

The stability of an enzyme is defined as its ability to maintain its active structural shape in the face of damaging influences, such as temperature rises. It is critical to ascertain by measuring an enzyme's initial activity and residual activity following storage at a specific temperature for a specified time.

The enzyme activity was reduced by 56% for the lipase at 5 mg/mL, 61% at 2.5 mg/mL and 36% at 1 mg/mL, respectively (Table 5.5). This shows that the enzyme activity has reduced over time during storage at 4 °C at all concentration of lipase prepared after 3 days' storage. The same tendency is observed in the three enzyme concentrations studied. From this stability study, it was concluded that the enzyme solution has to be prepared freshly prior to the immobilisation test due to the instability of the enzyme during the storage period.

Table 5.5. Lipase activity at different concentration and % of reduction of activity after 3 days storage at 4 °C.

Concentration (mg/mL)	Enzyme Activity Day 1 (U/mg _{Enzyme})				Enzyme Activity Day 4 (U/mg _{Enzyme})				% Reduction
	1	2	3	Mean	1	2	3	Mean	
5	0.11	0.11	0.11	0.11	0.05	0.04	0.05	0.05	55
2.5	0.12	0.14	0.13	0.13	0.05	0.05	0.05	0.05	62
1	0.14	0.15	0.05	0.14	0.10	0.08	0.06	0.09	36

5.3.2.2 Sample Miscibility

The BCP PMMA-*b*-P4VP microparticles synthesised in this study are hydrophobic and are not miscible with the phosphate buffer solution containing the enzyme. It floated on the surface, as shown in Figure 5.19 (a). Hence, an appropriate surfactant is needed to improve the miscibility of the particles and to facilitate enzyme immobilisation onto the copolymer surface. Two types of surfactant were studied; Tween-20, which was available in the laboratory; and poly(glycerol adipate) (PGA), a new renewable system that was synthesised by a colleague in the group.²¹ The enzyme solution was prepared in three different vials: with the addition of 0.5 wt.% PGA, 0.5 wt.% Tween-20 and mixture of 0.5% PGA and Tween-20, respectively.

As demonstrated in Figure 5.19b, the addition of these two surfactants reduced the hydrophobicity of the samples and increased their miscibility towards the buffer phosphate, with varying degrees of success. When Tween-20 was added alone to the phosphate buffer, many bubbles formed, resulting in poor measurement reproducibility. While the PGA alone provided less miscibility than the Tween-20, thus, it was determined that a mixture of Tween-20 and PGA was sufficient to increase the miscibility of samples in the phosphate buffer.

The lipase activity was unaffected by the addition of these two surfactants. This can be observed in Table 5.6, which shows the results of the control sample examined during lipase immobilisation. There was no significant difference in lipase activity between the start of the immobilisation process, $t = 0$, and the end of the immobilisation process, 2 hours later.

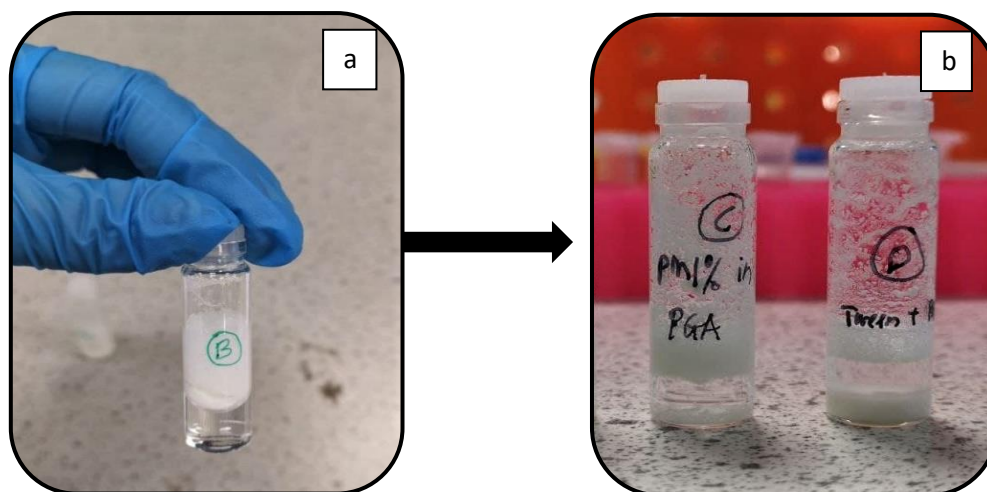


Figure 5.19. Miscibility of hydrophobic samples in phosphate buffer solution at pH=7; a) without the addition of surfactants b) with the addition of surfactants, left PGA and right mixture of Tween-20 and PGA.

5.3.2.3 Immobilisation of the Enzyme

The lipase solution (5 mg/mL) was immobilised onto the BCP microparticle samples. The mixture of Tween-20 and PGA was added to the enzyme solution, to improve the miscibility of the sample towards the lipase solution. The microparticles were left in contact with the lipase enzyme solution for 2 hours, under continuous mild shaking (mechanical shaker) on ice.

An immobilisation yield of 59% was recorded by the non-porous samples containing 1 wt.% DVB, 2.5PMMA₅₀₀-V₁₇₀-V₁₆₀/D1 (Table 5.6). When phase separated, these microparticles reveal SPH nanostructures, as previously discussed. Comparing non-porous microparticles with LAM nanostructure containing 2 wt.% DVB (PMMA₁₅₀-P4VP₄₀₀-P4VP₅₀/D2), we discovered relatively no notable difference with slightly decreased immobilisation yield (56%) (Table 5.6). When immobilised to non-crosslinked (0 wt.% DVB) LAM, PMMA₁₅₀-P4VP₄₀₀-P4VP₅₀ microparticles, the yield dropped to 51% (Table 5.6).

These results show that the lipase has been successfully immobilised under the stated conditions as a proof of concept. Both block copolymer microparticles, PMMA-*b*-P4VP, with SPH and LAM morphology of non-porous particles have the same potential to be used for this application. The amount of crosslinking tested, ranging from 0 to 2%, had no significant effect on the immobilisation yield of lipase into these BCP microparticles.

Enzyme immobilisation is a complex process which requires different factors to be optimised. Optimising parameters like protein load and immobilisation time should be developed to target an increased immobilisation yield. But protein immobilisation is a tailored process, as it will depend on each protein structure and the chemistry associated with the support used. Previously, there was a study of some different immobilisation strategies for the selective hydrolysis of fish oil performed by *Rhizomucor miehei* lipase (RML), the study showed that immobilisation varied from 11% up to 88% yields depending on the optimising approach.²²

Our data show (Table 5.6) that the BCP microparticles of this study can provide a good immobilisation structure for lipase enzymes.

Table 5.6. Lipase Immobilisation Activity of non-porous samples 2.5PMMA₅₀₀-V₁₇₀-V₁₆₀/D1 (SPH), PMMA₁₅₀-V₄₅₀ (LAM) & PMMA₁₅₀-V₄₀₀-V₅₀/D2 (LAM).

Condition	Sample	Mean Value of immobilisation				U/mL	U/mg	% Remaining	Immobilisation yield (%)
		1	2	3	Mean				
CTRL in PO₄ only	t=0	86.68	88.37	78.99	84.68	0.561	0.112	-	
	t=2 hrs	85.00	80.92	-	82.96	0.549	0.110	98	
CTRL in PO₄ mix PGA + Tween20	t=0	94.74	87.15	87.49	89.79	0.595	0.119	-	
	t=2 hrs	84.73	86.03	88.01	86.26	0.571	0.114	96	
t=2 hrs Immobilisation in PGA + Tween20	2.5PMMA ₅₀₀ -V ₁₇₀ - V ₁₆₀ /D1 (SPH)	38.74	40.58	31.76	37.03	0.245	0.049	41	59
	PMMA ₁₅₀ -V ₄₅₀ (LAM)	39.79	42.24	48.94	43.66	0.289	0.058	49	51
	PMMA ₁₅₀ -V ₄₀₀ - V ₅₀ /D2 (LAM)	36.11	34.13	46.73	38.99	0.258	0.052	44	56

5.3.3 Usnic Acid Adsorption Test

The usnic acid (UA) adsorption test was performed on the BCP microparticles with SPH nanostructure only. The effect of all other variation within microparticles including crosslinking degree, particle size and porosity was studied. This test was carried out by our collaborator, Iolanda Francolini in Rome, Italy.

Initially, the effect of UA concentration on the adsorption yield was investigated. An example of the adsorption yield vs. UA concentration is shown in Figure 5.20 for the porous BCP microparticle PorePMMA₅₀₀-V₃₃₀, which contained 0 wt.% DVB. As expected, the adsorption yield increased with the increase in UA concentration. A plateau was reached at 1 mg/mL and this concentration was chosen for the further experiments.

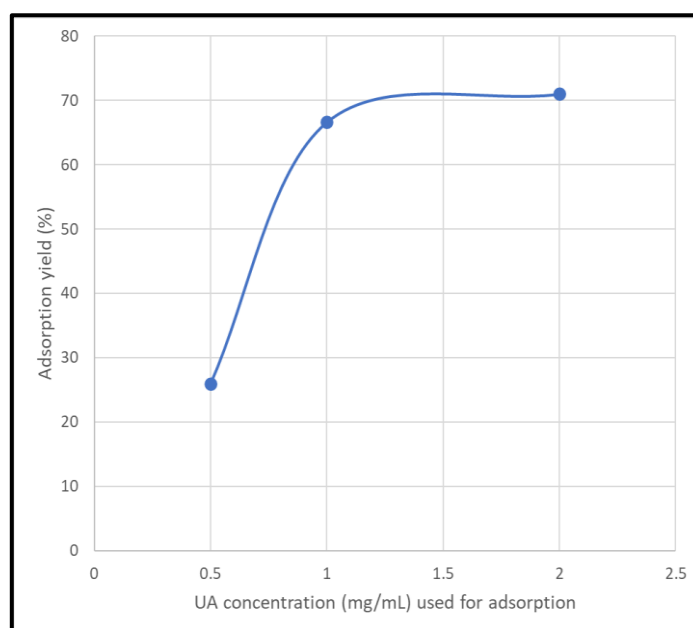


Figure 5.20 Effect of UA concentration on the adsorption yield

As for the adsorption yield, porous microparticles showed a higher absorption yield than non-porous particles as might be expected. That the lowest value 0.5 wt.% it is likely that the polymers are branched and not crosslinked as discussed in Chapter 4 and hence this showed much lower absorption. On average, both the porous and non-porous systems adsorb a drug amount ranging from 60 to 75% of the initially present drug, with the only exception being the BCP that contained 0.5 wt.% DVB, which showed a lower adsorption yield (45-55%) (Figure 5.21a). With regards to the drug absorbed per mg of particles (Figure 5.21b), the porous particles showed an increase in the adsorbed amount as the crosslinker content increased. In contrast, with the non-porous samples, the adsorbed amount of drug was independent from the crosslinking.

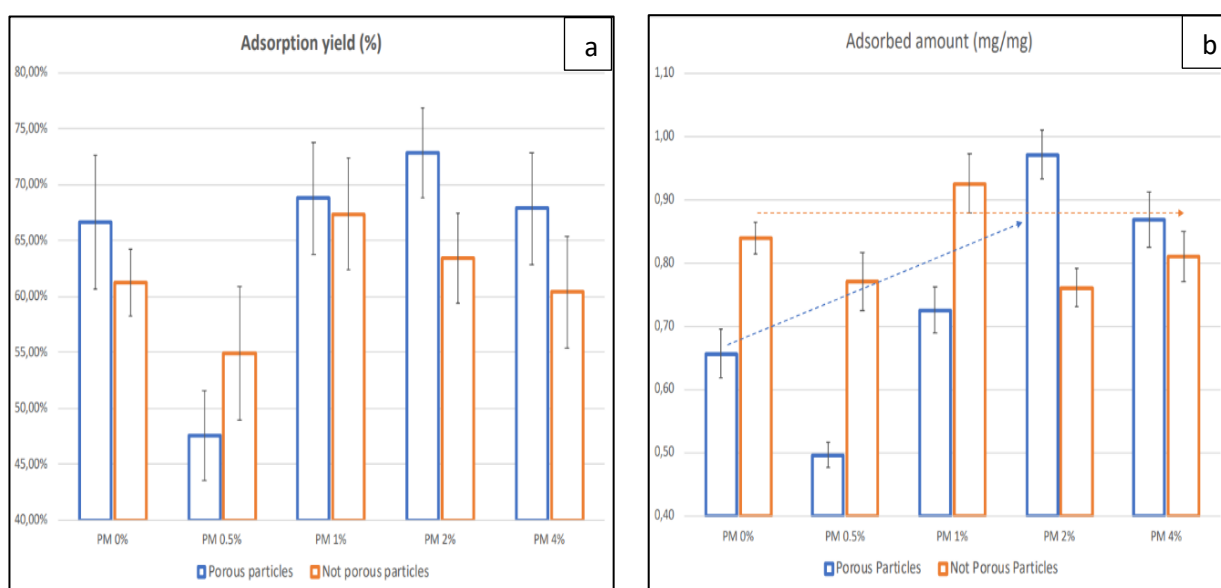


Figure 5.21. (a) Adsorption yield (%) and (b) adsorption amount per mg of particles for porous and non-porous particles obtained with different amount of crosslinker (0-4 wt.%). All particles synthesised with 2.5 wt. % of PDMS-MA. UA concentration 1 mg/mL.

Comparisons of the particles obtained with 2.5 and 5 wt.% stabilizers are shown in Figures 5.22a and 5.22b, including the adsorption yield and adsorbed amount, respectively. A similar adsorption yield was recorded for porous and non-porous particles. In addition, once, the crosslinker amount was fixed (either 0.5 or 1 wt.%), the presence of high stabilizer (5 instead of 2.5 wt.%) increased both the adsorption yield and the adsorbed amount per mg of particles for both samples.

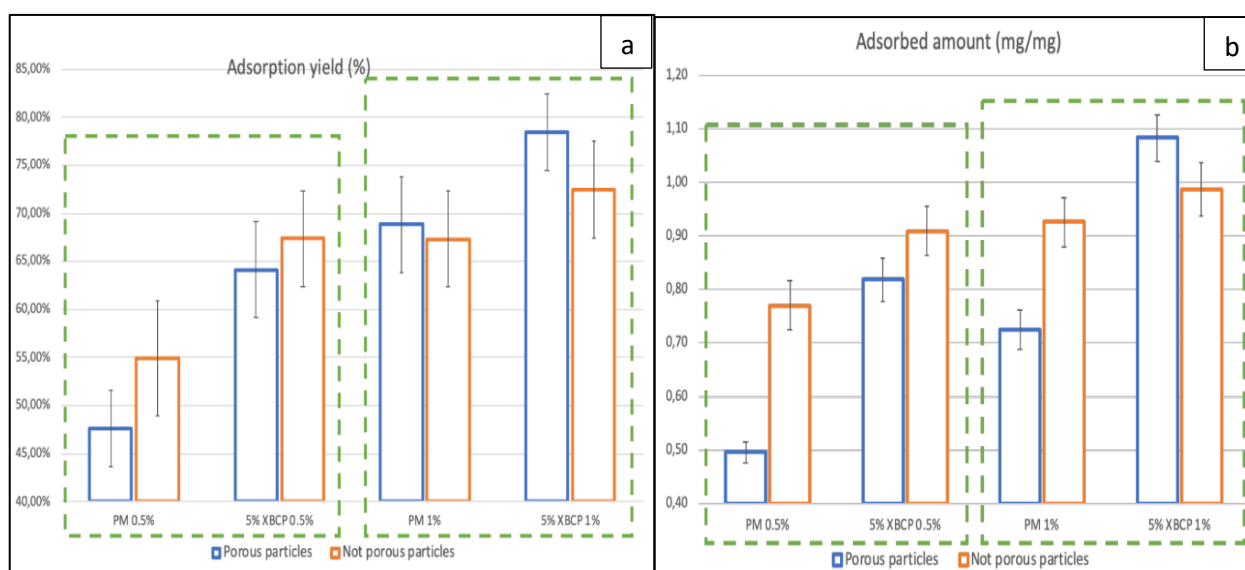


Figure 5.22 (a) Adsorption yield and (b) adsorbed amount for porous and non-porous particles obtained with different amount of stabilizer, PDMS-MA (2.5 or 5 wt. %). UA concentration 1 mg/mL. (Notes: PM denote samples with 2.5 wt.% , 5%XBCP denote samples with 5 wt.%).

Finally, the influence of particle size on the adsorbed amount per mg of particles for the porous (Figure 5.23a) and non-porous (Figure 5.23b) samples was investigated. In both cases, the adsorbed amount decreased with increasing particle size. However, in both cases the correlation was not good ($R^2 = 0.5161$ porous particles and $R^2 = 0.3008$ non-porous particles). These results corroborated the finding in Figure 5.22, which showed the effect of different amount of stabiliser, PDMS-MA added.

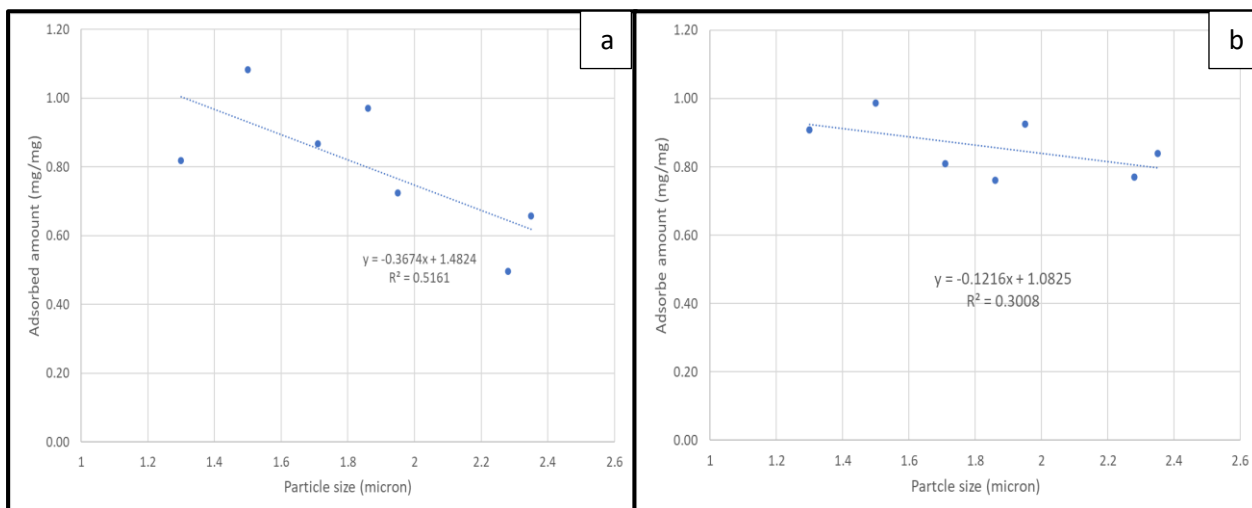


Figure 5.23 Adsorbed amount (mg/mg) vs. particle size for the (a) porous and (b) non-porous particles, showing the adsorbed amount decreased with increasing particle size.

In summary, the adsorption yields of porous microparticles are higher than the non-porous microparticles containing 0 wt.%, 1wt.%, 2 wt.% and 4wt.% respectively. Furthermore, the amount of drug adsorbed per mg of particle increased as the crosslinker concentration increased in porous particles, this was not the case for non-porous particles. These results show the positive effect of crosslinking in controlling the amount of drug adsorbed in porous microparticles. In both the particles synthesised with 2.5 and 5 wt.% PDMS-MA, the adsorbed amount decreased with increasing particle size in all porous and non-porous samples. All of the samples that were tested have had good adsorption yields of more than 60%, which shows that they could be good drug adsorption materials. The highest adsorption yield of UA recorded was 79% by porous particles produced with 5 wt.% PDMS-MA, which contained 1 wt.% of DVB.

5.3.4 Polymer Stationary phase for sample preparation

A few of the potential sorbent BCP microparticles materials were studied to evaluate their extraction capacities in an aqueous medium. This study could be regarded as a preliminary study since the aqueous sample was Milli-Q water. This test was carried out by our collaborator, Giovanni Dorazio in Rome, Italy.

The recovery data is a critical component of the extraction procedure. The recoveries and intra-day precision ($n = 2$) of Milli-Q water samples fortified with a solution of target analytes at a concentration of 10 g/mL were studied. The recovery study was conducted by calculating the percentage ratio between the peak area obtained from these samples and that obtained from spiked blank extract samples for each analyte.

Preliminary results demonstrated that certain compounds with a variety of different chemical structures, hydrophobic and hydrophilic properties might be extracted. In this study, the MarvinSketch tool (<http://www.chemaxon.com>) was used and estimated the hydrophilic lipophilic balance (HLB) value in the range of 2.7-7.5 and a value of partition coefficients ($\log P$) in the range of 2.8-4.6, general recovery data was estimated in the range of 35-75%, with a precision of less than 15% RSD (Relative Standard Deviation). $\log P$ is a ratio of concentrations of un-ionized compound between the two solutions.

A comparison of recovery data for the tested analytes allowed for the discovery of connections between extraction capacity and polymer structure. Initially, a comparison study was conducted in the absence of crosslinker (0 wt.% DVB) between a non-porous and porous BCP, which was synthesised using 2.5 wt.% PDMS. Figure 5.24 shows a data comparison of 2.5PMMA₅₀₀-V₃₃₀ and Pore2.5PMMA₅₀₀-V₃₃₀. There were no notable differences, which were less than 10% RSD. Although there was no

interest in analysing the structure of the polymer in the SPE application in this work, the extraction repeatability is an excellent outcome in terms of method validation.

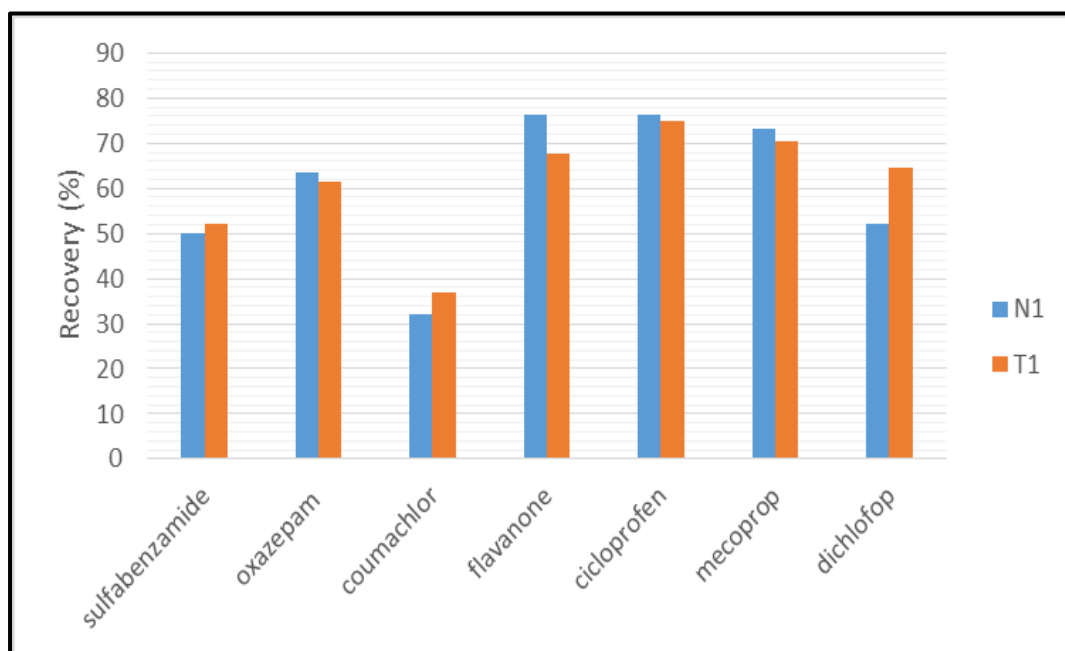


Figure 5.24. Comparative study of the extraction capacity of non-porous, 2.5PMMA₅₀₀-V₃₃₀ (N1) and porous, Pore2.5PMMA₅₀₀-V₃₃₀ (T1) BCP at 0 wt.% crosslinker. Experimental conditions: Capillary columns, 100 μ m I.D., packed length, 25.0 cm; effective length, 26.5 cm packed with XBridge™ C₁₈; flow rate, 210 nL/min, injection volume, 110 nL; room temperature; detection wavelength, 200 nm; Milli-Q water sample fortified at 10 μ g/mL of target compounds.

Comparing BCP containing the same crosslinker content (1 wt.% DVB) revealed relatively small trends. Figure 5.25 illustrates three BCP, 2.5PMMA₅₀₀-V₁₇₀-V₁₆₀/D1 (N3), Pore2.5PMMA₅₀₀-V₁₇₀-V₁₆₀/D1 (P2), and Pore5PMMA₅₀₀-V₁₇₀-V₁₆₀/D1 (T2), which differ in their porosity and PDMS concentration. Although there was no significant difference in extraction capacity when switching from a N3 to a P2 porous structure, the data implies a minor increase in recovery when switching from a N3 to a T2 porous structure. Additionally, with the smaller particles, that were

synthesised with 5wt.% PDMS-MA, a minor difference was detected (T2). The nano-LC-UV chromatogram after extraction, d-SPE, with the N3, P2, and T2 polymeric phase materials is shown in Figure 5.26.

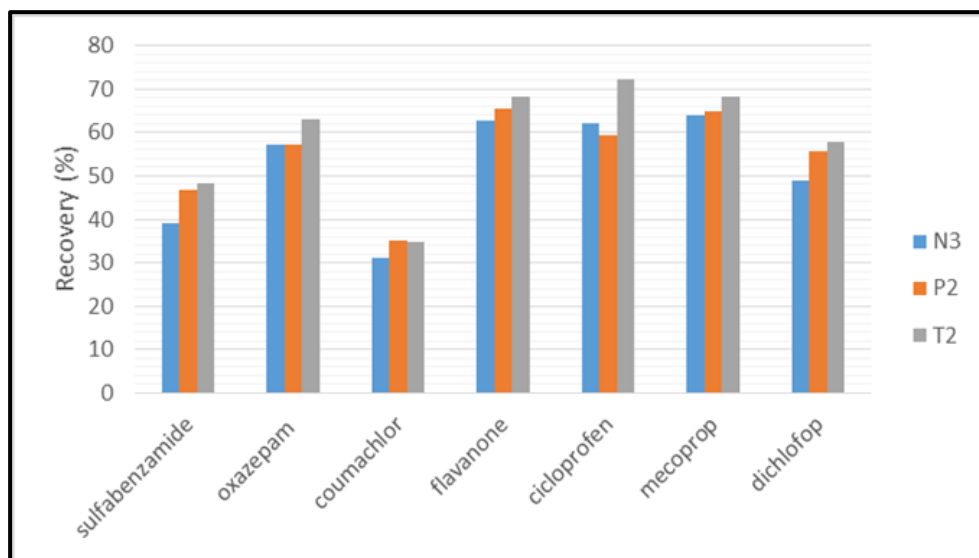


Figure 5.25. Comparative study of the extraction capacity of non porous or porous BCP microparticles with different % PDMS-MA. Experimental conditions: see Figure 5.25. (**Notes:** 2.5PMMA₅₀₀-V₁₇₀-V₁₆₀/D1 (N3), Pore2.5PMMA₅₀₀-V₁₇₀-V₁₆₀/D1 (P2), and Pore5PMMA₅₀₀-V₁₇₀-V₁₆₀/D1 (T2)).

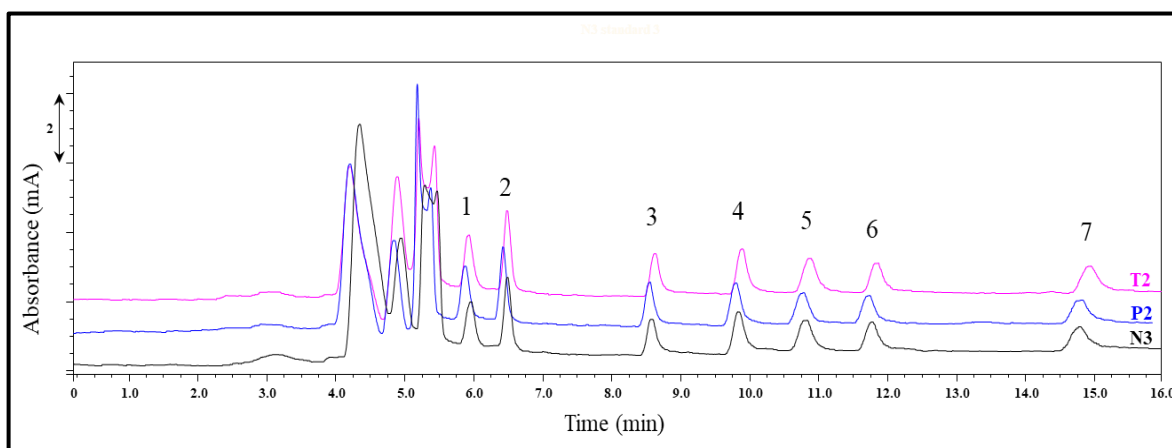


Figure 5.26. Comparison of nano-LC-UV chromatograms of fortified Milli-Q water sample after d-SPE using different polymer phase sorbent. For experimental condition see figure 5.25. (**Notes:** 2.5PMMA₅₀₀-V₁₇₀-V₁₆₀/D1 (N3), Pore2.5PMMA₅₀₀-V₁₇₀-V₁₆₀/D1 (P2), and Pore5PMMA₅₀₀-V₁₇₀-V₁₆₀/D1 (T2)).

The next comparison was between porous BCP, produced with the same amount of PDMS-MA (2.5 wt.%), but with different crosslinker percentage (Figure 5.27). With Pore2.5PMMA₅₀₀-V₁₇₀-V₁₆₀/D1 (P2), Pore2.5PMMA₅₀₀-V₁₇₀-V₁₆₀/D2 (P3) and Pore2.5PMMA₅₀₀-V₁₇₀-V₁₆₀/D4 (P5) only slight changes in recovery factor were observed. In contrast, the effect of increase both in crosslinker content and pore size, seemed to show a trend where the larger porosity (P2) gave higher recovery than smaller porosity (P3).

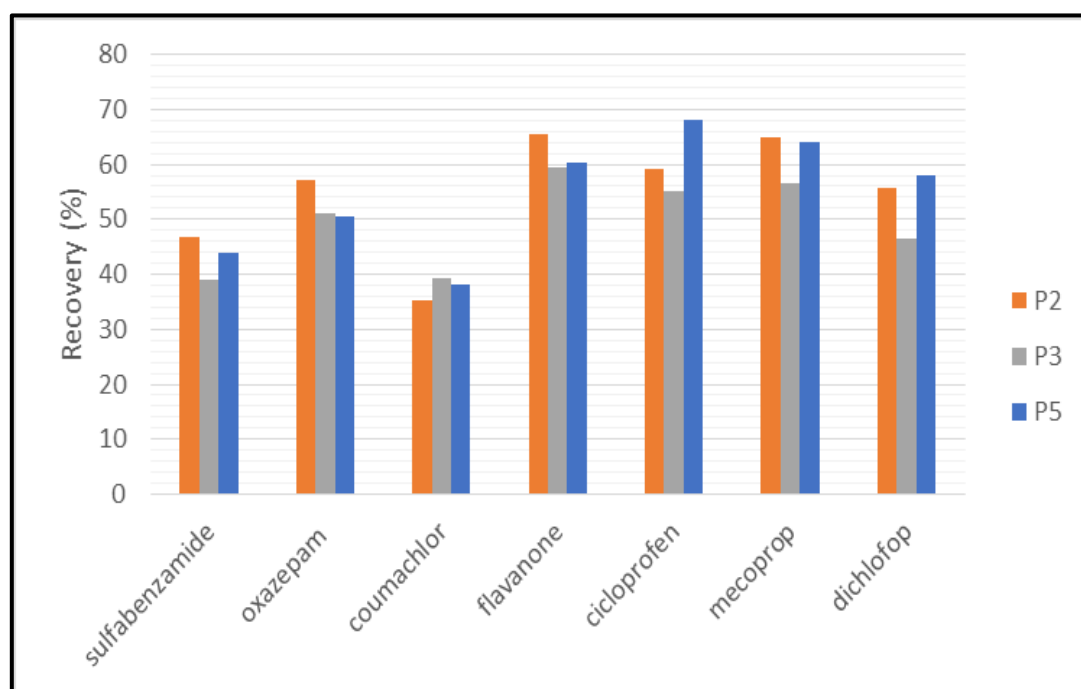


Figure 5.27. Comparative study of the extraction capacity of BCP microparticle at different degree of crosslinking (1 (P2), 2 (P3) and 4 (P5) wt.% of DVB)- Experimental conditions: see Figure 5.25. (**Notes:** Pore2.5PMMA₅₀₀-V₁₇₀-V₁₆₀/D1 (P2), Pore2.5PMMA₅₀₀-V₁₇₀-V₁₆₀/D2 (P3) and Pore2.5PMMA₅₀₀-V₁₇₀-V₁₆₀/D4 (P5)).

In general, the extraction capacity of all of the non-porous microparticles produced using 2.5 wt.% PDMS-MA containing DVB ranging from 0-4 wt.% gave satisfactory recovery 35-75% as estimated. However,

a few samples in the coumachlor analysis recorded slightly lower recovery around 30% (Figure 5.28). Comparing the non-porous to the corresponding porous particles, the recovery data showed, an increasing trend in most of the cases (Figure 5.29). These results highlighted that although the content of crosslinker changed (0–4 wt.%), the different pore sizes for non-porous (N1-N5), 32-69 nm to porous (T1-P5), 0.9-138 nm, played a discriminating role. Thus, it appeared that porous particles gave the highest recovery for higher surface development due to pore volume.

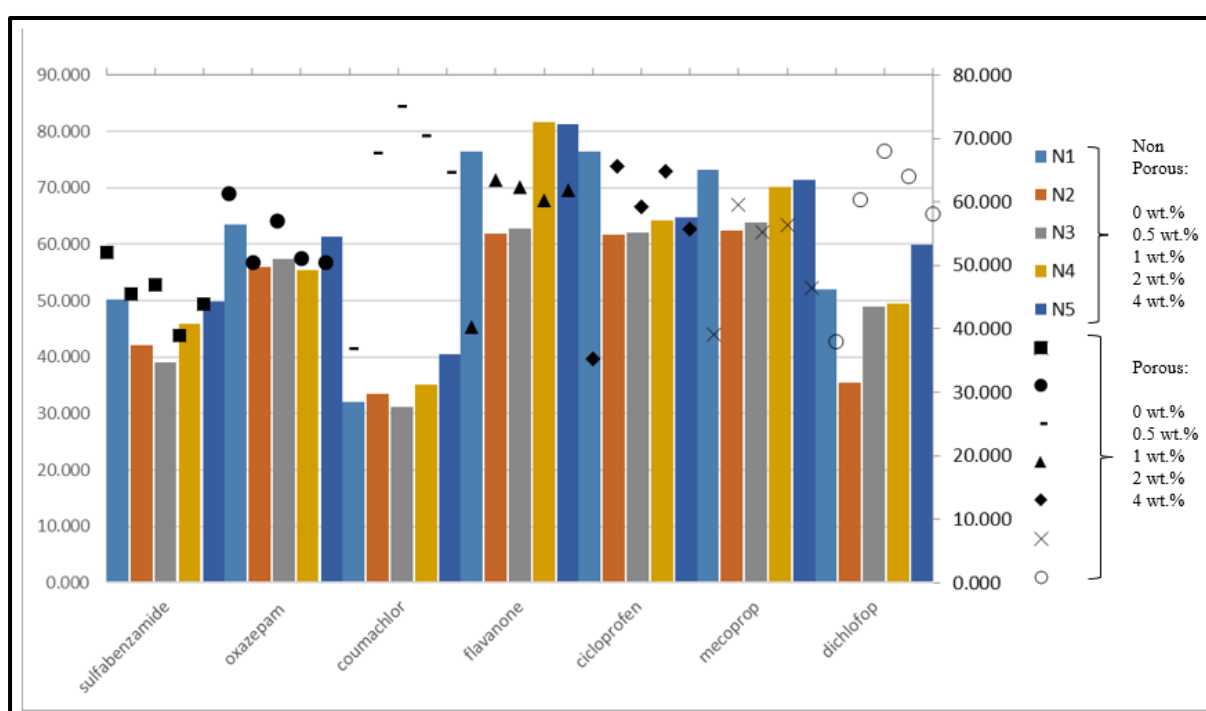


Figure 5.28 Comparative study of the extraction capacity of all the non-porous and corresponding porous BCP synthesised using 2.5 wt.% PDMS-MA at different crosslinking degree. Experimental conditions: see Figure 5.25.

5.5 Conclusion

Good control over the *in situ* crosslinking PMMA-*b*-P4VP particles was maintained when the surfactant level was reduced from 5 to 2.5 wt.%. This reduction in surfactant also yielded larger particles as expected.

Lipase has been successfully immobilised into the non-porous BCP microparticles with both SPH and LAM morphology. The immobilised yield was greater than 50% (51–59%), indicating that the material has proven to be viable for use as an enzyme support material.

Similar potential can also be seen in the UA adsorption test, where the adsorption yields of the majority of the substances tested was greater than 60%. The porous particles synthesised using 5 wt.% PDMS-MA, which contained 1 wt.% DVB, had the greatest UA adsorption yield of 79%.

The extraction capacity of the majority of microparticles produced by 2.5 wt.% PDMS-MA containing DVB ranging from 0–4 wt.% was also satisfactory, with the percentage of recovery meeting the estimated specification, ranging from 35 to 75 % after accounting for both the hydrophilic lipophilic balance (HLB) value and the value of partition coefficients ($\log P$).

In summary, this chapter shows that the size and porosity of the microparticle BCP can be controlled through polymer chemistry, and this control is then useful in turning the materials for different applications.

5.6 References

1. T. D. McAllister, L. D. Farrand and S. M. Howdle, *Macromolecular Chemistry and Physics*, 2016, **217**, 2294-2301.
2. S. Fanali, G. D'Orazio and M. G. Quaglia, *Chromatographia*, 2004, **60**, S239-S243.
3. G. D'Orazio, S. Rocchi and S. Fanali, *Journal of Chromatography A*, 2012, **1255**, 277-285.
4. U. Hanefeld, L. Gardossi and E. Magner, *Chemical Society reviews*, 2009, **38**, 453-468.
5. U. Hanefeld, L. Cao and E. Magner, *Chemical Society reviews*, 2013, **42**, 6211-6212.
6. J. Ge, D. Lu, Z. Liu and Z. Liu, *Biochemical engineering journal*, 2009, **44**, 53-59.
7. I. Mahmood, C. Guo, H. Xia, J. Ma, Y. Jiang and H. Liu, *Industrial & engineering chemistry research*, 2008, **47**, 6379-6385.
8. Q. Chen, H. Schönherr and G. J. Vancso, *Small (Weinheim an der Bergstrasse, Germany)*, 2009, **5**, 1436-1445.
9. E. Magner, *Chemical Society reviews*, 2013, **42**, 6213-6222.
10. F. M. Plieva, K. A. Kochetkov, I. Singh, V. S. Parmar, Y. N. Belokon and V. I. Lozinsky, *Biotechnology letters*, 2000, **22**, 551-554.
11. M. Pohanka, *Molecules (Basel, Switzerland)*, 2019, **24**, 616.
12. V. Taresco, I. Francolini, F. Padella, M. Bellusci, A. Boni, C. Innocenti, A. Martinelli, L. D'Ilario and A. Piozzi, *Materials Science & Engineering C*, 2015, **52**, 72-81.
13. A. M. Grumezescu, C. Saviuc, M. C. Chifiriuc, R. Hristu, D. E. Mihaiescu, P. Balaure, G. A. Stanciu and V. Lazar, *IEEE transactions on nanobioscience*, 2011, **10**, 269-274.

14. V. Grumezescu, A. M. Holban, A. M. Grumezescu, G. Socol, A. Fikai, B. S. Vasile, R. Trusc, C. Bleotu, V. Lazar, C. M. Chifiriuc and G. D. Mogosanu, *Biofabrication*, 2014, **6**, 035002.
15. F. Maya and B. Paull, *Journal of separation science*, 2019, **42**, 1564-1576.
16. G. Kibar and A. Tuncel, *Polymer bulletin (Berlin, Germany)*, 2015, **73**, 1939-1950.
17. G. He, T. M. Bennett, M. Alauhdin, M. W. Fay, X. Liu, S. T. Schwab, C.-G. Sun and S. M. Howdle, *Polym. Chem.*, 2018, **9**, 3808-3819.
18. G. He, T. M. Bennett, K. Alias, L. Jiang, S. T. Schwab, M. Alauhdin and S. M. Howdle, *Polymer chemistry*, 2019, **10**, 3960-3972.
19. S. J. Byard, M. Williams, B. E. McKenzie, A. Blanazs and S. P. Armes, *Macromolecules*, 2017, **50**, 1482.
20. M. Thommes, K. Kaneko, A. V. Neimark, J. P. Olivier, F. Rodriguez-Reinoso, J. Rouquerol and K. S. W. Sing, *Pure and applied chemistry*, 2015, **87**, 1051-1069.
21. P. L. Jacob, L. A. Ruiz Cantu, A. K. Pearce, Y. He, J. C. Lentz, J. C. Moore, F. Machado, G. Rivers, E. Apebende, M. R. Fernandez, I. Francolini, R. Wildman, S. M. Howdle and V. Taresco, *Polymer (Guilford)*, 2021, **228**, 123912.
22. M. Yousefi, M. Marciello, J. M. Guisan, G. Fernandez-Lorente, M. Mohammadi and M. Filice, *Molecules (Basel, Switzerland)*, 2020, **25**, 545.

Chapter 6

Conclusions and Future Work

This closing chapter summarises the main findings of the research presented in this thesis and suggests a few ideas for potential future research projects based on the results. This piece of research work has endeavoured to explore routes for the synthesis of novel nanostructured materials in supercritical CO₂. This was achieved through a facile crosslinking approach with the aim of maintaining the internal nanostructure of block copolymer microparticles. In addition, a few application tests were carried out as a proof of concept to highlight areas in which the BCP microparticles could be potential used.

6.1 Conclusions

A block combination between PMMA and P4VP, was desired to be explored further throughout this study. This monomer combination was of interest due to the differences in their CO₂-philicity coupled with their unique functionality. Furthermore, the potential application of this BCP, PMMA-*b*-P4VP had not previously been study in depth within the group.

Synthesis of PMMA-*b*-P4VP using RAFT dispersion polymerisation in scCO₂ was carried out and detailed in chapter three. The polymerisation process was optimised to produce BCPs with a range of sizes and phase-separated morphologies. The successful synthesis of BCP was confirmed by the GPC results, which indicated that chain extension of the PMMA had occurred by a shift in the peak to a higher M_n value in the final block copolymer. Good repeatability and reproducibility was established for the synthesis of SPH and LAM BCP microparticles, with M_n targeted value of 83,000 g/mol and 60,000 g/mol, respectively. The SPH BCP was synthesised via two consecutive RAFT polymerisation, while the LAM structure was obtained via RAFT in a series of shorter independent steps.

The utilisation of PMMA-CTA that had previously been synthesised and stored for future chain extension was a key success in obtaining a good quality of LAM BCP microparticles with a lower volume fraction of PMMA ($f_{\text{PMMA}} = 0.25$). Using the PMMA-CTA ensured that a sufficient amount of the first PMMA block is provided to induce the formation of the LAM morphology when phase separated during the chain extension copolymerisation with the second monomer, 4VP. The percentage yield and monomer conversion to polymer control over one-pot synthesis is partially lost when the volume

fraction value targeted is 0.25 ($f_{\text{PMMA}} = 0.25$). Thus, the amount of PMMA-CTA produced is insufficient and leads to failure of LAM formation.

The ultimate goal of this study to devise a crosslinking technique that can sustain the internal nanostructure of BCP in dispersion polymerisation in scCO_2 was achieved and discussed in chapter 4. RAFT dispersion polymerisation was successfully employed in developing a novel and facile method for *in situ* crosslinking copolymerisation in scCO_2 . It was possible to maintain the polymerisation-induced microphase separation within the microparticles and simultaneously crosslink the growing chains of the precursor by using a delayed addition of the crosslinker and a portion of the second monomer.

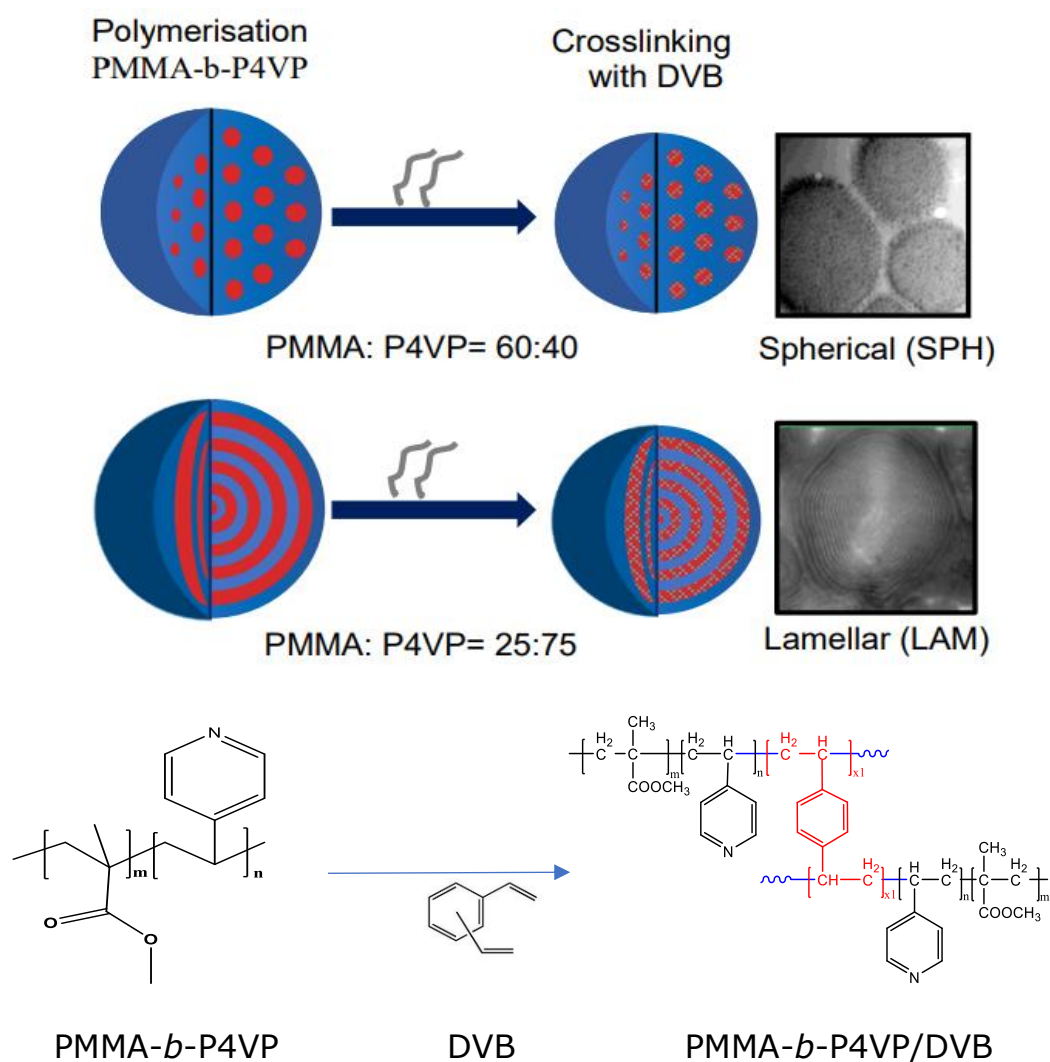


Figure 6.1. *In situ* crosslinking copolymerisation reaction of PMMA-*b*-P4VP via RAFT dispersion in scCO₂. The newly developed method for crosslinking the internal domain of P4VP has successfully preserved the internal nanostructure of BCP. The crosslinker used, divinylbenzene (DVB) consists of a combination of meta and para isomers of DVB and ethylvinylbenzene.

The method enables the preservation of the internal nanostructure of the BCP microparticles with either SPH or LAM internal morphology. The key discovery is the behaviour and performance of crosslinked microparticles, in particular the microparticles exhibiting the LAM internal morphology, which is a novel characteristic of this work. The crosslinking process was efficient, and both the particle size and domain size decreased in comparison to the non-crosslinked particles. The structural stability of the crosslinked PMMA-*b*-P4VP microparticles was successfully verified by dispersing them in suitable solvents, in which both the interior nanostructures and microparticulate scaffolds were preserved.

It was discovered that the amount of crosslinker supplied during the polymerisation of the SPH microparticles efficiently controlled the porosity formation during swelling in ethanol followed by deswelling in hexane. Macropores greater than 100 nm, mesopores 20 nm, sub-10 nm pores, and finally non-porous structures were all obtained by increasing the DVB concentration from 0 to 0.5, 1, and 4 wt.%, respectively. The maximum resistance point to swelling for SPH (PMMA₅₀₀-*b*-P4VP₃₃₀) and LAM (PMMA₁₅₀-*b*-P4VP₄₅₀) BCP was successfully determined at 4 wt.% for SPH and 2 wt.% for LAM.

Finally, in chapter five, it was demonstrated that the size and porosity of the microparticle BCP can be controlled through *in-situ* crosslinking copolymerisation by RAFT-dispersion in scCO₂, and this control is then useful in turning the materials for different applications. Lipase was

successfully immobilised into the non-porous BCP microparticles with both SPH and LAM morphology. The immobilised yield obtained, ranged from 51–59%, indicated that the BCP microparticles of this study provide a promising immobilisation structure for lipase enzyme in comparison to the previous study reported in 2020, in which the author reported a lipase immobilisation yields between 11 up to 88%.¹

All of the samples that were tested for usnic acid (UA) adsorption showed good adsorption yields of more than 60%, indicating that they could be utilised in drug adsorption applications. The highest UA adsorption yield was 79% and was achieved by the porous particles synthesised with 5 wt.% PDMS-MA and 1 wt.% DVB. On the other hand, the extraction capacity of the majority of the microparticles synthesised using 2.5 wt.% PDMS-MA, containing DVB ranging from 0-4 wt.%, was found to be satisfactory. The percentage of recovery met the estimated specification, ranging from 35 to 75 % after accounting for both the hydrophilic lipophilic balance (HLB) value and the value of partition coefficients ($\log P$). These results could be used as a good reference to assess the ability of this materials in a stationery phase application.

The work presented is not a complete task; there are always a variety of improvements and suggestions that will expand further on the current findings. Thus, a few recommendations for future work will be included in the following section.

6.2 Future Work

Promising results have been demonstrated by the PMMA-*b*-P4VP BCP system synthesised using methods developed in this study. The applicability of this method to other BCP systems and morphologies can be explored further. A preliminary study was carried out in the group by crosslinking the PMMA-*b*-PBzMA system with 0.5 wt.% of crosslinker.² However, more analysis, similar to what was demonstrated in this thesis, could be performed to evaluate the performance of this product and other BCP system.

In addition, there are two more scopes of work that are desirable: (1) Further investigation on the swelling/deswelling method in order to assess the porosity control over the LAM BCP microparticles and (2) an in-depth study on any of the potential applications proposed in this thesis, including enzyme immobilisation, usnic acid adsorption and polymer stationary phase applications for better optimisation and enhancement of the final results.

As discussed in Chapter 4, the swelling/deswelling method applied to LAM BCP microparticles was found not suitable. The method used could only be applied for swelling of a minority P4VP-block (less than 35 mol%) but the LAM BCP tested contained a majority of the P4VP-blocks (75%). Thus, the particles swelled too much as a result. This could be improved by using different swelling agents and perhaps optimisation of the exposure time which might have some impact on porosity formation. There was a study reported on the role of swelling agents in selective swelling induced pore generation of cylinder-forming diblock copolymer, PS-*b*-P2VP (S2VP) performed at different exposure time: 10 minutes, 1 hr, 4 hrs and 15 hrs.

The authors found that these two factors (swelling agents and exposure time) gave a significant impact on the porosity generation.³ A modification of the sample preparation before swelling/deswelling exposure could be one way of improving the method for LAM microparticles. There was another study on casting film of BCP PS-*b*-P2VP, which reported different stages of morphology reconstruction after exposure to an acidic environment.⁴

In Chapter 5, the lipase immobilisation test resulted in a promising immobilisation yield up to 60%. Protein immobilisation is a tailored process, as it will depend on each protein structure and the chemistry associated with the support used. Optimising parameters like protein load and immobilisation time should be developed to target an increased immobilisation yield. The same is true for the other application tests, in depth studies would give more information and could enhance the application possibilities. Finally, the usnic acid and polymer stationary phase application testing of the LAM BCPs for comparison with SPH BCP in term of materials performances is needed. The result of this would be a gain of knowledge about the properties of a wider range of the materials synthesis and their suitability for the application tested. In addition it would highlight if one material was better than another for a specific application.

6.3 References

1. M. Yousefi, M. Marciello, J. M. Guisan, G. Fernandez-Lorente, M. Mohammadi and M. Filice, *Molecules (Basel, Switzerland)*, 2020, **25**, 545.
2. G. He, T. M. Bennett, K. Alias, L. Jiang, S. T. Schwab, M. Alauhdin and S. M. Howdle, *Polymer Chemistry*, 2019, **10**, 3960-3972.
3. N. Yan and Y. Wang, *Journal of polymer science. Part B, Polymer physics*, 2016, **54**, 926-933.
4. Y. Wang, U. Gösele and M. Steinhart, *Nano letters*, 2008, **8**, 3548-3553.